PRESSURIZED WATER REACTOR LOSS-OF-COOLANT ACCIDENTS BY HYPOTHETICAL VESSEL RUPTURE

by

Phung Lien Doan
David D. Lanning
Norman C. Rasmussen

MITNE-141

August, 1972

Department of Nuclear Engineering
Massachusetts Institute of Technology

PRESSURIZED WATER REACTOR

LOSS-OF-COOLANT ACCIDENTS

BY HYPOTHETICAL VESSEL RUPTURE

by

Phung Lien Doan

Submitted to the Department of Nuclear Engineering on August 7, 1972 in partial fulfillment of the requirements for the degree of Doctor of Science.

ABSTRACT

The unlikely loss-of-coolant by pressure vessel rupture in a pressurized water reactor plant has been studied with the objective of probing the relative importance and consequences of principal blowdown processes. The computer codes WHAM and RELAP3 have been employed as the principal tools of analysis. To the fullest extent possible, design data for a large, 4-loop, 2758 MWt pressurized water reactor has been used to generate inputs for the accident simulation by the computer.

The rupture is hypothesized as a well-behaved hole located either at the top, bottom, or side of the vessel. For every such location, break sizes ranging from 1 to 4 times the loop flow area are investigated. Time for the break to open up is also studied parametrically to determine its effect on the subcooled and two-phase blowdown processes. Sensitivity studies have been made, encompassing emergency core cooling location and injection rates, fuel-clad gas gap conductivity, void reactivity coefficients and phase separation models. The accidents are followed sometimes to 40 seconds, but mostly only to 25 seconds after rupture initiation. At the end of this period, the accumulators have not completely discharged their water, and the lower plenum has not been filled.

Within the limitation of a priori assumptions used to define the accident and within the validity of the computer codes, several patterns of results are observed. The instantaneous rupture gives the highest subcooled loadings to vessel internals but otherwise the rupture time does not have much effect on parameters such as blowdown rate, blowdown time, heat transfer coefficients, and clad temperature. Flow reversal in the case of bottom and side breaks seems to exert a strong influence, insofar as RELAP3 is formulated, on the subsequent behavior of the clad temperature transient. The clad surface temperature is also sensitive to the fuel-clad gap conductance.

There is a tendency for the force and pressure loadings to level out to a maximum magnitude as the break increases in size. This maximum pressure loading is the difference between the normal subcooled pressure of the coolant and the saturation pressure. There is also a tendency for the blowdown rate, the mass remaining in the system, the pressure history in regions of the system other than the region with the break, and the average clad surface temperature to assume an asymptotic configuration when the break size increases. This behavior is seen to result from flow choking that exists at various flow paths whose areas are fixed irrespective of the break size. For all cases under investigation, the maximum of the average clad surface temperature at the hot one-third region of the core is about the same as the corresponding quantity for the loss-of-coolant accident by pipe break. This latter quantity is computed elsewhere with RELAP3 and with essentially the same plant data used in this study.

Thesis Supervisors: David D. Lanning
Norman C. Rasmussen
Title: Professors of Nuclear Engineering

Thesis Reader: Arden L. Bement
Title: Professor of Nuclear Materials

ORGANIZATION OF THIS DOCUMENT

This document consists of 9 chapters with titles as listed in the Table of Contents. The subtitles, tables and figures are listed in the beginning of the chapter in which they belong.

Immediately after the front title page are the Abstract, the Acknowledgements, the List of Abbreviations and the Table of Contents. Following the 9 chapters are Appendices A, B,C & D, the References and the Biographical Note.

The 9 chapters are numbered using arabic numerals, e.g. Chapter 5. The major subdivisions of each chapter are numbered using a decimal system based on the chapter number, e.g. 5.1, 5.2, 5.3, etc. Further subdivision of each chapter is identified by a second or third decimal system relating of the major division, such as 5.1.1, 5.2.1, 5.3.1.2, etc.

The references are classified in the alphabetical blocks (Block A, Block B ... Block Z), but no effort is made to further arrange the listings in each block in alphabetical order. The alphanumeric order of a reference, e.g. R5, is enclosed in parenthesis in the place of the text where it is mentioned.

Wherever possible, short explanation of the tables and figures is found on the tables and figures themselves. However, due to space limitation, the main explanation and discussion of the tables and figures must be found in the appropriate place in the text.

From beginning to the end, the pages of this document are identified by arabic numbers.

ABBREVIATIONS AND SYMBOLS

The following abbreviations and symbols are frequently used in this work. They are only written out where their use is for the first time.

A	Symbol used throughout to denote the size of the hypothetical hole in the vessel. The unit size is the pipe flow area.
ACRS	Advisory Committee on Reactor Safeguards
AEC	(United States) Atomic Energy Commission
AEC/DRL	Atomic Energy Commission/Directorate of Reactor Licensing
BWR	Boiling Water Reactor
CL	Charging Line
CHF	Critical Heat Flux
CHFR	Critical Heat Flux Ratio
DNB	Departure from Nucleate Boiling
DNBR	Same as CHFR, the ratio of the DNB flux to the actual surface heat flux
ECC	Emergency Core Cooling
ECCS	Emergency Core Cooling System
EOB	End of Blowdown
FLECHT	Full Length Emergency Cooling Heat Transfer (tests)
h	Symbol for fluid enthalpy
HPCIS	High Pressure Coolant Injection System
HSST	Heavy Section Steel Technology
HTC	Heat Transfer Coefficient
LOFT	Loss of Fluid Test
LPCIS	Low Pressure Coolant Injection System
LWR	Light Water Reactor
MIT	Massachusetts Institute of Technology
p	Symbol for pressure
PWR	Pressurized Water Reactor
RHR	Residual Heat Removal

SECCI	Start of Core Cooling Injection
SIS	Safety Injection System
t	Symbol for time
T	Symbol for temperature
t_b	Time over which the break opens from zero to its preassigned size
u	Symbol for internal energy

TABLE OF CONTENTS

*Contents of each Chapter, including Tables and Figures are listed in front of that Chapter.

CHAPTER 1

SUMMARY, CONCLUSIONS AND RECOMMENDATIONS

1. SUMMARY, CONCLUSIONS AND RECOMMENDATIONS

1.1 Summary

The principal processes and short-term effects of subcooled depressurization followed by two-phase blowdown as a result of a postulated pressure vessel rupture in a PWR plant have been topics of investigation in this work. The principal processes include the subcooled pressure and force loadings, the two-phase blowdown rates, pressures, flows, and heat transfer. The principal effects are the responses of the vessel internals to the loadings and the fuel clad surface temperature transients.

The plant chosen for analysis is a 4-loop 2758 MWt Westinghouse PWR plant similar to the Indian Point 2 plant that is scheduled to go on line in 1972. (Figs. 1.1.F1 and 1.1.F2). To the fullest extent possible, real plant data are used to put the analysis on a more practical plane (Appendix A). Where real data are missing or unavailable, realistic approximations are made and so indicated.

The tools of analyses include two computer codes, WHAM and RELAP3. Both of these codes have been developed for the USAEC and tested out on semi-scale experiments in the LOFT project. Although there are still many desirable improvements to be made, they represent the 1972 state of the art and have been widely used in the LOCA analyses for many PWR power plants.

The vessel is postulated to rupture or split in such a manner that the break area opens up linearly with respect to break time. Three locations of this window type blowout are analyzed, namely at the upper plenum, the lower

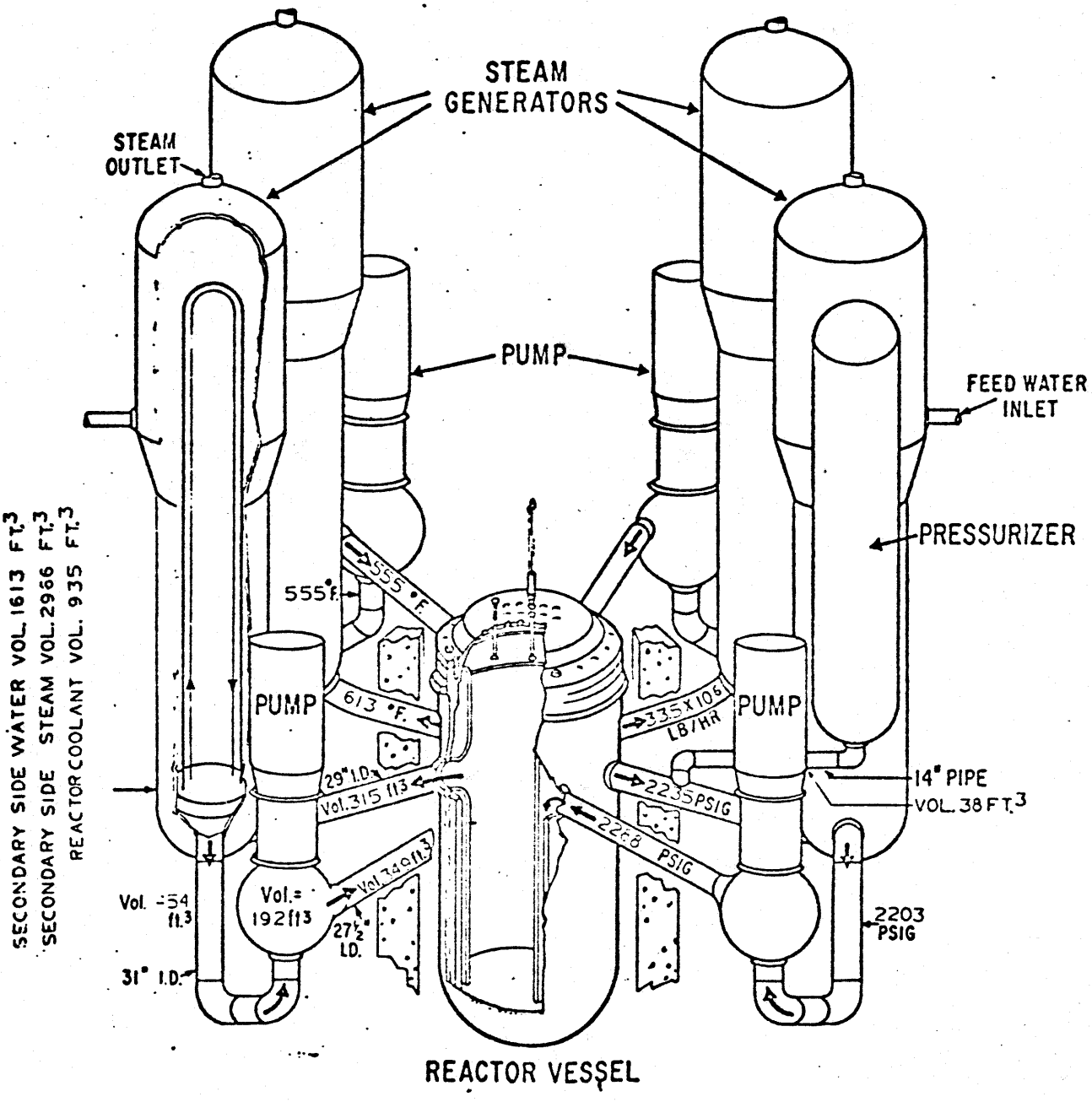

VIEW LOOKING WEST

Fig. 1.1.F1

Primary System Setup of A Typical Large PWR Plant Chosen For This Study (From Ref. C1)

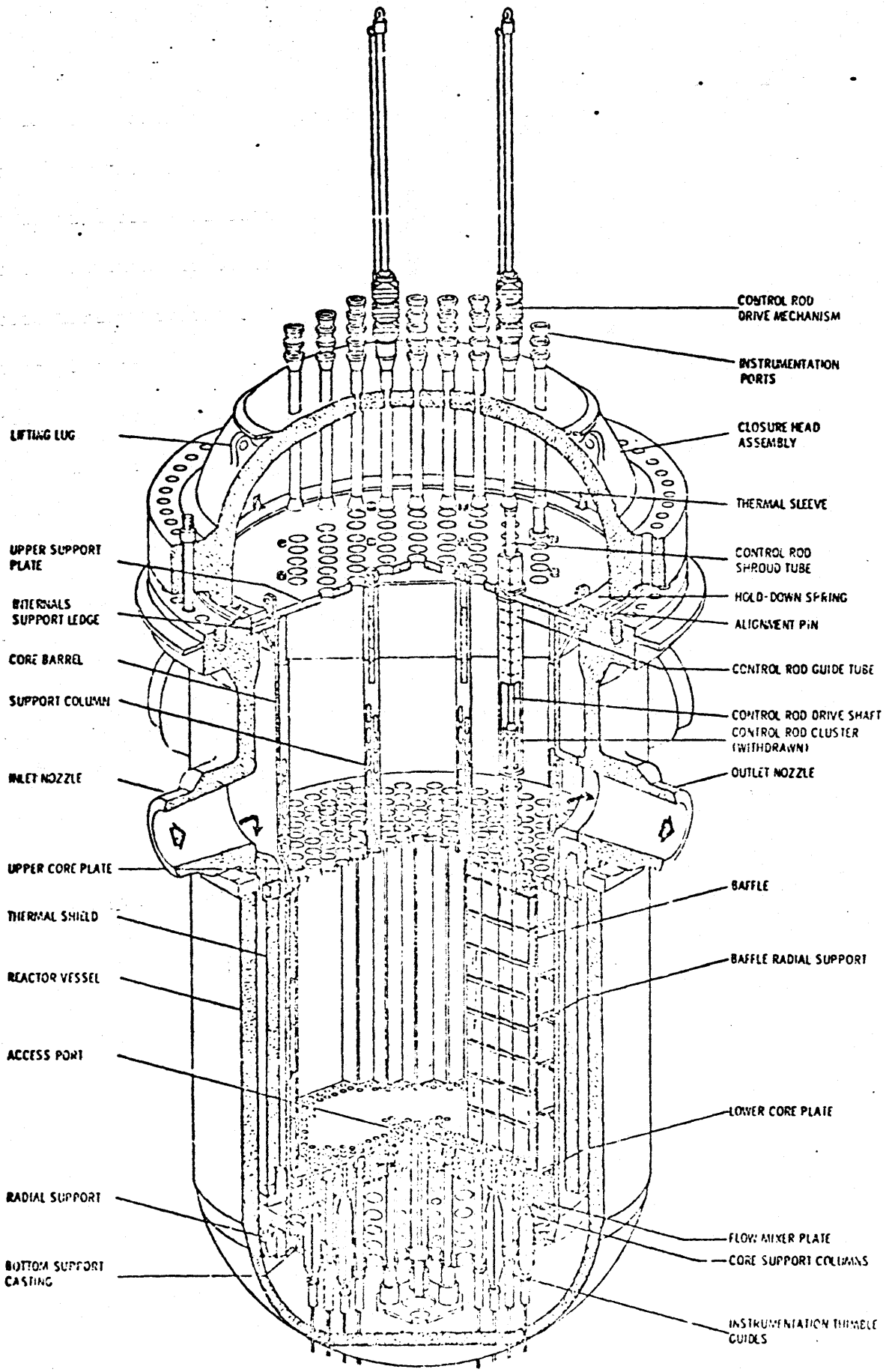

Fig. 1.1.F2

Reactor Vessel And Internals (From C1)

plenum and the annulus. They are respectively called the top break, the bottom break and the side break. For each location, four area sizes in the multiples of pipe cross sections are considered. The reason for the use of pipe cross sections is to establish some base line to compare the results with data already available for the single-ended and double-ended pipe breaks in the hot leg or the cold leg. Thus, for the top vessel break case, the unit break area is 4.587 ft^2, the flow area of the 29-inch ID hot leg. For the bottom and side break cases, the unit break area is 4.12 ft^2, the flow area of the 27-1/2 inch ID cold leg.

In postulating vessel breaks, it has been assumed that all the four recirculation loops are intact. This assumption is used to establish a base case analysis, because further deterioration of the rupture can be analyzed in somewhat similar ways. The safety control rods are assumed not to be activated till 30 seconds after the break, an assumption essentially the same as no control rod action at all. The steam generators are assumed to maintain their pressure and temperature on the secondary side, thus acting as a heat source in a substantial duration of the blowdown. The coolant recirculation pumps are assumed to be in a free-wheeling position, allowing the coolant to flow out of the break without pump constraint. Only three out of four on line accumulcators are used, and the ECC water is properly considered immediately after injection. This credit for the ECC water (i.e. no bypass) is not unconservative, because the assumption of thermodynamic equilibrium of RELAP3 effectively causes a delay of ECC water in reaching the lower plenum until well after end-of-blowdown (EOB).

System network setup for WHAM computation includes 30 legs and 28 connections. Friction and the effect of the recirculation pumps have been neglected on the basis of WHAM developmental information and test out. The effect of the pressurizer is also neglected because it appears in only one of the four loops and it is connected to the hot leg by a long, small surge line. However, other features such as internal volumes, flow bending, contraction or expansion are maintained. For the short subcooled decompression duration (less tham 60 msec.) considered, the above assumptions are well justified.

System network setup for RELAP3 consists of 17 volumes and 24 junctions. The volumes include 3 for the core, 3 for the downcomer, 3 for the steam generators, and 1 each for the core bypass, lower plenum, upper plenum, hot leg, cold leg, pump suction leg, pressurizer and accumulators. A constant pressure of 75 psia is prescribed for the containment. The junctions are the flow paths between the volumes. The junction between the accumulators and the cold legs has a swing check valve which is activated by the pressure in the cold legs. The junctions representing other pump-activated ECC lines (charging lines, low-pressure core injection lines and residual heat removal lines) are one-way junctions, allowing cold, borated ECC water to be pumped in at a preset time.

Initial conditions of the system are those of the 2758 MWth primary system operating at steady state, 100% power level.

Table 1.1.T1 summarizes the main features of the study.

TABLE 1.1.T1

MAIN FEATURES OF STUDY

1. Codes	
Subcooled blowdown	WHAM
Two-phase blowdown	RELAP-3
2. Rupture Conditions	
Location	Top, bottom or side
Size	4.12 ft^2 to 18.35 ft^2
Break time	0.25 msec to 100 msec
3. Time Lapse	
Subcooled blowdown	0 - 60 sec
Two-phase blowdown	up to 25 seconds sometimes to 40 seconds
4. Assumptions	
Core power before LOCA	100%
Scram mechanism	Void formation alone
Pump	Free wheeling
Coolant loops	All 4 intact
ECC	Accumulators and diesel pumps
5. Sensitivity Analyses	
Break time	0.25 msec to 100 msec
Break location	Top, bottom or side
Break size	4.12 ft^2 to 18.35 ft^2
Gap Conductivity	1 to 1/4 temperature dependent conductivity of helium
Accumulator Location	Cold legs, hot legs or upper plenum
ECC injection	2800 lbs/sec to 5200 lbs/sec, max.
Void reactivity	A factor of 1 to 4 base-case values
Phase separation	Bubble gradient of 0.8 and 0.5

Three break times are analyzed for each WHAM computation. These times are 0.00025 second, 0.01 second and 0.1 second respectively. The 0.00025 second duration is considered instantaneous because it is the size of only one time step while WHAM requires two time steps for the disturbance to travel through the break. Thus, a total of 36 cases have been studied for the subcooled depressurization, 12 each for the top, bottom and side breaks. The local pressure and subcooled liquid velocity at the ends of each leg have been computed for times up to 60 msec. For large breaks of 3-to 4-pipe-sizes, the computation stops at a shorter time when the pressure at any place in the system drops below the saturation pressure of the local liquid. The inertial force exerting on the walls of the legs is also computed by integrating the time-rate of change of the liquid momentum. The total force acting on any leg in a specified direction is then obtained by combining the components in that direction of the inertial force and hydrostatic force. Forces due to gravity, friction and monentum fluxes are small and have been neglected.

The break time of 0.1 second has been used in the majority of RELAP 3 blowdown calculations, but the break time of 0.01 second has been used also to obtain a sensitivity of different parameters to the break opening time. As indicated earlier, top, bottom and side breaks are analyzed for break size in the multiples of 1, 2, 3 and 4 pipe flow areas. Reactor scram is achieved by void formation solely. For each case, the following parameters are followed: blowdown rate, mass remaining in the lower plenum, start of accumulator ECC injection, flow rates, pressure and mass histories, end of blowdown time, fuel rod temperature redistribution, heat transfer, clad temperature transient and buildup of ECC water in the vessel. Only average values are obtained. The processes are followed only to 25 seconds with the exception of a few runs which are carried out to 40 seconds after break initiation.

1.2 Conclusions

The major conclusions of the study are listed below and are further elaborated in the conclusion sections of Chapters 6, 7, 8 and 9.

1. Loss-of-coolant accident by pressure vessel rupture is quite similar to the loss of-coolant accident by pipe break. The two most striking items commonly attributed to the former accident are a faster loss of coolant and the apparent inability to hold ECC water. These two items seem to be amenable to corrective actions that would effectively reduce their severity.

2. For the vessel window type breaks up to 18 ft^2 considered, the subcooled loadings are largest for the instantaneous break time, becoming smaller and smaller as the break time increases. The loadings are essentially negligible for break time of 0.1 second or longer.

For the same break time, the loadings increase with break area, but level out to a maximum value when the break area is large. This maximum value is the difference between the initial subcooled pressure and the saturation pressure which is assumed to exist just outside the break.

From design data of the internals, it appears that the core barrel has enough structural strength to withstand the subcooled loadings without failure. Subcooled loadings across the core would exceed 1000 psi in the case of large vessel breaks, therefore they may approach the support strength of the core. Other critical areas of concern would be the welded-on thermal shield which may be subjected to excessive loading in the case of a side break, and the control rod clusters which may be excessively deflected in the case of a top break. The dynamic response of these components to the loadings is not within the scope of the present study.

3. The blowdown is very fast for vessel breaks, ranging from just over 12 seconds for one-pipe-size break to 7 - 8 seconds for larger sized breaks. Flow choking exists not only at the break, but also at various flow paths in the system. This phenomenon is the most important process and has a pronounced influence on many blowdown parameters. End-of-blowdown, heretofore defined as the time at which leak flow through the break first stops, may need redefinition because of the violent fluctuating behavior of the blowdown at large breaks in the vessel. Thus, while the system pressure drops to the maximum containment pressure within 2 seconds when the break is 4 times the pipe flow area, there is still enough coolant in the system that the flow out the break is still intermittently significant after the first temporary pause. With the modified definition of EOB as the time when the flow out the break has dropped to a small, insignificant value, then EOB would range between 7 and 8 seconds irrespective of break sizes.

4. For any break location, there is still considerable coolant remaining in the lower plenum which flashes to supply steam for core cooling after EOB and before ECC water becomes effective. This applies even for a break in the lower plenum at the buckled area which joins the cylindrical section to the hemispherical head. When the break is at the lowest point of the bottom head, phase separation with bubble rise of the coolant in the lower plenum no longer helps, and practically all the coolant would be lost from the lower plenum.

5. For bottom and side vessel breaks, flow reversal takes place very fast, in less than 60 milliseconds for the cases considered. There is some anomaly in the clad temperature calculated by the RELAP 3 program during this period, the effect of which is carried for a long time after EOB. This anomaly, the flipping of heat transfer to the stable film boiling regime and locking it in that regime is thought to be due to the absence of a valid flow-dependent DNB correlation for flow reversal. The anomaly results in a higher clad temperature in certain cases.

6. The average clad temperature transients in the center core region assume the following general pattern: The temperature starts at the average steady state value, increases slightly during flow reversal, then decreases as the reactor has scrammed and the flow rate increases due to the greater pressure differentials. At a time close to EOB, the temperature turns around and increases. The excursion assumes a very steep slope (some 200°F/sec.) during the quiescent period following EOB due to stable film boiling and steam cooling. The temperature reaches a maximum in less than 25 seconds. curving slowly downwards as ECC water becomes slowly effective.

When the break size becomes larger and larger, there is a tendency for the average clad surface temperature to assume an asymptotic configuration the maximum of which is below 1500°F. This is equivalent to the maximum of the average clad surface temperature for the case of LOCA by guillotine pipe break reported in the literature for an equivalent large PWR plant investigated in RELAP 3 with practically the same initial conditions. This feature seems to be of great significance in the contingency plans for core cooling. It is thought to be due to the choking flow characteristics which leads to a

EOB of approximately 7 - 8 seconds for any break size. Thus, since the heat redistribution of the fuel rod has been essentially over, the heat production by fission products is more or less a constant, and the heat removal at the clad surface by steam cooling is low but not too different, then the clad surface temperature would of course assume an asymptotic pattern. It is believed that this fact will contribute substantially to the design of safeguards that can ultimately cool the core even at large vessel failures.

7. Various sensitivity studies have been made to evaluate the effects of important parameters in the blowdown process.

a) The bottom and side breaks result in worse loadings to the internals than the top break, and the peak of the average clad surface temperature at the center core region is also higher. But for the same location, the peak is about the same for all large break sizes.

b) The break times of 0.01 second and 0.1 second caused different subcooled pressure differentials across vessel internals, but do not give rise to any significant difference in blowdown rate, flow rates, mass remaining in the lower plenum, and temperature transients. There are only slight differences in the flow reversal time, reactor scram, and system pressure in a very short duration following break actuation. These differences have negligible effects on the EOB and clad temperature transients.

(c) The ECC injection rates from the same accumulator systems but with different maximum rates from some 2800 lbs/sec to 5200 lbs/sec have been studied. The higher rate of injection gives only a slightly lower peak for the average clad surface temperature. This is thought to be due to the fact that EOB takes place very fast while it takes some time for the ECC to build up from zero to a maximum value. Furthermore, the ECC water is slow in reaching the core due to the RELAP3 assumption of thermodynamic equilibrium in the leg where ECC water is injected into.

(d) The location of the ECC injection has a marked effect on the clad transient. When the location is at the hot legs or upper plenum, the peak temperature is higher than when the location is at the cold legs. This is thought to be due to the fact that as the ECC cold water is injected early in the blowdown, it lowers the pressure in the upper plenum and the hot legs thereby reducing the flow through the core. This is particularly prominent during the quiescent period when only a small pressure differential drives the steam through the channels for core cooling. However, it may also be due to the nature of the RELAP3 Code. At the present state, the code does not allow for any initial ECC water velocity nor any water entrainment both of which are obviously important if the core is to be cooled from the top.

(e) The gas gap conductivity has a strong effect on the temperature of the clad surface temperature. The lower the conductivity, the higher the peak of the clad temperature transient. For example, a difference of 400°F is seen when the gas gap conductivity changes from 1/2 to 1/4 the temperature-dependent conductivity of helium (1-pipe-size top break). This effect is due to the fact that a low conductivity interferes with the heat removal during the

beginning phase of the blowdown when the coolant flow through the core is high and effective. The redistributed heat is thus confined in the fuel, and will have to transfer out to the clad later when only steam is available on the outside to remove it.

A high conductivity. about 1/2 that of helium, is more probable for the gas gap at normal operation because the centerline temperature is 2800°F on the average, a value comparable to the design value. But very soon after the break, due to decreased coolant pressure, the clad may balloon, thus decreasing the overall conductivity of the gap. If the gap conductance has a strong effect on the clad surface temperature after EOB, then this phenomenon certainly is deleterious to the core cooling.

(f) A change of void reactivity coefficient from 1 to 4 times the base case values results in a relatively faster reactor scram, but otherwise is very insensitive to other parameters such as flow reversal, EOB, mass remaining in lower plenum, and clad surface temperatures.

(g) A change of the phase separation model from the base case to the more homogeneous model (smaller bubble gradient) results in a slightly faster blowdown and a slightly higher clad surface temperature. However, the quantity affected the most is the coolant mass remaining in the lower plenum. A more homogeneous phase model would leave less water. Thus, for the case of 1 pipe-size top break, only half as much water left if the phase model has a bubble gradient of 0.5, as compared to the base case with a bubble gradient of 0.8.

1.3 Recommendations

The following recommendations are proposed:

1.3.1 Break Time Determination

Sensitivity study in this work has indicated that the break time is not sensitive to the two-phase blowdown processes, but is very sensitive to the subcooled loadings. Therefore, it is highly desirable that the fastest break time of certain break size be determined with a reasonable degree of confidence. Work on fracture mechanics in the HSST project may in time provide this information. If it can be established that the break time is slower than "instantaneous", then the subcooled loadings are significantly reduced, and the integrity of the vessel internals can be counted on with more confidence.

1.3.2 Transient DNB Heat Flux Correlation

The determination of burnout is dependent on the DNB heat flux correlations which were established under steady state conditions. The extrapolation of the validity of these correlations to transient conditions may result in serious error, particularly in the cases involving flow reversal. The behavior of the clad at every moment has effects on the entire course of the blowdown, therefore, the use of a steady state DNB correlation to predict burnout results in conservative temperatures for the fuel clad but may lead to other incorrect information such as flow rates. Transient DNB heat flux correlations are, therefore, needed.

1.3.3 Different Modes of Emergency Core Cooling Injection

Results of this study indicate that the ECC water is most needed when the primary coolant has blown down almost completely. Furthermore, the time for EOB is almost the same for large breaks. Therefore, it is of interest to look into different modes of ECC injection both to render the ECC water more effective and to improve somewhat the economic and engineering penalties that may be associated with current ECC designs. The different ECC modes may include more redundant ECC injection locations, lower injection pressure, top and core sprays, vents to relieve the effect of steam binding, and even the use of the steam generators as a ECC water source.

1.3.4 Further Study of Vessel Break Consequences

For lack of time and resources, the present study has not included an analysis for the dynamic effects of the subcooled loadings on vessel internals and the temperature transient of the clad hot spots. Only comparison with data of LOCA by guillotine pipe break has been made. The data or responses of vessel internals have been used on faith that they are correct for the quoted low loadings. But for subcooled loadings approaching 1100 psi in magnitude and 100 cps in frequency such as those reported in this study, new analyses for vessel internals responses seem appropriate.

It has been concluded that in the first 25 seconds following the vessel rupture, the peak of the average clad surface temperature is below 1500°F and is similar to the same quantity for LOCA by pipe break. The use of THETA-1B to predict the temperature of the hot spots for the latter case has been made elsewhere with the result that the highest temperature is at no time exceeding

2300°F (A4). It is recommended that the THETA-1B or a similar code be used in conjunction with flow rates established in this work to compute the expected maximum hot spot temperature during vessel blowdown.

Furthermore, the study of the core behavior beyond 25 seconds is recommended to find out the long-term coolability of the core. In this case other modes of core cooling could be considered, such as top or core spray and the possibility of cold water flowing from the vessel cavity towards the inside of the vessel through the break.

Other consequences of a vessel rupture accident must be brought under consideration. These include the capability of the containment to withstand the fast pressure transient, the problems of missile generation, and the remote possibility of a slumped core.

1.3.5 Code and Model Improvements

The following improvements in the WHAM and RELAP3 codes and their use are proposed:

a. As WHAM uses the speed of sound at every time node to update the varying parameters (pressure, velocity and inertial force), it would be more accurate to input the sound speed as a function of pressure (still assuming that the enthalpy is basically constant in this very short duration). A slower sound velocity at lower subcooled pressure would effectively reduce the loadings and slow down the pulses. Experiments with semi-scale vessel rupture (G2) have indicated that WHAM overpredicts the loadings at large break sizes.

b. The one-dimensional simulation of the physical network for WHAM calculations seems to be justified for all sections of the primary system except the downcomer annuli, the vessel plena and the steam generator plena. In these regions, two- and even three-dimensional acoustic wave propagation is certainly significant, therefore, to model them as one dimensional short pipe is too coarse a simplification. Fabic (F5) has proposed the employment of rectangular or cubical networks for these regions, but no modification to the WHAM code has been available in the public domain. Efforts in this direction would result in lower but more accurate loadings to the vessel internals.

c. At present, RELAP3 seems to contain several shortcomings that can be improved with only moderate effort.

The cause must be found for the apparent persistence of the heat transfer in the film boiling regime in some calculations while in others the heat transfer proceeds with a seemingly more physical pattern. This cause is found in this study to be related to the flow reversal and the use of the various steady state DNB flux correlations. While it can be readily admitted that the current DNB flux correlations are inadequate for the flow reversal transient, it seems physical that the clad temperature should only rise very slightly during the few milliseconds of the reversal, then should again drop as the nucleate boiling regime is recovered due to the reversed but higher-than-normal mass flow rate.

d. This study has indicated that the maximum clad surface temperature is very sensitive to the gas gap conductivity of the fuel rods. The swelling and ballooning of the clad is most likely to occur when the coolant pressure

has dropped to a low value and when the clad surface temperature starts on a steep climb (T6). The effect of these phenomenologies to the transfer of the stored heat from inside the fuel must be evaluated if the clad surface temperature is to be computed more accurately.

e. There must be a provision in RELAP3 to account for the ECC injection velocity. When the ECC line is perpendicular to the cold leg, the injection velocity is effectively stopped at the injection location, but there have been designs (C5) with the ECC nozzles making an angle with the cold legs. In this case, a separate treatment of the injected, cold liquid, and of the two-phase (mostly steam) coolant would be desirable. In other words, the assumption of instantaneous mixing in these volume nodes should be substituted by a model of two-component flow in pipes with appropriate entrainment consideration. This effort is reported to have been made by some reactor manufacturers (C5), but no usable results presently exist in the public domain.

f. RELAP3 presently employs the forward finite difference technique to integrate the sensitive momentum equation. Even at very small time steps, which is computationally expensive, the flow rate fluctuates unrealistically in the core, particularly during the steam cooling period. It has been pointed out that the use of the backward finite difference technique allows larger time steps and renders the flow smoother (R6). It is recommended that this effort be undertaken for RELAP3.

g. Current practice in loss-of-coolant accident analyses includes the use of a series of large computer codes, the output of one is being fed as input into the other. The logic of these codes, such as RELAP3, is based on assumptions many of which are oversimplified. Experimental evidence is needed to provide some degree of confidence in the results calculated by these computer codes.

CHAPTER 2

Page

INTRODUCTION

2. INTRODUCTION

2.1 Perspective and Rationale

It has often been pointed out with pride, and may be rightly so, that no major human enterprise has ever been undertaken with the same excellent safety record as that of the nuclear industry. From the early days of the successful control over nuclear chain reactions, the exploitation of the energy from inside the nucleus has been conducted with the highest degree of care. This is possible thanks to the national, well thought-out nature of the enterprise, and perhaps also to necessity because of Man's first hand lesson that an unwise unleashing of nuclear energy can cause untold damages.

Commercial nuclear power has been a fact of life today and is proceeding to take over a larger and larger share of the power generating capacity in the foreseeable future. As of 1972, over 129 nuclear reactors totalling over 100,000 MWe have been operable or under construction or committed to be built in the United States (P3). Most of these reactors are of the light-water cooled and moderated category, although the high temperature gas-cooled reactors are beginning to come into the market. These powerful reactors, with power levels between 600 MWe and 1200 MWe, are usually sited as close to load centers as safety and regulation would permit. Often, large stations of multiple 1000 MWe units are sited within 30 miles from large metropolitan areas. Such siting is based upon the confidence that these nuclear plants are constructed and operated with no undue hazard to the safety and welfare of the public.

The basis for the confidence in the safety of nuclear plants is the provision for multiple barriers of protection, the so-called defense-in-depth concept. This concept stipulates that the nuclear plant must first be designed, built and operated with such quality and care that the probability of an accident occurring is very small. Then, protective systems are further provided to take corrective actions should certain plant functions not behave as expected. Finally, even these protective systems may be assumed to malfunction at the time they are called upon, and thus contingency measures must be available to mitigate the consequences. A very powerful technique commonly employed in the pursuit of this defense-in-depth concept is the single failure criterion. This criterion provides that any single component of the machine can be assumed to fail without causing undue safety hazard.

The general design criteria of 10 CFR 50 (Codes of Federal Regulation, Title 10, Part 50), Appendix A (A1) require current light water reactors to provide analyses and protection for the whole spectrum of pipe break sizes, the most severe being the guillotine cold leg break. Thanks to its compact geometry and its higher strength, the reactor pressure vessel failure is not included in this spectrum of requirements.

Current pressure vessels of light-water power reactors are built and operated in accordance to ASME Section III, Nuclear Vessels Code which was first promulgated in 1965 and has been subsequently subjected to many additions. A description of the pressure vessels is provided in Chapter 3 and a description of the Code is provided in

Appendix D.

To date, there is scanty statistics on the failures of pressure vessels. Some data exists on the failure probability of small boilers and pressure vessels which were built in accordance to an assortment of older, less stringent codes, (F1, K1, M12, S7). No pressure vessels built to ASME Section III has ever suffered a notable failure under operation. Most of the minor problems such as the existence of certain flaws within the vessel wall, or cladding cracks, or closure stud understrength... have been detected and subjected to corrective action by the Code's inherent program of quality assurance. Although better data is yet to be established, it is believed that the probability of a catastrophic failure under operation of a reactor pressure vessel of ASME Section III design is exceedingly small.

The present research is undertaken with the above perspective. In spite of the real superior quality of the reactor vessel, this work nevertheless postulates a hypothetical hole in it so as to initiate a loss-of-coolant accident by "vessel rupture". There is no basis for this postulate. The only justification of any credibility is that a pipe break if happened very close to the vessel can be viewed as a breach in the vessel. The objective of the postulate is to study the subsequent blowdown phenomenologies in order to understand certain aspects of the plant behavior under such a hypothetical accident. The merit of the understanding of things to be expected in certain hypothetical but important circumstances for prodent and economic planning is self-evident.

2.2 Outline of Study

Chapter 1 of this work contains the summary, conclusions and recommendations of this study. Chapter 2 is the present chapter dealing with the rationale and outline of the work. Chapter 3 describes the manufacture, service conditions and other characteristics of current light water reactor pressure vessels. Chapter 4 describes the subcooled blowdown computational technique and the computer code WHAM. Chapter 5 describes the two-phase blowdown computational techniques, the computer code RELAP 3, and the representation of the PWR primary system in a network of volume nodes and flow junctions. Results and discussions on top, bottom and side breaks are presented in Chapter 6, 7, and 8 respectively. Chapter 9 provides a sensitivity study for different parameters such as break location, break size, break time, ECC injection location, ECC injection rate, fuel-clad gap conductivity, and vapor-liquid separation models.

Efforts have been made to use the most up to date data on plant design and other physical properties. Appendix A contains design data of a 2758 MWt PWR plant that have been directly or indirectly used in the computation. Appendix B lists the physical properties of fuel, clad and other materials that are employed. Appendix C presents the heat transfer and DNB regimes and correlations used in RELAP 3. The requirements of ASME Section III, Nuclear Vessel Code and the status of current vessel failure analyses are presented in Appendix D.

The reference list is separated into sections according to

alphabetical order but no effort is further made to organize entries in each section.

2.3 Areas Not Under Study

There is understandably a multitude of phenomena, problems and concerns worthy of inclusive consideration in the event of a vessel rupture. However, in order to obtain some understanding in depth of a certain problem area, it has been found necessary to single out that area with clearly defined assumptions. The scope of this study has been described earlier as to include the subcooled blowdown and the two-phase blowdown phenomenologies. The time period covered is only up to 40 seconds following the initiation of the accident. No fracture mechanical analysis is provided as to why and how the vessel failure takes place. The standard ECC systems are included in the analyses but the flooding of the core beyond the indicated time period is not considered. Only average values of the heat transfer coefficients, flow rates, and temperature in certain regions of the primary system are investigated, i.e., no effort is made to study the behavior of the hot channel. It is believed that the overall study of the transient will tell more about the behavior of system and core coolability, whereas hot channel analysis is important to satisfy certain regulation criteria such as the temperature limit. Furthermore, it is believed that if the core remains its integrity and can be cooled in the first 40 seconds of the accident, there exist real possibilities to cool it in the longer term either by current ECC systems or by modified ones.

The problems of metal-water reactions and hydrogen production are only considered insofar as they are an integrated part of the coolant blowdown and clad heatup. No effort is made to consider them separately, either during the blowdown or after it. From the containment standpoint, a large hole in the pressure vessel would pose substantial pressure and missile problems which must be mitigated if the containment criteria are not to be violated. No efforts have been made in the current study to include these problems.

CHAPTER 3

REACTOR PRESSURE VESSELS

TECHNOLOGY, SERVICE CONDITIONS AND FAILURE POSTULATES

3. REACTOR PRESSURE VESSELS TECHNOLOGY, SERVICE CONDITIONS AND FAILURE POSTULATES

3.1 LWR Pressure Vessels

The reactor pressure vessel in light-water reactors performs the very vital function of housing the reactor core and providing a pressure-tight boundary for the primary system coolant. The safe performance of the pressure vessel throughout the life of the nuclear plant is a foremost requirement without which the plant cannot be permitted to operate. Because of this role, considerable importance has been attached to the design, fabrication, testing, quality assurance and inspection of these vessels.

3.1.1 Pressure Vessel Description

As part of the rapid growth of the LWR industry with the manufacture of ever more powerful reactor cores, the steel pressure vessels that house these cores have also gone through a dramatic increase in unit size. Current 1000 MWe BWR reactor vessels measure up to 60 feet in height, 23 feet in diameter and 6-1/2 inches thick. By reason of higher operating pressure but smaller core and primary coolant inventory, a 1000 MWe PWR reactor vessel is smaller but thicker, some 50 feet in height, 14 feet in diameter and 8-1/2 inches thick. Reactors with net electrical output up to 1500 MWe have been mentioned, and present heavy industry has the capability of fabricating steel pressure vessels to house such large reactor cores.

Figure 3.1.F1 shows a typical steel reactor vessel of a large PWR primary system. It is cylindrical in shape with hemispherical heads at the two ends. The top hemispherical head is attached to the cylindrical section by a system of flange, bolts, nuts and seals. Coolant inlet and outlet nozzles lie on the same plane on the upper portion of the cylinder. Other penetrations are for control rod sleeves at the top head and instrumentation thimbles at the bottom head. The wall thickness is larger at the cylinder than at the heads because hemispherical section can better distribute stresses due to internal pressure and because radiation effects are most prominent in the cylindrical section which is close to the core. Due to large number of penetrations, substantial reinforcements are seen at the region around the nozzles and flanges.

Figs. 3.1.F2 and 3.1.F3 show the main features of vessel internals. The core is placed in the cylindrical vessel section, below the nozzles. It is attached to the core barrel which hangs down from the flange and is supported by the upper and lower support system. The region of the vessel above the core is generally referred to as the upper plenum while the region below it is called the lower plenum. Subcooled inlet water flows in the vessel from the cold legs via the cold leg nozzles, then makes a 90 degree turn to flow down the annulus to the lower plenum. At the lower plenum, it makes a 180 degree turn to flow up to the core through a system of flow distributor plates. While in the core, the water is heated up to a temperature slightly below the saturation temperature. The heated water then flows to the upper plenum, mixed by turbulence, then flows to the hot leg via the outlet nozzles, to the steam generator for cooling, then is pumped back to the cold leg for another cycle.

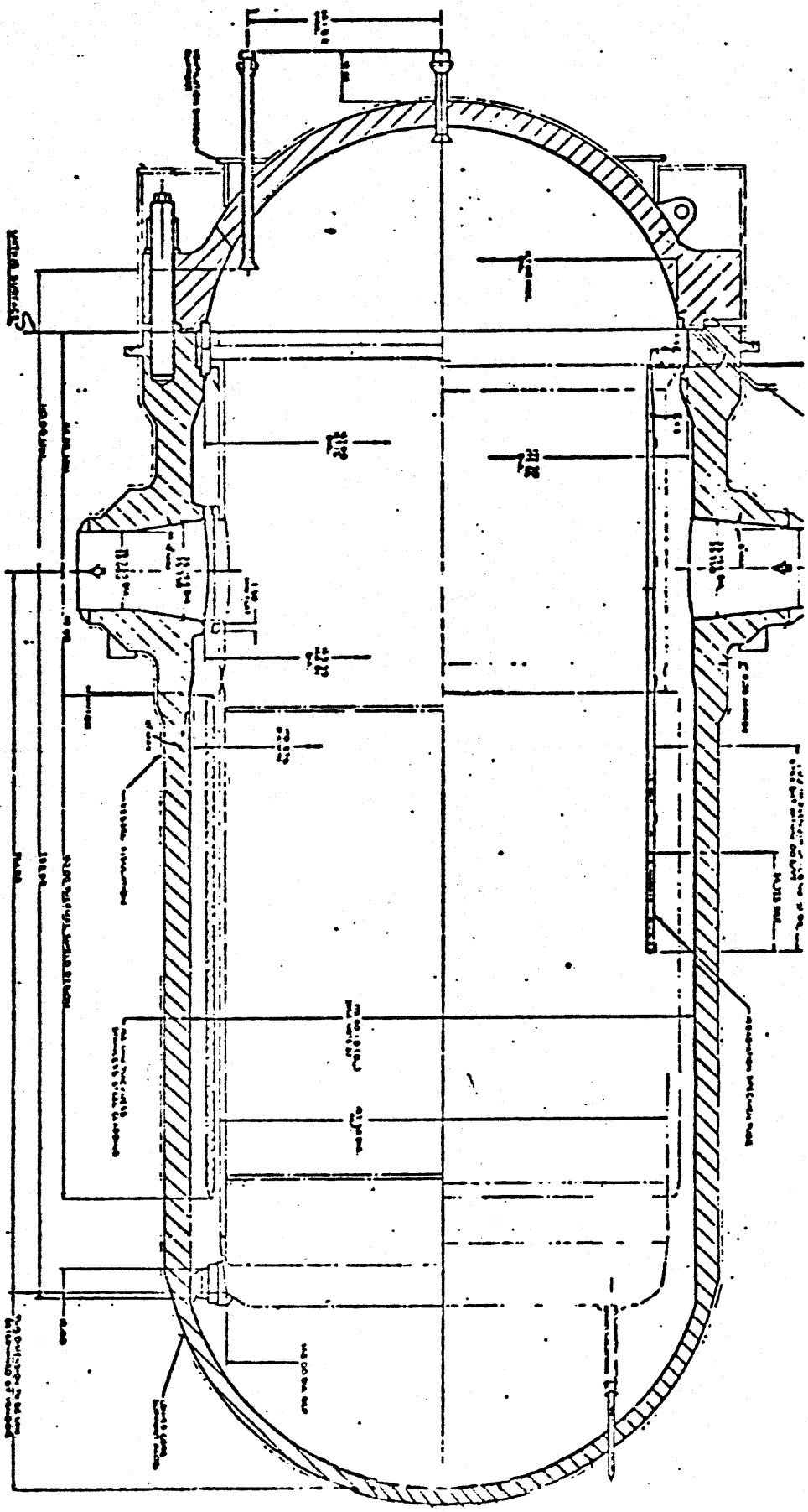

Fig. 3.1.F1

A Typical PWR Pressure Vessel (From Ref. I1)

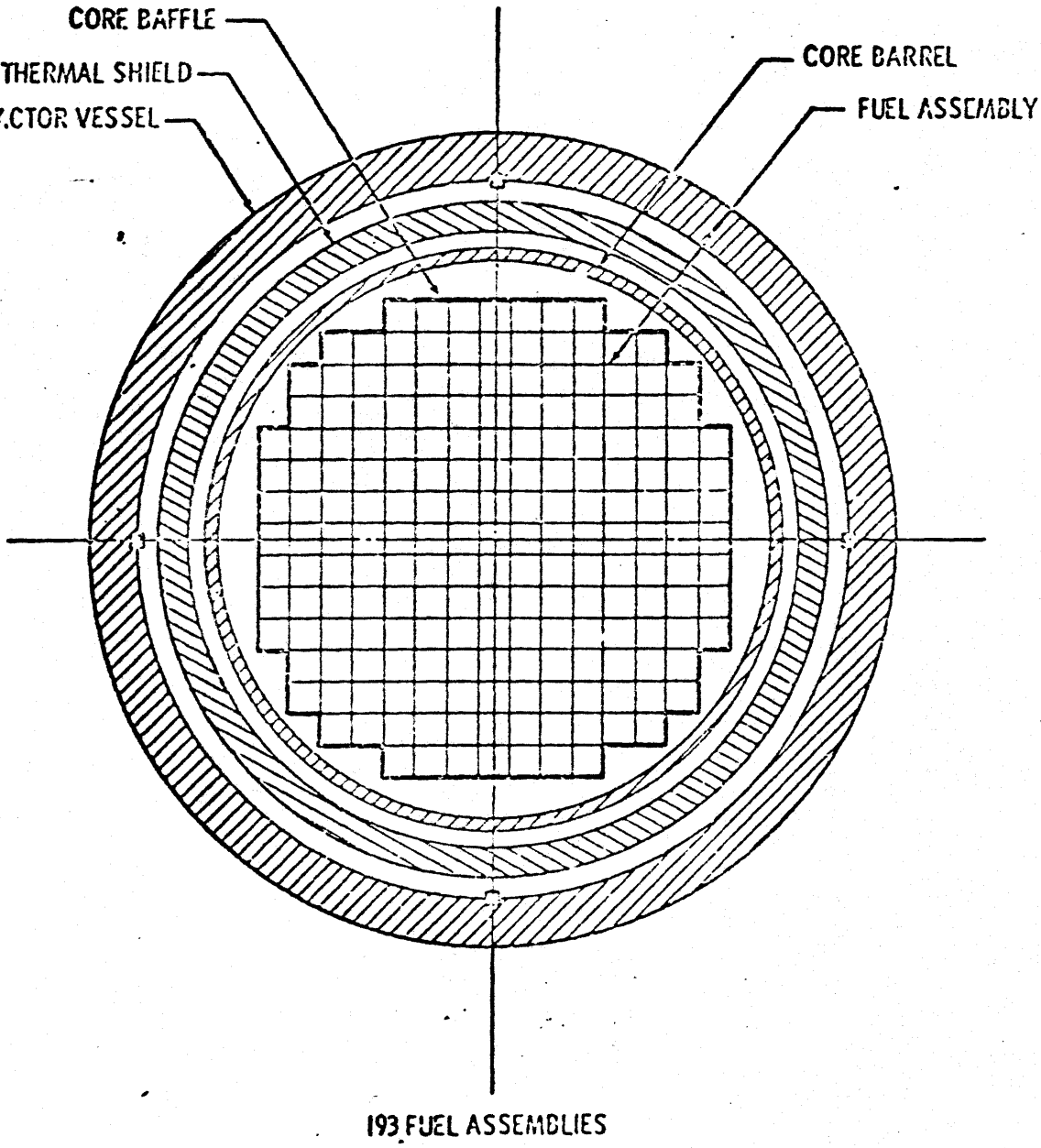

Fig. 3.1.F2

Plan View Of A Typical Large PWR Vessel and Internals
(From C1)

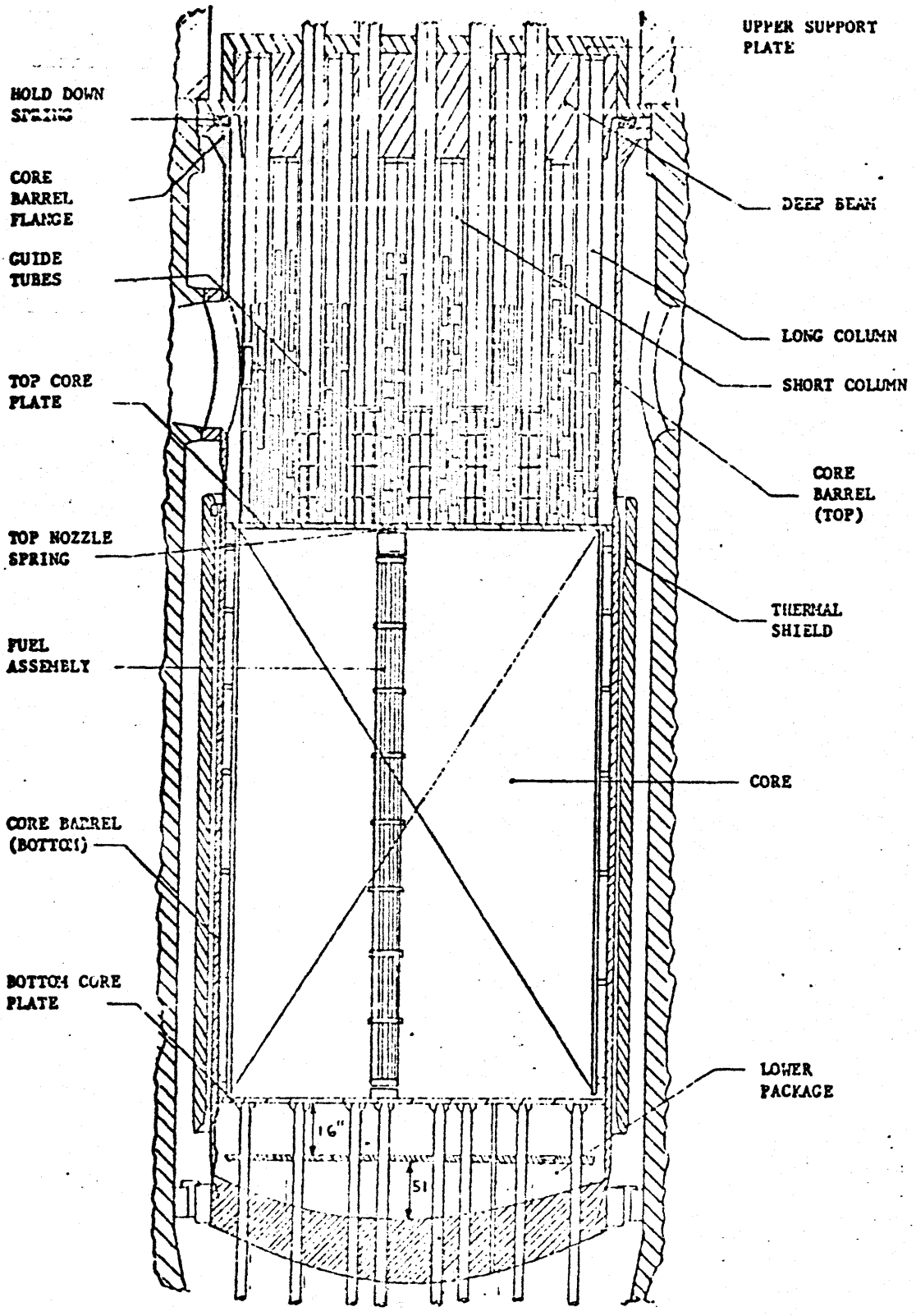

Fig. 3.1.F3

Vertical Section of A Typical Large PWR Vessel and Internals
(From C1)

3.1.2 Service Conditions

Current designs of BWR vessels are based on a temperature of 575°F and a pressure of 1250 psig. The corresponding bases for PWR vessels are 650°F and 2500 psig. These specified levels provide margin for operational maneuvering, transients, and set-point ranges for relief and safety valves.

The control of water conditions is important to preserve the integrity of the wetted surface of the vessels and its internals. Water must have less than 1 ppm of solids and 0.15 ppm of chloride. Dissolved gases such as xenon, krypton, nitrogen are kept at a constant low level through the use of gas stripper-deaerators. In PWR's hydrogen and a pH control agent, usually hydrazine, are introduced to control the dissolved oxygen to a pH level between 9.5 and 10. BWR's do not use the same scheme because the condenser tends to strip off the hydrogen without which hydrazine would break down to form nitric acid because of the high radiolytic oxygen level.

Special designs are made to minimize the effect of radiation on vessel walls. BWR vessels receive a lower neutron dose than PWR vessels by virtue of a greater clearance between the core and the vessel wall. A thermal shield consisting of a stainless steel plate approximately 4-1/2 inches thick has been used in most Westinghouse PWR's to reduce the total fast neutron fluence. Other PWR's such as those by Combustion Engineering, employ a thick core barrel to include the function of the thermal shield. The peak design life dose levels are less than 10^{18} nvt for BWR vessel walls (B6) and approximately 3×10^{19} nvt for PWR vessel walls. (W3).

TABLE 3.1.T1

TRANSIENT THERMAL AND LOADING CYCLES

FOR A 2758 MWt PRESSURE VESSEL (C1)

	Transient Condition	Design Cycles*
1.	Plant heatup at 100°F per hour	200 (5/yr**)
2.	Plant cooldown at 100°F per hour	200 (5/yr)
3.	Plant loading at 5% of full power per minute	14,500 (1/day)
4.	Plant unloading at 5% of full power per minute	14,500 (1/day)
5.	Step load increase of 10% of full power (but not to exceed full power)	2,000 (1/week)
6.	Step load decrease of 10% of full power	2,000 (1/week)
7.	Step load decrease of 50% of full power	200 (5/year)
8.	Reactor trip	400 (10/year)
9.	Hydrostatic test at 3110 psig pressure, 100°F temperature	5 (pre-operational)
10.	Hydrostatic test at 2485 psig pressure and 400°F temperature	40 (post-operational)
11.	Steady state fluctuations - the reactor coolant average temperature for purposes of design is assumed to increase and decrease a maximum of 6°F in one minute. The corresponding reactor coolant pressure variation is less than 100 psig. It is assumed that an infinite number of such fluctuations will occur.	

* Estimated for equipment design purposes (40-year life) and not intended to be an accurate representation of actual transients or to reflect actual operating experience..

** This transient includes pressurizing to 2235 psig.

Fatigue analyses involve the following categories of cycles (Table 3.1.T1):

a) Startup and shutdown cycles.

b) Load changes in normal operation.

c) Transients associated with safety action and integrity tests.

Mechanical loadings considered for the vessel are piping reactions, loading from mechanical devices that are appurtenances to the vessel, hydraulic loading, bolting action at flanges and seismic loading.

The reactor vessel is housed in a cavity with thick concrete walls which serve as biological shields. Normally, a 3 inch reflective steel or aluminum insulation layer cover the vessel on the outside to minimize temperature gradients in the vessel walls and to reduce thermal loss at the same time.

3.1.3 Fabrication

The techniques employed in the manufacturing of LWR vessels are similar to the techniques long practiced in the manufacture of heavy-walled petrochemical tanks. The principal vessel parts are the cylindrical shells, heads, flanges, nozzles, studs, nuts, supports, control rod sleeves and other penetrations. The material forms used are plates, forgings, bar stock and welding materials. Core internals, attachments supports and other appurtenances are also made from material forms such as castings, pipes, tubing, sheets strips and structural shapes.

Fig. 3.1.F4 shows an exploded schematic view of a typical LWR pressure vessel. The vessel is welded together from a number of courses. Depending on size, the head can be pressed from one steel plate or can be welded together from a number of hot-formed segments. The cylindrical shell may consist of integral rings circumferentially welded together or from rings which themselves are welded together from partial cylindrical courses. Therefore, a large LWR pressure vessel usually consists of many courses joined by circumferential butt welds and longitudinal weld joints. The welding techniques most commonly employed are the arc welding for the heads and arc welding or electroslag welding for the cylinder.

On the inside of the vessel, there is an austenitic stainless steel cladding. A nickel-based alloy overlay is sometimes used for flange faces or areas where stress corrosion may be of concern. The cladding thickness is 5/32 inch nominal and 1/8 inch minimum. No grinding or machining is done to the cladding, and the as-deposited single-layered clad is used in the vessel.

Upon completion of the vessel assembly, stress relief, annealing, and dimensional inspection, the body and closure head are finish machined. Among the most intricate tasks is the boring of penetrations. This requires accurate gauging, optical and calibration equipment for metrology for both setup and inspection, controlled environment and large machine tools.

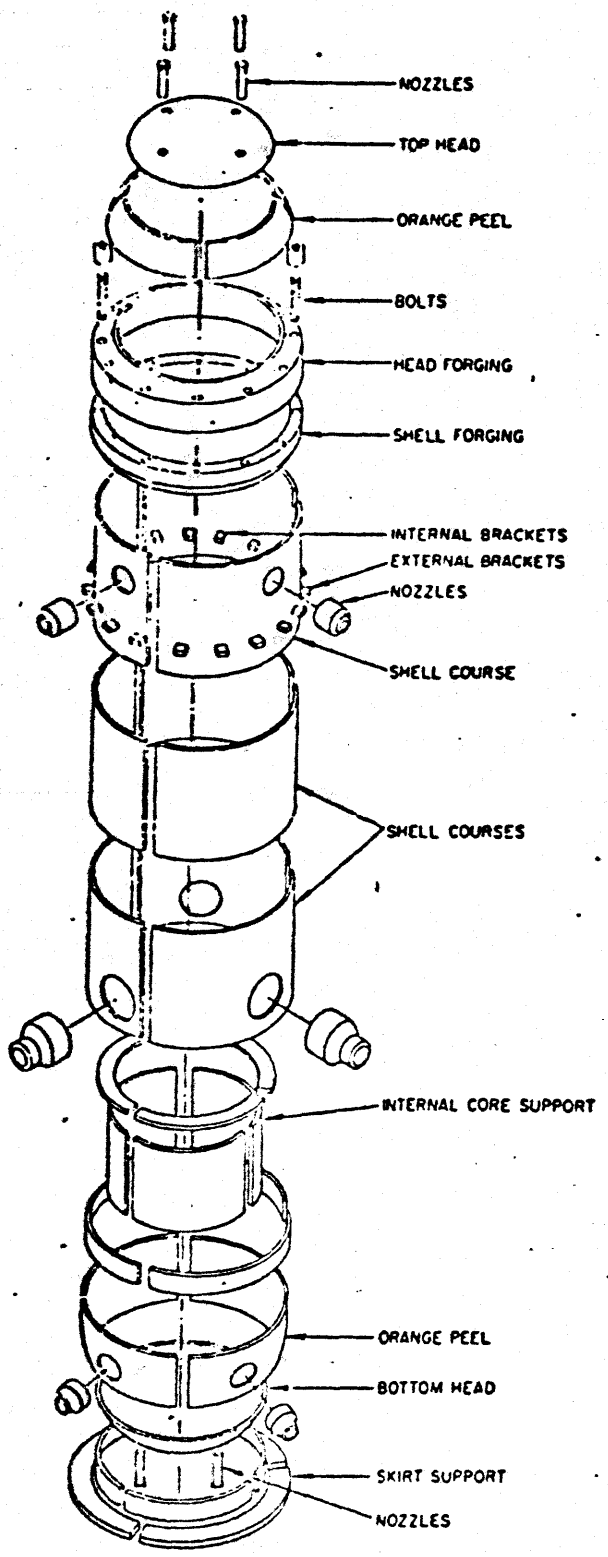

Fig. 3.1.F4

Exploded Schematic View of A Typical Reactor Vessel (BWR)
(From W3)

Early reactor vessels were fabricated from C-Mn ASTM A-212B steel. Since this steel shows deterioration of toughness in heavy sections, present vessels are fabricated from a nickel-modified version of ASTM A-302B plate, a Mn-Mo steel. The current designation for this material is ASTM A-533. The corresponding forging material is ASTM A-508 Class 2. The mechanical properties of these materials are generally satisfactory for the present requirements up to 12-inch thick sections, but the notch impact properties are marginal for heavier sections. For the next generation of LWR pressure vessels, ASTM A-542 and A-543 steels have been considered. These materials are hardened by quenching and tempering heat-treatment and have mechanical properties in the high-strength category.

3.2 Description of Reactor Vessel Failure Postulates

The previous section has described current LWR pressure vessel size, material, manufacture and operation conditions. Appendix D describes briefly ASME Section III-Nuclear Vessels and current design analytical techniques. This section presents factors contributing to the possible failure of a reactor vessel and the postulates of such a failure for this study.

3.2.1 Factors Contributing to the Possible Failure of a Reactor Vessel

The following factors may contribute to the failure of a nuclear pressure vessel.

a. Structural inadequacy resulting from design, underdesign, excessibely high localized stress concentrations, insufficient materials properties, materials defects, fabrication defects, and residual stresses.

b. Service deterioration due to corrosion or mechanical abrasion or to charges in material properties of thermal, mechanical, or radiation origin.

c. Progressive extension of flaws by mechanical or thermal stress cycling fatigue.

d. High-temperature failures from overheating or creep.

e. Short-time brittle fracture or ductile tear caused by over-loading, over pressurization, temperature charges, or accidential shock or impact.

f. Human negligence or error.

Most failures would involve a combination of these factors. Over the lifetime of the vessel, there could to be 29,000 cycles of unit loading or unloading at 5% of full power per minute, 4000 cycles of step load decrease or increase of 10% of full power, 400 heatup or cooldown events at 100°F/hr., 400 reactor trips of all kinds, 200 step load decrease of 50% of full power, 200 leak test at 2500 psi and 5 hydrostatic tests at 3110 psi. (Table 3.T1). In the assumption of PWR vessel failure, it is considered that flaws and cracks may be developed to such sizes as to propagate catastrophically when the reactor is at normal operating conditions, and particularly when an abnormal overpressurization condition occurs. Some incidents that create overpressure in a pressurized-water reactor are:

a. Turbine trip without reactor trip: The reactor is initially at full power when a turbine trip is caused by high pressure in the condenser. The pressure in the steam generator rapidly rises to 1200 psia, the relief valve set point. Lack of adequate heat transfer causes the pressure in the primary system to rise first to 2500 psia, the relief set point of the pressurizer, then to 4250 psia after the pressurizer has been filled with liquid (W1).

b. Loss of a feedwater pump without reactor trip: If no primary loop pressure control is allowed, the reactor coolant would reach an average temperature of 595°F. The pressurizer relief valves would limit the pressure to 2500 psi, but when the pressurizer is filled, then a pressure would build up to 4391 psi at 102 seconds after the incident (W1).

c. Large reactivity insertion accident caused either by faulty instrumentation, human errors, or by a rod housing blowout. It has been computed that, for a light water reactor, a fast withdrawal of the central control rod would result in a power surge that would produce a total energy of the order of half the energy inventoried in the coolant (B4).

For a PWR of 2758 MWt size, this represents some 150×10^6 Btu which is more than enough to fragment and vaporize the whole fuel. The resulting pressure surge would be of the order of the surge observed in the BORAX-1 destructive transient test, that is, about 6000 psi.

When an abnormal incident or series of incidents occur in the manner described above, the pressure vessel could fail catastrophically. One can consider the following hypothetical modes of failure:

a. Reactor vessel head opens up by zipper effect starting with one or a few failed bolts. In this case, the whole core may be lifted due to the hydrodynamic force.

b. A radial crack develops circumferentially above the nozzles and propogate catastrophically. The same consequences as in (a) above would follow.

c. Circumferential catastrophic failure below the nozzles. As the vessel is supported at the nozzles, the lower portion of the vessel would drop, exposing the core.

d. Cracks develop around the nozzle and a large window of the nozzle size or larger would be created. In this case, coolant blowdown would take place almost in the same manner as the pipe break accident. But due to lack of support at the blown out nozzle, the vessel would move under the influence of blowdown hydraulic forces.

e. A window type break at the bottom plenum region resulting in loss of all coolant and emergency core cooling water. The core would heat up and slump.

f. A longitudinal split at the beltline region. Hydraulic forces may dislocate the core and all coolant including emergency core cooling water may be ineffective.

The window type break is assumed mostly to take place at the heat-affected zone around the welds that join the vessel courses together. A somewhat exaggerated but real life example of the break is the December 22, 1965 ammonia tank accident in England as previously described (W3).

It must be emphasized that at the present state of technology, there is no evidence to support the above hypothetical vessel break assumptions. In fact, research in the Heavy Section Steel Technology program (T6) indicates that any such a break would be highly improbable.

3.2.2 Vessel Failure Postulates for This Study

In order to reconcile the firm belief on the part of the industry that the LWR pressure vessel cannot possibly rupture, and the understandable need to evaluate such an event for far reaching contingency planning, it is decided to postulate the following failures in this work:

a. A partial split or window-type break in the upper plenum of the vessel. This is called the top break.

b. A partial split or window-type break in the lower plenum of the vessel. This is called the bottom break.

c. A partial split or window-type break at the side of the vessel. This is called the side break.

For each break location, a number of break sizes will be studied. Other break modes such as the opening of the total head or the severance of the coolant legs at the same time as the vessel break are not dealt with in this study.

CHAPTER 4

SUBCOOLED DECOMPRESSION COMPUTATIONAL TECHNIQUE

4. SUBCOOLED DEPRESSURIZATION COMPUTATIONAL TECHNIQUE

4.1 Computer Code WHAM

4.1.1 Description of WHAM

The basic equations to be solved in order to obtain the force and pressure loadings as a function of time are the three conservation equations of mass, momentum and energy. However, due to their couplings, their simultaneous solution has not been easy. Many computer techniques have been developed to do this job, but few have been completely satisfactory insofar as computation time, versatility, and exactness are concerned. A few recent codes are BAM (B5), BURST (I2), WHAM (F3), FLASH3 (R5) and RELAP3 (R2). The last two use the technique of finite nodal volumes interconnected by junctions, thus invoking the concept of thermodynamic equilibrium but neglecting the effect of the wave interaction. BAM employs the subcooled relaxation method with acoustic wave reflection coefficients at area changes. It was found lacking in versatility and was accurate only for certain relatively simple geometries. BURST, in attempting to account for all space-time details, demands excessive computation time in addition to its difficulty in adapting to a complex system as the primary coolant loops.

WHAM, on the other hand, has been experimentally tested and widely used. It employs the wave superposition technique to account for the pressure and velocity while neglecting the energy conservation equation. In order to account for space dependence, it assumes the loop to consist of one-

dimensional segments (legs). Segment lengths, sonic velocity, and unit time interval for the wave to travel through the segment are all preset as input information so that the accounting of wave transmission, reflection and superposition can be accounted for as time progresses. The assumption of constant sonic velocity in each leg limits the validity of the code to the subcooled portion of the blowdown when sound velocity is not drastically altered by the two-phase mixture.

Advantages of WHAM are its versatility in modeling a complex three dimensional network with multiple junctions and parallel flow paths, ease of data preparation and low computation cost. Gruen (G2) and Hansen (H4) have used WHAM for the prediction of the Idaho 700 and 800 series semi-scale blowdown tests and have concluded that the calculated pressure histories match the measured values sufficiently well.

A disadvantage of WHAM is the assumption of plane wave propagation in one dimensional tubes. This assumption would work well for the core channels, the hot legs, the cold legs, the steam generator tubes but would fare poorly at the upper plenum, lower plenum and particularly at the downcomer annuli. Another disadvantage is the inability to extend the calculations for inclusion of the two-phase portion of the blowdown. This limitation is not of prime concern because the largest loadings always happen during the first few wave periods when the system is still substantially subcooled. BLODWN-2, a proprietary code by Westinghouse claims to have been able to link the subcooled portion of the loadings to the two-phase one. (F4). Examinations of the results from BLODWN-2 for the pipe break LOCA confirms that the first few loading periods involve the pressure differentials of highest magnitudes (C1).

4.1.2 Formulation of Basic Quantities

WHAM considers compressible liquid flow in one-dimensional, elastic pipes. The physical laws invoked are:

- The conservation of mass
- The conservation of momentum
- Linear relationship between compressed liquid density and pressure
- Linear relationship between internal pressure and pipe strain (Young modulus of elasticity).
- The linear superposition of plane acoustic waves.

The liquid velocity and pressure are cast into the following wave equations:

$$\frac{\partial 2u}{\partial t^2} = c^2 \frac{\partial 2u}{\partial z^2} \qquad (4.1)$$

$$\frac{\partial^2 p}{\partial t^2} = c^2 \frac{\partial^2 p}{\partial z^2} \qquad (4.2)$$

where u is the velocity, p is the pressure, t is the time, z is the distance along the pipe segment, and c is the speed of sound in that pipe segment.

Solutions of equations (3.1) and (3.2) are two waves traveling with the velocity of sound and in opposite directions:

$$p - p_o = \rho \left[F(t - z/c) + f(t + z/c) \right] \qquad (4.3)$$

$$u - u_o = \frac{g}{c} \left[F(t - z/c) - f(t + z/c) \right] \qquad (4.4)$$

where ρ is the fluid density.

The opening or closure of valves creates a series of disturbances because such a process must be described by a time-dependent loading impulses. The accounting for these disturbances is done in a similar fashion as in the case of one disturbance. At any instant t, an observer at position z sees only two waves, F and f, but these waves have histories that incorporate what has been going on from time zero. The first disturbance is created in the following manner: The valve opening is at a value A. Based on the liquid pressure and the back pressure at the break, a liquid discharge velocity can be computed. This discharge velocity then is fed into equation (4.4) to determine the value of the decompression wave, taking proper consideration for initial conditions.

The rupture is normally characterized by a linear function of time. It starts from 0 at time 0 and increases linearly to the rupture area A_{rup} at break time t_b. When t_b is very small, approximately 1 or 2 time steps in the computer iteration, then the break is termed "instantaneous". A time step is the time for the wave to travel from one subnode to the next. For a distance between subnodes of 0.8 ft. and a wave velocity of 3200 ft/sec., the time step size is 0.25 msec.

4.1.3 Pressure and Force Loadings

The principal items of interest that WHAM attempts to compute are the pressure and force loadings on different parts of the system. In the case of nuclear primary loops, the most important parts of the system are the core and core supports which must maintain a coolable geometry for long-term residual heat removal.

In the case of transients induced by the opening of a break, F(t-z/c) would represent a rarefaction wave traveling in the direction of positive z with sonic velocity, while f(t+z/c) would represent a compression wave traveling in the opposite direction.

The computer program WHAM codes equations (4.3) and (4.4) by making use of the fact that the wave at position z at time t is exactly the wave at position z-1 and at time t-1 (here both z and t have been nodalized). If an observer is posted at location z at time t, his "initial conditions" are the velocity and pressure of the liquid at the previous time t-1. At time t, he sees two waves converging on him. The first is the decompression wave F traveling from position z-1 and having magnitude F(z-1, t-1). The second is the compression wave traveling from position z+1 and having magnitude f(z+1, t-1). The current condition at z is thus the result of the superposition of F and f with the proper initial condition as previously described.

If only one disturbance, say decompression front, is sent through the pipe, then that wave would be the only wave traveling in the system, that is, F is finite but f is zero. But this wave would be reflected at the end of the pipe to become a compression of wave which travels in the opposite direction. Thus, one has a situation that the wave bounces back and forth at the two ends of the pipe until the wave magnitude is dampened out.

When the system consists of many pipes with contractions, enlargements, bends, and multi-connection joints, the waves suffer a series of reflection, transmission and dampening due to friction. WHAM accounts for these phenomena by using reflection, transmission coefficients which are normally used in fluid dynamics.

As WHAM calculates the pressure at every end point of each leg, the pressure differential across any leg or any number of legs can be readily computed by taking the difference of the proper values.

The force acting on any part of the system consists of the fluid inertial force, the hydrostatic (pressure) force, the momentun flux force, the friction force and the body force. In WHAM formulation, it is:

$$-F_m = \frac{\partial}{\partial t}\iiint_V G.\vec{m}\, dV + \left[p + \frac{G^2}{\rho}\right]_1 A_1 (\vec{n}_1.\vec{m}) + \left[p + \frac{G^2}{\rho}\right]_2 A_2 (\vec{n}_2.\vec{m}) + \sum_i \left[K_i \frac{G|G|}{2\rho} A (\vec{n}.\vec{m}) + \iiint_V g\ \vec{k}.\vec{m} dV\right]$$

where F_m is the exerting force

G is the mass flux

$\vec{m}$ is the direction of interest

$\vec{n}$ is the normal to the surface of interest

Index 1 and 2 refer to inlet and exit planes of the control volume V.

All un-indexed values refer to average values throughout the control volume V.

Of the above force components, WHAM calculates only the inertial component. The other components can be readily evaluated from other information such as the pressure and velocity which are also given in WHAM printout. The body force is usually neglected because it is very small compared to other terms.

In this work, only maximum force loadings on the core, the core barrel and the thermal shield are evaluated.

4.2 WHAM Model for LOCA by Vessel Rupture

A sudden break in the piping or at the pressure vessel will send disturbance waves throughout the system. WHAM has been reasonably successful in accounting for these waves, and the degree of success depends to a great extent on the modeling of the primary loops. In general, the more detailed the inputs, with proper setting of initial conditions, the closer the predicted pressures and force loadings are to measured values.

The normal modeling of the pipe break accident is to represent the core, the core bypass, the downcomer and two loops, one for the broken loop and one for the other intact loops lumped together.

For the vessel break accident, only one lumped loop needs be presented because the legs have been assumed to be intact in this study.

Figs. 4.2.F1, 4.2.F2 and 4.2.F3 represent the models developed for WHAM calculation of subcooled loadings subsequent to the pressure vessel breack at the top, bottom and side. The three diagrams are almost the same, due to the obvious fact that they represent the same primary system. However, it is noted that the location of leg 1, the artifice employed by WHAM to represent the breaks, is different in the three cases. Starting with leg 1, the break, all other legs are numbered sequentially in such a manner that their order must increase in the (positive) direction away from the break (the direction that the decompression waves travel).

Some special features of the model include:

a) The four primary coolant loops of the PWR plant have been lumped into one loop in the model. This one loop has seven segments representing the hot legs, the steam generator inlet plena , the U tubes (2 segments), and steam generator outlet plena and the cold legs. Between the steam generator outlet plena and the cold legs are the primary system circulating pumps which raise the pressure in the cold legs some 80 psi above that in the steam generator outlet plena when the loops are functioning normally.

b) The pressurizer has been ignored during subcooled blowdown.

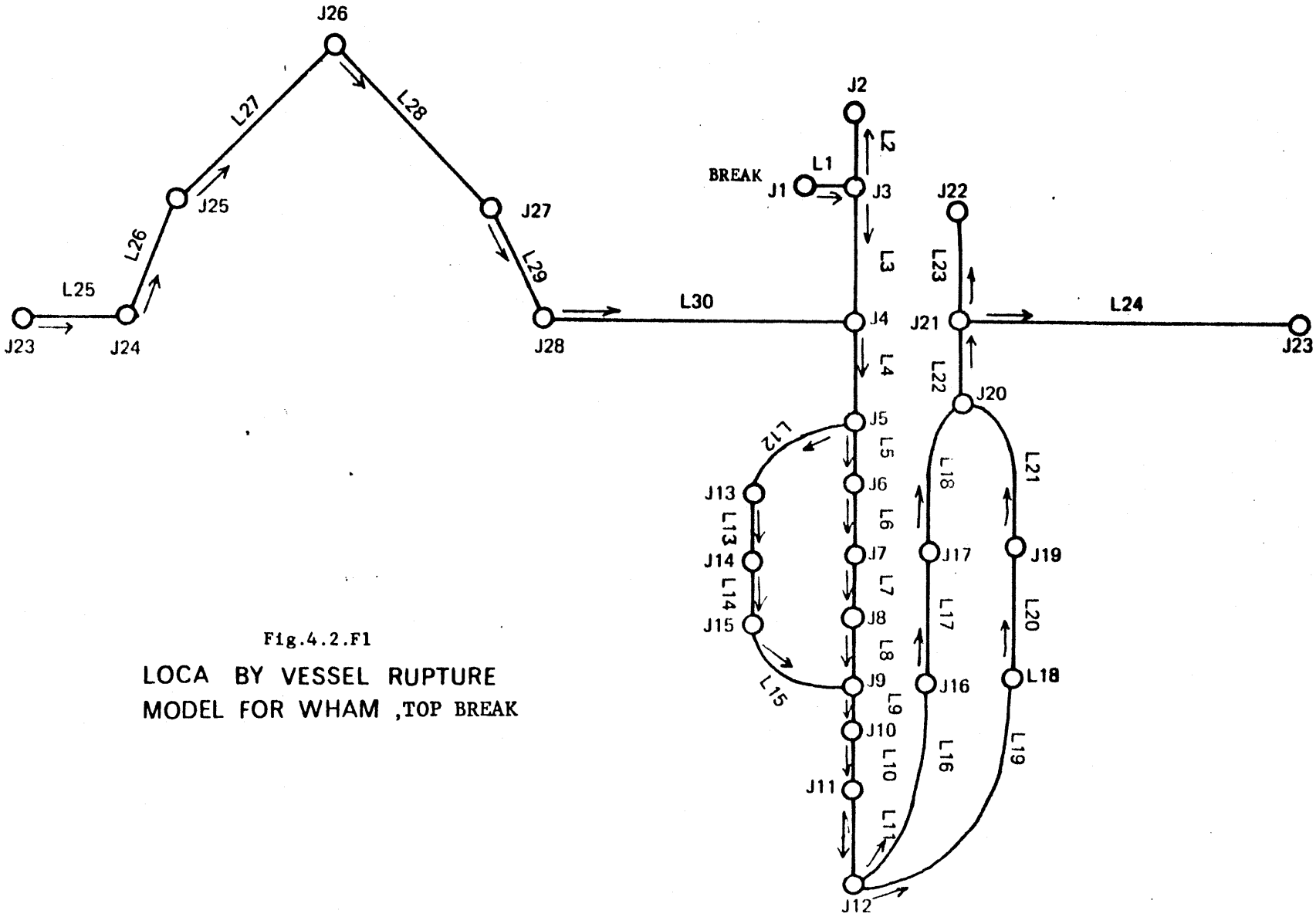

Fig.4.2.F1

LOCA BY VESSEL RUPTURE
MODEL FOR WHAM ,TOP BREAK

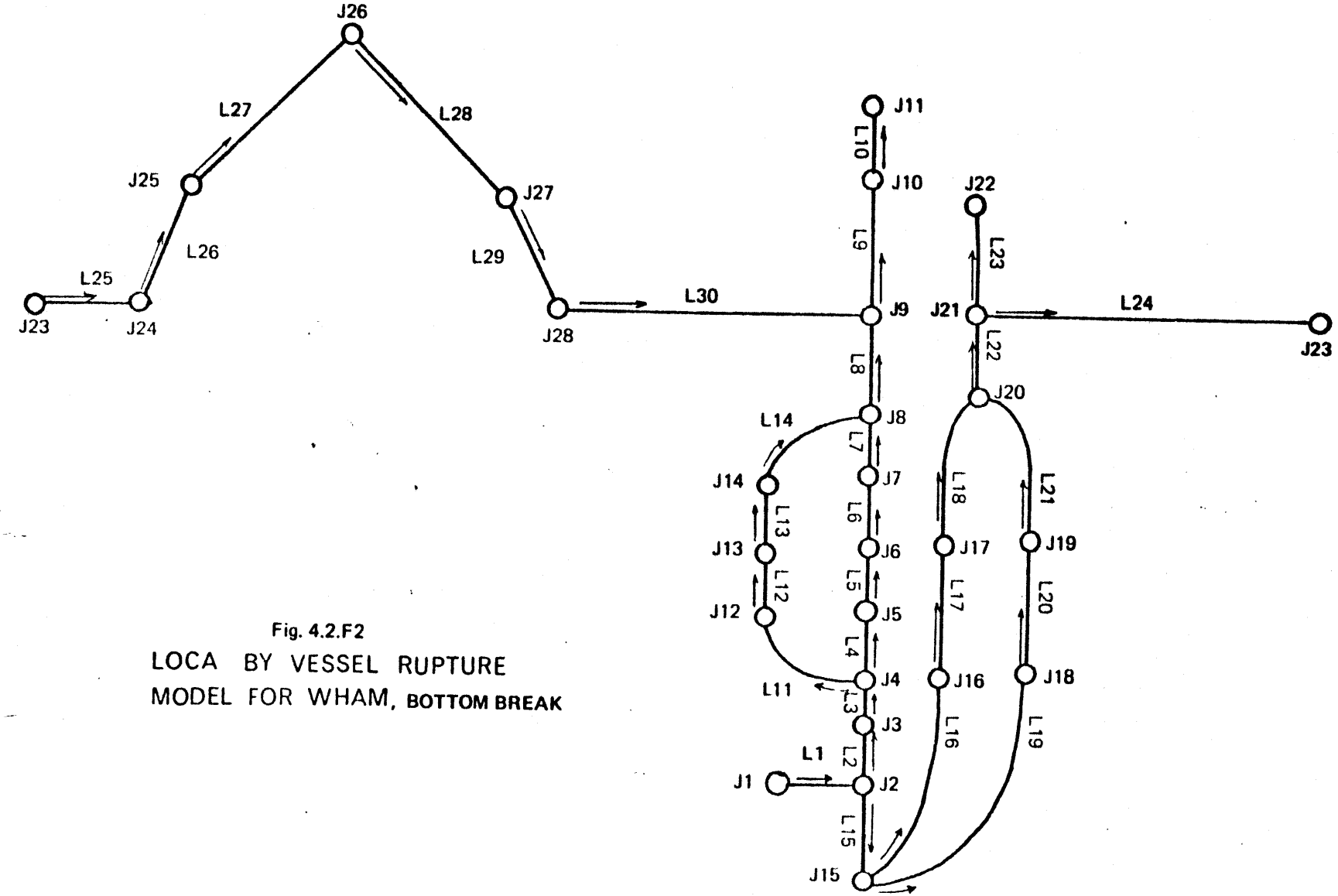

Fig. 4.2.F2

LOCA BY VESSEL RUPTURE MODEL FOR WHAM, **BOTTOM BREAK**

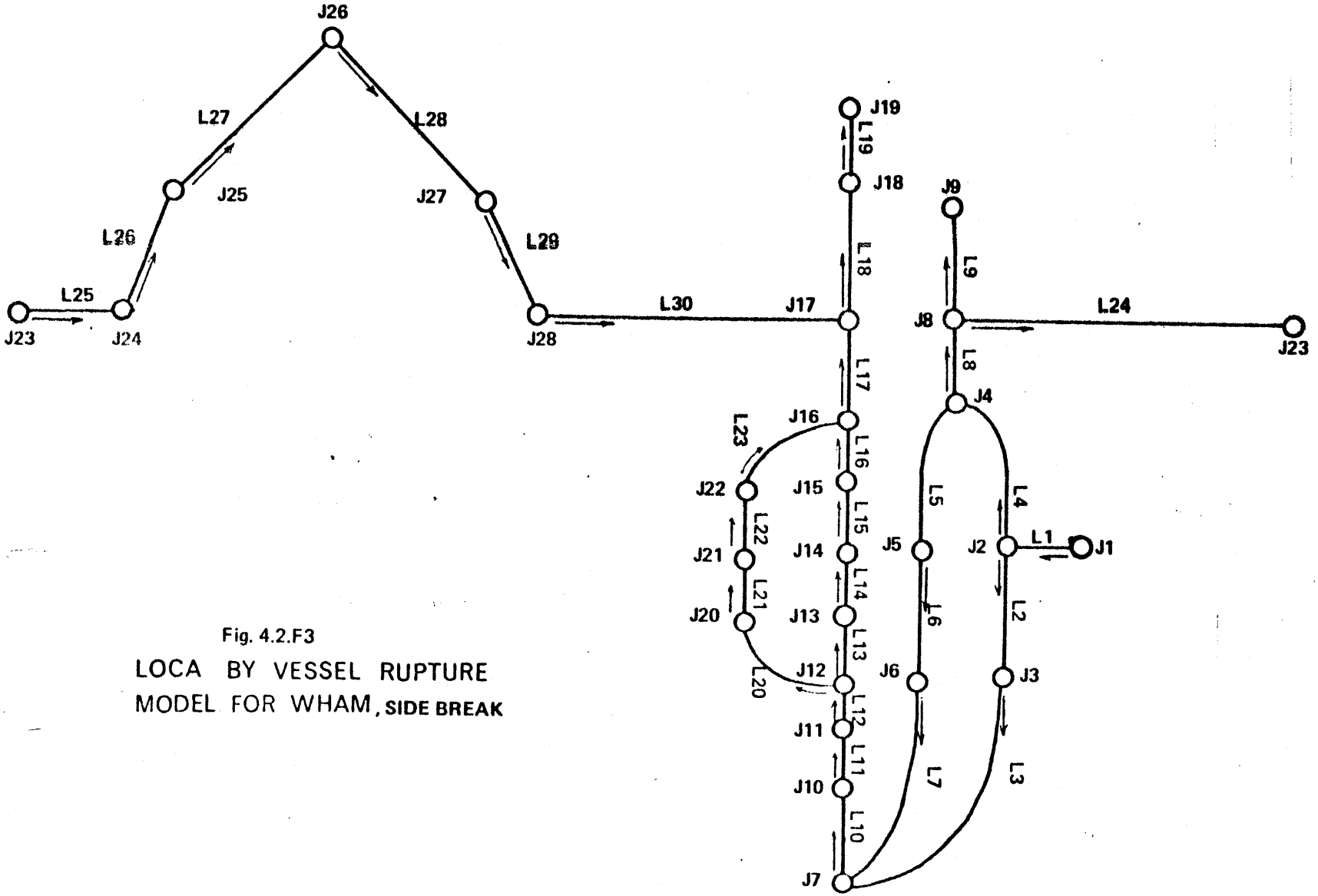

Fig. 4.2.F3

LOCA BY VESSEL RUPTURE MODEL FOR WHAM, SIDE BREAK

Table 4.2.T1

DESCRIPTION OF SYSTEM LEGS MODELED FOR WHAM

Leg Serial Number			
Top Break	Bottom Break	Side Break	Description
1	1	1	Break opening
2	10	19	Portion of vessel above upper support plate
3	9	18	Upper plenum above nozzles
4	8	17	Upper plenum below nozzles
5	7	16	Upper 1/4 core
6	6	15	Middle 1/4 core
7	5	14	Middle 1/4 core
8	4	13	Lower 1/4 core
9	3	12	Region between core bottom and flow plate
10	2	11	Region between flow plate and flow inlet casting
11	15	10	Lower plenum
12	14	23	Upper 1/4 of bypass
13	13	22	Middle 1/4 of bypass
14	12	21	Middle 1/4 of bypass
15	11	20	Lower 1/4 of bypass
16	16	7	Lower 1/3 of annulus between barrel and shield
17	17	6	Middle 1/3 of annulus between barrel and shield
18	18	5	Upper 1/3 of annulus between barrel and shield
19	19	3	Lower 1/3 of annulus between shield and vessel
20	20	2	Middle 1/3 of annulus between shield and vessel
21	21	4	Upper 1/3 of annulus between shield and vessel
22	22	8	Annulus above shield but below nozzles
23	23	9	Annulus above nozzles
24	24	24	Cold legs
25	25	25	Pipes between heat exchangers and pump
26	26	26	Outlet plenum of HX
27	27	27	1/2 of U tubes
28	28	28	1/2 of U tubes
29	29	29	Inlet plenum of HX
30	30	30	Hot legs

Notes: Arrows in the diagrams represent the positive direction in the indicated legs.
Pump and pressurizer actions have been neglected in the subcooled blowdown calculations.

In effecting the above lumping, it has been inherently assumed that the four loops behave exactly in the same manner. This is not exactly true because one loop is connected to the pressurizer while the other three are not. But the pressurizer surge line is long and small in comparison to the legs, and the pressure in the pressurizer is practically constant, therefore, the effect on the wave propagation is small. This conclusion has been arrived at by modeling the system both with pressurizer and without it in the trial period of this computation.

c) The downcomer is represented by three annuli. The first annulus, consisting of two legs, is the portion of the downcomer above the core region, where water flows in from the cold legs before making a 90 degree bend downward. The second and third annuli are similar, each consisting of three legs. These two annuli are separated by the thermal shield. If a vessel side break was not to be studied, they can effectively be lumped into one because they behave in exactly the same manner as waves traveling from the core to the cold legs or vice versa. But since the study includes a break at the side of the vessel, large pressure differentials are expected across the thermal shield, thus justifying the need to represent this portion of the downcomer by two annuli.

The representation of annuli as a tube for WHAM calculation is a rather stretched out extension of the validity of WHAM. One can stipulate that, since WHAM assumes one-dimensional flow and plane wave propagations, then its validity would break down at the annuli where significant cross flow may take place. This is particularly true when a break at a cold leg or at the vessel side happens. Efforts have been made to represent the downcomer by

a bundle of tubes interconnected in various places to simulate cross flow, but results have not been as successful as the one-tube downcomer model insofar as comparison with experimental data is concerned.

d) A core bypass loop has been incorporated into the model to account for the fact that some 4.5 percent of the flow is not effective in channel cooling. This core bypass loop is mainly the region between the core baffle and the barrel, having a cross section of 23.4 ft^2 and a volume of 290 ft^3. It is assumed that there are considerable structures in this region, the coolant flow speed there is very small, of the order of 1.4 ft/sec.

CHAPTER 5

TWO-PHASE BLOWDOWN COMPUTATIONAL TECHNIQUE

5. TWO-PHASE BLOWDOWN COMPUTATIONAL TECHNIQUE

5.1 Blowdown Computer Codes

Even with many simplifying assumptions, the two-phase blowdown phenomenon is so complicated that it would defy any attempt to predict it in closed form. When the complex physical configuration is further considered, then even a hand numerical computation is practically impossible. The use of a large computing machine is therefore a must if the predicted results are to be compared to experimental values.

One of the earliest computer codes written specifically for the blowdown of a high pressure light water system is FLASH (1966). It is a digital program which calculates the flows, inventories, pressures and temperatures in a 3-volume primary system. A priori assumptions are made concerning the water-steam mixture, heat transfer coefficients, and ECC injection. Improvements of FLASH have resulted in steadfastly better FLASH-2 (1967), FLASH-3 (1969) and FLASH-4. FLASH-3 (R5) and FLASH-4 (R6) have both reached a stage of development that can predict reasonably well experimental blowdown data from the LOFT semiscale tests. FLASH-3 uses the forward finite difference numerical technique to account for the momentum conservation in flow junctions, while FLASH-4 employs the backward finite difference numerical technique, a method that gives better convergence and requires less computation time. Both codes lump the physical system into volume nodes

interconnected by flow junctions. The maximum number of nodes and junctions are 20 and 40, respectively, although one can modify the program to account for more nodes. Thermodynamic properties are stored in tables to be searched by the computer. Reactor kinetics are included by a point kinetic model. Moody choked flows in tubes and through the leak are also stored in tabular form. (M9, M10, M11).

FLASH-3 and FLASH-4 have been widely used in the analyses of loss-of-coolant accidents for PWR's. The codes require the service of a large CDC computer. For certain plant configuratio or need, the codes can be altered to respond to the specific situation. Such has been the case with the creation of the code CEFLASH-4 (Confidential) by Combustion Engineering and CRAFT by Babcock and Wilcox Company. (B7).

The Code SATAN-V (System Accident and Transient Analysis of Nuclear Plants) of Westinghouse (B8) has been similarly developed. It attempts to cover the accident in all three stages, namely the subcooled decompression, the two-phase blowdown, and the refill stages.

For boiling water reactors, the blowdown has been analyzed by a General Electric code temporarily called Short-Term Thermal Hydraulic Analysis (STTA) by the AEC. This code calculates the vessel pressure, core flow, and core inlet fluid enthalpy as a function of time using the equation of mass, energy and momentum conservation. The analysis assumes one-dimensional non-slip flow using the Martinelli - Nelson two-phase friction pressure drop multipliers. The reactor primary coolant system is represented by nine nodal volumes (lower plenum, core, core bypass, upper plenum, separation zone, steam dome, downcomer, and the recirculation loops). Moody critical flow is also used at the break.

The RELAP series of codes is more or less similar to the FLASH series in system modeling and numerical techniques. They were developed at the Idaho Nuclear Testing Station in support of the LOFT project. A special feature of RELAP-3, the 1971 release version of the series, is the structure of the code in modular form, this greatly facilitating the access to it for change. RELAP-3 has been chosen as the analysis instrument for this study. (R2).

5.2 RELAP3 MOD.36

5.2.1 General Description

The two-phase blowdown code used in this study is RELAP3, Mod. 36, prepared by the Aerojet Nuclear Corporation and sent to MIT in December, 1971. (A5). This code has been chosen on the basis of compatibility with our computer systems and upon the recommendation of the ECCS Task Force as expressed in the Interim Acceptance Criteria of 1971. (A2).

RELAP3 represents the PWR system as a set of nodal volumes interconnected by flow junctions. Mass and energy calculations are made for each volume in small time increments by accounting for the inflow, outflow, and production terms. Momentum calculations are made for flow junctions and are governed by pressure, inertia, flow area and junction friction. There are many features and options to simulate the volume-junction network as close to the physical system as realizable. These include provisions for bubble rise and phase separation in each volume, gravity head, choked flow, energy addition or removal, pump head and coastdown as well as emergency core cooling systems.

The RELAP3 Mod. 36 is written in FORTRAN IV, double precision. It consists of some 50 subroutines which can be overlayed to render the computation more efficient. Allowance exists for up to 200 volumes and 250 junctions, but a LOCA modeling very seldom needs more than 40 volumes and 50 junctions. As the number of volumes and junctions increases, the time increment must be made smaller in order for the various numerical calculations to converge, the overall computation time consequently increases to cover the same LOCA period desired. A sample 34-volume LOCA problem needs six and one half hours of IBM 360/75 to cover a blowdown period of 60 seconds.

5.2.2 Mass, Energy, Momentum and State Determination

Thermodynamic equilibrium assumption requires that the equation of state is valid in any volume at the end of each time increment. The equation of state for water has been incorporated into the code by inclusion of thermodynamic property tables for water and steam. When the enthalpy and quality of the mixture is known(through mass and energy calculations), a systematic search and interpolation is made to find out the volume pressure, temperature and other properties.

The basic mass and energy equations employed are:

$$\frac{dM_i}{dt} = \sum_{j=1}^{N} W_{ij}$$

$$\frac{dU_i}{dt} = \sum_{j=1}^{N} W_{ij}\, h_{ij} + Q_i$$

where M_i = total mass in Volume i

W_{ij} = flow rate into Volume i through junction j

U_i = energy in Volume i

h_{ij} = enthalpy of flowing fluid

Q_i = heat production in (or removal from) Volume i

The basic momentum equation employed is:

$$\frac{1}{144 g_c}\left(\frac{\ell}{A}\right)\frac{dW_j}{dt} = P_i - P_{i+1} + \Delta p_p + \int_{V_j}\frac{\rho\, dz}{144} - \frac{K_j W_j |W_j|}{\rho_j}$$

where g_c = gravitational conversion constant

$\frac{\ell}{A}$ = junction inertia

W_j = average flow from Volume i to Volume i+1

$P_i - P_{i+1}$ = thermodynamic pressure differential across the fluid contained in the flow volume

P_p = Pump head

$\int \frac{\rho\, dz}{144}$ = Gravitational head across fluid column

K_j = net friction coefficient including normal friction losses

ρ_i = fluid density in volume i.

Mass loss due to leak is calculated by the orifice equation. In the case of great pressure differentials, the limiting flow is calculated by Moody's two-phase choked flow model.

Energy removal by a heat exchanger is calculated from an input table or by the flow dependent equation:

$$Q_{HE} = \frac{W}{W_o} H_{HE} (T_{pri} - T_{sec})$$

where Q_{HE} = heat removal rate by the heat exchanger

$\frac{W}{W_o}$ = ratio of flow at the time considered to the nominal flow.

H_{HE} = total heat transfer coefficient during steady state full power operation.

T_{pri} = temperature of primary coolant in the heat exchanger

T_{sec} = temperature of secondary coolant in the heat exchanger.

A few moments after blowdown T_{pri} often drops below T_{sec}, and the heat exchanger acts as a heat source to whatever mass of coolant flowing on the inside of the U tubes.

The core always acts as a heat source, during normal operation or during blowdown. One dimensional heat conduction in cylindrical rods is assumed to calculate the heat transfer from inside the fuel rod to the coolant. The conduction subroutine is patterned after the HEAT1 Code with accommodation for 31 radial modes, six different concentric regions and six different materials. PWR fuel rods can be seen as consisting of three regions, the uranium pellet, the gas gap and the zircaloy cladding. At steady state operation, temperature distribution in the rod is such that the difference in the clad surface temperature and the coolant, together with the proper heat transfer coefficient in the proper heat transfer regime, are just right to transfer the energy generated inside the rod by nuclear fission. During blowdown, reactor power drops, but the heat transfer regime also changes, thus subjecting the cladding to a temperature transient, the calculation of which is a principal feature of RELAP3.

5.2.3 Heat Transfer Correlations

RELAP3 uses a series of heat transfer correlations to cover the wide spectrum of environmental conditions during blowdown. A tabulation of these correlations and terminologies is listed in Appendix C. The basic parameter for choice of correlations is the quality $^{(x)}$ of coolant in the channels. Second in line for correlation application are factors such as fuel pin surface temperature, surface heat flux, and bulk coolant temperature. The five regimes in which seven modes of heat transfer are used are: (x being the quality of the coolant).

a) $X < 0$, Subcooled Regime

When $T_s < T_{NB}$ subcooled forced convection, Seider-Tate correlation

When $T_s = T_{NB}$ subcooled nucleate boiling, Thom correlation.

b) $0 \leq X < 0.1$

The heat transfer coefficient is calculated by interpolating between Thom correlation and Schrock-Grossman correlation.

c) $0.1 \leq X < 0.6$, Forced convection boiling, Schrock-Grossman correlation with Wright constant.

d) $0.6 \leq X < 1$, Forced convection boiling. The heat transfer coefficient is obtained by interpolation with respect to quality between Schock-Grossman correlation and Dittus-Boelter correlation.

e) X = 1 and superheated steam: single phase steam heat transfer, Dittus-Boelter correlation.

f) Stable Film Boiling when the surface heat flux has exceeded the critical heat flux, Dougall-Roshenow correlation.

5.2.4 Critical Heat Flux

In order to establish whether or not film boiling takes place, the critical heat flux is computed in order to compare it with the real heat flux. The critical heat flux is also obtained from a series of correlations, each of which is applicable to a certain regime of environmental conditions. The parameters that are used to define CHF regimes are the coolant pressure and mass flux. The six CHF regimes are:

a) $p < 725$ psi, Modified Barnett Correlation.

b) $725 \leq p < 1000$ psi, the CHF is calculated by linear interpolation with respect to pressure between Modified Barnett Correlation and Barnett Correlation.

c) $1000 \text{ psi} \leq p < 1500$ psi, Barnett Correlation.

d) $1500 \text{ psi} \leq p < 1800$ psi, the CHF is calculated by linear interpolation with respect to pressure between Barnett Correlation and BAW-2 Correlation.

e) $p \geq 1800$ psi, $G > 0.5 \times 10^6$ lb/hr ft^2, BAW-2 Correlation.

f) $p \geq 1800$ psi, $G \leq 0.5 \times 10^6$ lb/hr ft^2, Average value between Barnett and BAW-2 Correlations.

The inlet enthalpy used in the critical heat flux correlations is dependent on the flow direction. It is determined by using the enthalpy of inlet coolant if direction of flow is the same at both ends of the channel. The average enthalpy of coolant in the channel is used when the flows are zero or are in opposite directions.

5.2.5 Other Basic Features of RELAP3

Power generation is determined by either a tabular input of power versus time or a reactor kinetic calculation. Point reactor kinetic equations are solved. Data for 1 prompt neutron group, 6 delayed groups and 11 gamma groups are stored in the program. Options to the user includes the input of power distribution between various portions of the core, Doppler, void and coolant reactivity coefficients.

The two-phase separation model used in RELAP3 is a semi-empirical fit to a number of experimental, high pressure blowdowns. (C8, M8). It uses two numbers as inputs. One number, C_o determines the gradient of the bubble population as a function of the mixture height. The second number, V, determines the velocity of steam bubble relative to the mixture interface, as the bubble moves up and breaks at the interface. On the basis of experimental blowdown tests, a value of 0.8 for the bubble gradient and 3 ft/sec. for the bubble rise velocity have been recommended (R2, R5).

Emergency core cooling systems can be included as part of the RELAP3 nodal volume-junction system. Passive, on-line systems such as accumulators are represented by a node which is connected to the cold legs by a valved

junction which is open at a certain pressure differential across the swing check valve. Other power driven ECC systems such as the charging lines (CL) the safety injection lines (SIS) or the residual heat removal lines (RHR) can be represented by junctions which are activated by preset conditions and which would follow preset injection curves.

5.2.6 Advantages and Deficiencies of RELAP 3

RELAP3 has the advantage of being developed in support of the LOFT project; therefore, it has been tested out in a series of semi-scale blowdown simulations. Its modular structure is easy to get access to, thus facilitating improvements as more experimental data, better numerical techniques, and different methods of problem solution are obtained.

However, like most blowdown codes currently available, RELAP3 has the following deficiencies:

a) It is a one-dimensional code, assuming that fluid in a junction can flow in one direction only at a time. It thus fails to recognize the effect of cross flow in the PWR open lattice. This cross flow is of negligible importance during the blowdown when the mass flux is large, but would be meaningful at the quiescent and refill stages when the pressure differential across the core is small. The cross flow effect may be both beneficial and detrimental. It is beneficial to cool the upper portion of partially or fully blocked channels, a phenomenon already observed and measured in the FLECHT program. It may be detrimental if it diverts the coolant away from hot spots where temperature and pressure are higher than in other places.

The effect of this RELAP3 deficiency in this loss-of-coolant accident computation is expected to be negligible because only the average properties of the core (coolant state, heat transfer coefficient, clad and fuel temperature) are being looked for. By invoking the assumption of complete mixing, one has in fact assumed 100 percent cross flow at any elevation in the core volume.

b) RELAP3 does not account for flow blockage due to clad ballooning and rupture. Calculations and experiments have indicated that quite early in the blowdown, when pressure, flow and therefore heat transfer coefficient drop drastically, the cladding in certain hot spots fail under the influence of steep temperature transient and internal gas pressure. Flow channel blockage may, therefore, be considerable. RELAP3, however, assumes a constant channel flow area. Although the FLECHT program has indicated increased heat transfer due to cross flow and due to better heat transfer regime, these phenomena are neglected in RELAP3.

c) The forward difference numerical technique employed in the solution of balance equations requires very small time steps to be taken. This often results in excessive computation time, even at the fastest currently available computer. Furthermore, flow through the core fluctuates unrealistically in the late stages of the blowdown. Current effort by the Aerojet Nuclear Corporation is to adapt the backward finite difference technique from FLASH4 to smooth out the flow and to reduce computation time (R6).

d) The assumption of complete and instantaneous mixing of the fluid and thermodynamic equilibrium in any control volume has been successfully verified by experiments except in two situations. The first situation occurs in the relatively large volume where conditions exist for steam bubbles to separate from the two-phase mixture. This situation has been quite successfully accounted for by the incorporation into the code of a phase separation model with bubble population gradient and bubble rise velocity as inputs. The second situation occurs when the cold ECC water is injected into the cold legs. Due to the assumptions of complete mixing and thermodynamic equilibrium in the cold legs, RELAP3 features the injected water as slowly filling up the cold legs, receiving higher-enthalpy coolant from either end and mixing it to raise the overall mixture enthalpy. ECC water does not start to flow into the next volume until the cold legs have been filled. The situation starts over again at the next volume and so on.

In reality, it is known that the circulating, high quality fluid in the loop can entrain ECC water to the next volume right from the start of ECC injection. Conditions may also exist to allow a certain annular flow in which the high quality fluid would flow in the middle while the cold ECC water would flow at the periphery adjacent to the pipe wall. In some ECC systems, a nozzle making an angle with the cold leg in the direction of the pressure vessel is included, thus enabling some credit to be taken for the initial velocity of the injected water (C5).

This RELAP3 deficiency is conservative in that it gives rise to water chugging, steam binding and the slower the flow of ECC water towards the core.

e) Another disadvantage of RELAP3 is the need to represent the system by many nodes. The representation of the core by 3 nodes and the heat exchanger by 7 nodes have been recommended for the analysis of loss-of-coolant accidents by pipe break. (A2).

5.3 Model for Loss-of-Coolant Accident by Pressure Vessel Rupture

Fig 5.3.F1 shows the diagram of the model for the analysis of the loss-of-coolant accident by pressure vessel failure. Table 5.3.T1 shows details of the nodes and junctions.

This model designed for RELAP3 analysis of the two-phase blowdown portion of the accident is consistent with Figs. 4.2.F1, 4.2.F2 and 4.2.F3, which are designed for the WHAM analysis of the subcooled portion of the accident. Basic physical data and setups are the same although they may appear in different forms to adapt to the requirements of a specific code.

5.3.1 Nodes

Seventeen nodes altogether have been chosen to represent the 4-loop large PWR primary system under investigation. These nodes include 1 for the vessel upper plenum, 1 for the lower plenum, 3 for the core, 1 for the core bypass, 3 for the downcomer (thus altogether 9 for the vessel),

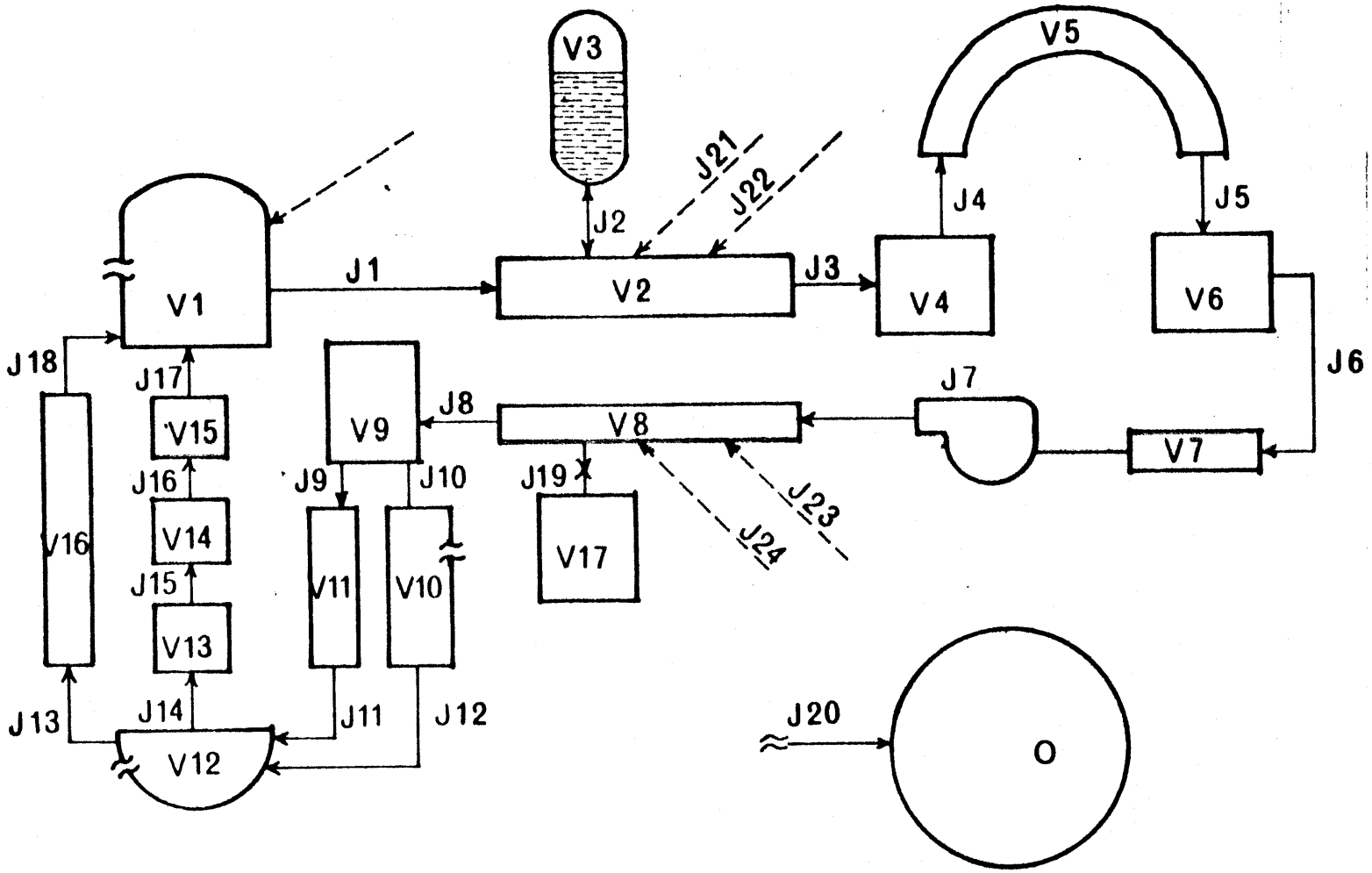

LOCA BY VESSEL RUPTURE
MODEL FOR RELAP-3

Figure 5.3.F1

Table 5.3.T1

DESCRIPTION OF MODEL NODES AND JUNCTIONS

Node	Description	Junction	Connects
V1	Upper plenum	J1	Vol. 1 to Vol. 2
V2	Hot Legs	J2	Vol. 3 to Vol. 2
V3	Pressurizer	J3	Vol. 2 to Vol. 4
V4	HX Inlet Plenum	J4	Vol. 4 to Vol. 5
V5	HX U Tubes	J5	Vol. 5 to Vol. 6
V6	HX Outlet Plenum	J6	Vol. 6 to Vol. 7
V7	Line Between HX and Pump	J7	Vol. 7 to Vol. 8
V8	Cold Legs	J8	Vol. 8 to Vol. 9
V9	Upper Downcomer Annulus	J9	Vol. 9 to Vol. 11
V10	Annulus Between Shield & Vessel	J10	Vol. 9 to Vol. 10
V11	Annulus Between Barrel & Shield	J11	Vol. 11 to Vol. 12
V12	Lower Plenum	J12	Vol. 10 to Vol. 12
V13	Lower Core	J13	Vol. 12 to Vol. 16
V14	Central Core	J14	Vol. 12 to Vol. 13
V15	Upper Core	J15	Vol. 13 to Vol. 14
V16	Core Bypass	J16	Vol. 14 to Vol. 15
V17	Accumulators	J17	Vol. 15 to Vol. 1
V0	Containment	J18	Vol. 16 to Vol. 1
		J19	Vol. 17 to Vol. 8
		J20	Break, Vessel to Containment
		J21 - J24	One-Way ECC Pumped Lines

1 for the pressurizer, 1 for the hot legs, 1 for the cold legs, 3 for the heat exchangers, and 1 for the pipings between the heat exchangers and the coolant pumps. To the fullest practicable extent, the physical dimensions and properties of these volumes have been extracted from the final design data as presented in the Indian Point 2 Final Safety Analysis Report and recapitulated in Appendix A. Thermodynamic conditions of coolants in these volumes are those when the plant is in steady state, full power operation.

The core has been represented by three nodes of equal volume, height and flow passage. The characteristics of core power distribution, heat exchange surface area, and reactor kinetic are explained in Section 5.3.6. The region between the core baffle and the core barrel constitutes the core bypass because coolant flowing through it does not directly touch the fuel rods. The representation of the downcomer as three nodes is important to study the side break situation. Furthermore, due to different flow area between the barrel and the shield on the one hand, and between the shield and the vessel on the other hand, flow choking under large break conditions is not the same for these two nodes.

Four hot legs have been lumped into one node. This is feasible because of the assumption that only the vessel breaks while the loops remain intact. The connection of the pressurizer into this lumped node is not really correct, but it is expected that the error introduced into the overall mass flow as passing by the vessel to the break is negligible.

Four cold legs are likewise lumped into one node. This lumping is more rigorous than in the case of the hot legs because every cold leg should behave in a similar manner as the others, since each has the same characteristics and the same connection with a passive accumulator.

The representation of the containment as a dummy node with index 0 and with a preset pressure needs clarification. Frequently, a pipe break loss-of-coolant accident modeling counts the containment as one node connected to the broken volume by a junction with valves, which would be activated by a computer trip signal. This is considered rather inadequate because the containment is a complex, large structure, the attainment of thermodynamic equilibrium, mixing and adiabatic conditions in which is not possible for the short duration of the blowdown. A feature of this extra containment node is some back flow later in the blowdown when the pressure and temperature in the primary system is quenched more quickly by the ECC water. It is not clear how this backflow would help in the core cooling. By using a dummy containment node with a preset pressure, one avoids addressing this mixing and equilibrium question in the containment. The maximum pressure buildup in the adiabatic containment of the Indian Point 2 design has been calculated to be about 75 psia. It is possible that the pressure in the reactor vessel cavity may be higher at the earlier stages of the blowdown, but this would not influence the blowdown in any manner because the critical flow through the break is independent of the back pressure. At later stages,

the blowdown simply stops when the pressure in the primary coolant has reached or dropped below 75 psia. No backflow is thus credited for. To be more conservative, a lower containment pressure may be prescribed in order to make sure that the ECC water in the refill stage is not assumed to completely stay in the primary loops. However, this prescription would be unconservative when steam binding effects are in question (A2).

5.4.2 Junctions

Twenty four junctions have been used to connect the volumes together in a closed loop, or to act as one-way lines for the ECC water injected by pumps. Flow cross sections of a junction are the smallest cross section that exists at the end nodes. Length and friction coefficient of a junction is the combined lengths and frictions of the two end nodes, the combination being done in such a manner that at steady state (time 0) the computed flow faithfully reflects the expected real flow in the system.

Junction 19 connecting the passive accumulators (node 17) to the cold legs (node 8) has a swing check valve which is normally closed but which would automatically open when the pressure in the cold legs drop to a certain value.

Junction 20 represents the break, thus connecting the vessel to the containment which has a dummy index of 0. Depending whether the break under investigation is at the top, side or bottom, the upstream node of the

break is 1, 10 or 12, respectively. The elevation of the break is not of real importance to the blowdown, although it may have some significance at later stages when phases start to separate and settled, or when the pressure has been significantly reduced for the ECC water gravity head to come into play. For this study, the elevation of the top break has been assumed at the top head flange. The bottom break has been assumed to take place at the weld zone between the lower head and the cylindrical section. The side break has been assumed to take place at the middle core elevation.

The ECC systems consist of the three subsystems. The first subsystem is the on-line, passive, check-valve actuated accumulators. This has been represented by node 17 and junction 19. Injection of ECC water is through the cold legs, node 8, although a sensitivity study will be made to see how an injection into the hot legs or even the upper plenum would help in the case of a bottom or side break. The second ECC subsystem is the high pressure core injection system (HPCIS). This is represented in the model as three one-way junctions. Junction 21 is the small high-pressure charging lines, connecting to the hot legs (node 2) and normally operating at reactor pressure. The high pressure safety injection lines can bring ECC water to either the cold legs or the hot legs. They are thus represented by two junctions, 22 and 23. Finally, the third ECC subsystem is the residual heat removal lines (RHR). They are represented by junction 24.

Flows in junctions 21, 22, 23, 24 are determined by preset curves which have pressure differentials between the injection lines (pump driven) and the receiving nodes as parameters. The junctions start to inject water when the diesel-driven pumps are up to speed, normally 25 to 30 seconds after start of LOCA.

5.3.3 Coolant Pump Model

The response of the coolant recirculation pumps to the LOCA is complex as it depends on time, flow, pump inertia and pump friction. Upon LOCA and loss of on-site power, the pumps would be left in a free-wheeling situation. If the break occurs at the bottom or side of the vessel, coolant would rush towards the vessel in the normal direction, thus accelerating the pump speed. If the break occurs at the top of the vessel, the pump would be accelerated or decelerated depending on which flow path (normal or reverse) presents the least resistance to the depressurization.

Representation of the coolant pump is done through a set of input data. A conservative cavitation constant of 0.001 has been used. The pump coastdown curve is taken from plant design data. The pump head versus flow is presented in Appendix A.

5.3.4 Phase Separation

Homogeneous mixing of steam and water is assumed for all volumes except the pressurizer, the accumulators and the vessel plena. The pressurizer is prescribed with a preset temperature, pressure and liquid level. The accumulators are prescribed with a liquid temperature, liquid level,

and gas pressure. The upper and lower plenums of the pressure vessel are considered large enough for phase separation to take place, hence a separation model with C_o = 0.8, V = 3 ft/sec has been used. (C8, M8, R2, R5). These values have been shown to reflect experiments well in section 5.2.5.

5.3.5 Reactor Kinetics

Seven neutron groups (one prompt, six delayed) and eleven delayed gamma groups have been used to account for the core kinetics following start of LOCA. Negative reactivity contributions include void formation, fuel Doppler coefficients and coolant temperature coefficient. Void formation is almost solely responsible for the fast shutdown of the chain reaction.

To the fullest possible extent, kinetic input data are those designed for the typical PWR plant under investigation. Other data have been estimated. For example, the division of the core into three equal volumes necessitates the determination of the power fractions that are generated in those volumes. By numerical integration of a measured power distribution late in life of Yankee, and by consulting with typical PWR pipe break analyses, fractions of 0.31, 0.46 and 0.23 have been assigned for the bottom, central, and top section of the core, respectively. The Doppler effectiveness for those sections, 0.26739 0.59014 and 0.14247, are similarly obtained from pipe break analysis done at Idaho Nuclear Testing Station. The negative void coefficients are -0.0049, -0.0328, 0.0079 $/%void for the bottom, central and top section respectively. These values fall within the range of data put forth by Elbaum in his investigation of void effect on reactor transients. (E2). Since void formation is almost solely responsible for the shutdown of the

reactor, a sensitivity study has been made to evaluate its effects on other blowdown parameters. At present, a variable void coefficient as a function of void fraction cannot be inputted into RELAP3.

5.3.6 Time Step Selection

The selection of time step is very important for RELAP3. A large time step usually results in numerical instabilities which frequently cause failure of the run. A time step too small would be uneconomical on computer time. A time step size smaller than the time for an acoustic wave to travel the shortest pipe in the system is usually suggested. Rettig et al propose the following (R2):

$$\Delta t = \left(2\pi / nC\right)\sqrt{V(L/A)}$$

where

C = velocity of sound, ft/sec

L = path length, ft.

n = a constant between 5 and 10

A = path area, ft^2

V = volume of fluid, ft^3

When the blowdown is rapid, such as in this study, the time step should also be smaller than the ratio of mass in a volume (lbs) over the rate of change of that mass (lb/sec), and the ratio of total enthalpy of the volume (Btu) over the rate of enthalpy change by mass loss (Btu/sec).

When the coolant is subcooled, the speed of sound is higher, requiring the use of smaller time steps. As steam forms in the coolant, the speed of sound decreases, allowing the use of larger time steps. A good time step has been selected when a run with a smaller time step does not produce any significant changes in the results.

For the model under study, at computed by the above formula is 0.9 msec. for the subcooled conditions. The following 5 sets of time steps in 6 blowdown intervals have been selected.

Set	Time Step (sec)	End of Intervals (sec)
1	0.0002	0.2
2	0.0004	0.5
3	0.0005	2.0
4	0.001	10.0
5	0.0025	40.0

For break sizes of the order of 3 and 4 pipe sizes, set numbers 2 and 3 are also reduced to 0.0002 sec. step sizes to avoid noticeable fluctuations.

CHAPTER 6

TOP BREAK: RESULTS AND DISCUSSIONS

6. TOP BREAK: RESULTS AND DISCUSSIONS

The top break is located in the upper plenum in the area of the top flange. The actual location of the break is not important in the overall results so long as it remains in the upper plenum and is not at a hot leg nozzle. A break at the hot leg nozzle could be analyzed in the same manner but needs a modification of the system model and, therefore, has not been included in this study.

The unit break size is 4.587 ft^2, the cross-sectional area of the hot leg. Break sizes in the multiples of 1, 2, 3, and 4 that area have been studied. The rupture is assumed to open up linearly from zero to the specified break size over a break time t_b. The break time can be anywhere from a very small time duration to a fraction of a second, with the higher limit being probably more realistic. An objective of the study is to find out how sensitive the break time is to the results. For the subcooled depressurization, three break times of 0.00025 (instantaneous), 0.01, and 0.1 sec. are studied. For the two-phase blowdown. two break times of 0.01 and 0.1 sec. are studied.

6.1 Subcooled Loadings On Vessel Internals

Upon break initiation in the upper plenum, sudden loss of fluid results in decompression waves which travel from the break to other parts of the primary system. As the waves encounter changes on their travel path, they are partially reflected. Reflected decompression waves are in reality the compression waves that travel from other parts of the system towards the break. WHAM uses the principle of wave superposition to combine these two trains of waves to arrive at the pressure and fluid velocity at any

point in the system. The formulation of the technique has been presented in Chapter 4. The model diagram for the top break accident has been shown in Fig. 4.2.F1. Table 6.1.T1 provides a legend for Fig. 4.2.F1 in order to serve as a basis for the understanding of the results presented in this section.

6.1.1 Transient Pressure Differentials

Fig. 6.1.F1 shows the history of the pressure differential across the core. Fig. 6.1.F2 shows the pressure differential across the core barrel. The break time for these cases is 0.25 msec. which can be termed as "instantaneous" because it takes twice that duration for the disturbance to travel through the break. The location of the break has been placed at the level of the vessel flange at which the closure head is bolted to the vessel cylindrical section.

Fig. 6.1.F1 indicates that the pressure differential across the core is oscillatory with magnitudes significantly damped after the first pulse. Loading period is of the order of 20 msec. The corresponding loading frequency is 50 cps.

At normal operation, the pressure differential across the core is 31.5 psi in the upward direction. This value remains the same for about 3 msec. after the break because the disturbance waves take that much time to travel from the break to the upper core plate. When the decompression waves have reached the upper core plate, then the pressure differential starts to increase. A maximum value is reached just before reflected waves have returned to the top and transmitted waves have arrived at the bottom of the core.

Table 6.1.T1

TOP BREAK

CHARACTERISTICS OF NETWORK MODELED FOR WHAM

Leg	Initial Pressure (psi)	Initial Velocity (1) (ft/sec.)	Area (ft^2)	Length (ft)	No. of (2) Subnodes
1	2236.5	0	4.587 x (1,2,3,4)	1.5	2
2	2236.5	0	1.0	4.37	6
3	2236.5	0	134.24	6.32	8
4	2236.5	-6.9	134.24	4.67	6
5	2238.5	-15.5	47.9	3.292	4
6	2246.6	-15.5	47.9	3.292	4
7	2254.6	-15.5	47.9	3.292	4
8	2262.5	-15.5	47.9	3.292	4
9	2265.8	-6.5	119.5	1.34	2
10	2269.2	-6.5	119.5	3.25	4
11	2272.5	-6.0	129.4	5.33	4
12	2238.6	-1.4	23.44	3.292	4
13	2246.6	-1.4	23.44	3.292	4
14	2254.6	-1.4	23.44	3.292	4
15	2262.5	-1.4	23.44	3.292	4
16	2276	-29	10.18	6.67	8
17	2279.5	-29	10.18	6.58	7
18	2283.0	-29	10.18	6.58	8
19	2276	-29	16.54	6.67	8
20	2279.5	-29	16.54	6.58	7
21	2283	-29	16.54	6.58	8
22	2286.5	-29	36.4	4.67	5
23	2286.5	0	36.4	4.67	5
24	2288	-47.54	16.48	21.16	24
25	2203	-37.8	20.81	11.5	13
26	2203	-7.5	105.8	6.22	6
27	2210.5	-15	54.56	26.16	26
28	2225.5	-17.51	54.56	26.16	27
29	2233	-9	105.8	6.22	6
30	2235	-50.47	18.35	17.22	23

(1) Sign of water velocity is relative to the positive direction of increasing subnodes in each leg.

(2) Number of subnodes is the integer closest of $L/c\Delta t$

Fig.6.1.F1
TOP BREAK
HISTORY OF CORE PRESSURE DIFFERENTIAL

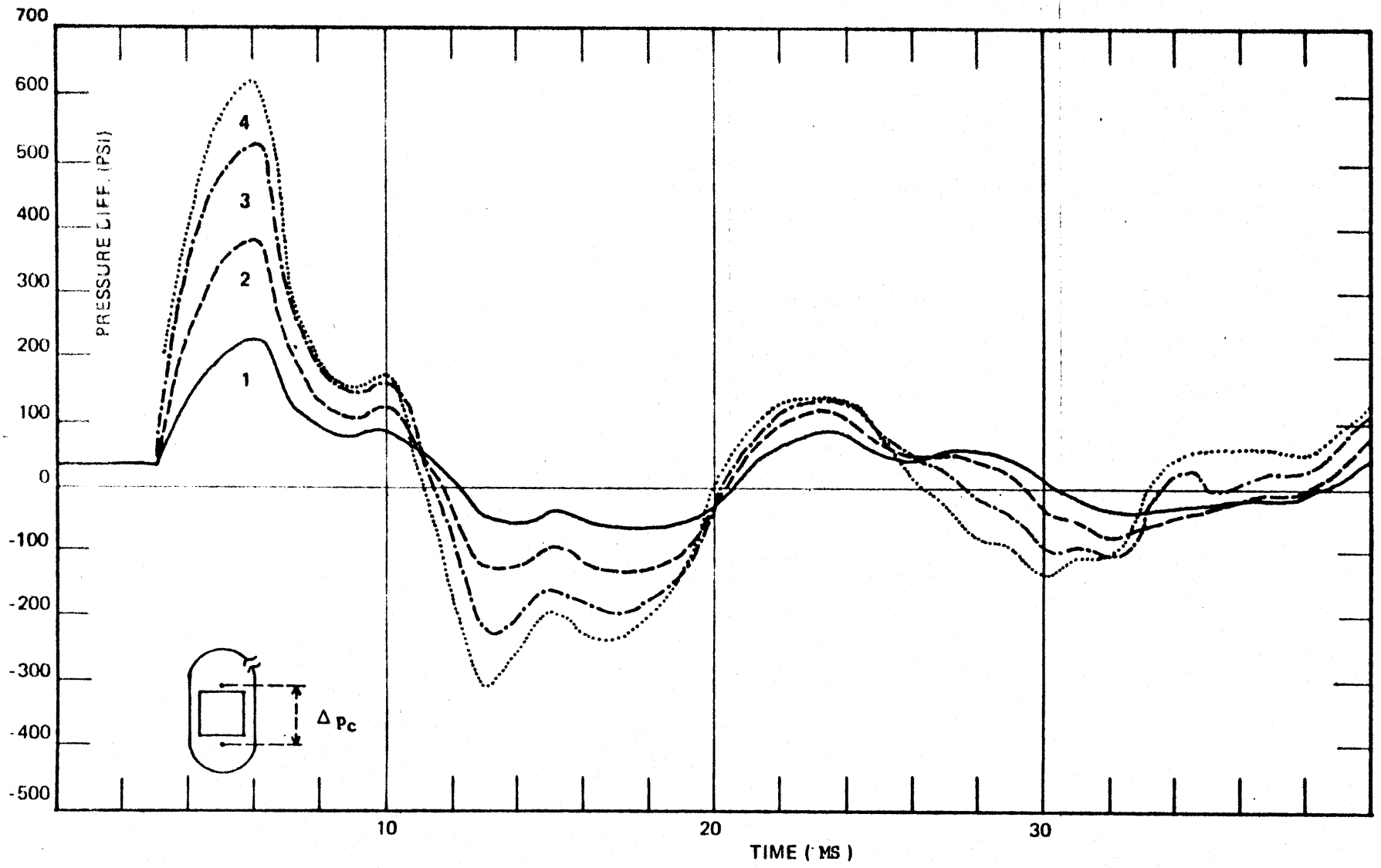

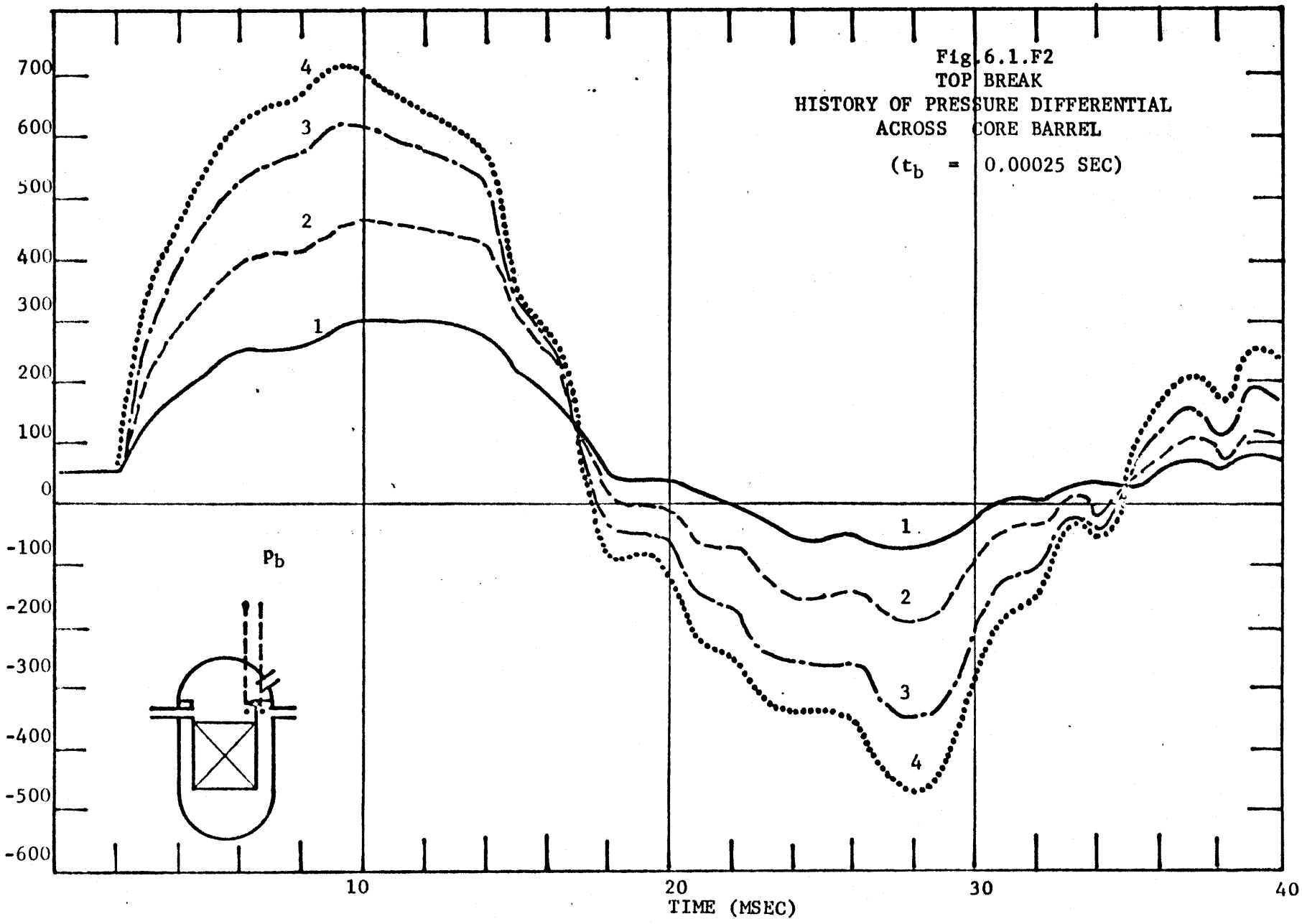

Fig. 6.1.F2
TOP BREAK
HISTORY OF PRESSURE DIFFERENTIAL
ACROSS CORE BARREL
(t_b = 0.00025 SEC)

The pressure differentials across the core barrel as shown in Fig. 6.1.F2 are both higher in pulse magnitude and broader in pulse time than the corresponding ones across the core. This is easily understood due to two reasons: a) the initial subcooled pressure at the cold leg nozzles is higher than the initial subcooled pressure just below the core: and b) The wave travel path from the upper plenum to the cold leg nozzles is considerably larger than the core height. Thus. the oscillation period of the pressure loadings across the upper portion of the core barrel is approximately 33 msec., corresponding to a frequency of 31 cps. This is about the same as the frequency of the pressure loadings on the same core barrel location caused by a break at the vessel side as described in Section 8.1.1.

The pressure loadings on the thermal shield is essentially nil because disturbance waves traveling upwards from the lower plenum should be the same on both sides of the thermal shield.

6.1.2 Sensitivity of the Pressure Differentials on Break Time and Break Size

Figs. 6.1.F3 and 6.1.F4 show plots of the maximum pressure differentials across the core and the upper core barrel, respectively. The changing parameters are the break size and break time.

It is noted that, as the break size increases, the magnitude of the largest pressure pulse also increases, but not linearly. There is a tendency for the loadings to level out as the break size increases. For very large break sizes, the pressure differential should approach 780 psi, which is the difference between the initial subcooled pressure at the cold leg nozzles (2280 psi) and the saturation pressure corresponding to the 613°F in the upper plenum (1500 psi).

Fig. 6.1.F3

EFFECTS OF BREAK SIZE AND BREAK TIME ON MAXIMUM PRESSURE DIFFERENTIALS ACROSS REACTOR CORE

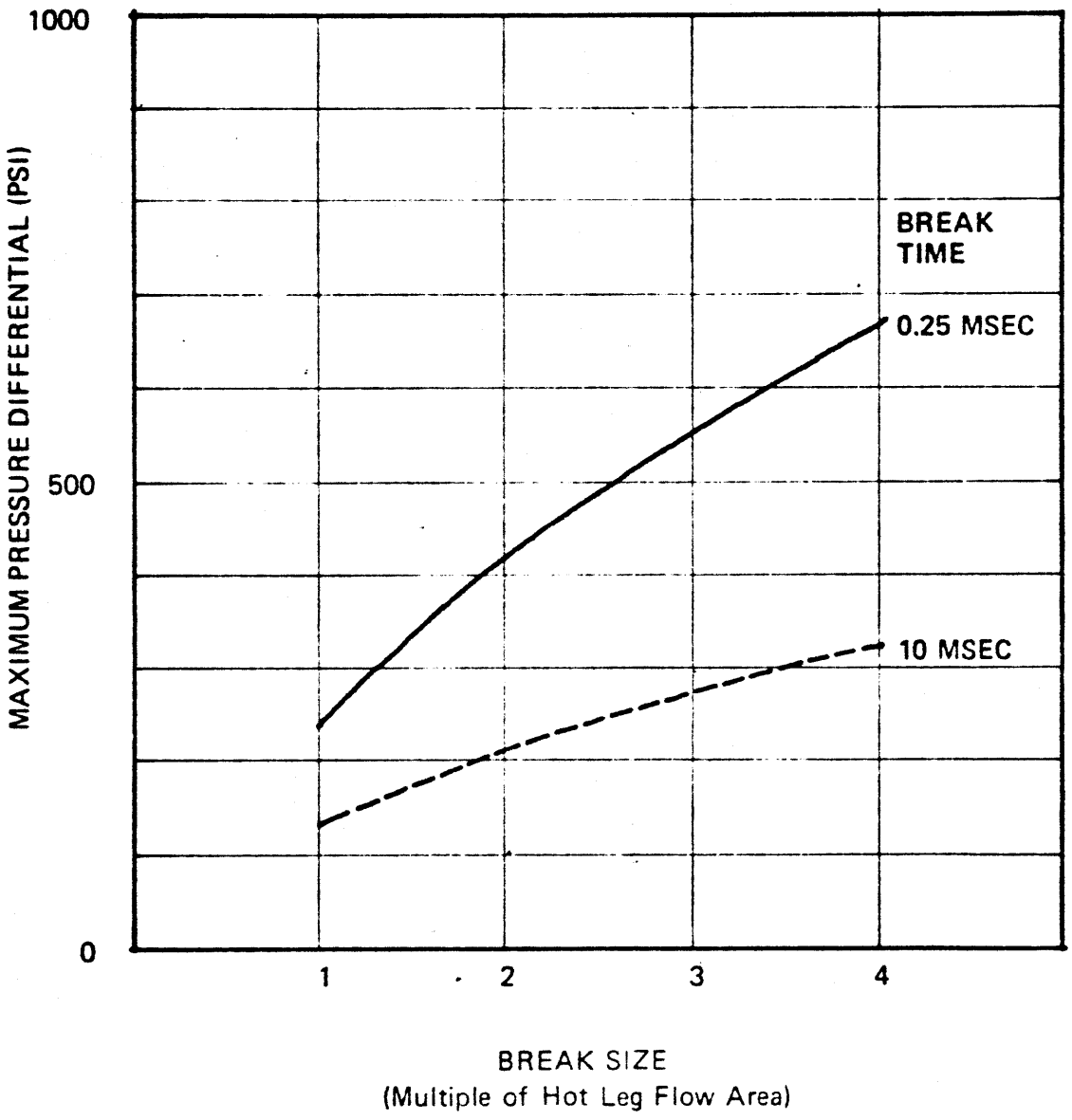

Fig. 6.1.F4

EFFECTS OF BREAK SIZE AND BREAK TIME ON MAXIMUM PRESSURE DIFFERENTIALS ACROSS CORE BARREL

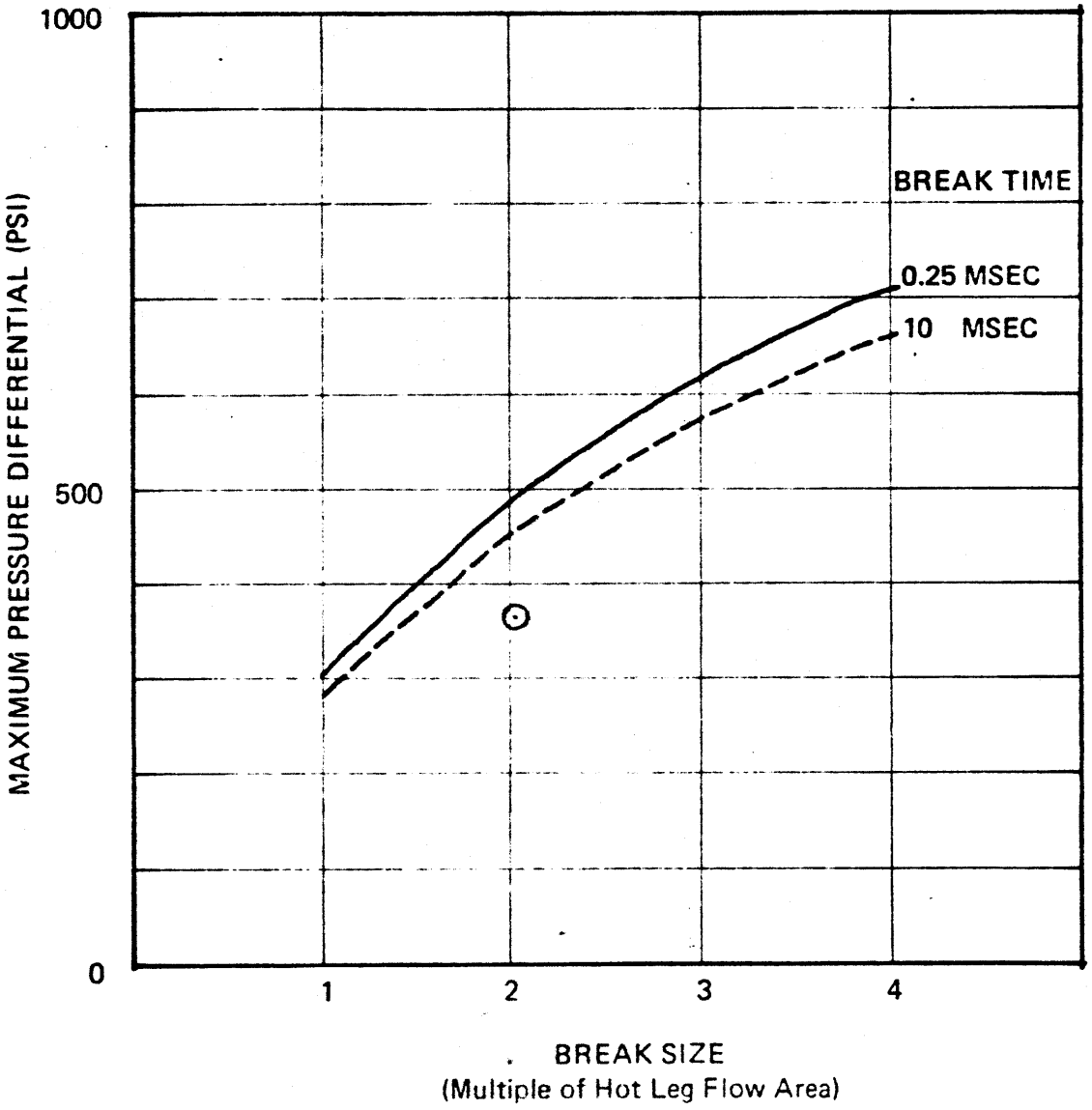

⊙ Manufacturer's value for hot leg double-ended break, break time 1 to 20 MSEC (C1).

The effect of break time on core loadings is more pronounced than the effect on barrel loadings. The reason is again the long travel path from one side of the barrel to the other side, allowing the outside to be still at the initial pressure while the inside has been decompressed to a low value even for larger break times.

The circle in Fig. 6.1.F4 represents the value of the largest pressure loading on the upper core barrel as presented by the manufacturer for the double-ended hot leg break (C1). It is 360 psi as compared to 450 psi for the case of upper plenum break considered in this study.

6.1.3 Force Loadings

The force loadings on vessel internals consist of hydrostatic force (due to pressure differentials), friction force, inertial force. gravity, and force due to change in momentum flux. The magnitude and direction of the net force is the vector sum of these components, and therefore, is quite complicated to account for. In reality, however, the friction force, momentum flux change, and gravity are very negligible when compared to the hydrostatic and inertial forces. In this work, only the hydrostatic and inertial forces are considered.

Table 6.1.T2 lists some values of force loadings across the core. No similar listing is made for the core barrel because in this case the forces are both time and space dependent. Furthermore, at any given elevation of the core barrel, the force simply has two perpendicular components; namely the inward or outward hydrostatic force and the inertial force which is parallel to the surface on both sides of the barrel.

Across the core, the net force is the vector sum of the hydrostatic force which directs upward (during the first pulse) and the inertial force which is opposite to the hydrostatic force. Because in the formulation of WHAM, there is a one-to-one relationship between the fluid pressure, velocity and inertial force, the time behavior of the force loading should be similar to that of the pressure differential. Only two values of the loadings (at the 6 msec. peak and at 10 msec. low) are presented in Table 6.1.T2.

In order to understand the effect of the loadings on the core, it is necessary to look into the composition of the core. There are 193 fuel assemblies in the core. Each assembly has 225 rod positions, 204 of which are occupied by the fuel rods, 20 by the control rod cluster guide thimbles and 1 by the instrumentation thimble. There are nine grid assemblies along the length of the fuel assemblies with clip springs to hold the fuel rods in place. At either ends of each fuel assembly are the box-like plena for coolant inflow and outflow. The weight of the entire assemblies and the loads resulting from control rod insertion are transmitted by the lower ends of the assemblies to the bottom core plate. Leaf springs are mounted between the top ends of the assemblies and the upper core plate to provide hold down loading for the core.

Under oscillatory loadings caused by a vessel break, the assemblies may move upward, touch the upper core plate, then fall down on the bottom core plate, causing oscillation in all vessel components. The manufacturer (C1) has estimated that a maximum longitudinal force of 5700 pounds per assembly would result upon a LOCA by hot leg break. Table 6.1.T3 lists the corresponding values for the cases of vessel top break with break size ranging from one to

Table 6.1.T2

TOP BREAK

SOME VALUES OF FORCE LOADINGS ACROSS THE CORE*

Cases	Inertial Force (10^6 lbs.)	Hydrostatic Force (10^6 lbs.)	Total (10^6 lbs.)
At 6 msec. peak			
Break size A = 1	1.330	-3.041	-1.711
A = 2	2.368	-5.253	-2.886
A = 3	3.354	-7.188	-3.834
A = 4	4.003	-8.571	-4.568
At 11 msec. low			
Break Size A = 1	0.352	-0.829	-0.477
A = 2	0.486	-0.829	-0.343
A = 3	0.542	-0.829	-0.288
A = 4	0.452	-0.829	-0.375

* Forces due to momentum flux change, friction and gravity are negligible. Cross section of the core is taken as the area inside the baffle, or 96 ft^2. Positive direction of the force is downwards (arrow in Fig. 4.2.F1).

Table 6.1.T3

TOP BREAK

LARGEST SUBCOOLED FORCE LOADING PER FUEL ASSEMBLY

Break Size	Peak Loading (lbs)
A = 1	8,700
A = 2	14,700
A = 3	19,600
A = 4	23,400
LOCA by Hot Pipe Break*	6,700

* From Reference C1, Section 14.3.2.2.6

Table 6.1.T4

SOME VESSEL INTERNAL MECHANICAL CHARACTERISTICS (C1)

Item	LOCA		Design	
	Stress (psi)	Deflection (in.)	Stress (psi)	Deflection (in.)
LOCA by Hot Leg Break				
Upper Support Structure	12,000	0.12	n.a.	1
Lower Support Structure	15,000	n.a.	n.a.	n.a.
Upper Core Barrel	13,500	n.a.	(1)	3
RCC System Cluster Bending	6,000	n.a.	n.a.	1
Thimble Compression	16,800	n.a.	n.a.	0.035
LOCA by Cold Leg Break				
Upper Support Structure	n.a.	n.a.	n.a.	n.a.
Lower Support Structure	11,000	n.a.	n.a.	n.a.
Upper Core Barrel	20,300	n.a.	(1)	n.a.
RCC Guide System	n.a.	n.a.	n.a.	n.a.

(1) Short-cylinder characteristics of the upper core barrel have been determined as (Ref. C1, Section 14.3.2.15) Buckling Pressure: Between 850 psi and 2400 psi. Extensional Natural Frequency: Larger than 1180 cps. Bending Natural Frequency: Between 60 cps and 100 cps.

four times the hot leg flow area. It is seen that the vessel top breaks generally cause maximum loadings two or three times larger than the value caused by LOCA by hot pipe break.

Table 6.1.T4 lists a few calculational effects presented by the manufacturer (C1) when the vessel internals are under excitation by subcooled loadings by pipe break. The determination of the corresponding results for the vessel break cases does not fall into the scope of the present study.

6.2 Two-Phase Blowdown

The two-phase blowdown following a break in the upper plenum of the vessel has been studied with RELAP3, Mod 36. The principal processes followed with respect to time after the break are: normalized power history, flow rates, fuel temperature redistribution, coolant quality heat transfer coefficient, total mass loss, coolant remaining in the lower plenum, ECC water injection, and clad surface temperature in the middle region of the core. All quantities are average values for the system or the portion of the system considered, and are stepwise calculated over very small time intervals such as already indicated in Section 5.3.6.

As mentioned previously in this chapter, the location of the break can be postulated anywhere in the upper plenum except at the hot leg nozzles. Breaks at the hot leg nozzles can be analyzed in the same way, but modification of the model (Fig. 5.3.F1) must be made to account for the intact loops and the broken loops.

Four break sizes have been studied with areas being 4.587 ft^2, 9.174 ft^2, 13.761 ft^2 and 18.348 ft^2 respectively. These areas are 1, 2, 3 and 4 times the flow area of the hot leg.

A break time of 0.01 second has been used for the majority of the cases but some studies have also been made with a break time of 0.1 second. The sensitivity of different parameters with respect to break time are presented in Chapter 9, and the general conclusion drawn is that the break time is relatively insensitive to the principal parameters under investigation.

6.2.1 Normalized Power

Fig. 6.2.F1 shows the normalized power history of the core for break sizes 1, 2, 3 and 4 (terminology has already been defined). The parameters that have bearing on the normalized power curves are delayed fissions, void negative reactivity, and to a lesser extent, Doppler coefficient. Mechanical rod action has been neglected to the extent that it is not assumed to take place until 30 seconds later when the reactor has been well shutdown.

Observation of the normalized power curves indicate that void formation alone is enough to scram the reactor in less than 1 second, much less for larger sized breaks.

For the case of one-pipe-size rupture, the power drops slower than for the case of a double-ended hot leg break reported for the same 2758 Mwt reactor. The two plateaus around 1 and 1.5 seconds correspond to flashing sequences in the upper and lower plena during which the pressures and rod remain practically constant. As break sizes increase, void formation is faster while the effect of flashing is less obvious due to predominance of flow induced by large pressure differentials.

Fig.6.2.F1

TOP BREAK
NORMALIZED POWER HISTORIES

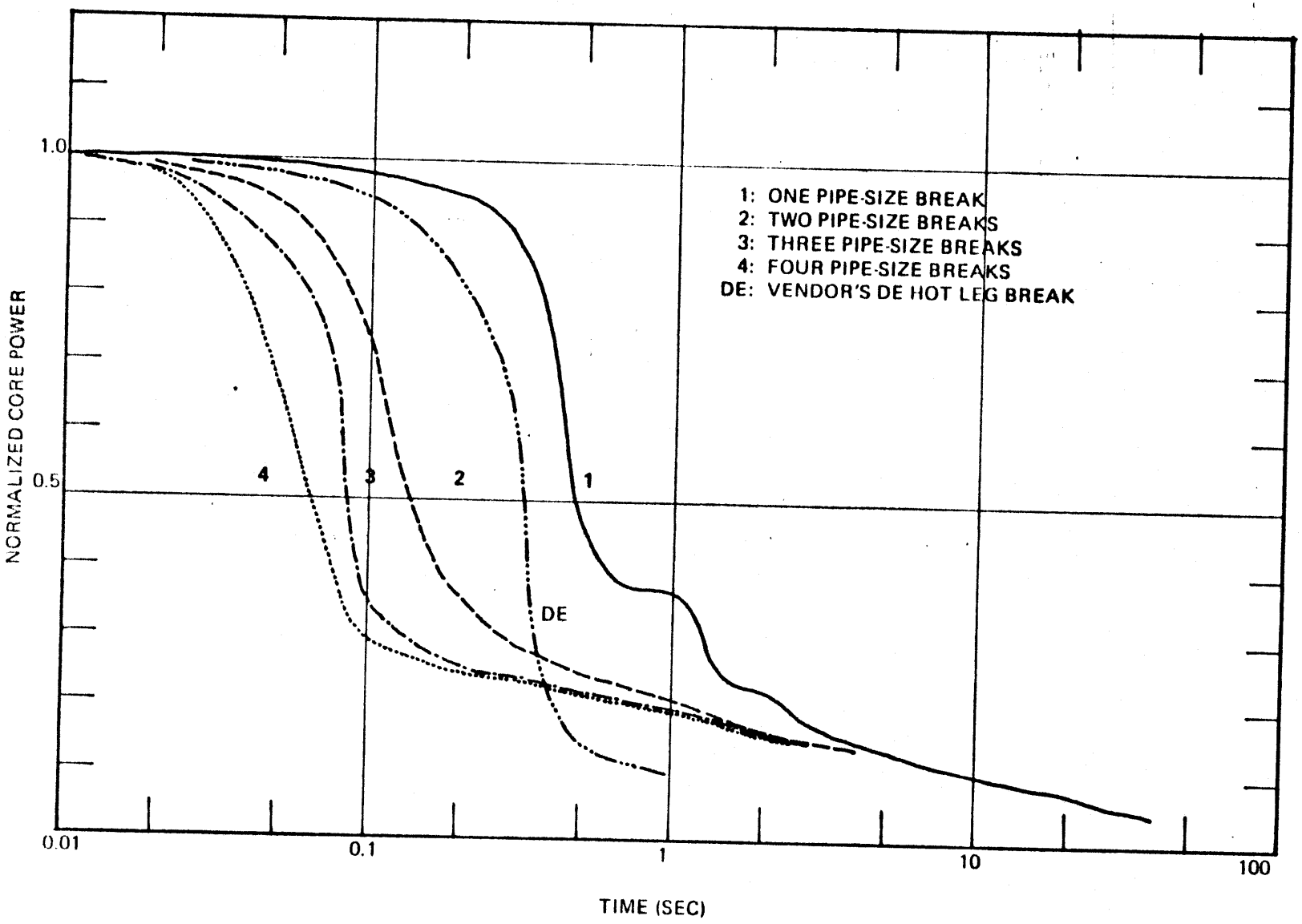

All normalized power curves become asymptotic at and beyond EOB. This is the period when the core is only filled with saturated steam. The normalized power curve in this period is the decay heat curve of the fission products.

6.2.2 Flow Rates

Figs. 6.2.F2 and 6.2.F3 show the flow rates at the break (Curve J20), in the hot legs (Curve J1) and at the core midplane (Curve J15) as a function of time.

Marks on the curves indicate the time after which the flow is no longer choked. Choking flow is the feature that becomes more and more prominent as the break increases in size. Flow at the break (Curve J20) is characterized in the beginning with metastable orifice flow, but quickly turns into choking, two-phase flow as the pressure in the upper plenum has dropped enough for the coolant in the vicinity of the break to flash. The flow in the hot legs reverses very fast and the reversed flow is also featured by choking when the break is larger than twice the hot leg flow area. Flow rate through the core starts out at the steady state value of 36,160 lbs/sec., increases to approximately twice, three times, and four times that value for break sizes of 1, 2 and 3 hot leg flow area. The flow through the core never experiences flow reversal such as the case for bottom and side breaks, but does go through some fluctuation at low break sizes which may be due to flashing sequences at different parts of the vessel. As the combined flow area of the channels is 47.9 ft^2, more than twice the largest break considered,

Fig. 6.2.F2
TOP BREAK
FLOW RATES AT BREAK (J20), HOT LEGS (J1)
AND CORE MIDPLANE (J15)
(✕ Indicates the time when Flow Choking stops.)

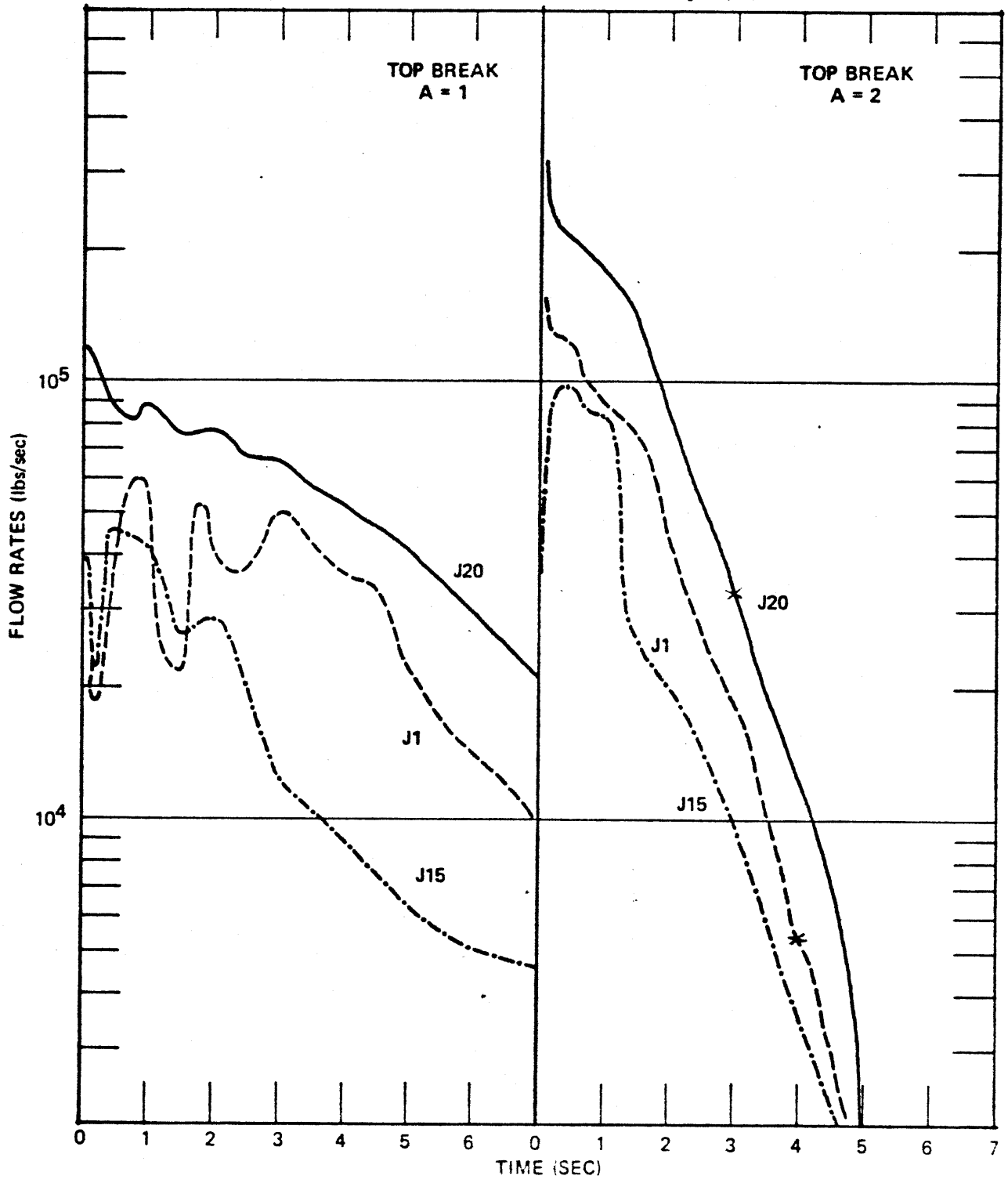

Fig. 6.2.F3
TOP BREAK
FLOW RATES AT BREAK (J20), HOT LEGS (J1)
AND CORE MIDPLANE (J15)
(X indicates the time when Flow Choking stops)

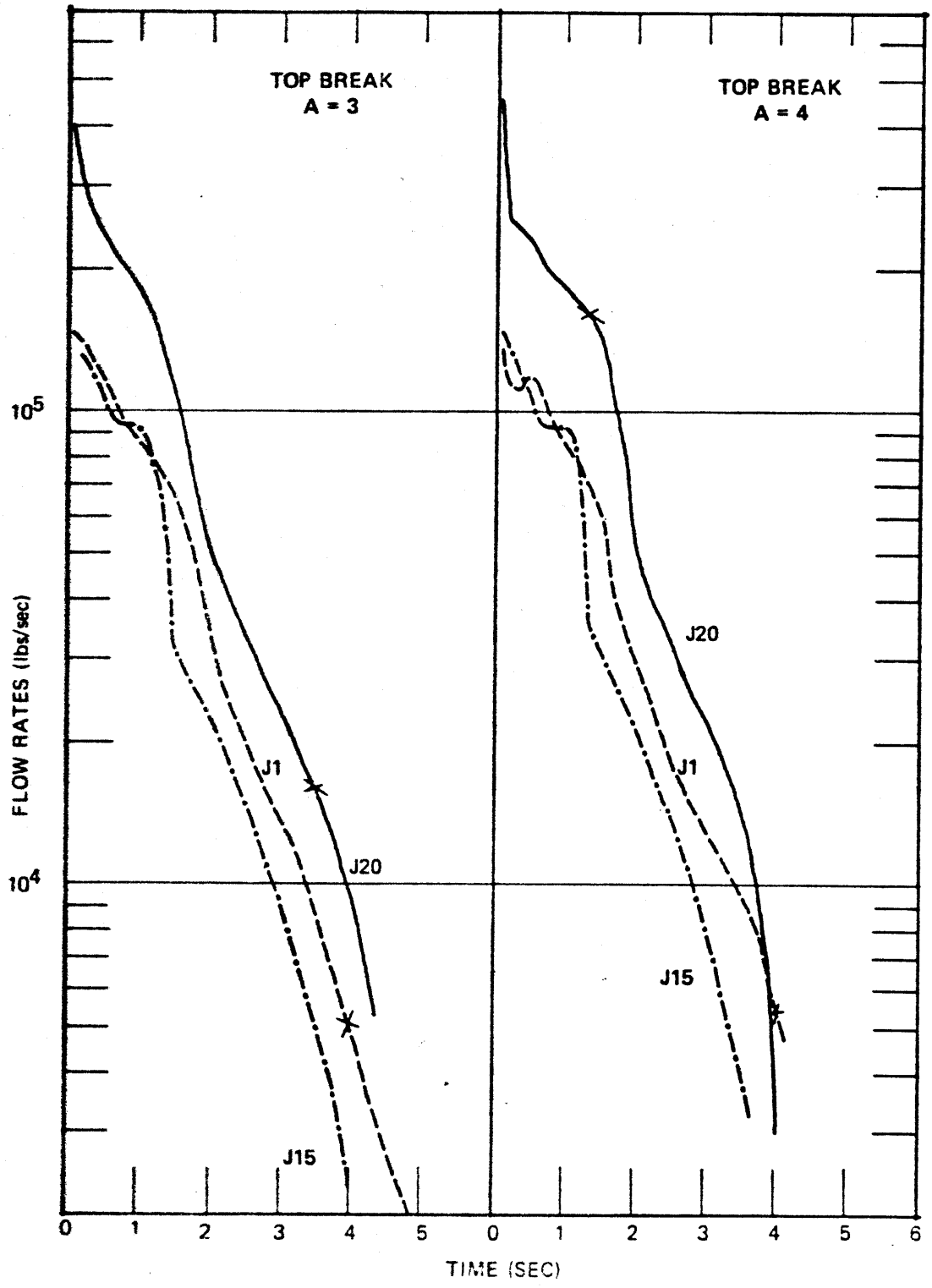

the flow through the core is not choked even though the pressure differential across the core may be many hundred psi for large breaks. It is not clear whether this computer result reflects the physical reality or not. By assumption, RELAP3 has treated all the flow channels as one flow path with the area as the combined flow area and with a friction factor to reflect the steady state pressure drop. This friction factor is maintained throughout the blowdown. A better model may be obtained if the flow channel is dealt with individually and the total flow rate multiplied by the number of flow channels to satisfy the conservation equations.

The sum of curves J1 and J15 in Figs. 6.2.F2 and 6.2.F3 does not add up to curve J20 because the break flow also includes input from the core bypass and depletion of the upper plenum.

For the case of top break with the size of one hot leg flow area, the flow pattern shows some fluctuation as manifested in Fig. 6.2.F2. These fluctuations seem to be caused by the influence of flashing in different parts of the primary system. This influence does not show prominently at larger break sizes because it cannot compete with the fast depressurization of these cases.

Table 6.2.T1 lists the values of time for start of emergency core cooling injection (SECCI) and end-of-blowdown (EOB). When the cold leg pressure has dropped to 660 psi, cold borated water from the accumulators starts to inject into the cold legs. The start of injection is at 4.68 second, 1.54 second, 1.34 second, and 1.30 second for break sizes of 1, 2, 3 and 4 times the hot leg flow area, respectively. Thus, the indication is that the pressure in the cold leg does not drop in the same linear pattern as the

Table 6.2.T1

TOP BREAK

START OF EMERGENCY CORE COOLING INJECTION (SECCI)

AND END OF BLOWDOWN (EOB)

Break Size (1)	Time (Sec.) SECCI	EOB(2)
Break time = 0.1 sec.		
A = 1	4.68	12.8
A = 2	1.54	6.4 - 8.6
A = 3	1.34	4.58 - 8.3
A = 4	1.30	3.96 - 8.2
Break time = 0.1 Sec.		
A = 2	1.58	6.4 - 8.6

(1) Break size A, is in multiple of hot leg flow area, which is 4.587 ft^2.

(2) Where a range of EOB is given, the first number is the time when break flow first pauses but then again resumes significantly, and the last number is the time when no significant flow exists.

increase in break size, and there is a trend for SECCI to reach an asymptotic value around 1.30 second. The injection flow rate has the same pattern for either top, bottom or side breaks, and the pattern can be seen in Fig. 8.2.F7 The flow rate is zero at SECCI, builds up to a maximum value of approximately 2800 lbs/sec. in about 2 seconds and then slowly drops to about 2000 lbs/sec. at 25 seconds.

End-of-blowdown has been defined (A3) as the time at which flow out of the break first becomes zero. This definition is only clear cut for smaller sized breaks such as when the break is one hot leg flow area. For larger breaks, there is considerable flow fluctuation at the break when EOB is drawing close, therefore, the flow out of the break may be temporarily zero at an instant but may again resume at a significant rate for some time. The range for EOB is therefore listed in Table 6.2.T1. The first number of the range is the time when the break flow first becomes zero. The second number is the time when significant flow no longer exists. If EOB is liberally interpreted as the time when flow out of the break has dropped to an insignificant value, then EOB is around 7 to 8 seconds for the break sizes under investigation. For even larger break sizes, EOB should still be within that range because of the choking characteristics of the flow in various parts of the primary system.

Table 6.2.T2 lists values for SECCI and EOB for loss-of-coolant accident by guillotine pipe break as reported for some PWR plants (B6, A5, C9). It is seen that SECCI and EOB take place much later than for vessel break cases.

Table 6.2.T2

SECCI AND EOB FOR GUILLOTINE

PIPE BREAK LOCA IN SOME PWR'S (B6, A5, C9)

Plant	SECCI	EOB
Oconee-Type, 841 MWe	13	21.5
Cook-Type, 1060 MWe	16	26
Ft. Calhoun-Type, 530 MWe	13	16

6.2.3 Mass Loss History

Fig. 6.2.F4 shows the mass loss history for the four break sizes under investigation.

The total coolant inventory in the primary system is approximately 470,000 lbs. at the onset of the accident. The mass loss curves as presented in Fig. 6.2.F4 can exceed this value beyond EOB because there is an additional 130,000 lbs. of ECC water which may also flow out the break as time goes on. But for times smaller than EOB, the mass loss curves would build up and level out at 470,000 lbs.

The evidence of flow choking and limiting end-of-blowdown can be seen in this figure. At small breaks, the mass loss history is almost linear over the first 6 or 7 seconds because over this time period the flow out of the break is choking and approximately constant. When the break increases in size, the mass loss curve becomes bent, being very steep at the beginning and leveling out as time goes on. The curves for break sizes of 2, 3 and 4 pipe flow areas are very close together, suggesting an asymptotic pattern. This asymptotic configuration would allow the same insignificant amount of coolant remaining in the primary system at EOB which has been noted in the previous section as being between 7 and 8 seconds.

6.2.4 Pressures in the Upper and Lower Plena

Figs. 6.2.F5 and 6.2.F6 show the pressure histories in the upper and lower plena for the 4 top break sizes considered. The DE curve in these figures is the history of "System" pressure for the LOCA by pipe break reported by the manufacturer for the same PWR plant under consideration. (C1).

Fig. 6.2.F4
TOP BREAK
MASS LOSS HISTORY
(Curves 1, 2, 3, 4 Correspond to Break)
(Sizes in Multiples of Hot Leg Flow Areas)

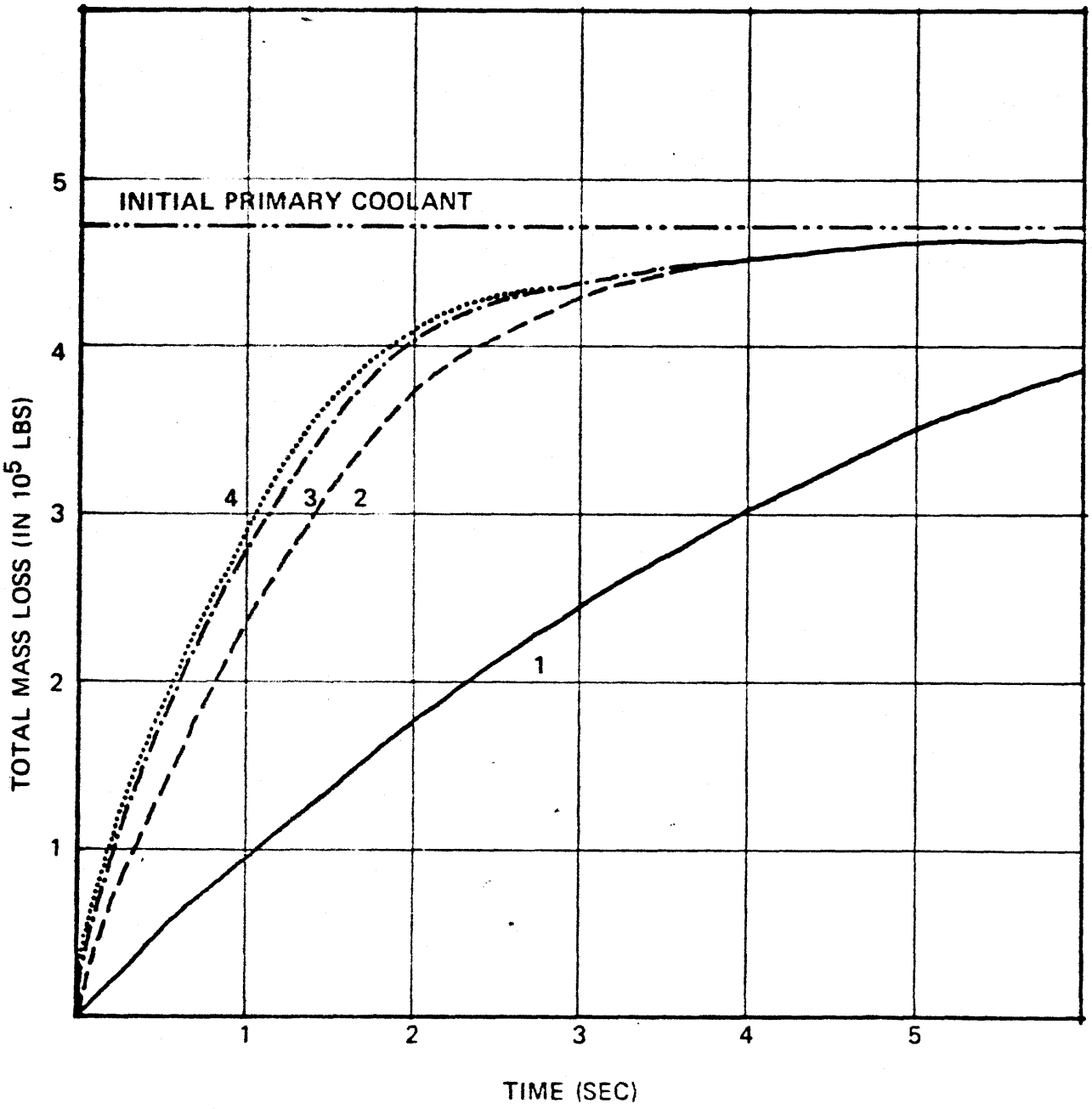

Fig. 6.2.F5
TOP BREAK
PRESSURE HISTORY IN UPPER PLENUM

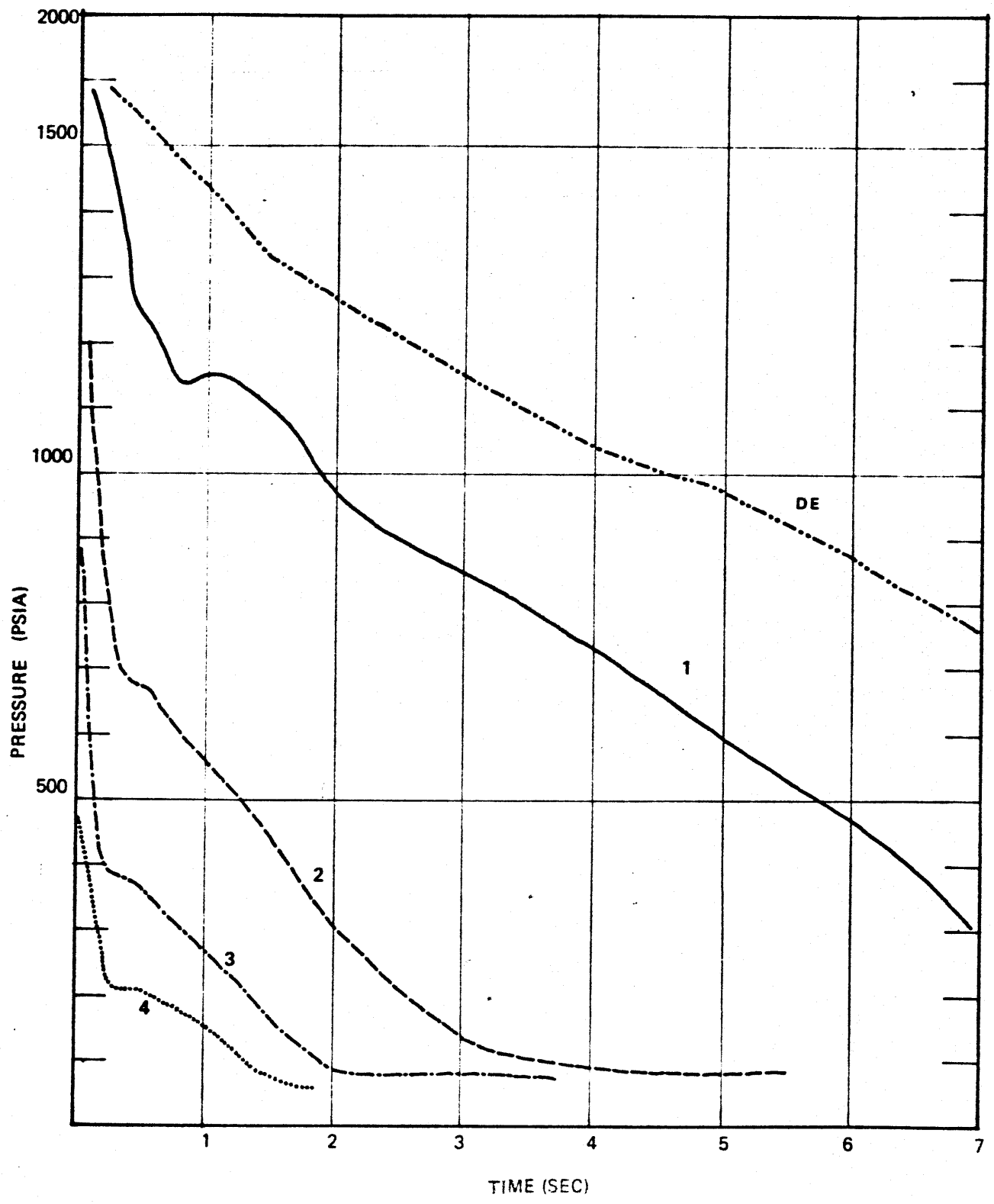

Fig. 6.2.F6
TOP BREAK
PRESSURE HISTORY IN LOWER PLENUM

(Curves 1, 2, 3, 4 Correspond to Break Sizes in those Multiple Hot Hot Leg Flow Areas. DE is the Curve Provided by the Manufacturer for the Double-Ended Pipe Break.)

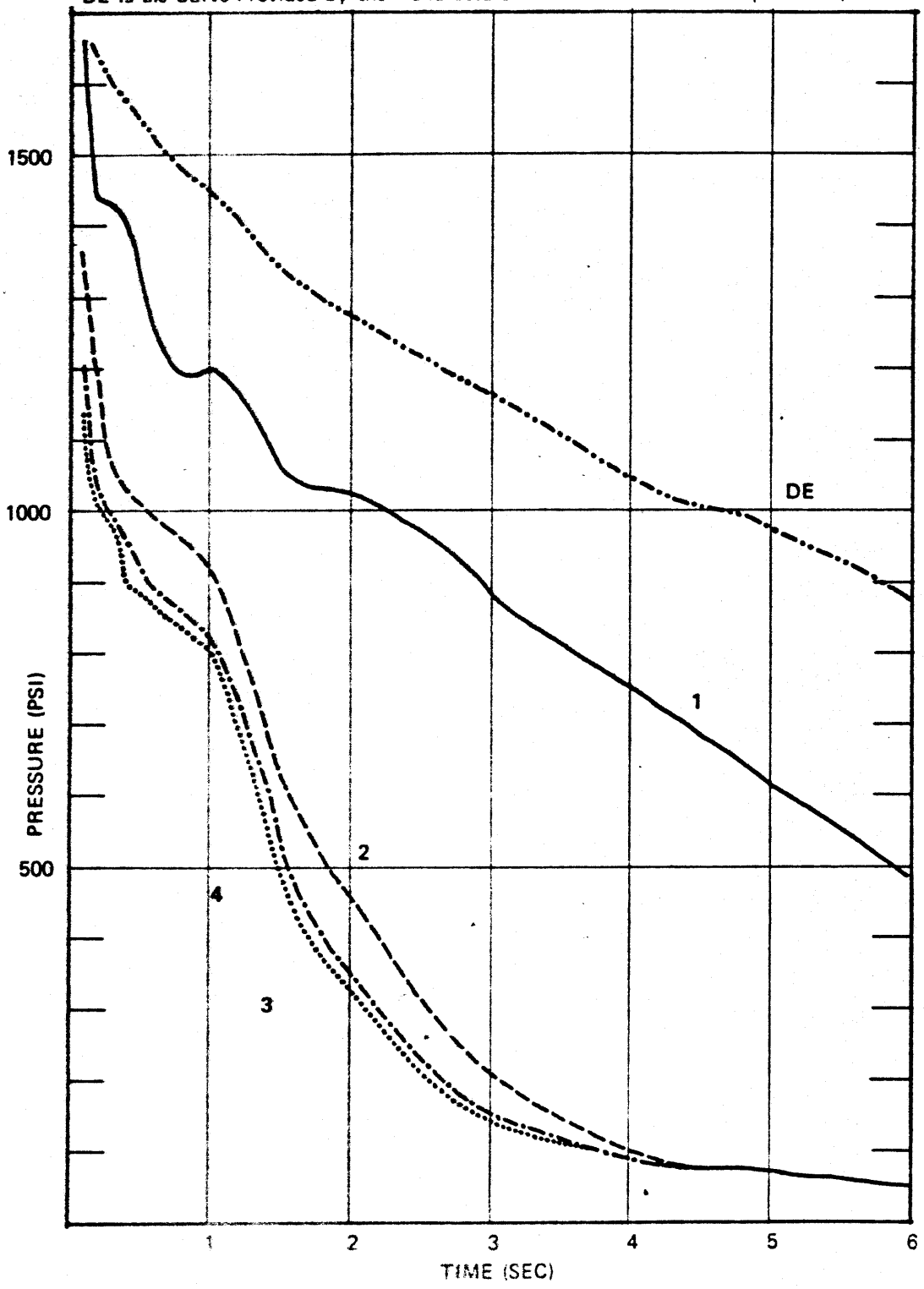

It is seen that the depressurization is much faster for vessel break than for the pipe break even though the latter has a break size two times larger (double-ended break) than the former. But as the vessel break increases in size, the pressure history curves tend to approach an asymptotic configuration. This asymptotic configuration is particularly evident for portions of the system further away from the break, such as in the case of the lower plenum.

The pressure histories for the case of one-pipe-size break show the influence of flashing in the upper plenum, core, and the lower plenum respectively at about 1450, 1200 and 1050 psi. For larger break sizes, the leveling out of the pressure at approximately 0.5 second is more due to the predominance of the two-phase flow over the subcooled flow.

The difference of the lower and upper plenum pressure as calculated by RELAP 3 may be 600 - 700 psi for times smaller than 0.5 second. This value approaches the differentials computed by WHAM for the subcooled depressurization.

6.2.5 Coolant Remaining In Lower Plenum

For all break sizes under investigation, the minimum mass remaining in the lower plenum is practically the same, around 8500 lbs. or 16% of the initial mass in the volume.

The lower plenum has been specified as a place where phase separation can take place. The bubble gradient parameters is 0.8. The bubble rise velocity is 3 msec. These values are experimentally derived by Curet and others (C8). and have been recommended as indicative of the flowdown for a large volume.

Fig.6.2.F7

TOP BREAK

COOLANT MASS IN LOWER PLENUM

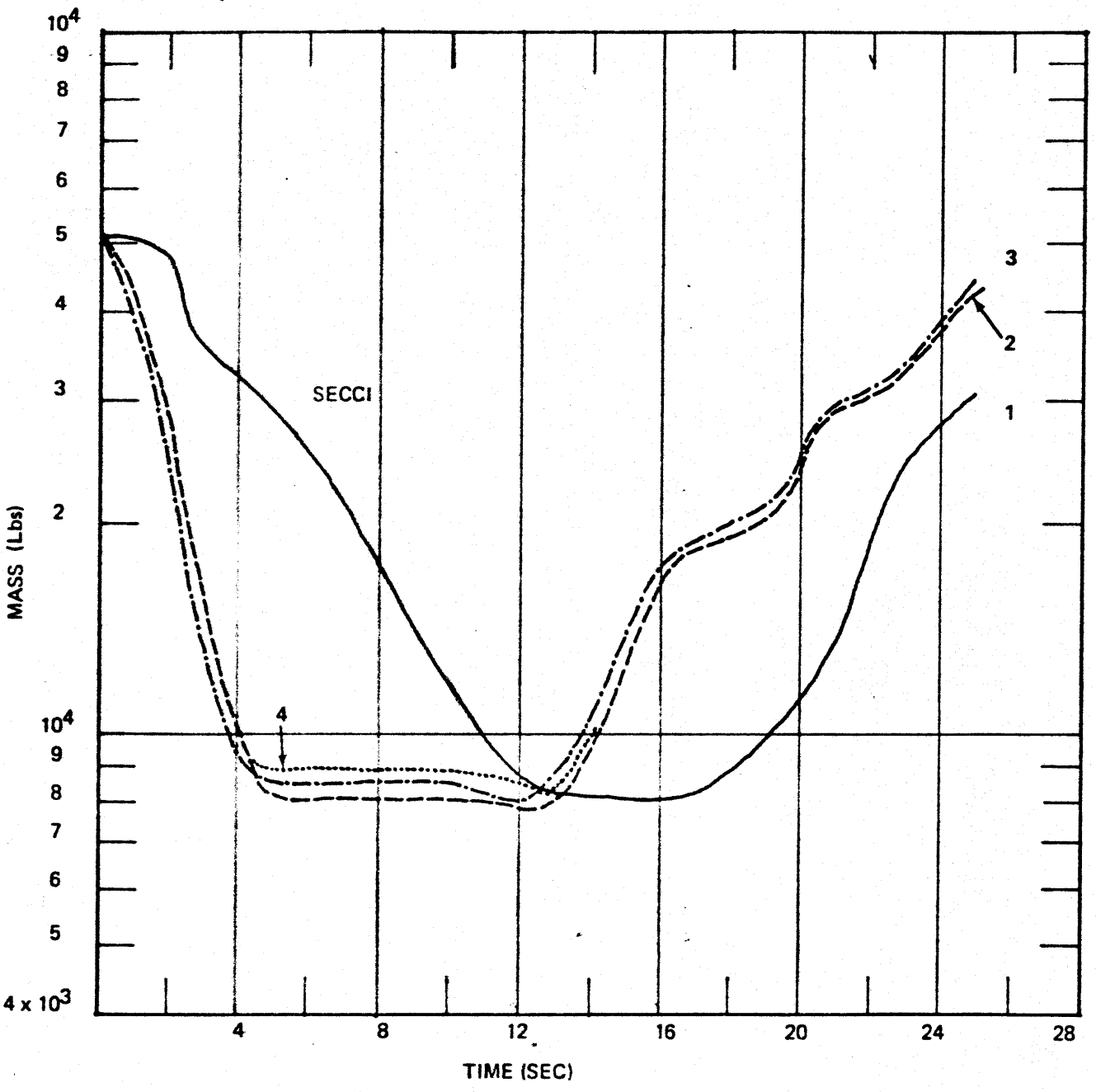

The loss of mass in the lower plenum, mostly by flow through the core to the upper plenum, is almost exponential for the duration of the blowdown. This is manifested as straight lines in the semi-log plot of coolant mass versus time shown in Fig. 6.2.F7. During this time, the replenishment (from downcomer annuli) rate and loss rate (to upper plenum, through core) are governed mainly by pressure differentials. As the pressures approach 75 psia, the prescribed pressure of the containment, the leak tapers off. The 8500 lbs. remaining in the lower plenum corresponds to the amount of saturated water and steam in a volume of 1100 ft^3, at 75 psia, 320°F.

The flattening of the curves around 8500 lbs. is part of the relatively quiescent period when only steam rises from the fluid to flow through the core. ECC water from the accumulators continues to be injected into the cold legs, but remains there until the legs are filled with water before flowing towards the lower plenum. When this takes place. the mass in the lower plenum rises, but at a somewhat unsteady rate. The ECC water continues to be injected well beyond 25 seconds due to the relatively conservative model of a rather small injection rate.

6.2.6 Heat Transfer Coefficient, Critical Heat Flux Ratio, Flow Quality and Average Clad Surface Temperature

Upon upper plenum rupture, the onset of void formation immediately introduces negative reactivity which by itself is capable of shutting down the reactor. Centerline and average fuel temperatures, therefore, never increase because core power never increases beyond its steady state value. Circumstances exist by which the power increases slightly before dropping (positive void coefficient before negative coefficients override it), but these do not constitute any significant change in the overall temperature transient. Further-

more, even some rod ejection may occur due to the great subcooled loadings. This situation deserves a separate study, but for the moment, it suffices to point out that mechanical constraints, hydraulic drag, and inertia would prevent rod ejection at such a fast rate that would allow the resulting positive reactivity to compete with very fast forming voids.

During blowdown, core temperature transient is characterized by the fuel temperature redistribution and changes of heat transfer regimes at the clad surface. At the prescribed gap conductivity, the steady state fuel average temperature is 1845°F and the centerline temperature is 2897°F. A sensitivity analysis of temperature transient with respect to gap conductance is presented in Section 9.7. Figure 9.7.F1 of that section shows the energy redistribution history for the middle core region for two values of gap conductance. It can be seen from that figure that the typical time constant of the fuel is of the order of 10 - 12 seconds.

Figs. 6.2.F8, 6.2.F9 and 6.2.F10 show the histories of the critical heat flux ratio (DNBR or CHFR), heat transfer coefficient (HTC) and average clad surface temperature for the middle core region. Only the cases of 1, 2 and 3-pipe-sizes breaks are presented, but for larger break sizes, the pattern is similar to that of the 3-pipe-sizes break. For approximately 4 seconds in the initial stage of the blowdown, the clad surface temperature drops due to increased mass flow and consequently increased heat transfer coefficient. The flow transients can be seen in Figs. 6.2.F2 and 6.2.F3 (Curves J15). After this period, the mass flow decreases drastically due to depletion and low system pressure, the HTC also drops equally fast because the flow is essentially in the steam regime. Fig. 6.2.F9 is a typical quality history for the flow at core midplane. It begins at subcooled

Fig. 6.2.F8

TOP BREAK, A = 1

AVERAGE DNBR, HTC AND CLAD SURFACE TEMPERATURE
IN MIDDLE CORE REGION

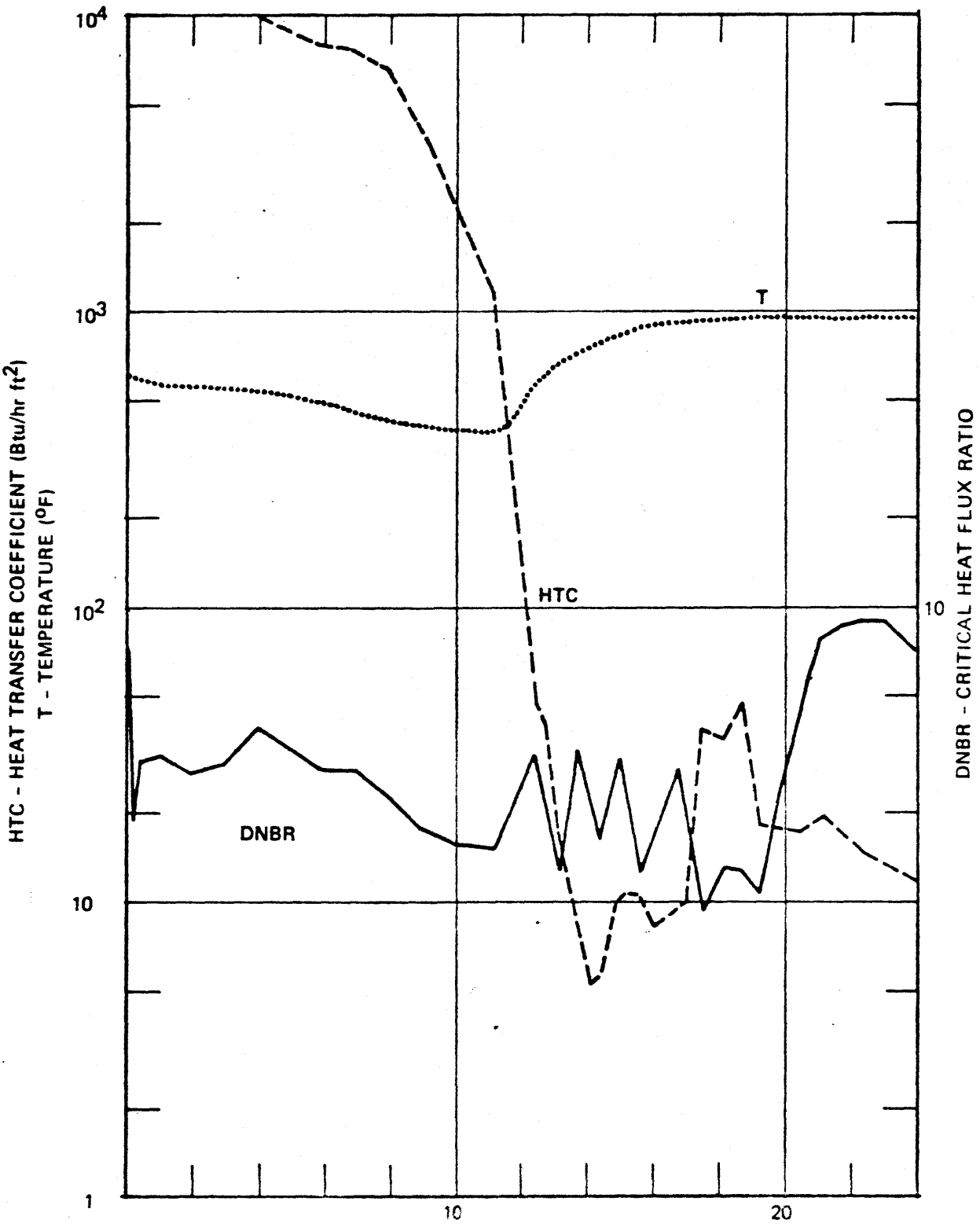

Fig. 6.2.F9
TOP BREAK, A = 2
AVERAGE DNBR, HTC AND CLAD SURFACE TEMPERATURE
IN MIDDLE CORE REGION

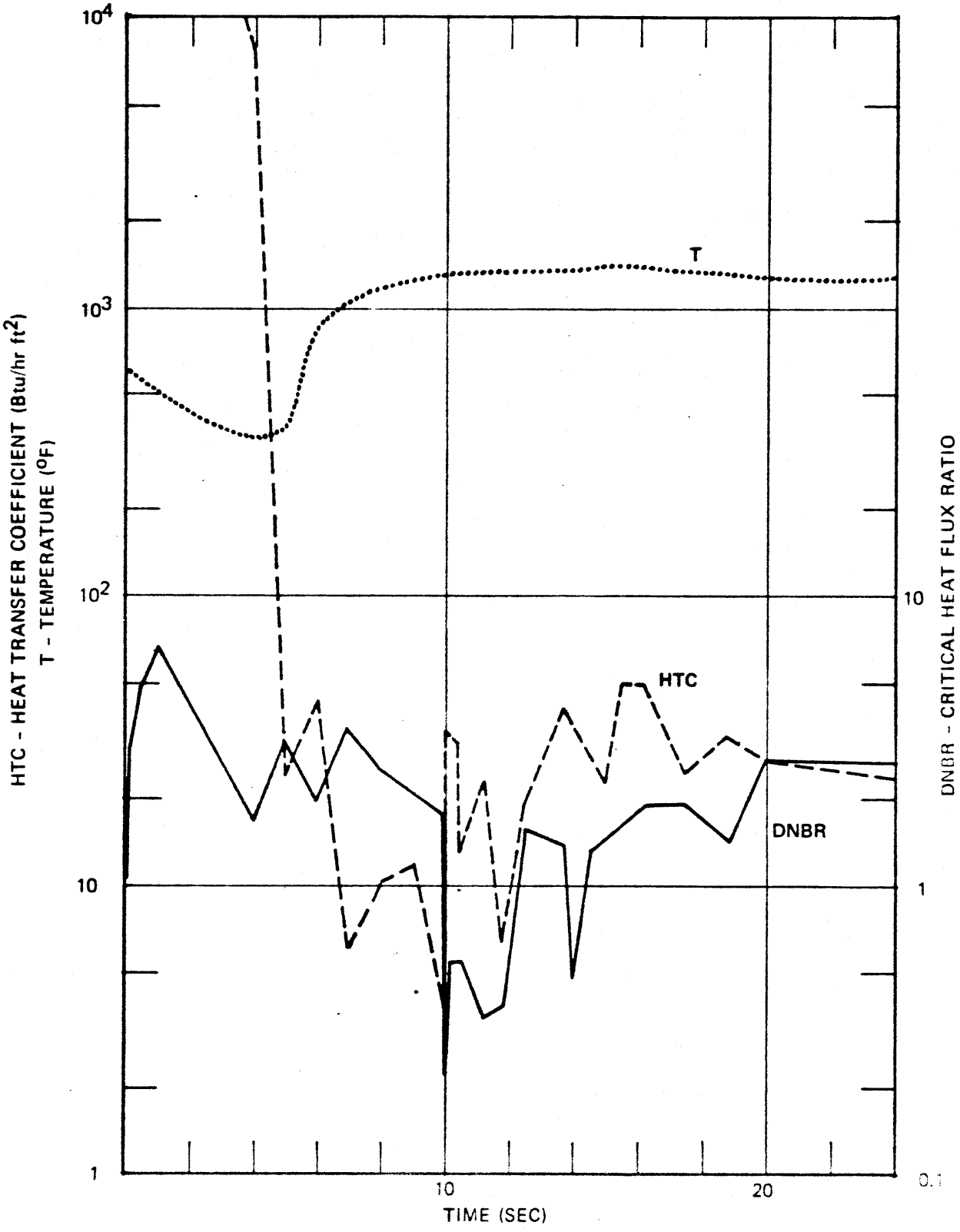

Fig. 6.2.F10
TOP BREAK
AVERAGE DNBR, HTC AND CLAD SURFACE TEMPERATURE
IN MIDDLE CORE REGION

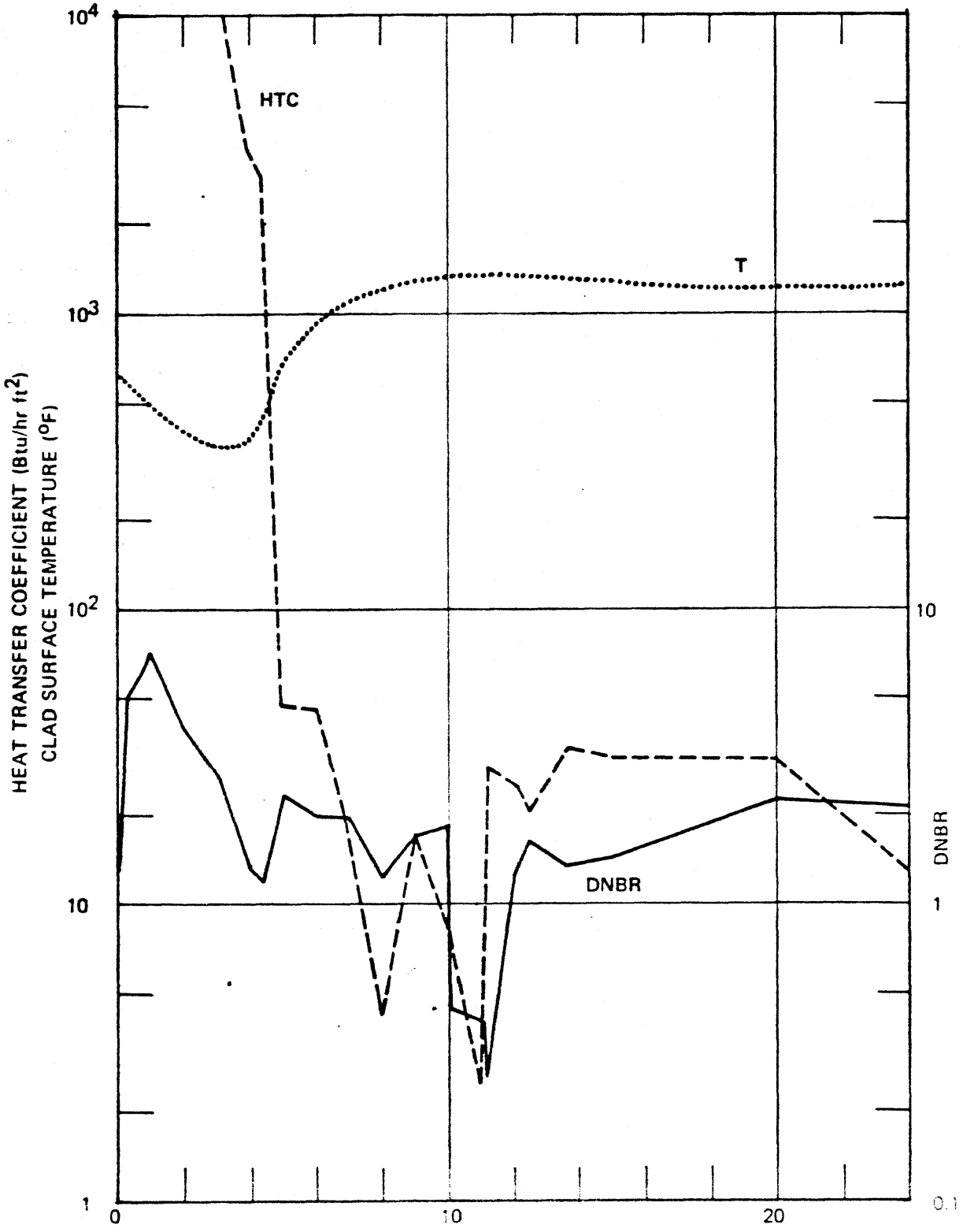

quality (smaller than zero), then increases to 1.0 within 4 to 5 seconds and remains there for a while until ECC water becomes effective. The clad surface temperature climbs most steeply when the flow and the HTC drop steeply. Highest clad surface temperature is reached at the quiescent stage during which only steam is available to cool the core.

The HTC and DNBR curves in Figs. 6.3.F8, 6.3.F9 and 6.3.F10 are not smooth curves. They have been obtained by plotting a few values at finite time intervals, and noting that they are subject to fluctuations due to fluctuations in flow rates, only straight lines have been used to connect these points. The DNBR for small break sizes is above 1 for most of the blowdown period, but for larger break sizes, the DNBR may drop below 1 for a substantial duration beyond 10 seconds. Again, it is during this same duration that the flow quality is 1.0 and the clad surface temperature attains its maximum value.

The observation of the above pattern for the clad surface temperature transient is, in part, due to the nature of RELAP3. As the code uses the assumption of thermodynamic equilibrium, the injected ECC water would be instantaneously mixed first in the cold legs, dropping the enthalpy and pressure of the coolant there. This necessitates the filling of the cold legs before the water can be transported to other parts of the primary system. The core mass flow in the quiescent period between 4-5 seconds and 14-16 seconds consists mainly of steam evaporating from the primary coolant that remains in the lower plenum. At about 14-16 seconds, the cold legs have been filled, and the ECC water starts flowing towards the downcomer, the lower plenum, and becomes effective in cooling the core. The clad surface temperature

subsequently drops. In reality, some ECC water is expected to be entrained before the cold legs are filled, thus the clad surface temperature should not reach as high a maximum as shown in Fig. 6.2.F11.

Fig. 6.2.F12 also shows a most interesting feature of the clad surface temperature transients. This feature is the asymptotic configuration assumed by clad surface at the middle core region as the break size is larger than twice the flow area of the cold leg. The maximum of this asymptotic configuration is some 1320°F, a value that compares well with LOCA by pipe break. Explanation of this behavior can be stated as follows: The clad temperature transient is determined by the energy inventory in the fuel for redistribution, the fission products decay heat, and the heat removal at the clad surface. The fission products decay heat is practically the same for all break cases. The initial energy inventory in the fuel is also the same. Previous sections concerning core flow rates and HTC have shown that the heat transfer is very effective in the first 4 seconds for large break sizes. Thus the clad temperature drops and reaches practically the same minimum as shown in Fig. 6.2.F10. At this time, the fuel energy has been substantially redistributed. Moreover, the leftover inventory for removal does not differ greatly for different break sizes. At the steam cooling stage, HTC is of the order of 10 - 30 Btu/hr. ft^2, again not varying too much for different break sizes. With all these factors taken into account, that is, with the almost same heat inventory, the same heat production, the same starting temperature, and almost the same HTC, then it is not surprising that the clad temperature should assume almost the same transient.

Fig. 6.2.F11
TOP BREAK, A = 2
FLOW QUALITY (X) AND AVERAGE CLAD SURFACE TEMPERATURE (T) IN MIDDLE CORE REGION

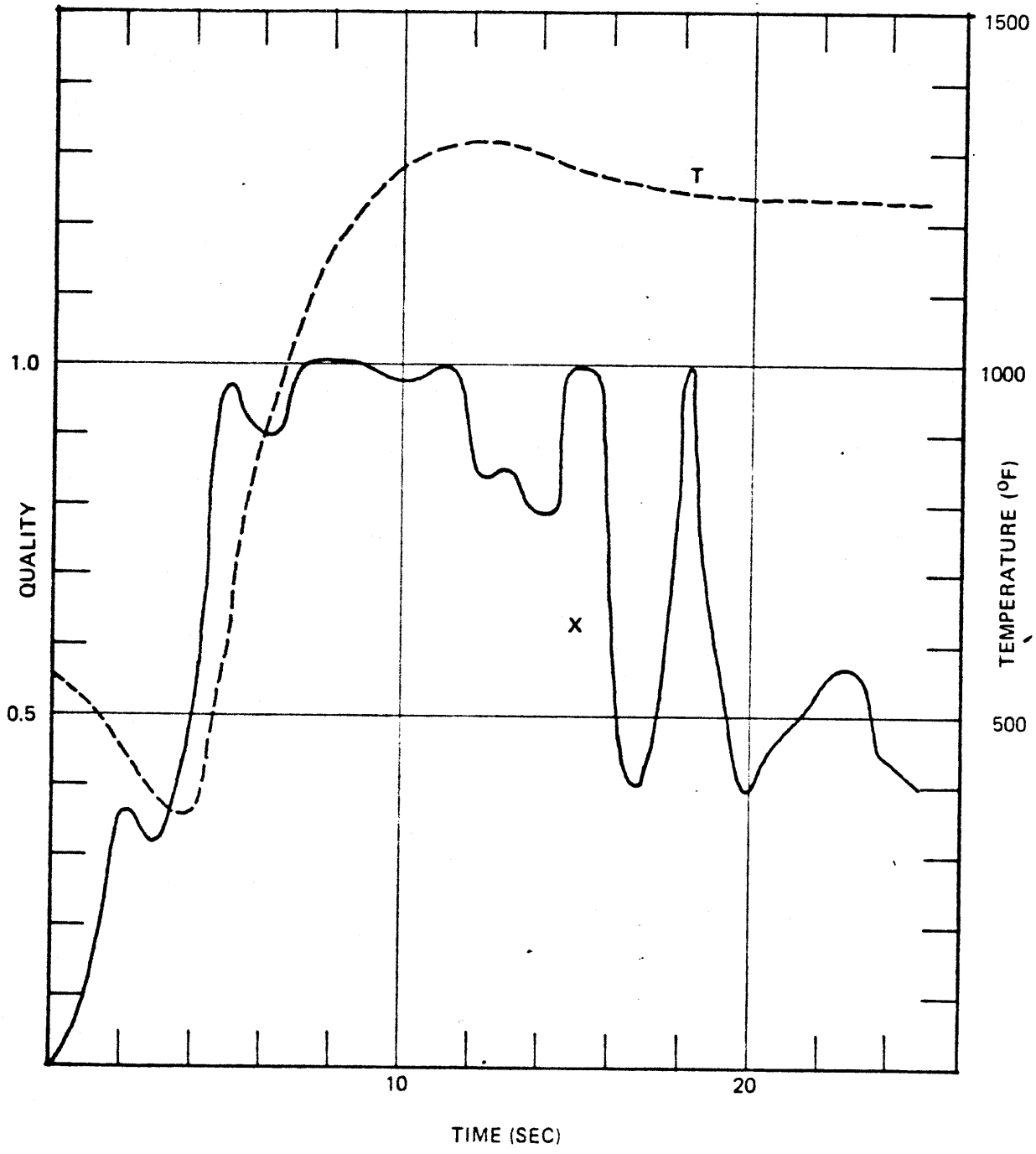

Fig.6.2.F12

TOP BREAK
AVERAGE CLAD SURFACE TEMPERATURE
AT MIDDLE CORE REGION

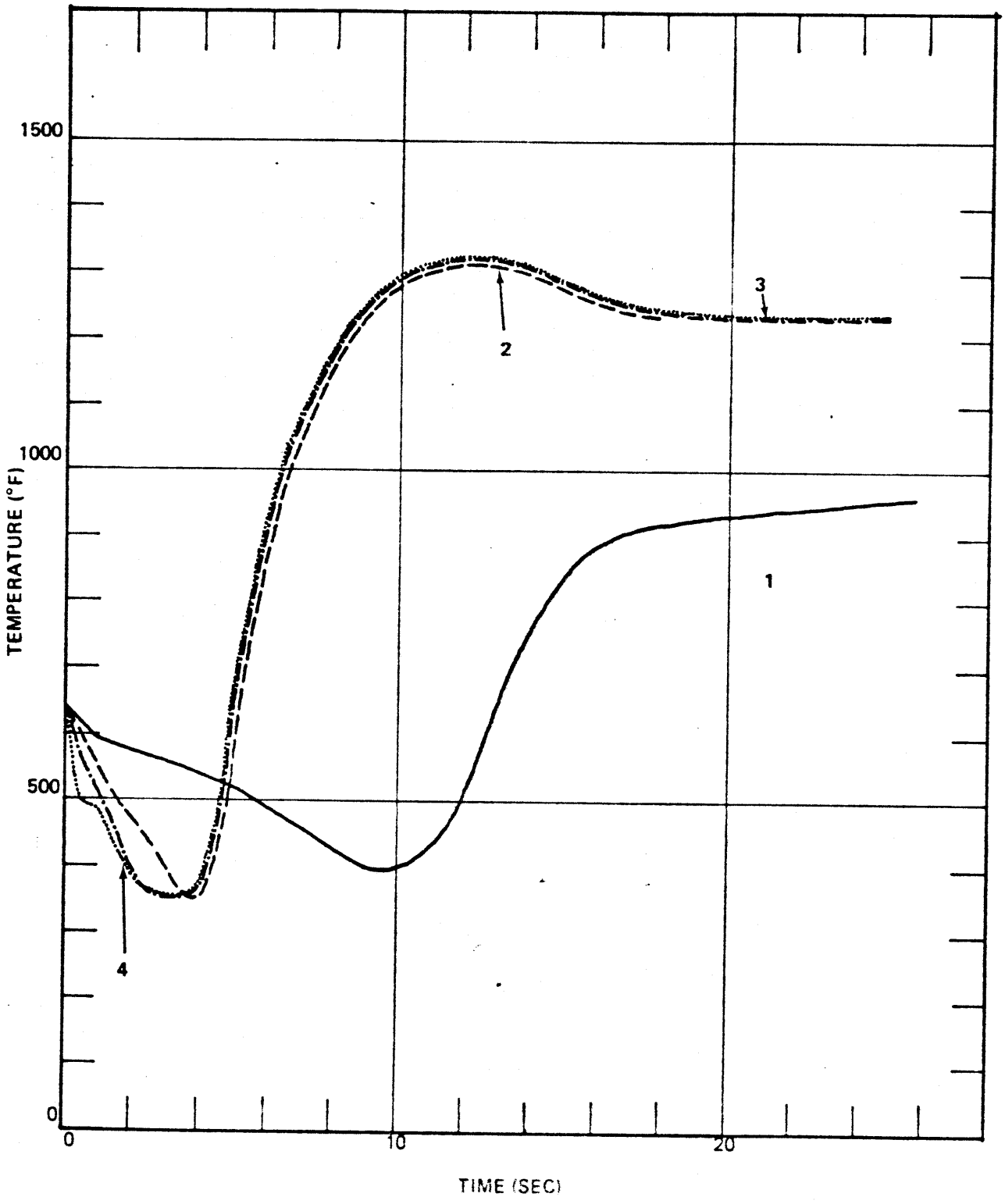

For break sizes larger than 4 hot leg flow area, the asymptotic temperature configuration should still be the same.

6.3 Conclusions

The loss of coolant accidents by hypothetical reactor vessel break at the top have been studied with the WHAM and RELAP3 computer codes. The principal parameters and processes under investigation are the subcooled pressure differentials across the core and core barrel, the peak subcooled force loadings, the normalized power history, the flow rates, and mass loss histories, the coolant remaining in the lower plenum, and the average clad surface temperature transient in the middle region of the core. The parameters that have been changed to investigate their sensitivity to the blowdown processes are the break time, break size, and fuel clad gas gap conductivity.

It is found that the pressure and force loadings on vessel internals increase with increasing break size but would level out to a maximum value as the break size becomes large. For a given break size, the loadings decrease as the break time increases. The loadings arisen in the case of a one-pipe-size instantaneous top break are slightly higher than those reported for the case of a LOCA by double-ended hot leg break.

Void formation caused by system depressurization has been solely responsible for tripping the reactor. The normalized power history for the cases of one-pipe-size and two-pipe-sizes break brackets pretty well the normalized power history reported for the same plant for the case of LOCA by double-ended hot leg break.

Unlike bottom and side vessel breaks, the break at the top does not lead to flow reversal in the core for break sizes of one pipe size or smaller, there is some fluctuation in the flow across the core and in the hot legs which are caused by the combination of the depressurization by mass loss and the flashing of liquid at various regions of the system. When the break size is two-pipe-sizes or larger, the depressurization by mass loss has the overriding influence, and the fluctuation is no longer noticeable except at the steam flow stage at the end of the blowdown.

The end of blowdown is approximately 12.8 seconds for the one-pipe-size break. For break sizes twice the flow area of the hot leg or larger, the flow out of the break may be temporarily zero at around 4 seconds, but would again resume significantly because there is still considerable coolant in the primary system. With the slight modification of EOB as the time when no significant flow exists out of the break, EOB for all large break sizes falls into the range of 7 to 8 seconds, i.e. similar to the case of bottom and side breaks.

The blowdown and its consequences in the case of a top break seems to be better behaved than in the case of a bottom or side break. Typical examples are the behavior of the coolant mass remaining in the lower plenum, the pressure history in the lower plenum, and the transient of the average clad surface temperature in the middle core region. As the break increases in size, the coolant mass remaining in the lower plenum and the lower plenum pressure assume asymptotic configurations which clearly indicate a limiting value for these quantities. The clad surface temperature starts out at the steady state value (around 621°F), drops to approximately 350°F in about 4 seconds, then

rises steeply to reach a peak just above 1300°F at 12 to 14 seconds. This transient pattern is the same for 2-, 3-, and 4-pipe-size breaks. It is argued that this is the limiting configuration for the average clad surface temperature in the case of a vessel top break without change in core geometry. This configuration is comparable and not worse than the transient of the clad temperature in the case of a LOCA by double-ended pipe break reported in the literature.

The break time is sensitive to the subcooled loadings but is rather insensitive to the two-phase blowdown processes. The correct determination of the fuel-clad gas gap conductivity, however, is quite important for the transient of the clad surface temperature.

CHAPTER 7

BOTTOM BREAK: RESULTS AND DISCUSSIONS

LIST OF FIGURES AND TABLES

7. BOTTOM BREAKS: RESULTS AND DISCUSSIONS

The location of the bottom break has been selected at the weld zone between the lower hemispherical head and the cylindrical section of the vessel. A break at a lower elevation should not change the basic phenomenologies except a possible smaller mass remaining in the lower plenum after end-of-blowdown. A sensitivity study has been made to examine the effect of a break at a lower elevation on the processes and parameters under investigation.

Irrespective of break elevation, a break at the lower vessel plenum would foreclose any chance of reflooding the core. In the event of such a break, alternate emergency core cooling location beside the cold legs is, therefore, warranted. The present analyses include cases when the ECC injection nozzles are shifted from their ordinary cold leg location to the hot legs of upper plenum.

The unit break size under study is 4.12 ft^2 which is the flow area of the 27-1/2 inch cold leg. Break sizes in multiples of 1, 2, 3 and 4 that area have been investigated.

Similar to the cases of top breaks and side breaks, two different sets of break time have been used. For WHAM computations of subcooled pressure and force loadings which involve the velocity of sound in the subcooled fluid, break times of 0.00025 second, 0.01 second, and 0.1 second have been investigated. The 0.00025 second break time has been termed "instantaneous" because it takes twice that time for the sound wave to travel across the break.

TABLE 7.0.T1

BOTTOM BREAK

CASES UNDER INVESTIGATION

Regime	Break Size (1)	Break Time (sec)	Accident Time Investigated (sec)	Remarks
Subcooled Depressurization	1.2	0.00025	0.06	Three break time for each break size
	3&4	0.01&0.1		
Two-Phase Blowdown	1	0.01	25	
	1	0.1	40	
	2	0.01	25	
	2	0.1	25	cold leg ECC injection
	2	0.1	25	hot leg ECC injection
	2	0.1	25	upper plenum ECC injection
	2	0.1	25	Break at lowest point
	3	0.1	25	
	4	0.1	40	

(1) Break size is in multiples of 4.12 ft^2, the flow area of the cold leg.

(4/80)

For RELAP 3 computations of two-phase blowdown, the break time of 0.1 second has been employed throughout, except for a few cases when a break time of 0.01 second has been used to find out the sensitivity of basic blowdown parameters to the break time.

Table 7.0.T1 lists the cases investigated.

7.1 Subcooled Depressurization

Similar to the top break, the subcooled depressurization of the primary system has been studied with the WHAM computer code. Description and verification of this code have been given in Chapter 4. The logical network used to describe the primary system with a bottom vessel break is shown in Fig. 4.2.F2. The dimensions, fluid conditions and noding characteristics of this logical network are presented in Table 7.1.T1.

At normal operation and during the entire duration of the subcooled depressurization, the fluid in the primary system is subcooled. Initial conditions are that of the coolant at normal operation. In the nodalization of the primary system, it has been necessary to lump the space-dependent conditions into discrete ones for each node, with proper consideration for the geometry of the flow paths. Two factors have been neglected, namely the effects of friction and of the coolant pumps. Both of these effects have been shown by Fabic (F3) and Gruen (G2) to be negligible when the decompression is violent and fast.

Table 7.1.T1

BOTTOM BREAK

CHARACTERISTICS OF NETWORK MODELED FOR WHAM

(For Use in Conjunction With Fig. 4.2.F2)

Leg	Initial Pressure (psi)	Initial Velocity(1) (ft/sec.)	Area (ft^2)	Length (ft)	No. of(2) Subnodes
1	2272.5	0	4.12 x (1,2,3,4)		2
2	2269.2	6.5	119.5	3.25	4
3	2265.8	6.5	119.5	1.34	2
4	2262.5	15.5	47.9	3.292	4
5	2254.6	15.5	47.9	3.292	4
6	2246.6	15.5	47.9	3.292	4
7	2238.5	15.5	47.9	3.292	4
8	2236.5	6.9	134.24	4.67	6
9	2236.5	0	134.24	6.32	8
10	2236.5	0	1.0	4.37	6
11	2262.5	1.4	23.44	3.292	4
12	2254.6	1.4	23.44	3.292	4
13	2246.6	1.4	23.44	3.292	4
14	2238.6	1.4	23.44	3.292	4
15	2272.5	-6.0	129.4	5.23	4
16	2276	-29	10.18	6.67	8
17	2279.5	-29	10.18	6.58	7
18	2283	-29	10.18	6.58	8
19	2276	-29	16.54	6.67	8
20	2279.5	-29	16.54	6.58	7
21	2283	-29	16.54	6.58	8
22	2286.5	-29	36.4	4.67	5
23	2286.5	0	36.4	4.67	5
24	2288	-47.54	16.48	21.16	24
25	2203	-37.8	20.81	11.5	13
26	2203	-7.5	105.8	6.22	6
27	2210.5	-15	54.56	26.16	26
28	2225.5	-17.51	54.56	26.16	27
29	2233	-9	105.8	6.22	6
30	2235	-50.47	18.35	17.22	23

(1) Sign of fluid velocity is relative to the positive direction of increasing subnodes in each leg.

(2) Number of subnodes is the integer closest to $L/c\Delta t$.

In this analysis, the pressure and force loadings on principal vessel internals have been studied. The principal vessel internals are the core, the core barrel, the thermal shield and certain components of the reactor core. The vessel break is initiated by prescribing a time t_b over which the leak at the bottom of the vessel opens up from zero to a prescribed size A. Four break sizes, which are respectively 1, 2, 3 and 4 times as large as the flow area of the cold leg, have been studied. For each break size, three break times of 0.00025 second, 0.01 second, and 0.1 second are used.

7.1.1 Transient Pressure Differentials

Fig. 7.1.F1 shows the history of the pressure differentials across the core. Fig. 7.1.F2 shows the pressure differentials across the core barrel. The break time for these cases is 0.00025 sec. which can be termed as "instantanious" because it takes twice that duration for the disturbance to travel through the break. The location of the break is at the buckled zone between the vessel cylinder and the bottom head.

The pressure differentials across the core is oscillatory with magnitudes significantly damped after the first two pulses. The pulse period is approximately 20 msec. which corresponds to a frequency of 50 cps. At normal operation, the pressure differential across the core is 31.5 psi. As the break is located practically at the same elevation as the bottom of the core, the transient starts almost immediately after the start of the break. The net magnitude of the differential increases until the decompression waves have traveled up the top of the core to reduce the pressure there, at which time the pulse turns around and increases past zero to the other direction.

Fig. 7.1.F1

BOTTOM BREAK: HISTORY OF PRESSURE DIFFERENTIALS ACROSS THE CORE

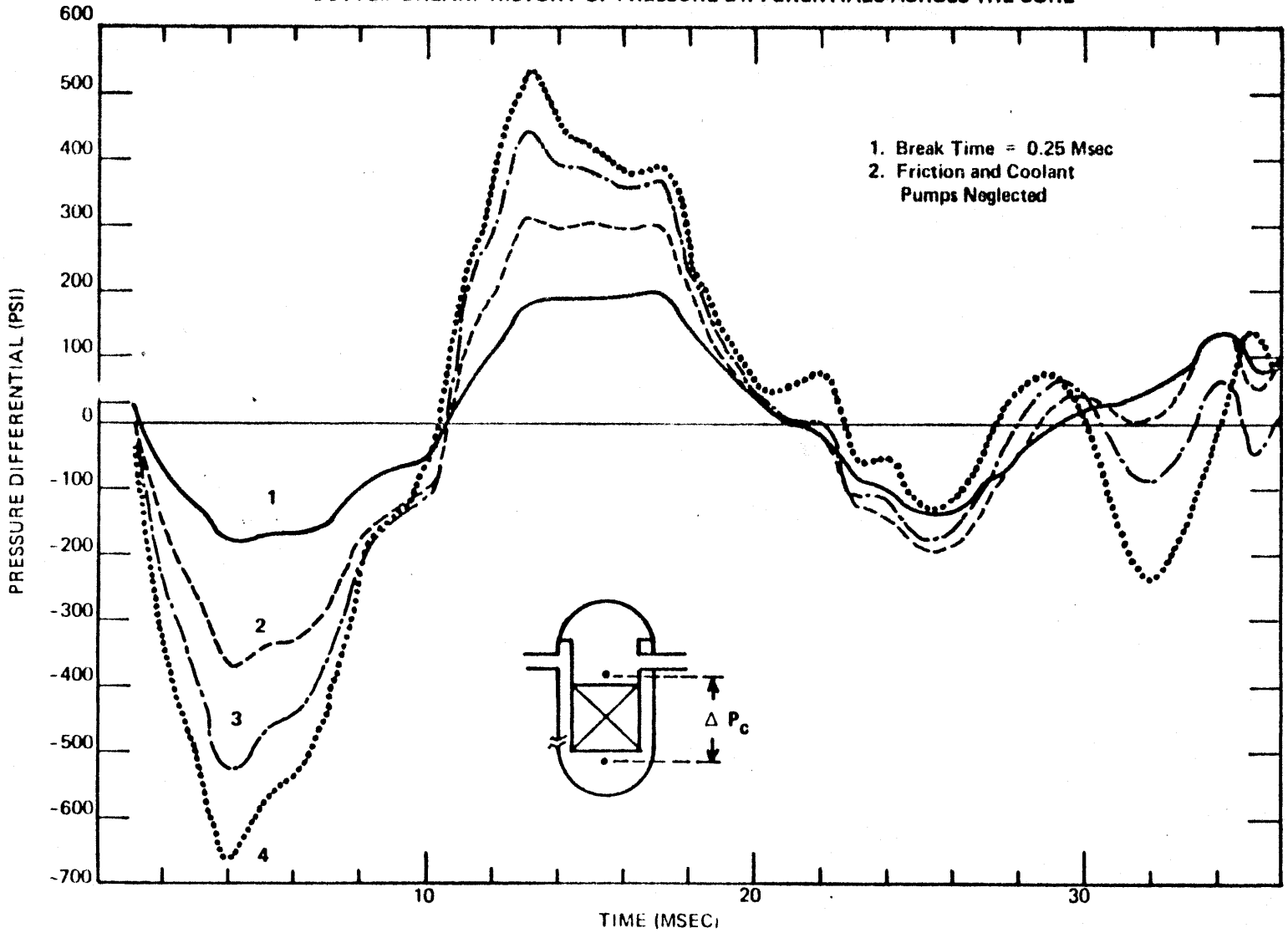

Fig. 7.1.F2
BOTTOM BREAK: HISTORY OF PRESSURE DIFFERENTIALS ACROSS THE CORE BARREL

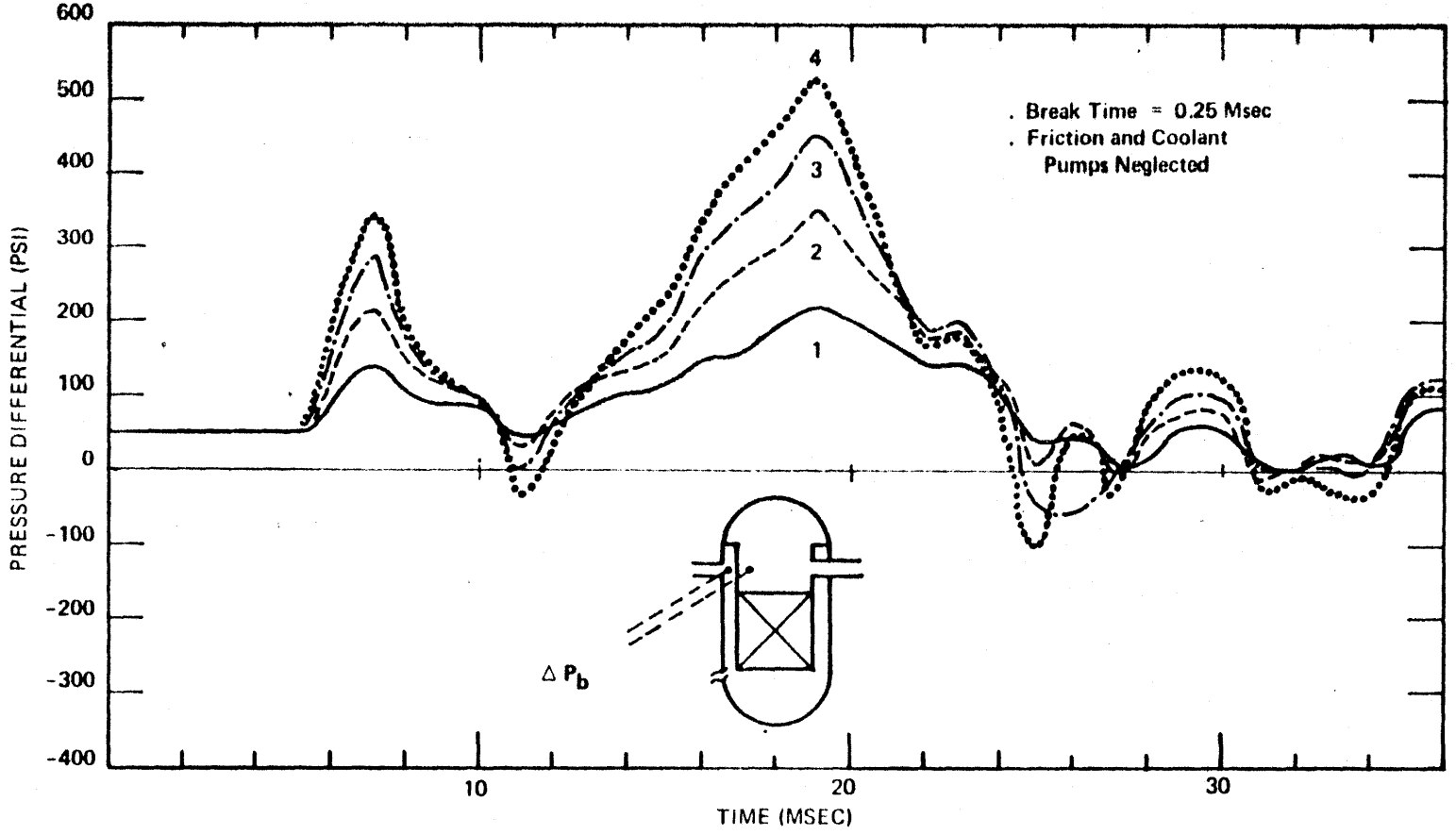

The oscillatory behavior of the pressure loadings is entirely due to the reflection characteristics of the acoustic waves in a closed system. Upon break initiation in the lower plenum, the sudden loss of fluid results in decompression waves which travel from the break to other parts of the system. As the waves encounter changes on their travel path, they are partially reflected. Reflected decompression waves are actually compression waves that travel from other parts of the system towards the break. The combination of these two opposing trains of waves at any point, with proper consideration for its initial conditions, results in the new physical conditions for that point. As the closed system is well defined with fixed dimensions, the oscillations have a more or less fixed period. (The period actually changes slightly as the sound velocity changes with pressure.)

The history of the pressure differentials across the upper core barrel is interesting in that the differentials are almost always in the inward direction, and that the second pulse is larger than the first pulse. This preferential direction of the pressure differential is due to the fact that the WHAM model (Fig. 4.2.F2) employed in this study has placed the bottom break approximately 10.66 ft. farther from the cold leg nozzles than from the hot leg nozzles (twice the length of Leg L15). It is noted that the differential across the upper core barrel is the difference between the pressure at the cold leg nozzles and the pressure at the hot leg nozzles. The value of this difference at normal operation is approximately 50 psi. Due to the shorter path, the same disturbance can travel to the upper plenum faster than to the cold leg nozzles, thereby depressurizing the pressure in the upper plenum a few milliseconds in advance.

The fact that the second pulse is larger than the first pulse is not readily explicable on the basis of available data. It seems to be due to the complicated combination of waves which go through series of transmission and reflections as well as the time-dependent buildup of these phenomenologies.

In reality, however, it seems that a bottom break would give rise to much less pressure differential across the upper core barrel such as shown in Fig. 7.1.F2. The reason is that it would take the disturbance about the same time to travel to two points on the two sides of the upper core barrel. This argument would be proved by connecting Leg 1 (the break) to Junction J15 (the lowermost point of the lower plenum), or by remodeling Fig. 4.2.F2 in such a way that the downcomer annuli join the break at Junction J2 (Fig. 4.2.F2). These changes have not been included in this study.

The pressure differential across the thermal shield should be nil because disturbance waves traveling upwards from the lower plenum should be the same on both sides of the thermal shield.

7.1.2 Sensitivity of the Pressure Differentials with Respect to Break Time and Break Size

Fig. 7.1.F3 shows a plot of the maximum pressure differential across the core versus break size for two break times of 0.00025 second and 0.01 second. Fig. 7.1.F4 shows a plot of the maximum pressure differential across the core barrel versus break size for three break times of 0.00025 second, 0.01 second and 0.1 second.

Fig. 7.1.F3
BOTTOM BREAK
EFFECT OF BREAK TIME AND BREAK SIZE
ON PEAK PRESSURE DIFFERENTIAL ACROSS REACTOR CORE

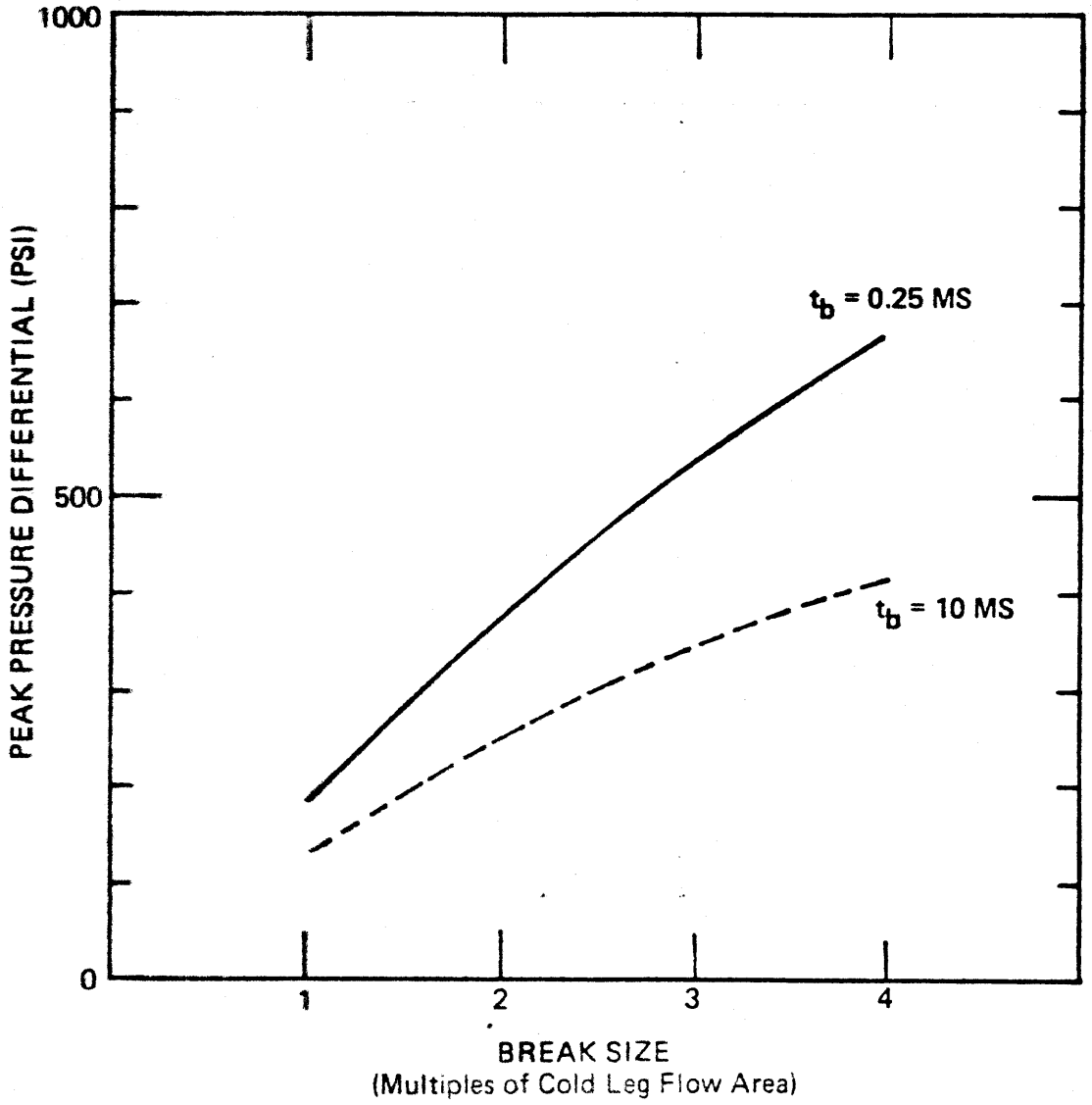

Fig. 7.1.F4
BOTTOM BREAK

EFFECT OF BREAK TIME AND BREAK SIZE ON PEAK PRESSURE DIFFERENTIAL ACROSS THE CORE BARREL

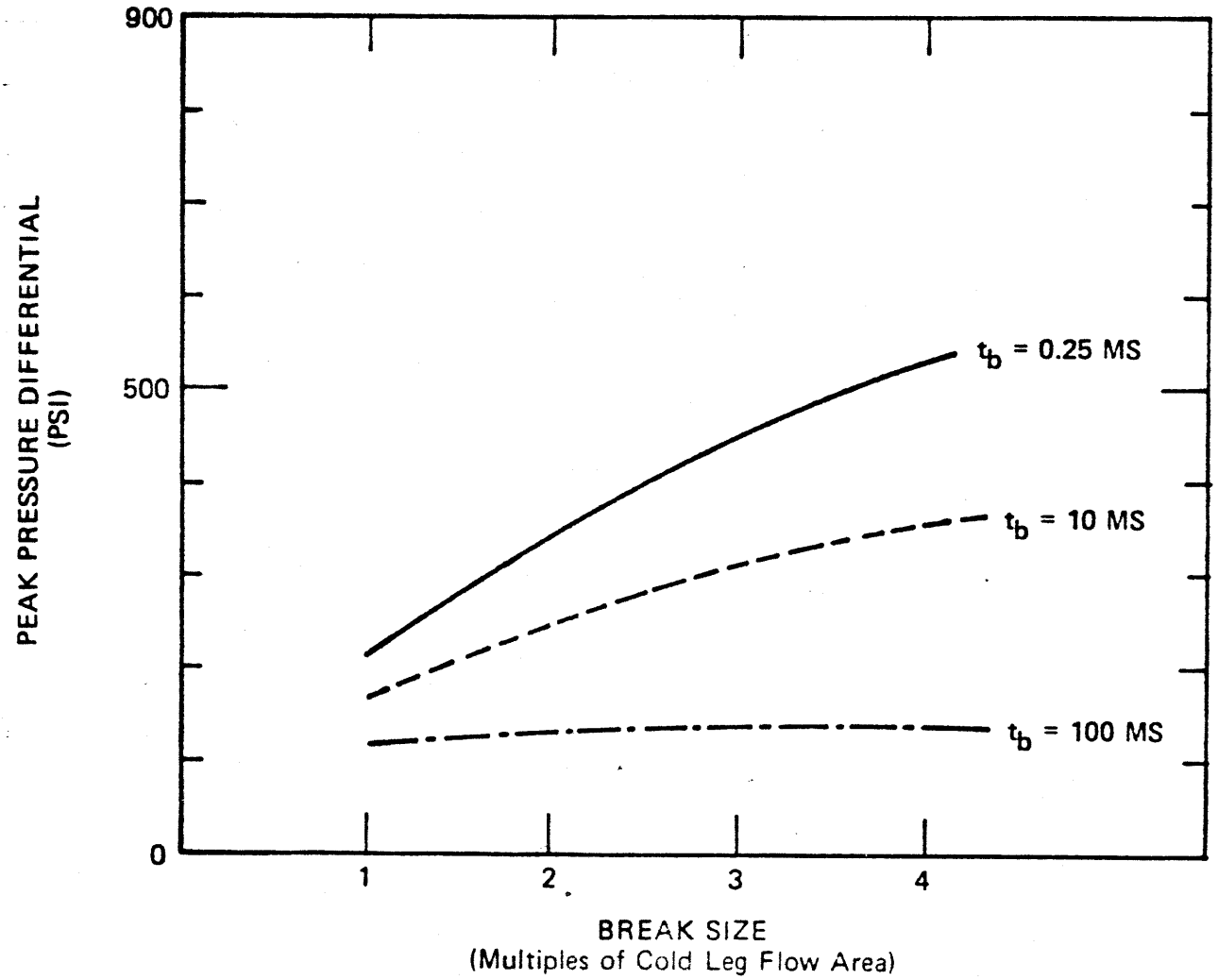

It is seen that as the break size increases linearly from 1 to 4 times the flow area of the cold leg, the maximum pressure differential also increases, but not linearly. There is a trend for the differential to level out as the break size becomes large. Based on the structure of the WHAM code, which assumes a break back pressure the same as the saturation pressure of the subcooled liquid just upstream (p_{sat}), then the largest pressure differential across any vessel internal should be the difference between the local initial pressure and p_{sat}. This largest pressure differential is approximately 1150 psi for the bottom break. The Idaho series of semi-scale blowdown tests has shown that the selection of a break back pressure as p_{sat} yields results close to measured ones (G2), and most LOCA analyses to date have used the same selection (C1, I1). It is felt that if such selection is true for a double-ended pipe break with coolant being discharged directly into the containment, it must also be true for a vessel break which discharges the coolant to the containment via the vessel pit.

When the break time is larger than "instantaneous," the peak pressure differential is smaller. For example, the peak pressure differential decreases approximately 30% when the break time is 10 milliseconds instead of "instantaneous." When the break time is further increased to 100 milliseconds, the reduction is such that the peak pressure differentials are smaller than 150 psi, a value quite negligible indeed in view of the severity of the accident.

The decrease in the pressure loadings at the increase of the break time is, of course, due to the manner disturbance waves travel upstream from the break. The time step of these WHAM computations is 0.25 millisecond. If the break time is 0.25 millisecond, then in only one time step after break initiation, the magnitude of the decompression wave is proportional to the entire break size. On the other hand, if the break time is 10 milliseconds, then the first decompression wave has a magnitude proportional only to 1/40 of the break size. The train of decompression waves in this case, however, consists of waves with increasing magnitudes for the duration of the break time, thereafter the wave magnitudes decrease with respect to time due to lower system pressure. The transmission and reflection of these waves in the primary coolant system would result in a pressure differential pattern with a peak not occurring at the first pulse such as usually the case for the "instantaneous" break.

Comparison with pressure loadings on vessel internals in the case of a vessel side break presented in Chapter 8 indicates that the bottom break is not as severe. The reason has already been mentioned earlier in this section as due to the proximity of the break to the core and to the parallel travel of decompression waves on both sides of the core barrel.

7.1.3 Force Loadings

The force loading on a vessel internal is the vector sum of the hydrostatic force, the friction force, the inertial force, and the body force (gravity). The hydrostatic force is by far the dominant one which gives rise to inertial and frictional forces because it is due to the pressure differen-

tial that the flow is maintained of altered. Gravity is very small compared to the other forces and can be safely neglected. Friction force is also neglected in this work on the basis of analytical and experimental verification by Fabic (F3) and Gruen (G2) that such a practice does not give rise to significant errors.

Table 7.1.T2 lists some values of force loadings across the core. In this case, the combination of the hydrostatic and inertial forces are straightforward because they are both parallel to the flow channels. The inertial force has been computed by WHAM as to represent the accelaration or deceleration of the fluid in the core. The hydrostatic force has been obtained by multiplying the pressure differential across the core to the cross section of the core inside the baffle, which is 96 ft^2.

Since the relationship between the fluid pressure, velocity and force loading is one to-one, the time history of the loadings should be similar to that of the pressure differentials such as presented in Fig. 7.1.F1. Due to this reason, only two values of the loadings for each break case have been presented in Table 7.1.T2, one at the time of a peak pressure differential, the other at a time when the pressure differential is essentially nil. The corresponding net loadings in this table attest to the statement that the loadings are high when the pressure differentials are high.

Similar to the top break cases, an approximate loading on each fuel

Table 7.1.T2

BOTTOM BREAK

SOME VALUES OF FORCE LOADINGS ACROSS THE CORE*

Cases	Inertial Force (10^6 lbs)	Hydrostatic Force (10^6 lbs)	Total (10^6 lbs)
At 4 msec. peak			
A = 1	1.2758	-2.4980	-1.2222
A = 2	2.4029	-5.0458	-2.6429
A = 3	3.3952	-7.2770	-3.8818
A = 4	4.2659	-10.5753	-6.3094
At 21 msec. low			
A = 1	0.1523	0.0567	0.2090
A = 2	0.2717	-0.0843	0.1874
A = 3	0.2638	0.1106	0.3744
A = 4	0.0710	0.7451	0.8161

* Forces due to momentum flux change, friction and gravity are neglected. Cross section of the core is taken as the area inside the baffle, or 96 ft^2. Positive direction of the force is upwards (arrow in Fig. 4.2.F2).

TABLE 7.1.T3

BOTTOM BREAK

LARGEST SUBCOOLED FORCE LOADING PER ASSEMBLY

Break Size	Peak Loading (lbs)
A = 1	6,332
A = 2	13,694
A = 3	20,113
A = 4	32,691
LOCA By Cold Leg Break*	9,900

* From Reference C1, Section 14.3.2.2.6 (Revised)

assembly can be obtained by dividing the net core loading by 193 fuel assemblies. The results lts for the four break cases together with the value given by the manufacturer for the LOCA by pipe break are given in Table 7.1.T3. It is seen that the force loadings on each fuel assembly is larger the larger the break size, but for the 1-pipe-size break case, the loading is only 65% of value presented by the manufacturer for the LOCA by cold leg break.

This analysis has not included computations of force loadings on the core barrel and other vessel internals. It is because the force loadings on the core barrel are both space and time dependent. It is further complicated by the argument presented in Chapter 4 that the approximation of the downcomer annuli as one-dimensional flow tubes may not be a rigorous (although conservative) representation of the physical system. However, the force loading on the core barrel should be recognized as consisting of three components. The first component is the hydrostatic force which is always perpendicular to the barrel surface, hence is alternating between compression and tension in effect. The second is the combination of friction and inertial forces which act parallel to the surface and on both sides of the core barrel. These two components should be simple to calculate for every elevation of the barrel, hence for its whole length by numerical integration. The third component is the horizontal or torsional inertial force resulting from cross flow in the downcomer annuli is not assessable with the techniques and assumptions employed in this study.

7.2 Two-Phase Blowdown

As having been mentioned at the beginning of this chapter and elsewhere in this study, the basic tool of analysis for the two-phase blowdown

processes is RELAP 3, Mod 36 (R2). Plant initial conditions are as described in Chapter 5. The break location is selected at the weld zone between the hemispherical head and the cylindrical section of the vessel. Break sizes are in multiples of cold leg flow area, which is 4.12 ft^2. The basic break time is 0.1 second, although a break time of 0.01 second has also been studied to examine the effect of this parameter on the blowdown processes. The main blowdown processes under investigation are the normalized power history, the flow reversal, the coolant flow in different parts of the primary system, the history of mass loss, the pressure history in the upper and lower plenum, the heat transfer coefficient, the critical heat flux ratio, and the behavior of the average clad surface temperature transient.

All values computed by RELAP 3 are averaged values in the nodal volumes of junctions modeled to represent the physical primary loop. This model has been shown in Fig. 5.3.F1.

7.2.1 Normalized Power History

Fig. 7.2.F1 shows the normalized power history for the four bottom break cases and the case for LOCA by double-ended pipe break which is provided by the manufacturer (C1).

Void formation has been solely responsible for reactor scram because control rod action has been assumed not to take place until 30 seconds after the start of the break. Fuel, moderator and other metal temperature coefficients are practically constant and negligible for the first fraction of a second.

(157)

Fig. 7.2.F1
BOTTOM BREAK
NORMALIZED POWER HISTORY

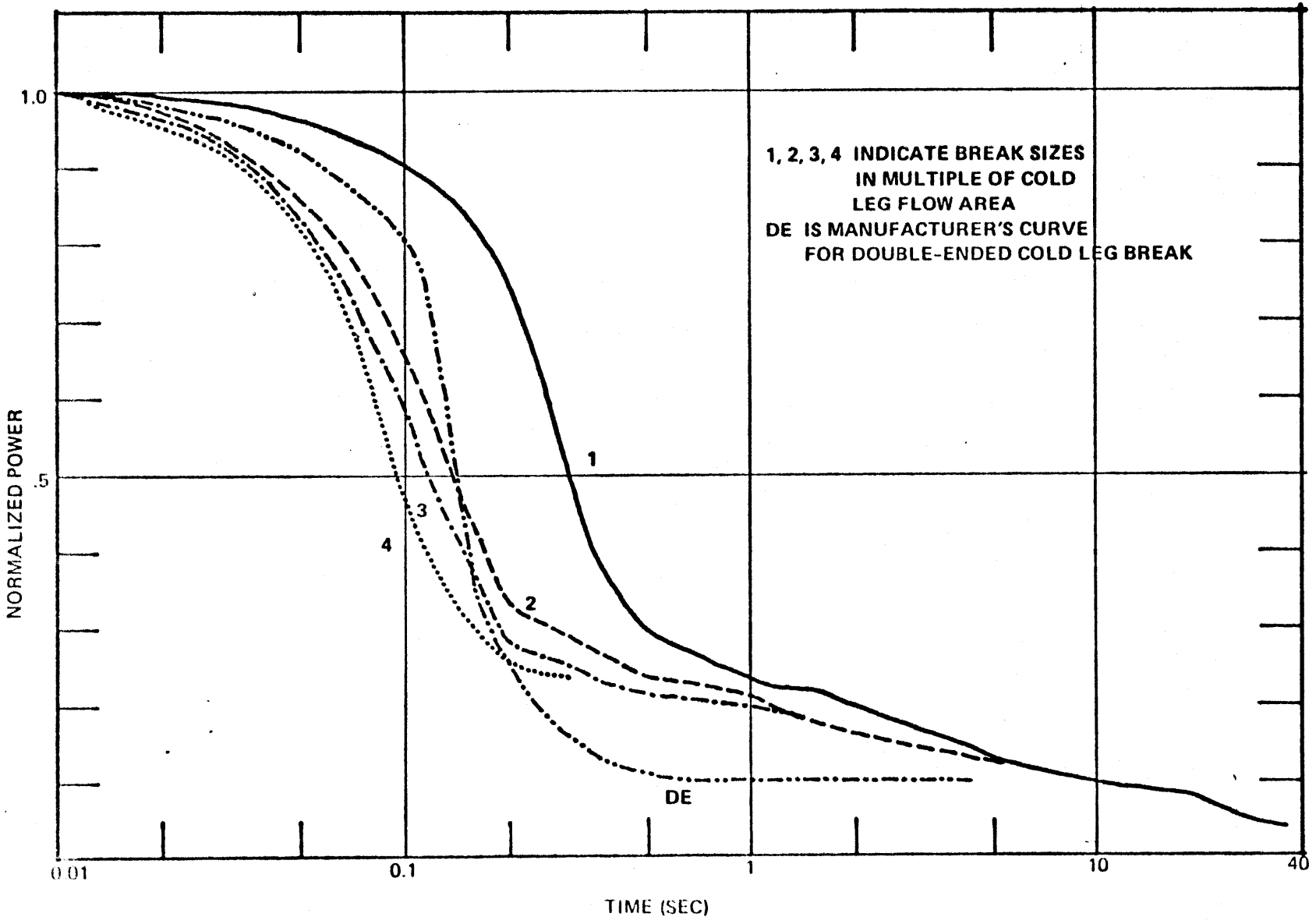

(157)

(158)

Fig. 7.2.F2
BOTTOM BREAK
EFFECT OF BREAK TIME ON NORMALIZED POWER HISTORY

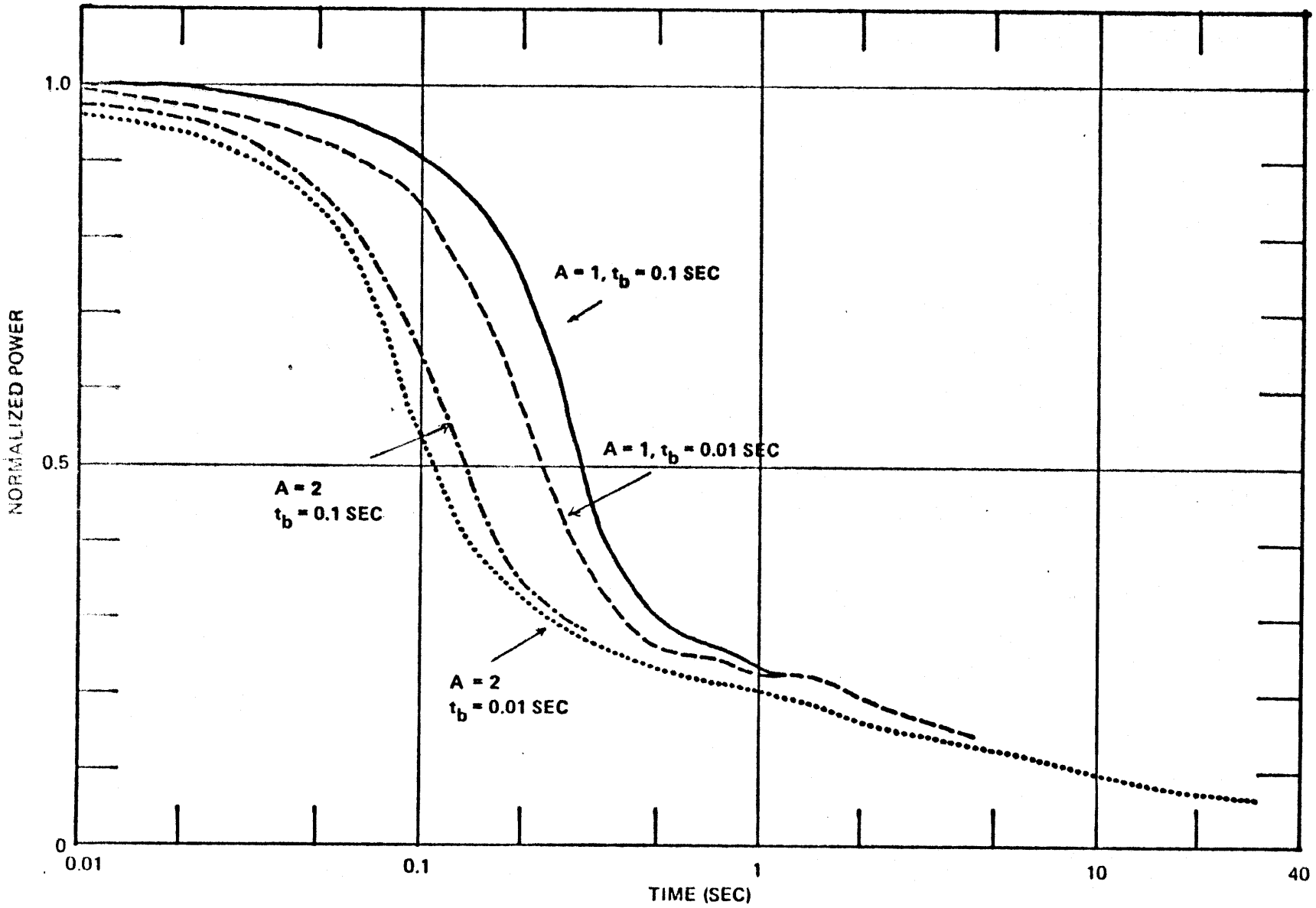

(158)

It can be seen that the larger the break size, the faster the reactor scrams. Cases for break sizes of 1 and 2 times the flow area of the cold leg bracket pretty well the case for double-ended pipe break. At times larger than 0.1 second, the normalized power curves for all vessel break cases in this study lie above the curve for double-ended pipe break supplied by the manufacturer. This is due to the fact the present study has conservatively overlooked control rod action and other coolant and metal reactivity coefficients while the DE curve takes these into account.

Superposition of curves in Fig. 7.2.F1 on corresponding curves for the top break (Fig. 6.2.F1) show that the bottom break cases cause a faster reactor scram. This is true despite the top breaks are slightly larger in net sizes and the break times are also shorter. Furthermore, the power curve for the case of one-pipe-size break does not show the obvious power leveling at around 1 second as in the case of the top break. The only reason for these observations is that a break at the bottom involves more subcooled liquid and thus a faster depressurization.

Fig. 7.2.F2 further shows that a smaller break time (0.01 second instead of 0.1 second) would bring about a faster reactor scram. However, the time needed for the power to drop to a certain level, say 30%, is only slightly different for the two cases. It is shown in Chapter 9 that except for these small differences which do not bring about significant consequences, the break time is rather insensitive to most of the two-phase blowdown processes.

7.2.2 Flow Reversal

A break in the lower plenum is different from a break in the upper plenum in that there is a flow reversal across the core in the former case. As the break opens up, allowing subcooled liquid to escape, the pressure in the lower plenum quickly drops. Whereas the pressure differential across the core in normal operation is of the order of 30 psi, the upper plenum now has a much higher pressure than in the lower plenum. The flow through the core, therefore, slows down and reverses its direction in order to allow coolant from the upper plenum to flow towards the break.

Flow reversal takes place faster the bigger the break and the smaller the break time. For the relatively long break time of 100 msec, the reversal happens at 55 msec for 2-, 3-, and 4-pipe-sizes breaks. In all cases, trip signal for break actuation occurred at 5 msec, a preassigned value inputted into RELAP 3. For a break time of 10 msec instead of 100 msec, the flow reversal happens within 10 msec after the break actuation, indicating that the flow reversal is entirely governed by the pressure differential across the core.

Fig.7.2.F3 shows the flow reversal for the different break cases. Except the lower plenum, coolant in the entire primary system is still subcooled when flow reversal occurs.

Fig. 7.2.F3
BOTTOM BREAK, t_b = 0.1 SEC
FLOW REVERSAL

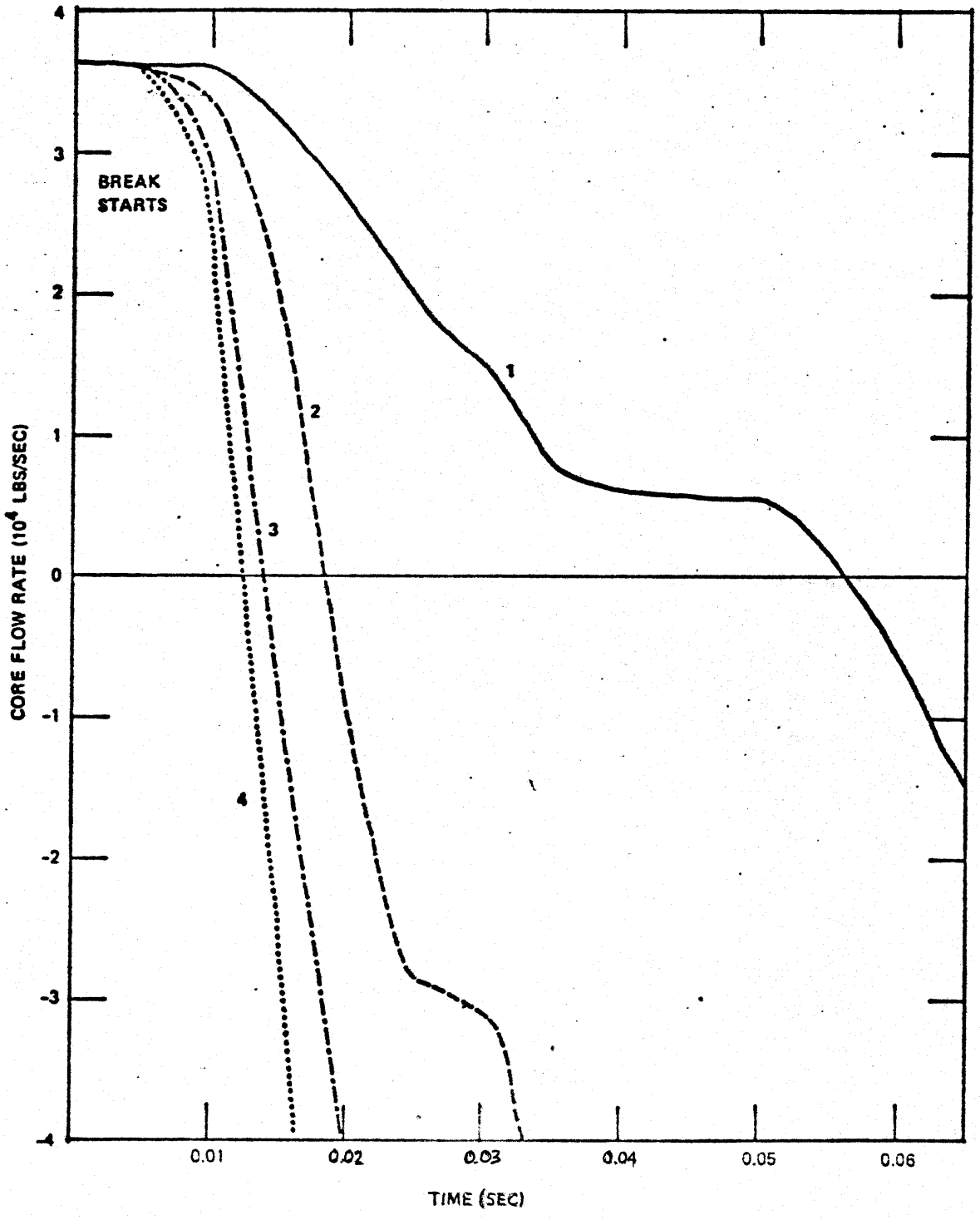

7.2.3 Pressure Histories in the Upper and Lower Plena

At normal operation, the coolant in the lower plenum is approximately at 555°F, 2272 psi, while that in the upper plenum is approximately at 613°F, 2236 psi. The pressure drop across the core is 31.5 psi.

Figs 7.2.F4, 7.2.F5, and 7.2.F6 show the pressure histories in the upper plenum and lower plenum respectively for the break sizes of 1, 2, 3 and 4 times the area of the cold leg cross section.

As having been pointed out previously, the largest pressure differential across the core occurs during the subcooled blowdown period. The portion of the curves in Figs. 7.2.F4 and 7.2.F5 between 0.01 second and 0.1 second would not tell the same kind of details as Fig. 7.1.F1 would. However, beyond 0.1 second, the obvious trend is that the difference in pressure between the upper and lower plena is larger the larger the break size. The drop in pressure in the lower plenum is very rapid while the drop in pressure in the upper plenum is slower thanks to the farther location of the upper plenum from the break.

Figs. 7.2.F4 and 7.2.F5 show some evidence of flashing at around 0.2 second when the pressure in the upper plenum has a plateau at approximately 1500 psi and the pressure in the lower plenum has a plateau at approximately 1100 psi. Another plateau between 0.5 and 1 second is due to limiting flow that takes place in various flow paths of the primary system.

Fig. 7.2.F4
BOTTOM BREAK, A=1
PRESSURE HISTORY IN UPPER AND LOWER PLENA

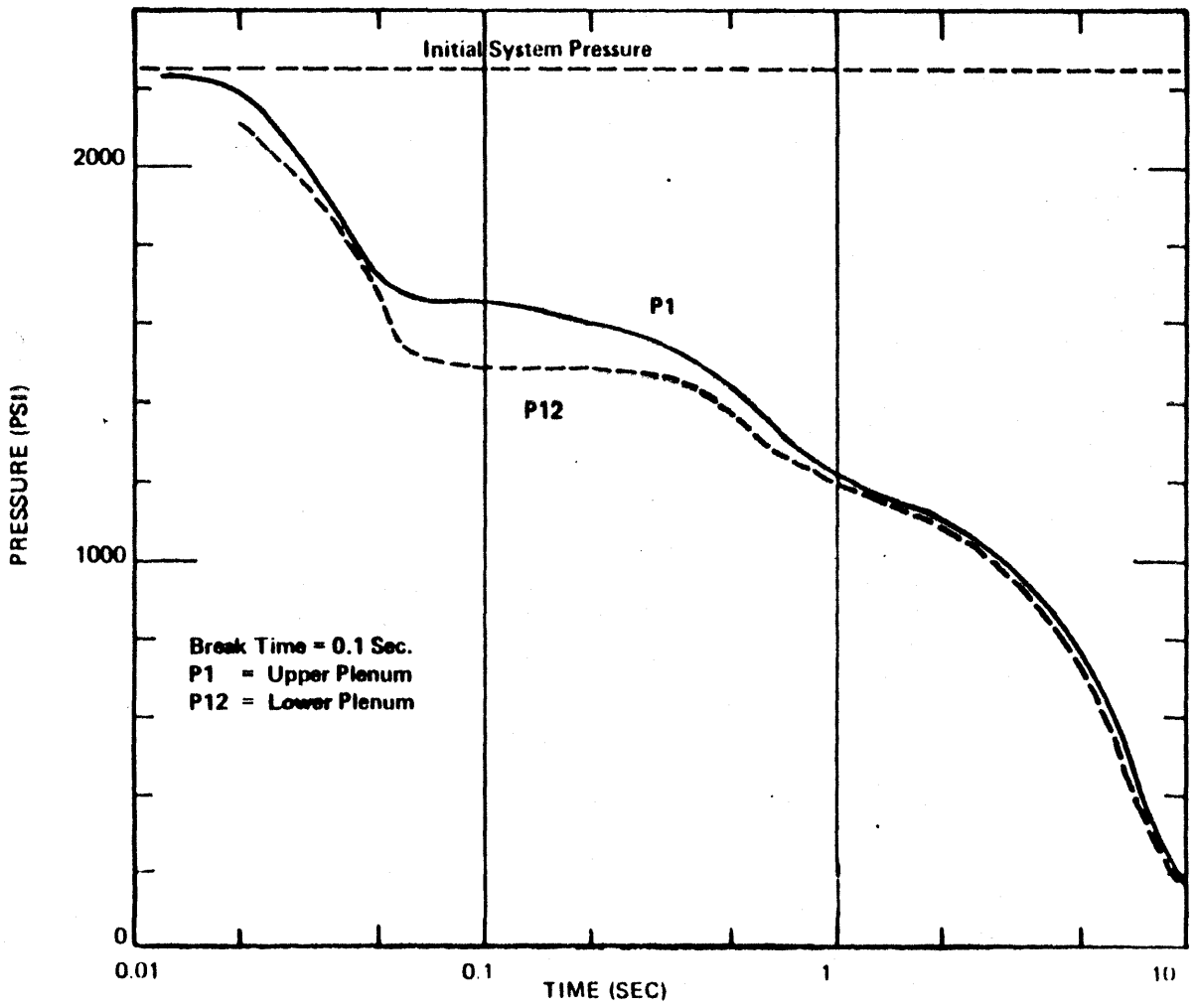

Fig. 7.2.F5
BOTTOM BREAK, A=2
PRESSURE HISTORY IN UPPER AND LOWER PLENA

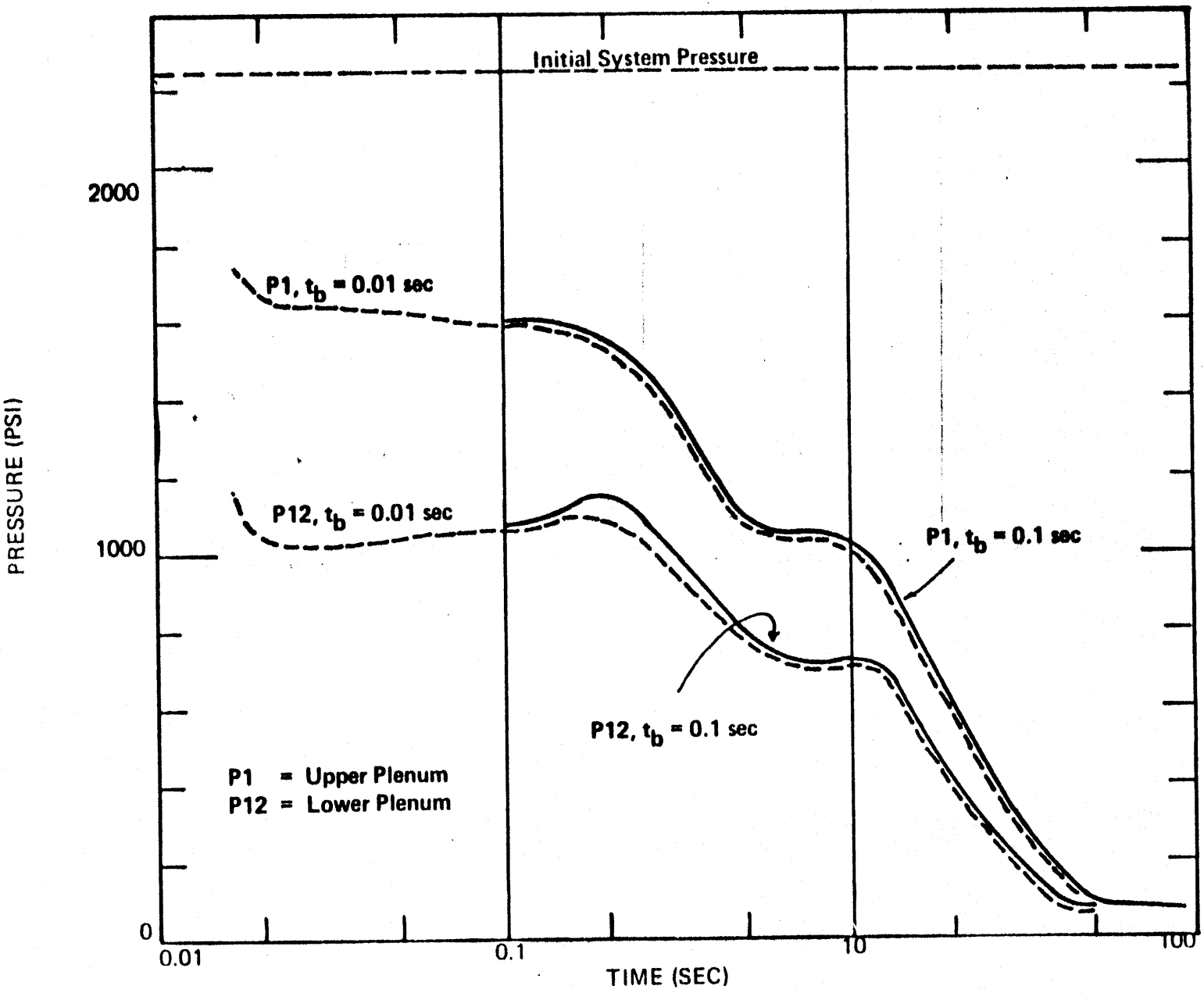

Fig. 7.2.F6
BOTTOM BREAK, A = 3 & 4
PRESSURE HISTORY IN UPPER AND LOWER PLENA

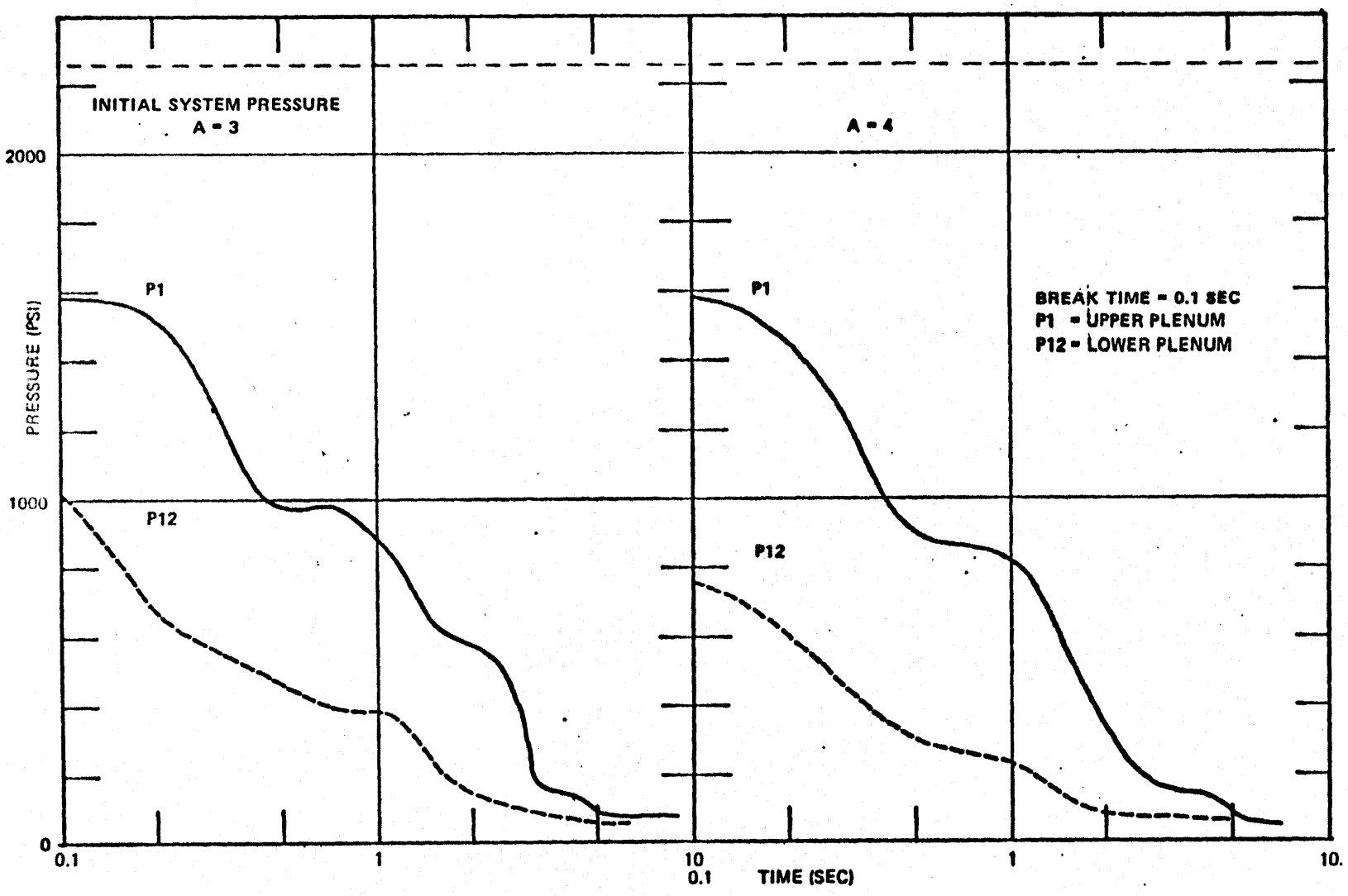

7.2.4 Flow Rates

Figures 7.2.F7, 7.2.F8 and 7.2.F9 show the flow histories for a certain flow paths of the primary system after onset of the bottom break. Notations of the curves correspond directly to the flow junctions of the model as presented in Fig. 5.3.F1. Thus, J19 represents the ECC injection flow rates, and J20 represents the flow out of the break. The flow rate at the midplane of the core has been taken as the average of the flow rates at Junctions J15 and J16 which constitute the two ends of the middle core region.

A prominent feature of the flow pattern in the primary system subsequent to a vessel break in the flow choking that takes place in junctions of small cross sections and high friction. This feature has not been displayed satisfactorily in Figs. 7.2.F7, 7.2.F8 and 7.2.F9 except for the break flow in those figures. A close examination of the flow pattern for the case studied reveals the following flow paths that are most likely to be the site of choking flow: the break, the downcomer annuli, the cold legs, the hot legs, and the pressurizer surge line.

Choking flow at the break is established almost immediately at the break, after an initial short time of liquid loss for the lower plenum to drop the pressure fast enough for the two-phase flow to come into prominence. Flow out of the break is choked so long as the pressure in the lower plenum is still high. For large break sizes, the pressure in the lower plenum drops very fast, therefore, choking flow through the break is also fast to cease, e.g. at 1.5 to 2.0 seconds for the breaks three and four times the flow area of the cold leg.

Fig. 7.2.F7
BOTTOM BREAK, A=1, t_b = 0.1 SEC
FLOW HISTORIES IN SOME FLOW PATHS

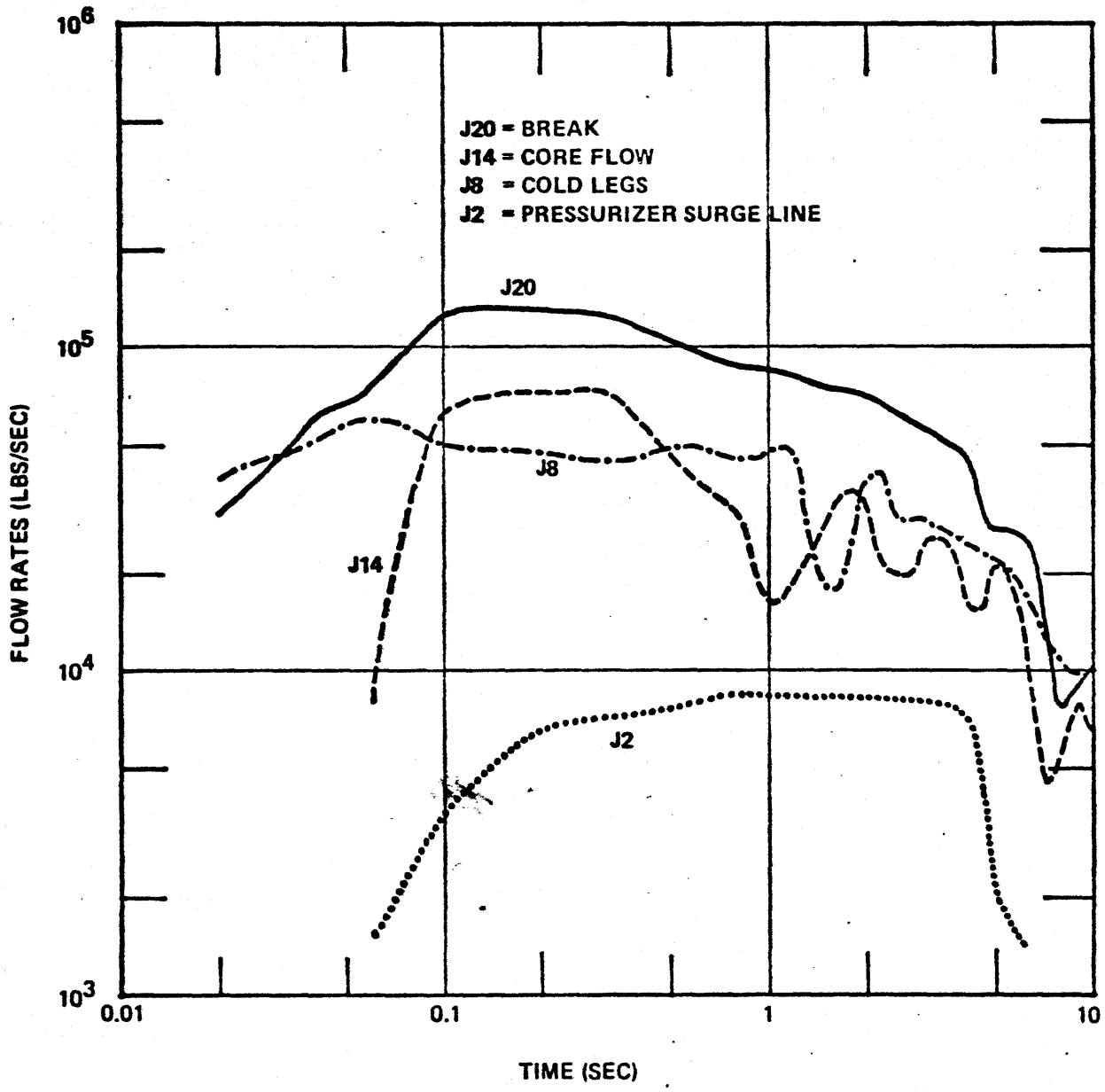

Fig. 7.2.F8
BOTTOM BREAK, A=2, t_b = 0.1 SEC
FLOW RATES IN SOME CRITICAL PATHS

J20 = LEAK
J11 & J12 = DOWNCOMER
J8 = COLD LEGS
J2 = PRESSURIZER SURGE LINE

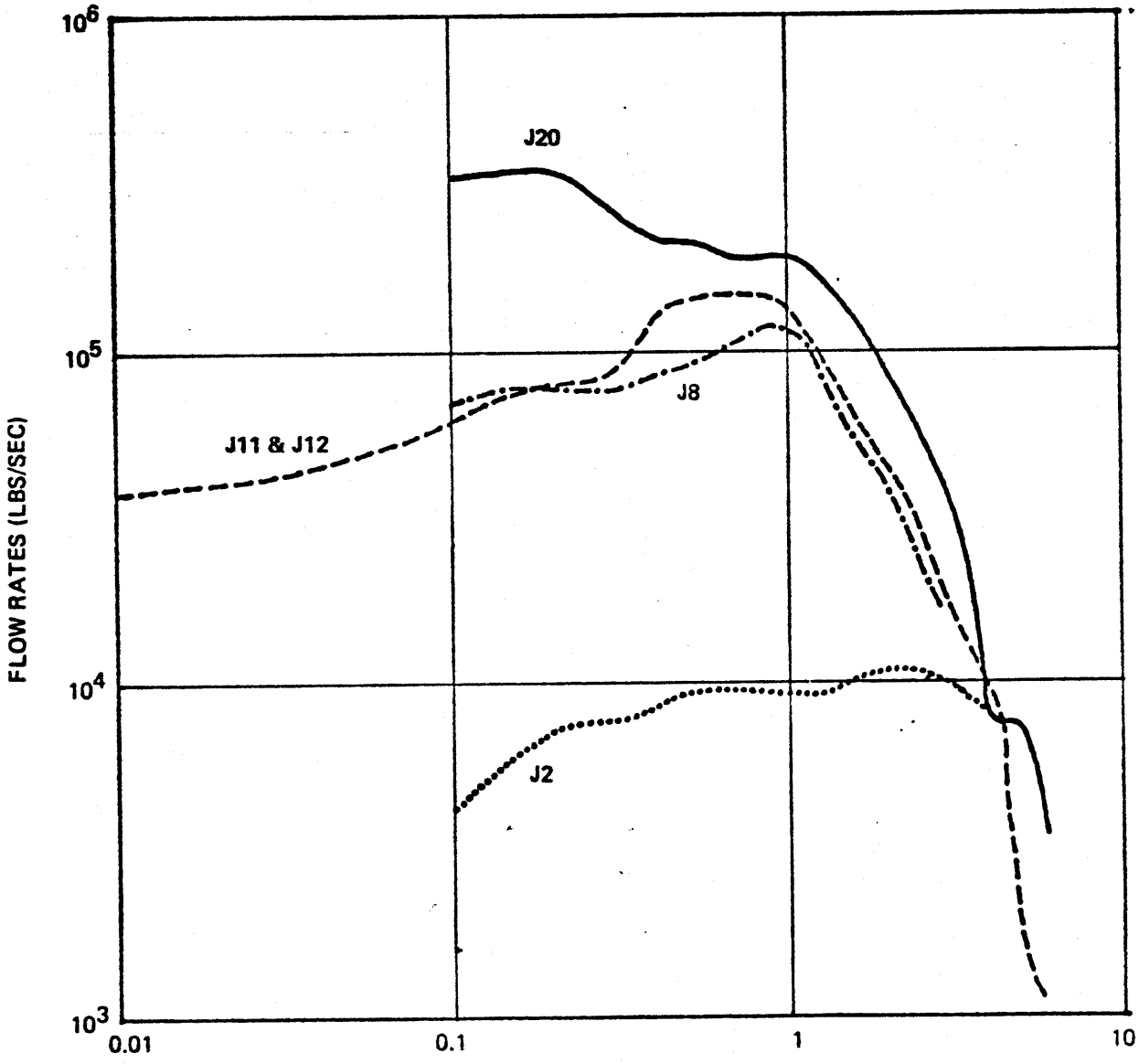

Fig. 7.2.F9
BOTTOM BREAK, A = 3
FLOW IN SOME CRITICAL PATHS

J20 = LEAK
J11 + J12 = DOWNCOMER
J8 = COLD LEGS
J2 = PRESSURIZER SURGE LINE

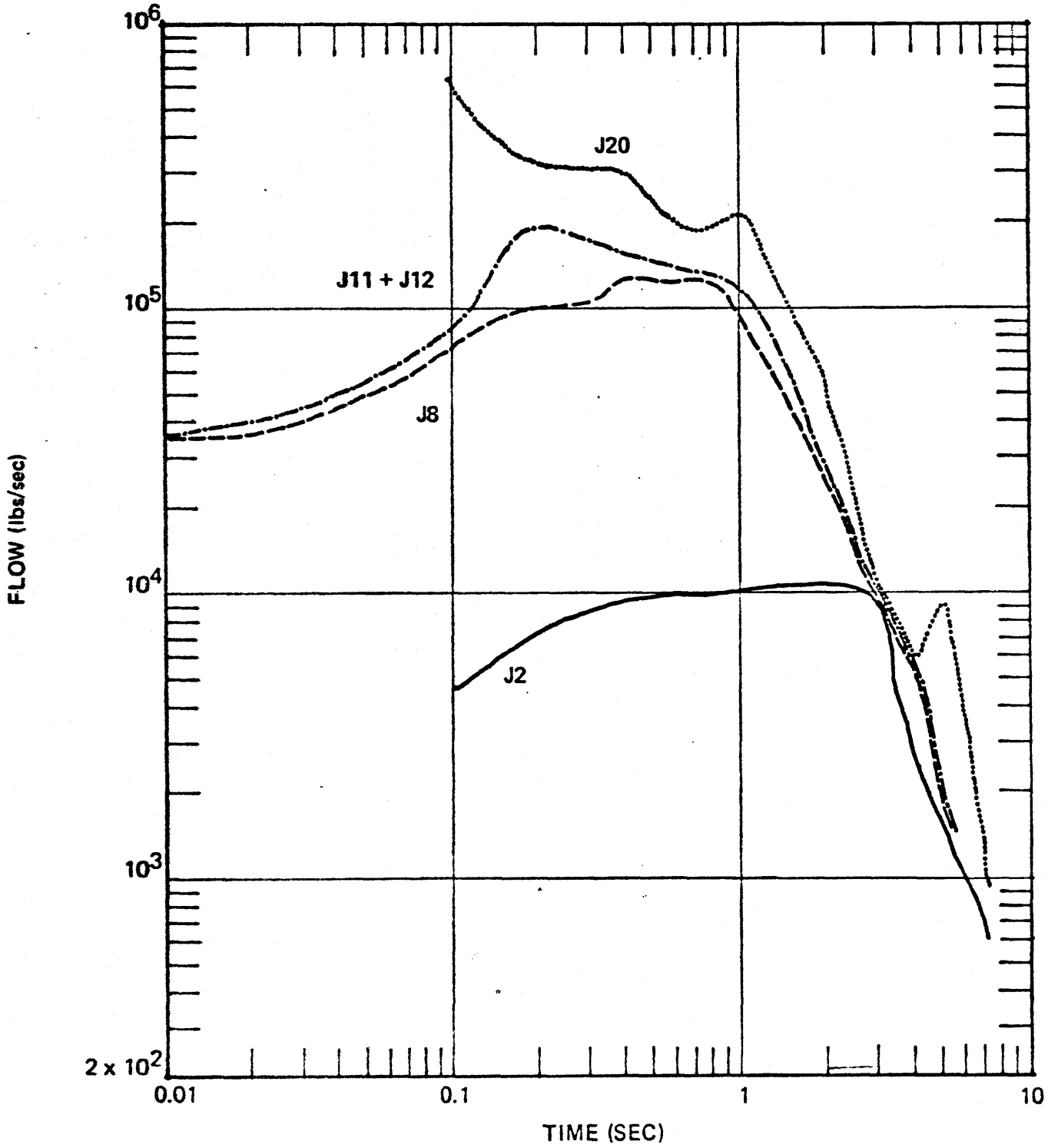

The fast drop of the pressure in the lower plenum creates a large pressure differential across the downcomer annuli, and the flow there is also choked. This choking feature would travel up to the cold legs, hot legs and the surge line of the pressurizer.

No flow choking is seen across the core and the steam generator U tubes. This is due to the large lumped flow areas of these flow paths (47.09 ft^2 for the core and 54.46 ft^2 for the steam generators). Whether this is a physical fact or not is unclear at present. It seems that a large pressure differential in the order of several hundred psi (Figs. 7.2.F4, 7.2.F5, and 7.2.F6) across the core would create flow choking in the small flow channels. In order to check this possibility it is necessary to represent the flow channel individually (instead of a lumped, fictitious tube for the whole core.) Mass and momentum conservation in this case can be achieved by multiplying the individual channel flow by the total number of flow channels. Some changes of the RELAP 3 code is necessary for such a representation.

7.2.5 End of Blowdown (EOB) and Start of Emergency Core Cooling Injection (SECCI)

End of blowdown has been defined (A3) as the time when the flow out of the break first stops. This definition seems to be unacceptable for breaks larger than the pipe break because in the former case there is such a violent fluctuation in the flow rate that the flow may temporarily pause, but then resumes again at large rates. Therefore, it has been decided to interpret

EOB as the time when the flow out of the break has dropped to an insignificant value, say 100 lbs/sec. With this definition, EOB of larger vessel breaks tends to be between 7 and 8 seconds irrespective of break size.

Table 7.2.T1 lists EOB and the time for the start of emergency core cooling (SECCI) for the bottom break sizes considered. When the flow fluctuation is violent, a range is given in which the break flow may become zero for an instant and then resumes again at respectable rates.

SECCI is defined as the time when emergency core cooling water starts to be injected into the primary system. This is the time when the pressure in the receiving node has dropped to 660 psi. Unlike EOB, the time for SECCI is unambiguous. It takes place between 1.0 and 2.0 seconds for large vessel break sizes.

7.2.6 Mass Loss History

Fig. 7.2.F10 shows the mass loss history for the four break sizes under consideration. At normal operation, the total inventory of primary coolant in the system is approximately 470,000 lbs.

It is noted that the mass loss curves tends to crowd together as the break increases in size. When the break size is 3 to 4 times the flow area of the cold leg, then the mass loss curve seems to reach an asymptotic configuration. This is the result of flow choking which tends to limit the mass flow rates out of the break even though the break size has become very large.

TABLE 7.2.T1

BOTTOM BREAK

END-OF-BLOWDOWN (EOB) AND START OF

EMERGENCY CORE COOLING INJECTION (SECCI)

Break Case[1]	SECCI (sec)	EOB[2] (sec)
A = 1		
t_b = 0.1 sec	5.73	12.2
t_b = 0.01 sec		
A = 2, cold leg ECC		
t_b = 0.1 sec	1.655	7.25-7.92
t_b = 0.01 sec	1.61	7.53-8.04
A = 2, hot leg ECC		
t_b = 0.1 sec	1.915	6.93-7.88
A = 2, upper plenum ECC		
t_b = 0.1 sec	1.92	6.61-7.65
A = 3		
t_b = 0.1 sec	1.13	7.04-8.01
A = 4		
t_b = 0.1 sec	1.075	6.53-7.97

(1) 'A' is the break size in multiple of cold leg flow area (4.12 ft^2). t_b is the break time over which the break opens up from zero to its full size.

(2) Where two numbers are shown for EOB, the first number is the time when the flow out of the break temporarily pauses, and the second number is the time after which no significant leak exists.

Fig. 7.2.F10
BOTTOM BREAK
MASS LOSS HISTORY

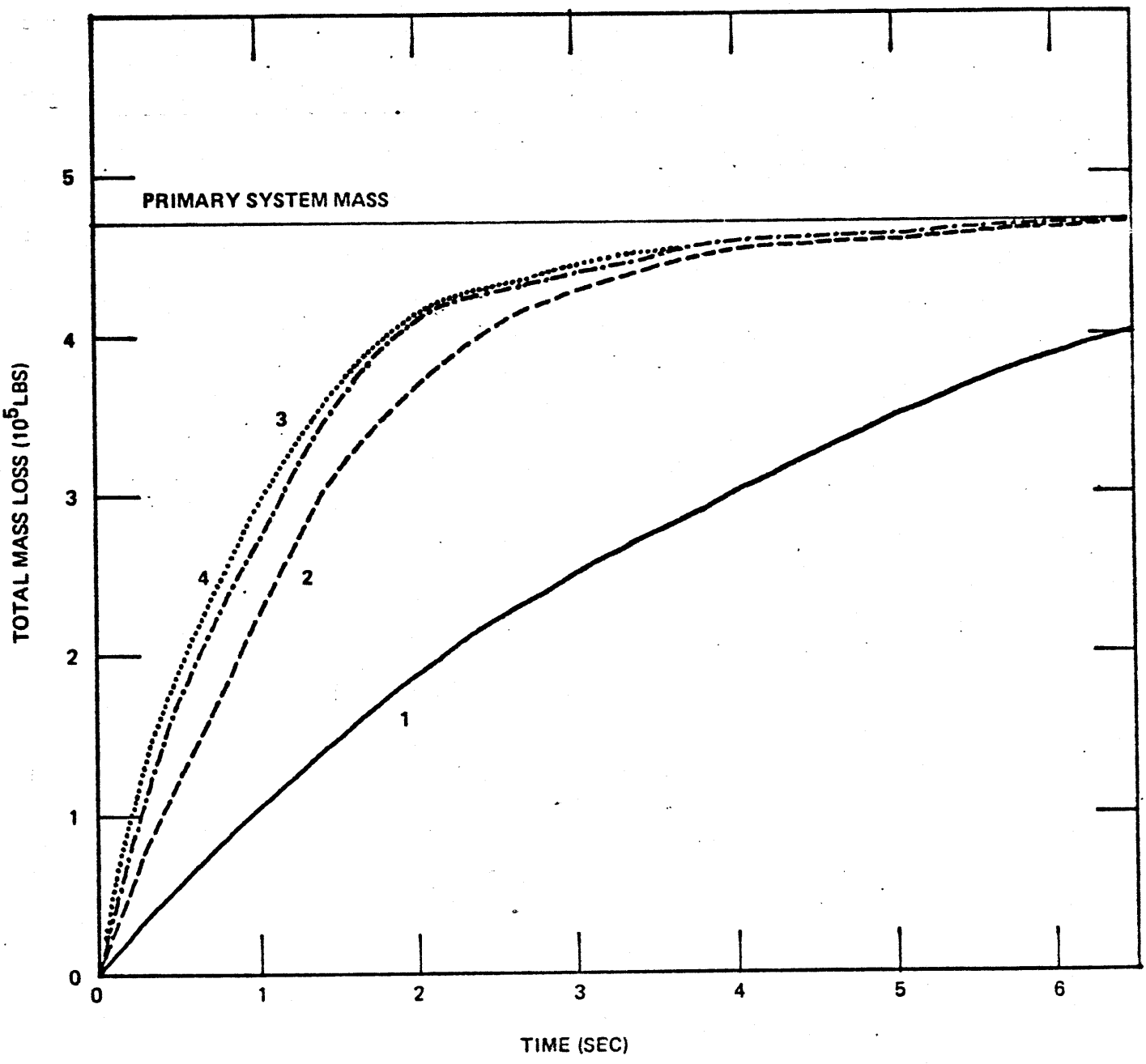

The mass loss for the bottom break is slightly faster than for the top break in spite of the fact that the break area is 10% smaller for corresponding cases. This is because a break in the bottom would allow more subcooled fluid to be lost before two-phase equilibrium and flow choking can be established.

7.2.7 Coolant Mass In Lower Plenum

The coolant mass in the lower plenum following a bottom break depends on the postulates of the break and the relative pressure in other parts of the system, particularly the upper plenum and the cold legs.

A plot of the coolant mass versus time is illustrated in Fig. 7.2.F11. It shows a more complicated pattern than in the case of top or side break. As the break has been assumed at the weld zone between the cylindrical part and the hemispherical part of the vessel, there is room in the lower head to contain significant amount of coolant during the blowdown. Upon break initiation, loss rate from the break is much larger than the make up rates as results of flow towards the lower plenum from the annulus and upper plenum, thus the total mass drops rapidly. This drop rate levels out until EOB when the total mass remains practically constant, around 10,000 lbs. This is the period when pressure differentials between various contiguous nodes are small, and only evaporating steam from the lower plenum is available for core cooling. When the cold legs have been filled with ECC water and this water starts flowing towards the downcomer and down the lower plenum, then the coolant mass in the lower plenum starts to rise, between approximately 16 to 22 seconds after the rupture.

Fig. 7.2.F11
BOTTOM BREAK AT BUCKLED ZONE
COOLANT MASS IN LOWER PLENUM

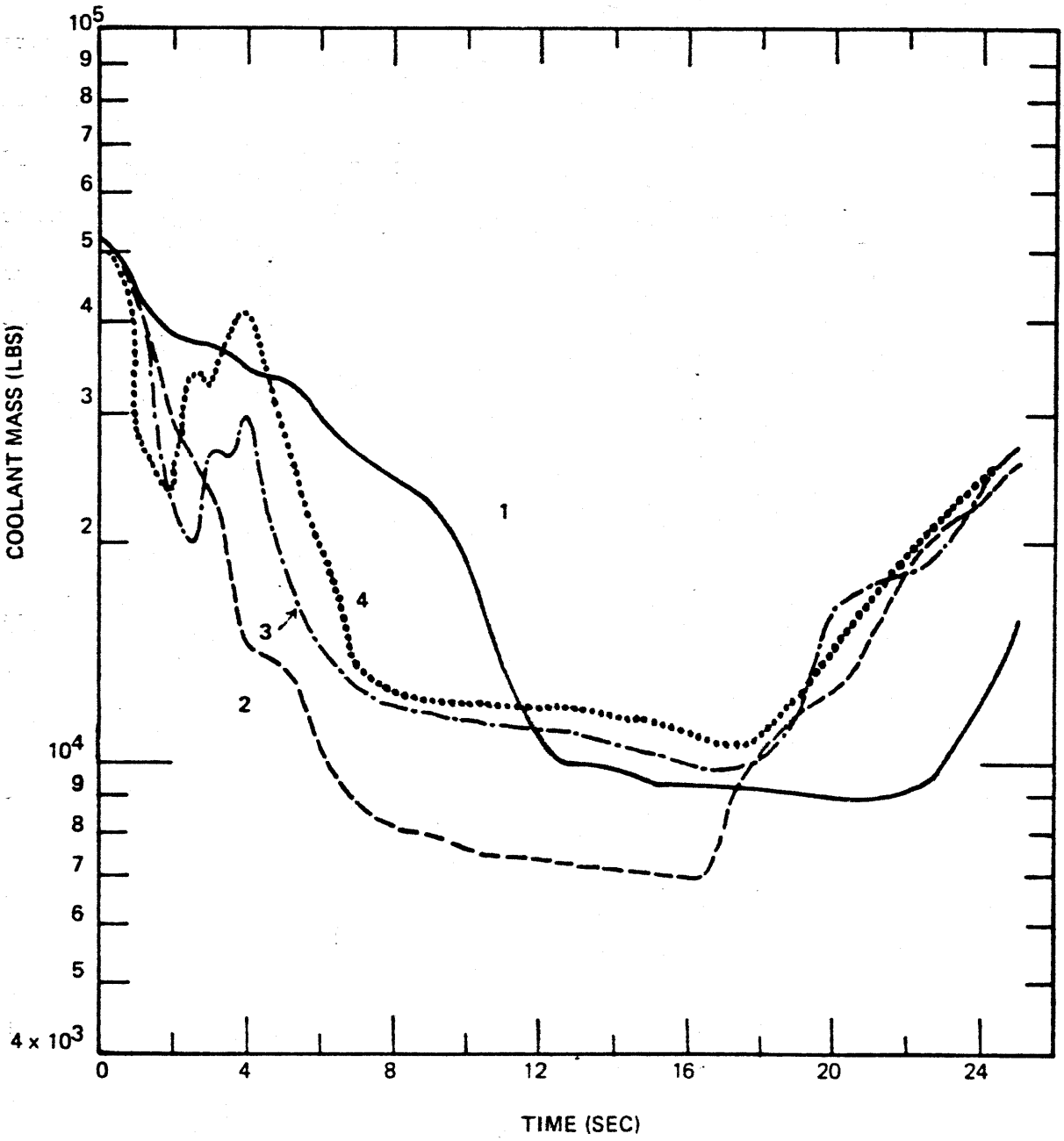

Fig. 7.2.F11 shows a conspicuous mass surge in the lower plenum around 4 seconds for the cases of break sizes 3 and 4 times the cold leg flow area. A study of pressure and flow rate histories, such as shown in Figs. 7.2.F5 and 7.2.F9 indicates that this surge is the result of the assumption on the back containment pressure, and to a lesser degree, to the flow imbalance between inflow and outflow of the lower plenum. The model for RELAP 3 in this series of calculations has used a containment back pressure of 75 psi, the justification for which has been presented in Chapter 5. When the break is large, the pressure in the lower plenum drops to this value very fast, at around 4 seconds. When this pressure has been reached, then RELAP 3 does not allow any further leak. On the other hand, considerable mass and pressure still exist in the upper plenum and the cold legs, and the coolant continues to flow into the lower plenum. Figs. 7.2.F12 and 7.2.F13 illustrate the effect of inflow and out flow imbalance on the coolant mass history in the lower plenum. Outflow rate is that of the break. Inflow rate is the sum of the flow rate through the core and the flow rates of the core bypass and the downcomer annuli. It is seen that the mass history is explainable rather well on the basis of inflow and outflow rates.

A comparison of Fig. 7.2.F11 with Fig. 6.2.F4 shows the surprising result that the minimum mass remaining in the lower plenum is larger for the bottom break than for the top break.. The reason for this result may be due to the phase separation model. When the break is at the buckled zone of the lower plenum, phase separation is reached faster, allowing more steam to flow out of the break, whereas when the break is at the upper plenum, the flow out

Fig. 7.2.F12

BOTTOM BREAK, A=2
INFLOW, OUTFLOW AND MASS IN LOWER PLENUM

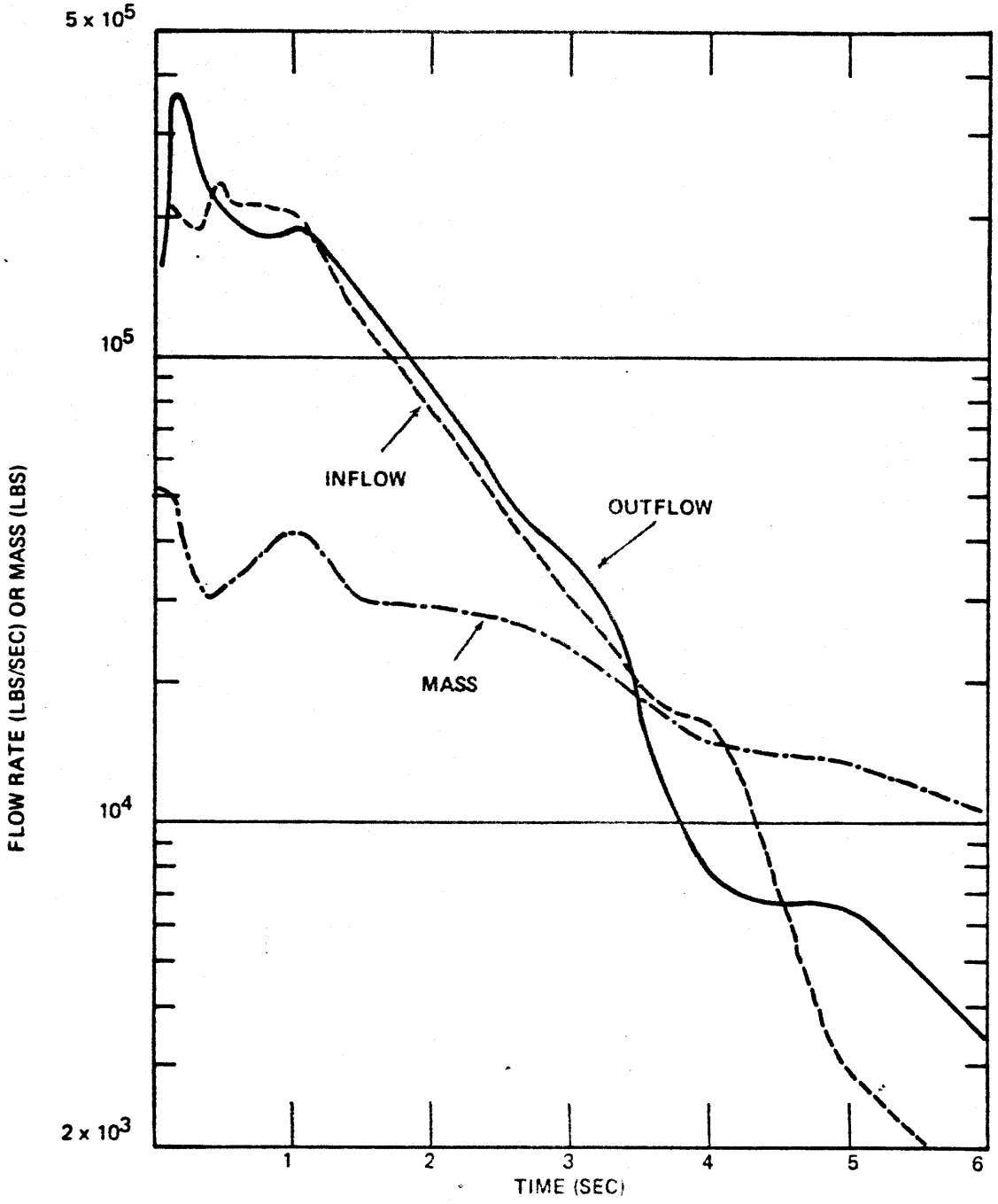

Fig. 7.2.F13
BOTTOM BREAK, A=3
INFLOW, OUTFLOW AND MASS IN LOWER PLENUM

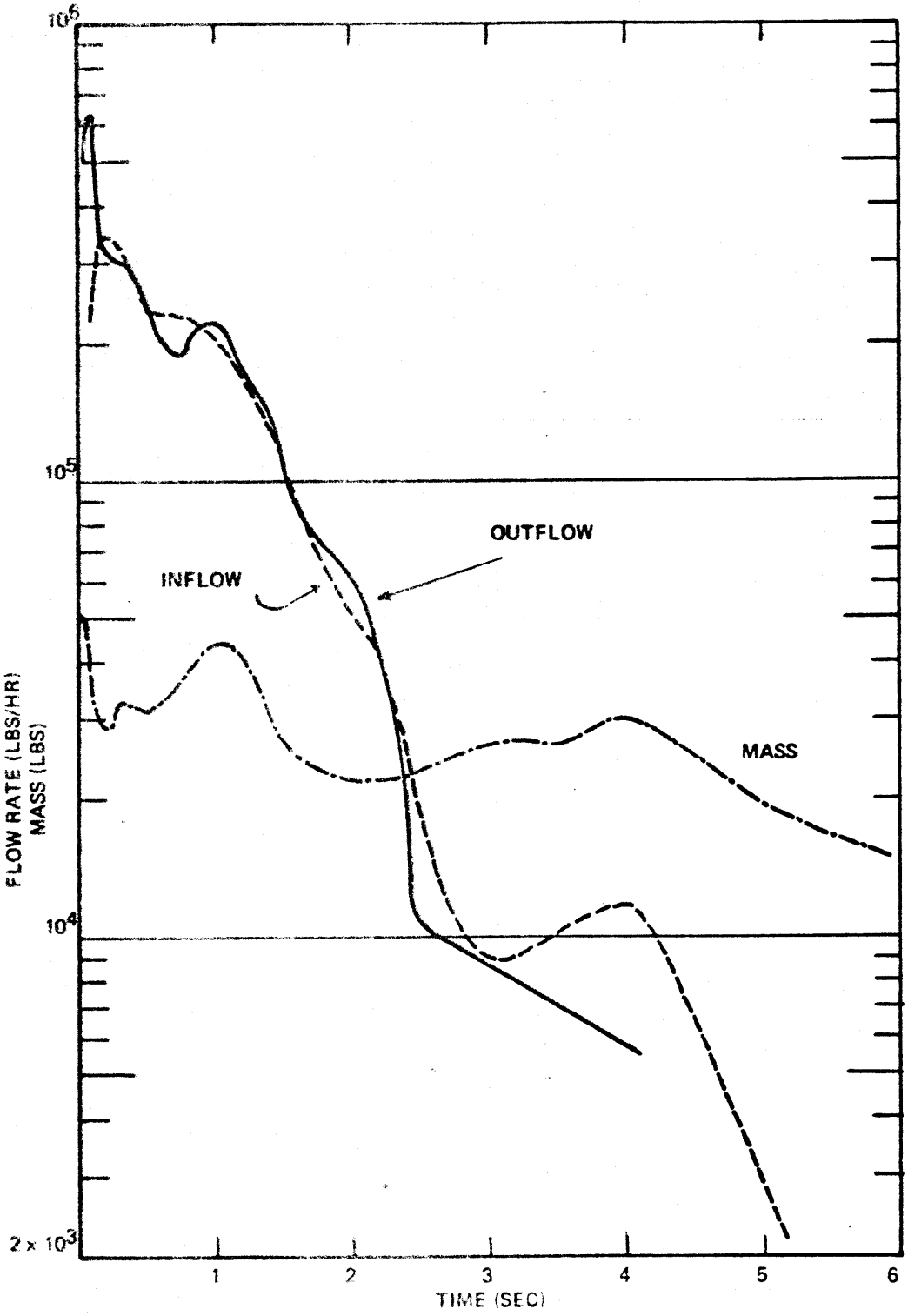

Fig. 7.2.F14
BOTTOM BREAK AT LOWEST POINT, A = 2
COOLANT MASS IN LOWER PLENUM

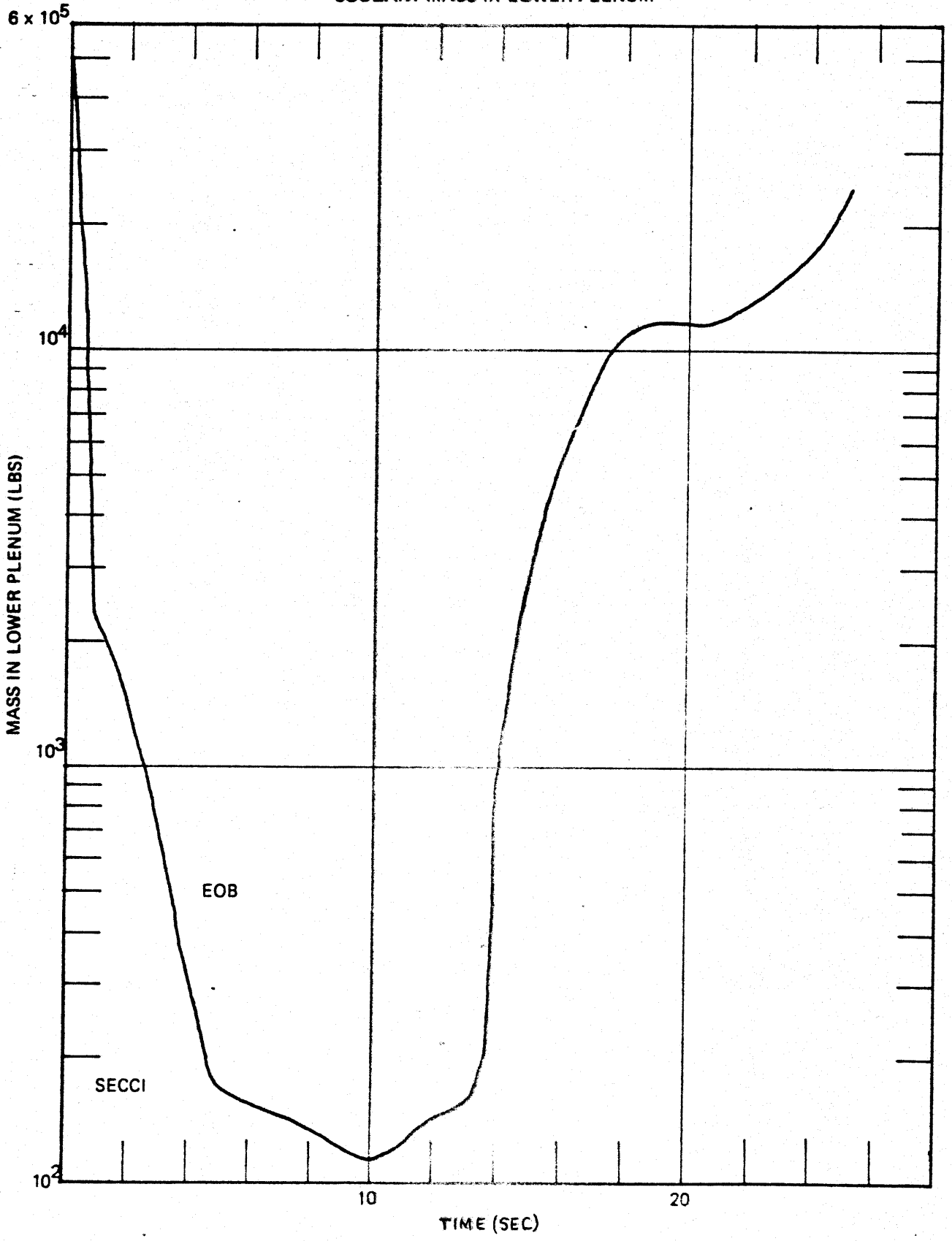

of the break entrains more water droplets. This explanation is plausible due to the result presented in Chapter 6 that a more homogeneous phase separation model would cause less coolant to remain in the lower plenum after EOB.

A break at the lowest point of the bottom head would cause an almost complete loss of coolant from the lower plenum after EOB. Fig. 7.2.F14 illustrates this result for the case of a break size twice the cold leg flow area. The minimum mass remaining at 10 seconds is 120 lbs which is the mass of saturated steam at 75 psia in a volume of 1100 ft^3. Fig. 7.2.F14 shows further a build up of water in the lower plenum when ECC water starts flowing in from the cold legs. This result seems to be due to programming logic, because this logic calls for a complete stoppage of inflow or outflow at the break when the pressure in the lower plenum has dropped below 75 psi. In reality, even when the pressure immediately outside the break is 75 psi or higher, the cold ECC water would drop out of the plenum. Thus when the break at the lowest point of the bottom head, it is doubtful that the ECC water would ever be effective. Steam rise from the lower plenum, if any, is more likely to flow out of the break due to the steam binding effect in the core. Therefore, alternative ECC injection location seems to be needed, such as a location in the hot legs or at the upper plenum.

7.2.8 Quality of Coolant In Middle Core Region

The quality of the coolant in the reactor is a factor which determines the heat transfer regime of the core.

Fig. 7.2.F15a is a typical history of coolant quality in the middle core region. The coolant in that region is subcooled at normal operation. After the start of the break, the pressure in the core drops to saturation pressure very quickly, allowing steam to form. The coolant quality increases from 0 to 1.0 in about 4 seconds and remains at 1.0 until ECC water becomes effective. Stable film boiling occurs when the surface heat flux is higher than the DNB flux, and this generally happens when the coolant quality is high. At around 4 seconds when the coolant quality becomes 1.0 and remains there for many seconds, the clad surface temperature starts a steep climb. This temperature rise is turned around later when ECC water becomes effective in lowering the quality of the flow through the core.

7.2.9 Heat Transfer Coefficient (HTC), Critical Heat Flux Ratio (DNBR) and Clad Surface Temperature

Fig. 7.2.F15 shows the temperature transient of the average clad surface temperature such as the pattern shown in Chapter 6 for the top break. Except for the case of two-pipe-sizes break, the other breaks cause the clad surface temperature to rise from the very start of the accident, reach a high at around 1 to 2 seconds, then level off before a second steep rise to to a new peak. But when the break is twice the flow area of the cold leg, the clad surface temperature shows a small increase before flow reversals, then decreases to a low value of approximately 370°F at 5 seconds, then starts a steep climb when coolant flow through the core is predominantly steam.

Some insight into the behavior of the clad temperature can be obtained by examining the flow rate of the coolant through the core, the heat transfer coefficient and the critical heat flux ratio such as those in Figs. 7.2.F16 and 7.2.F17.

Fig.7.2.F15a

AVERAGE QUALITY OF COOLANT IN MIDDLE CORE REGION

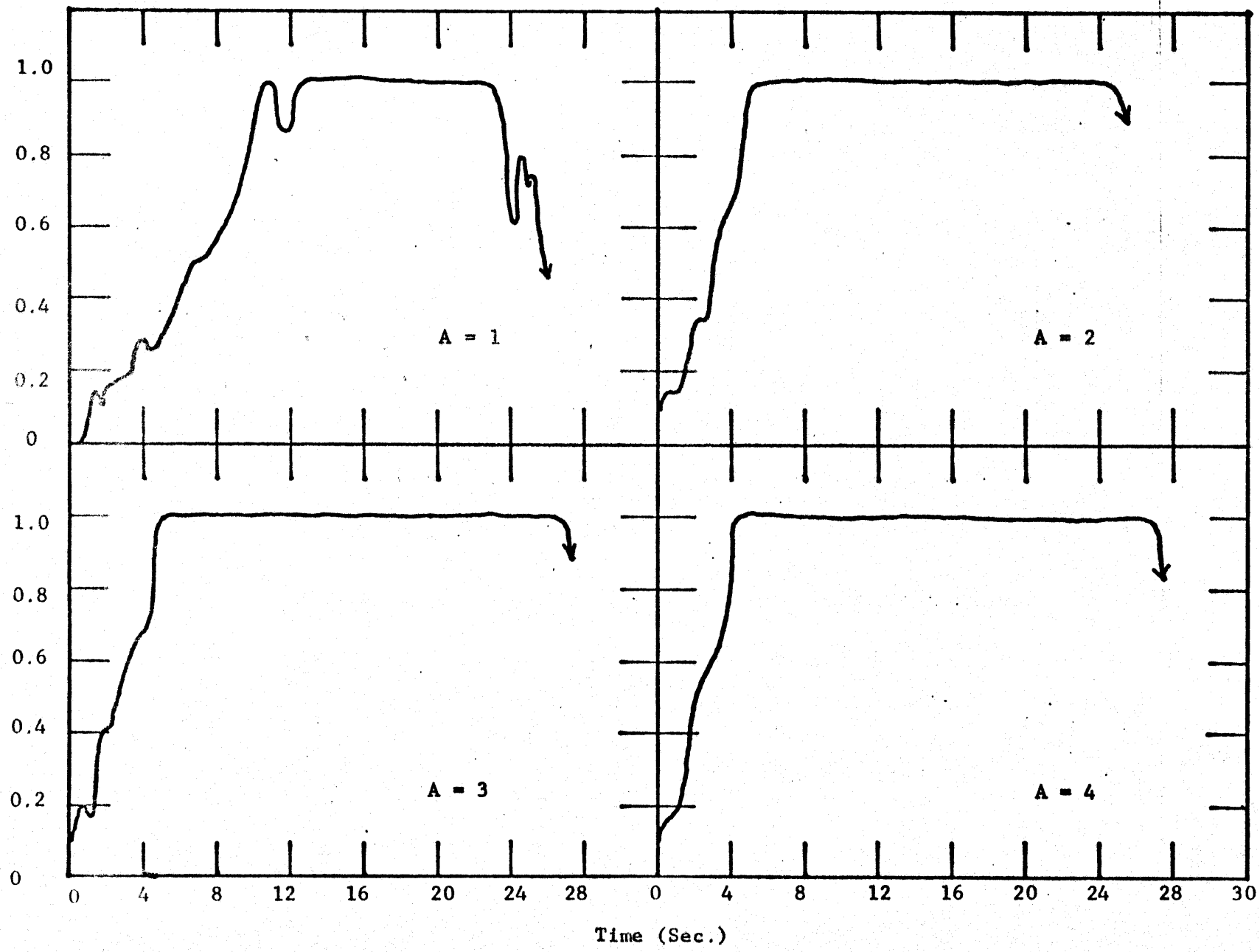

Fig. 7.2.F15
BOTTOM BREAK
CLAD SURFACE TEMPERATURE IN MIDDLE
CORE REGION

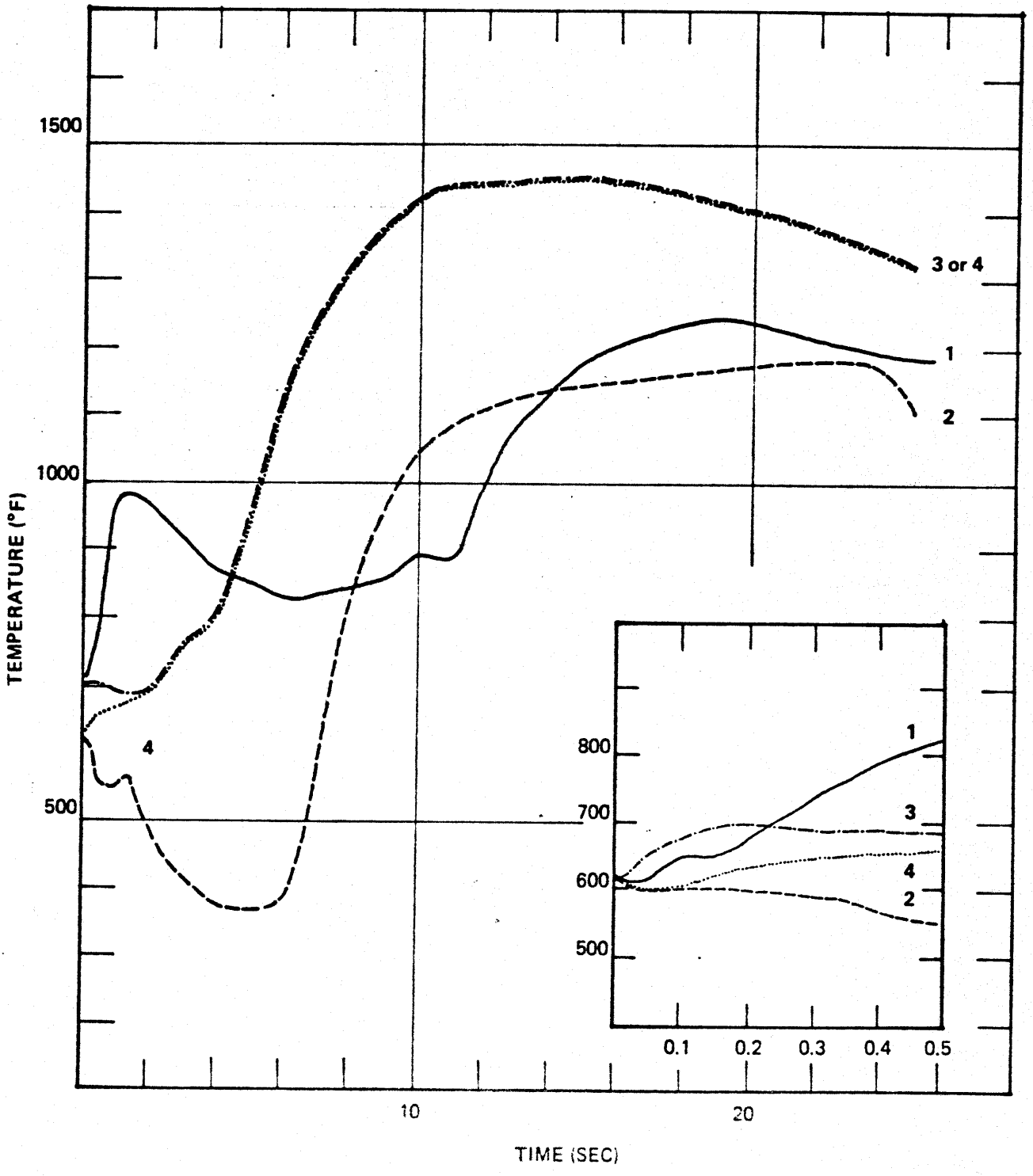

Fig. 7.2.F16
BOTTOM BREAK, A=2
AVERAGE FLOW, HEAT TRANSFER COEFFICIENT (HTC),
DNB RATIO AND CLAD SURFACE TEMPERATURE
(T) IN MIDDLE CORE REGION

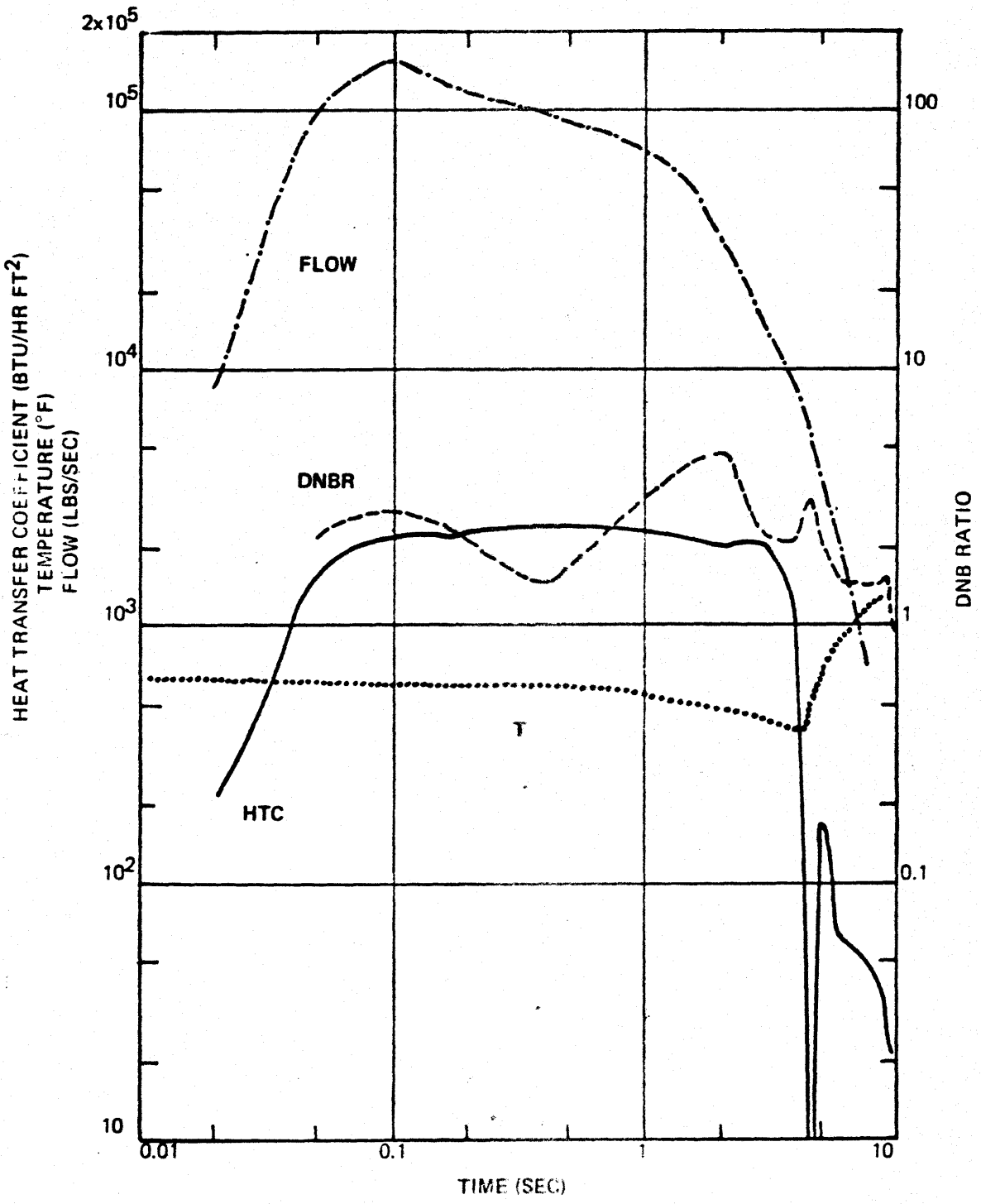

Fig. 7.2.F17
BOTTOM BREAK, A=3
AVERAGE FLOW, HEAT TRANSFER COEFFICIENT (HTC)
DNB RATIO AND CLAD SURFACE TEMPERATURE
(T) IN MIDDLE CORE REGION

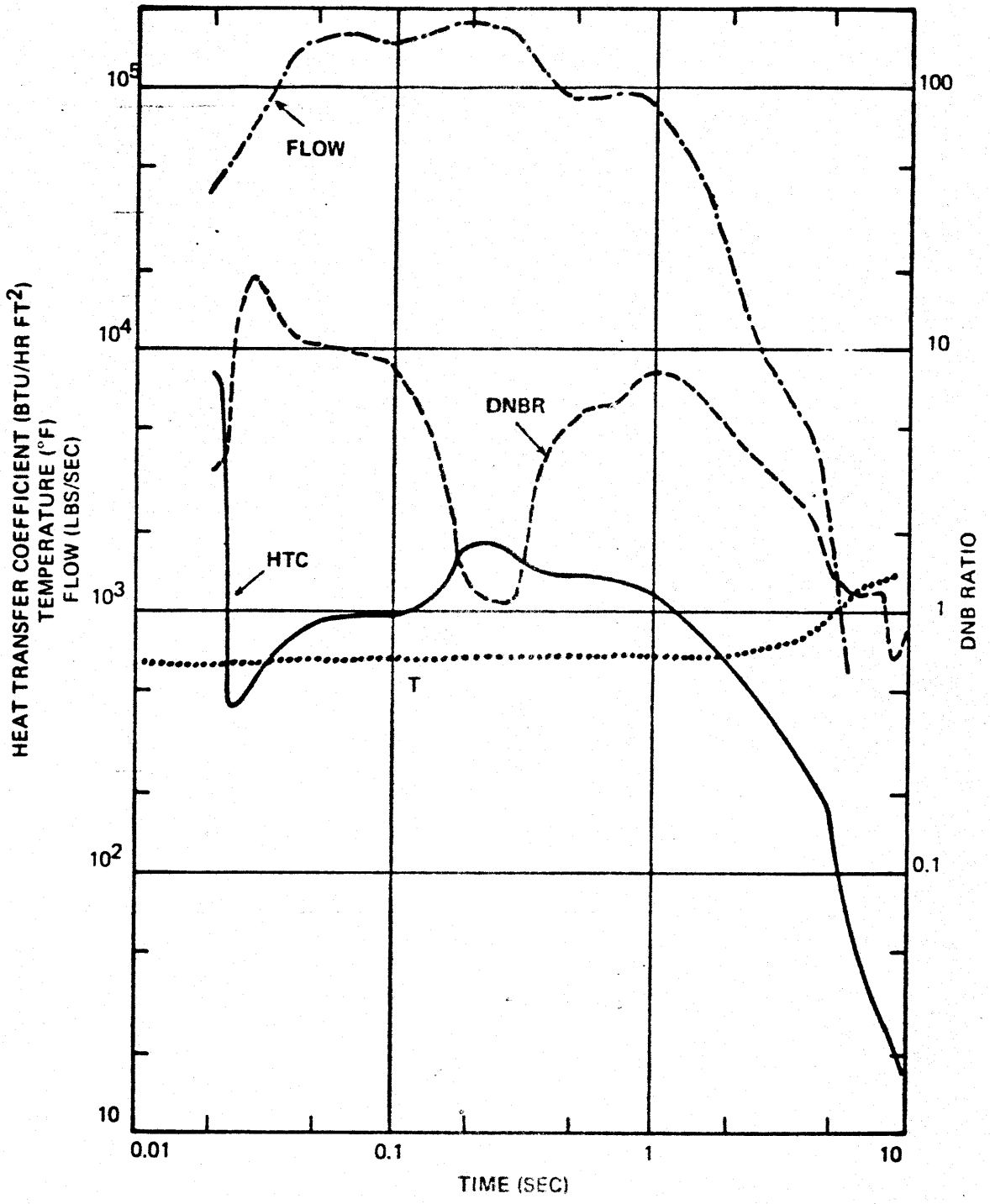

Fig. 7.2.F18
BOTTOM BREAK, t_b = 0.1 SEC
AVERAGE HTC IN MIDDLE CORE REGION
DURING PERIOD OF FLOW REVERSAL

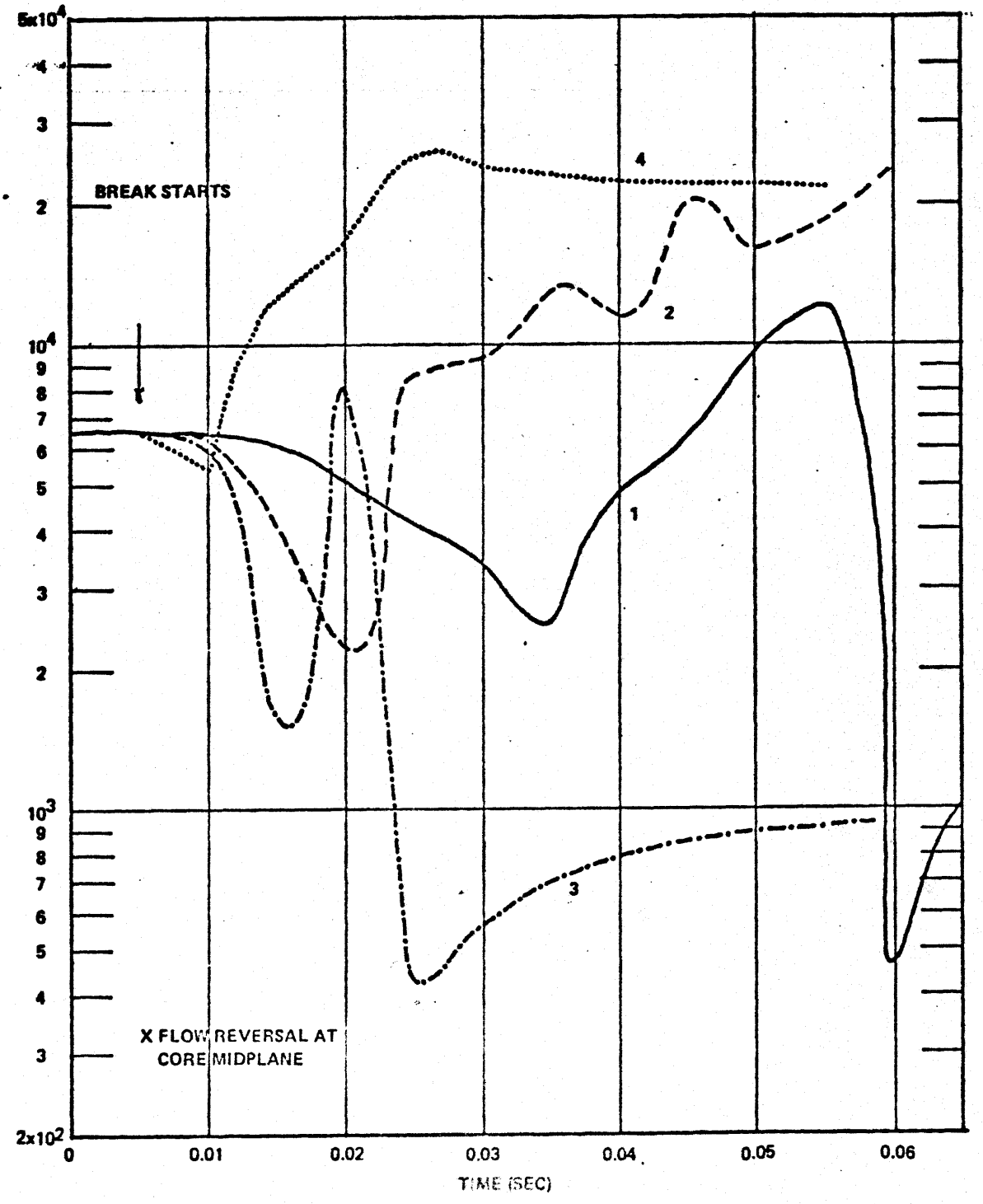

Fig. 7.2.19
BOTTOM BREAK, t_b = 0.1 SEC
AVERAGE DNB RATIO IN MIDDLE CORE REGION
DURING PERIOD OF FLOW REVERSAL

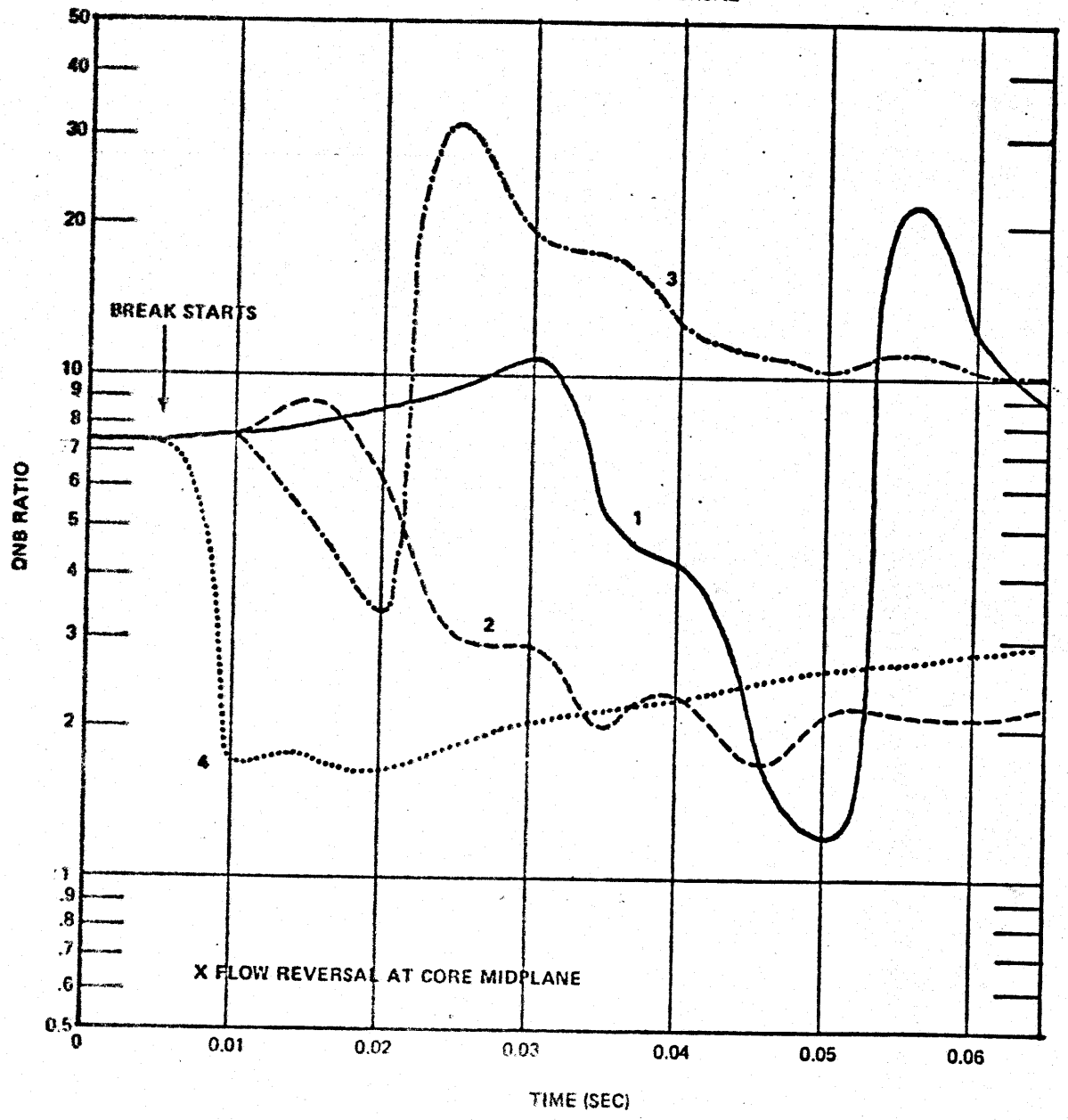

Fig. 7.2.F20
BOTTOM BREAK, t_b = 0.1 SEC
AVERAGE CLAD SURFACE TEMPERATURE IN MIDDLE CORE REGION
DURING PERIOD OF FLOW REVERSAL

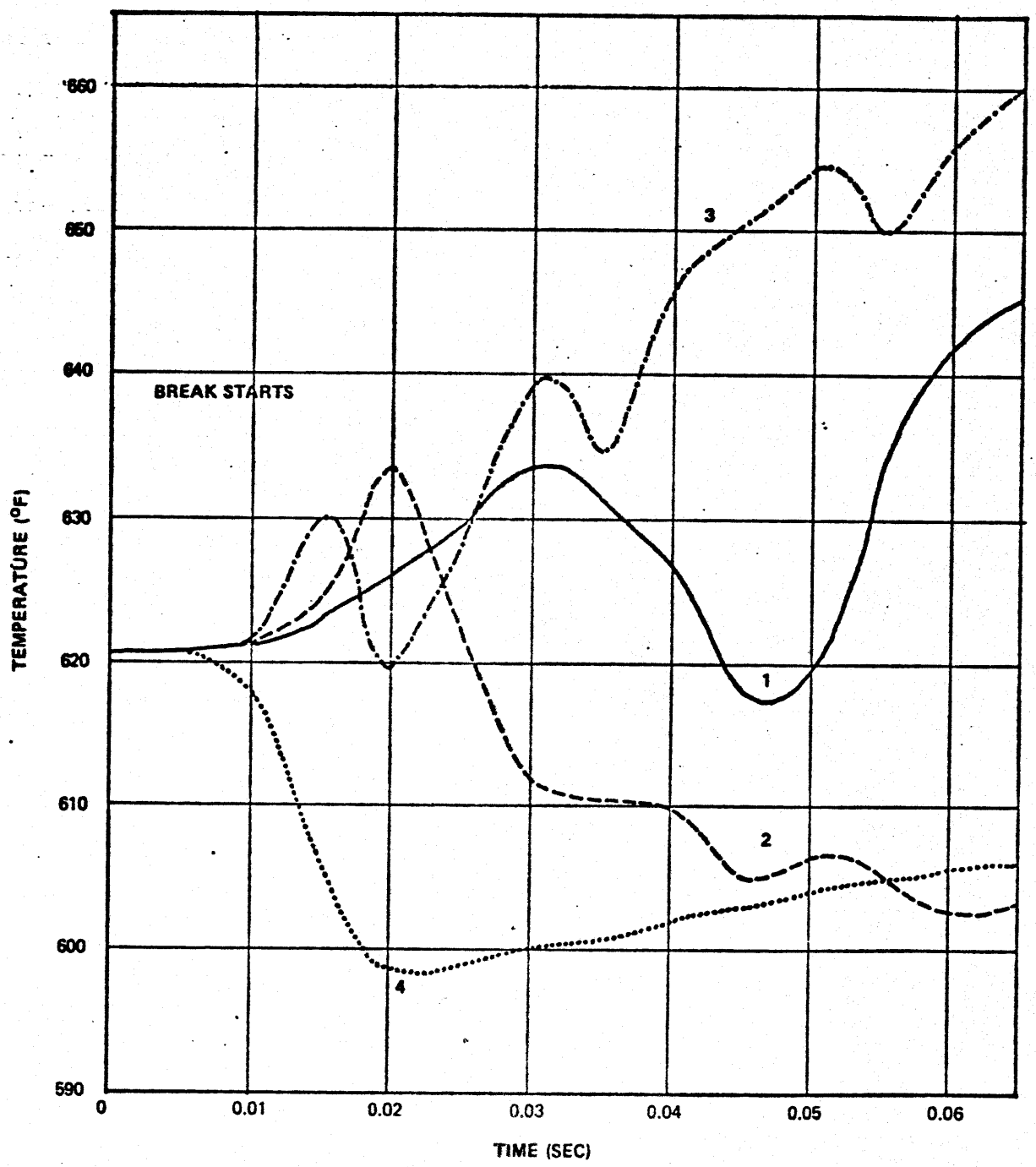

For a break size larger than twice the flow area of the cold leg, flow reversal at the core midplane takes place in less than 0.02 second. The behavior of the heat transfer coefficient, the DNB ratio and the clad surface temperatures in the period between 0 and 0.02 second is not shown in Figs. 7.2.F16 and 7.2.F17, but can be seen in more details in Figs. 7.2.F18, 7.2.F19 and 7.2.F20. Typically, the heat transfer coefficient starts out at the steady state value of approximately 6400 BTU/hr ft^2. It decreases after the actuation of the break because the flow through the core slows down. After flow reversal, the coolant is still subcooled and the mass flow through the core is large, the heat transfer coefficient thus rises again to a value in the order of 1000-2000 BTU/hr ft^2 and remains there for 4 to 5 seconds.

The heat transfer coefficient of cases 1, 3, and 4 (break soze is equal to 1, 3 and 4 times the flow area of the cold leg) does not demonstrate the same pattern as described above. After flow reversal, it does not stay at a high value of 1000-2000 BTU/hr ft^2, but drops down an order of magnitude and remains there for the duration of the blowdown. This is possible if there is onset of DNB which may be caused by the following interrelated factors: a) A DNBR smaller than 1, b) A high coolant quality so that stable film boiling takes place. Both of these factors are not seen to take place in Figs. 7.2.F19 and 7.2.F15. The reason for the calculated steady rise of the clad surface temperature after flow reversal for the case of 1, 3 and 4 pipe sizes breaks is therefore, not obvious on the basis of present evidence.

7.2.10 DNB Correlation Involving Flow Reversal

The previous section reveals an apparent anomaly in the way the heat transfer coefficient is calculated after flow reversal. Figs. 7.2.F21 and 7.2.F22 serve to further illustrate this anomaly. For the bottom break size twice as large as the cold leg flow area, the clad surface temperature transient assumes two different paths for the break times of 0.01 second and 0.1 second. It is shown in Chapter 9 that the break time is very insensitive to most parameters of interest in the two-phase blowdown. These parameters include the flow rates, the rate of mass loss, the rate of ECC water injection, and the clad surface temperature transient. The flow rates through the core such as shown in Fig. 7.2.F22 attest to this conclusion. The heat transfer coefficients in the same figure, however, differ by a factor of approximately 20.

It is obvious that the low heat transfer coefficient (t_b=0.01 sec.) results from the stable film boiling correlation. It is not obvious, however, that the heat transfer should be in that regime when the coolant flow through the core is still two to three times its value at normal operation.

Two possible causes of this anomaly are:

a) There may be a programming error in RELAP 3 which locks the heat transfer into the stable film boiling regime once that regime is entered. The previous section has shown that the DNBR is generally larger than 1.0 for the first fraction of a second. Thus, the error, if any, may be due to a logical decision which does not involve a direct comparison of the surface heat flux to the DNB flux.

Fig. 7.2.F21
BOTTOM BREAK, A=2
EFFECT OF HEAT TRANSFER CORRELATION
ON AVERAGE CLAD SURFACE TEMPERATURE *

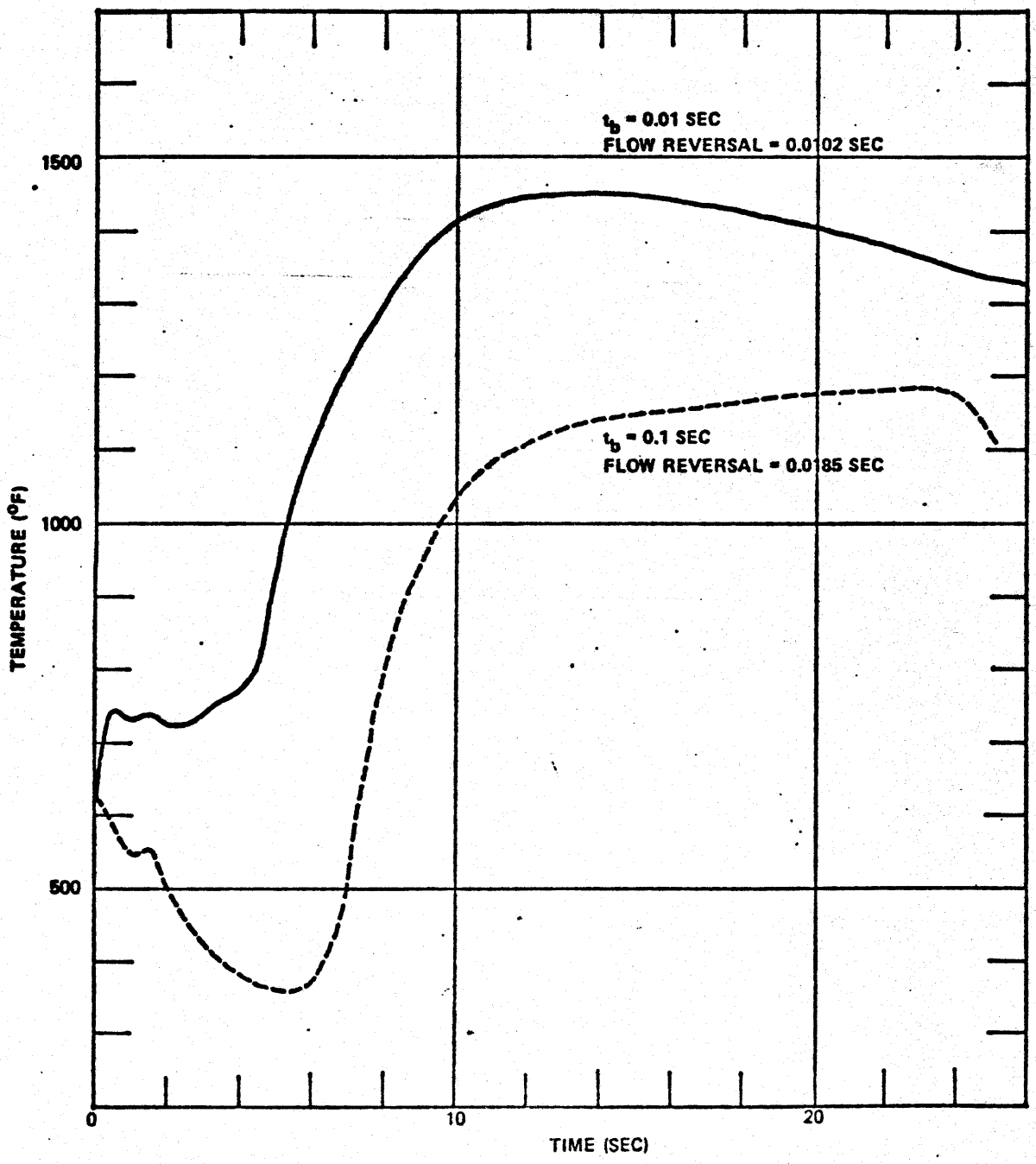

* The only apparent changing parameter here is t_b, but it is argued in text that the real cause of the difference in the two curves is probably the heat transfer correlations in RELAP 3.

Fig. 7.2.F22
BOTTOM BREAK, A=2
AVERAGE CORE FLOW RATE AND HTC
t_b = 0.01 SEC and t_b = 0.1 SEC

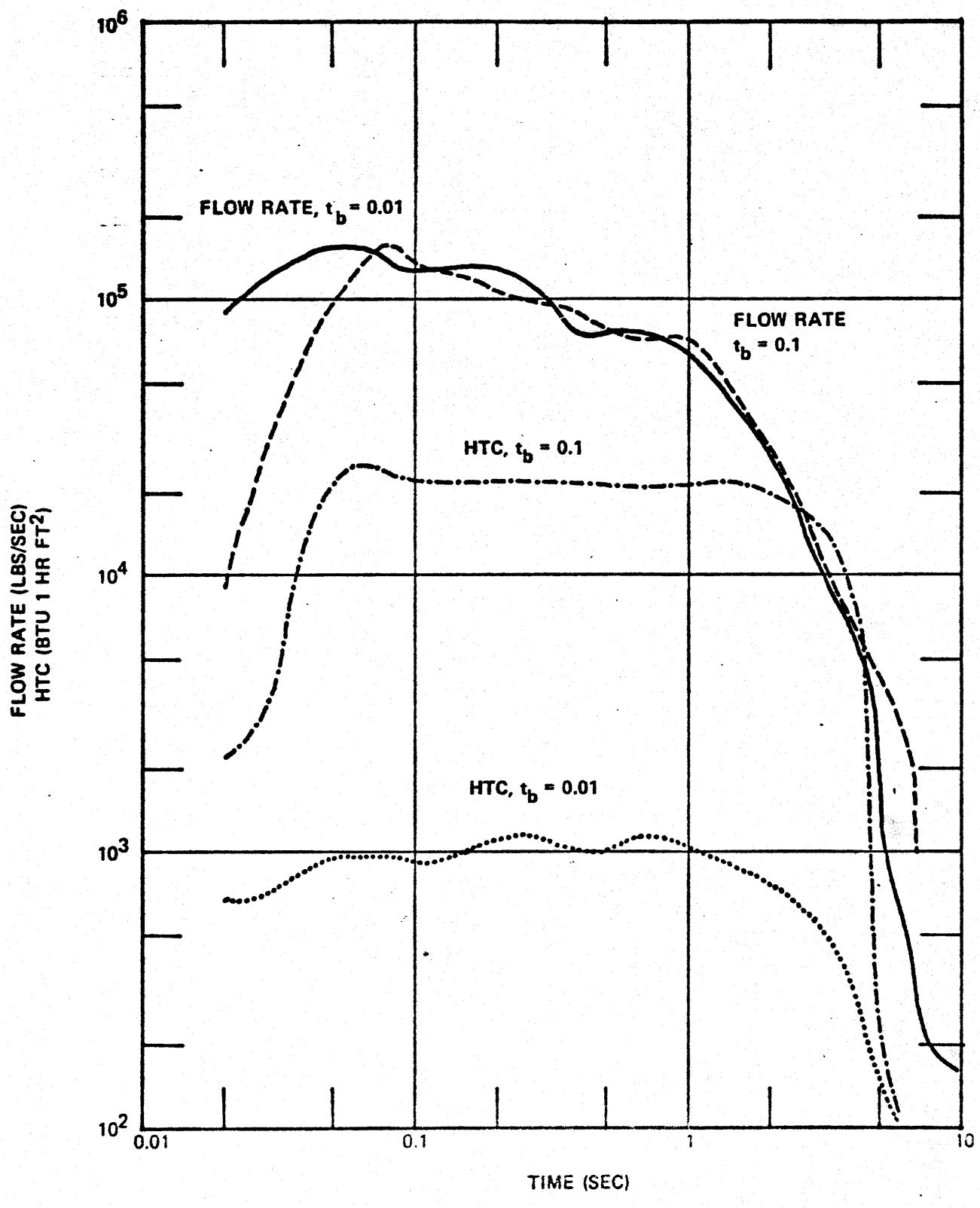

b) The DNB heat correlations employed by RELAP 3 are steady state correlations which feature the mass flow rate (G) as a direct parameter. For the complicated geometry of a nuclear plant, these correlations at best are valid only within the range of conditions upon which they were formulated. Extrapolations of the calculations beyond the range of validity of the correlations would yield unreliable results. But this extrapolation has been practiced for the bottom and side breaks because these cases involve flow reversals when the mass flow rate slows down from a high value to zero and then to a high value in the opposite direction.

Griffith (G3), in examining results of calculations by Aerojet Nuclear Company for the 1-1/2 Loop Semi-Scale System (A7), has suggested that departure from nucleate boiling (DNB) may not have a chance to take place during the fast flow reversal in the early stages of a LOCA. Recent tests on a BWR-type fuel element (L6) show that the predicted CHF does not occur until approximately 4 seconds after coolant shut off, and this is the case for various coolant shutoff times. Both Griffith's suggestion and Lahey's results (L6) seem to be of importance if the anomaly of the clad surface temperature transient presented in this section is to be resolved.

On the basis of the increased flow rates after flow reversal, and the results of the top break cases, it is possible that the correct pattern for the average clad surface temperature transient is a slight increase before flow reversal, then a steady decrease to a low value of some 370°F at about 4 seconds, and finally a steep increase to a peak just before ECC water is effective. This peak, as can be inspected in Fig. 7.2.F15, is below 1500°F, and is comparable to that of a LOCA by cold leg break.

A recent, unpublished series of experiments by Lawson (L5) involving a simulated loss of coolant in a high pressure system equipped with heated tubes, indicate that the clad surface temperature did indeed drop following flow reversal.

7.2.11 Bottom Breaks with ECC Injection Above Reactor Core

As mentioned at the beginning of this chapter (Table 7.0.T1), studies have been made with ECC injection at the hot legs and in the upper plenum. The purpose is to find out the behavior of the clad surface temperature transient as compared to the case of ECC injection at the cold legs.

Principal results of these studies are presented in Chapter 9. In general, the basic blowdown phenomenologies do not change when the ECC injection location is changed. One should intuitively suspect that when the vessel has a hole at the lower plenum, then the cold leg ECC water would all flow out the break. Therefore, if the core is to be cooled, ECC water must be available from the top.

This insight, however, is not observed during the first 25 seconds of the blowdown. In fact, Section 9.4 even indicates that an injection from the top may give a higher clad surface temperature in the first 25 seconds of the blowdown. The tentative explanation for these calculational results is that an early ECC injection at the reactor top would hinder flow through the core. However, the model for these studies is not detailed enough to account for effects such as ECC injection velocity and the period of analysis is not long enough to account for longer term coolability of the core. Further study in this area is warranted.

7.2.12 Average Clad Surface Temperature Transient in a LOCA by Double-Ended Cold Leg Break

Fig. 7.2.F23 is a plot of the average clad surface temperature of the three core regions (lower, middle, and upper) following a postulated LOCA by a double-ended cold leg break. Data of this plot is extracted from a RELAP3 34-volume sample problem that was included in the RELAP3 package (A5). The sample problem is intended to represent a LOCA by double-ended cold leg break in a 3411 MWt PWR plant. Most of the plant characteristics are similar to those used in this study except the following: a) the break is truly instantaneous in that no break time is assigned, b) a rather high gas gap conductivity is used (0.4687 Btu/hr ft^2 F), and c) the lower portion of the core is assigned the largest power fraction.

Examination of Fig. 7.2.F23 reveals the following observations:

a) The average clad surface temperature is highest for the lower core region.

b) The peak of the average clad surface temperature is just below 1500°F, that is, not better off than the worst vessel break so far under investigation.

c) The pattern of the average clad surface temperature transient is a steep initial climb characteristic of an early DNB. This has been argued in previous sections as probably not physical. Further studies on transient DNB correlations involving flow reversal is necessary.

Fig. 7.2.F23
AVERAGE CLAD SURFACE TEMPERATURE
FOLLOWING A DOUBLE-ENDED COLD
LEG BREAK ACCIDENT IN A 3411 MWt PWR
(Data Plotted from Ref. A5)

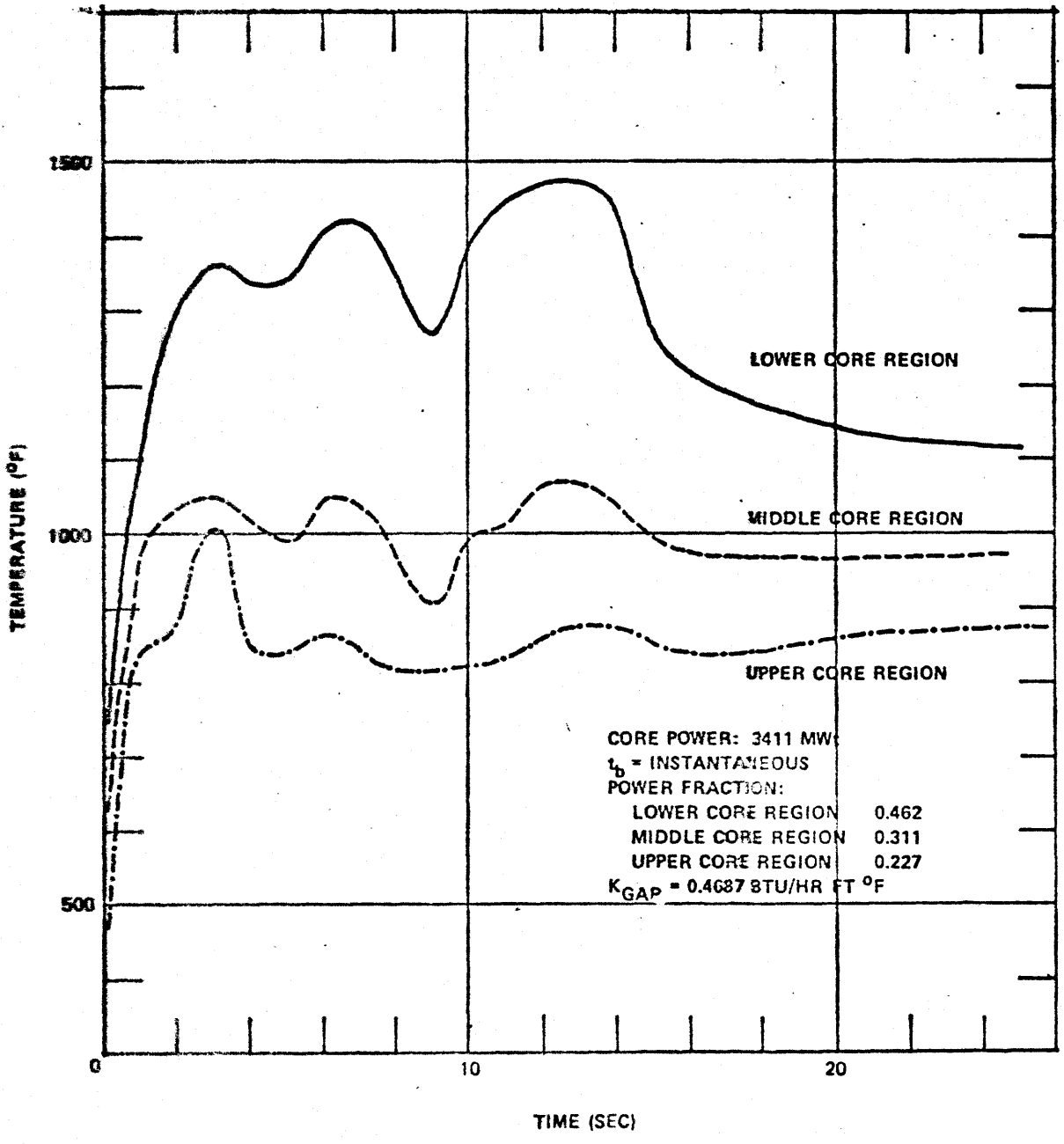

7.3 Conclusions

A break in the lower plenum of the reactor vessel causes the system to depressurize faster than when the break of the same size is situated in the upper plenum or at the side. The fast depressurization allows void to form in the core at the earliest stages of the blowdown and this void formation alone is capable of scramming the reactor.

The analysis of the blowdown has been based on the assumption that the vessel internals, particularly the core, maintain their integrity and geometry. Subcooled pressure and force transient loadings on vessel internals have been analyzed with the WHAM computer code. Results indicate that the loadings depend very strongly on the break time which is the duration (of the order of fractions of a second) over which the break opens up from zero to the preassigned size. The highest loadings are associated with the "instantaneous" break. The peak pressure loadings across the core is of the order of 600-700 psi and 50 cps (for a 16.48 ft^2 break). The peak force loading across the core for the same case is of the order of 6000 kips. The peak pressure loadings across the upper core barrel is between 500-600 psi which is smaller than for the case of the side break of the same break size.

As the break size increases, the loadings on vessel internals also increases, but not linearly. There is a tendency for the pressure loadings to level out and to be asymptotic to a maximum value which is the difference between the subcooled pressure and the saturation pressure of the fluid in the lower plenum.

The break time is not as sensitive in the two-phase blowdown as in the subcooled period. The only change introduced by a change of break time from 0.1 second to 0.01 second is a slightly faster scram and a slightly faster flow reversal. Other parameters such as the histories of flow rates, mass loss, coolant remaining in the lower plenum, and average clad surface temperature remain essentially the same for the duration of the blowdown.

Flow reversal is a special feature of the bottom break as compared to the top break. The reversal takes place very fast, some 56 msec. for the case of one-pipe-size break and less than 20 msec for larger breaks.

The flow of coolant in various flow paths is very turbulent and often choked. Choking flow occurs at the flow paths with small cross sections and high friction. These include, in the order of occurrence, the break, the downcomer annuli, the cold legs and the pressurizer surge line. Flow through the core coolant channels and through the steam generator U tubes is not choked for the cases under study because the cross section of these flow paths is quite large. It is suggested that, with the presence of many hundred psi across the flow channels, the flow in the channels may be critical, and this can be assessed only by treating an individual channel as a flow path.

The existence of choking flow in various critical flow paths leading to the break is the cause for the asymptotic behavior of many blowdown parameters as the break increases in size. These parameters include system pressure, mass loss rate, coolant mass remaining in the lower plenum, and clad surface temperature. The end-of-blowdown has been defined (A3) as the time when the flow out of the break first stops. It is argued that, due to the violent fluctuation of the flow in the case of large vessel breaks, EOB could be inter-

preted as the time when the flow out of the break is no longer significant. In this light, EOB is between 7 and 8 seconds for any large break size under investigation.

The mass remaining in the lower plenum after EOB is larger for a bottom break at the buckled zone than for a top or side break. This result is rather surprising and is tentatively explained as due to phase separation model and to the present containment pressure. However, when the break is located at the lower most point of the lower plenum, there is essentially no more coolant remaining in the lower plenum after EOB.

The average clad surface temperature transient in the middle region of the core is shown to assume an asymptotic configuration as the break increases in size. The peak of this asymptotic configuration is below 1500°F, a result not worse off than existing data on LOCA by double-ended pipe break. The clad surface temperature, however, sometimes goes through a drop before a steep climb, sometimes starts the steep climb from the onset of the break. This erratic behavior exists for different break sizes and the same break time, or for the same break size with different break times. It is argued that the correct pattern is the transient with a very slight rise before flow reversal, then a steady drop till close to EOB, then finally a steep climb after EOB and before the ECC water becomes effective. That the temperature sometimes rises steeply from the start of the accident and keeps on rising throughout the blowdown is attributed to either an error in the RELAP3 decision logic, or to the inadequacy of the existing DNB correlations in the case of transient flow with reversals.

CHAPTER 8

SIDE BREAK: RESULTS AND DISCUSSIONS

LIST OF FIGURES AND TABLES

8. SIDE BREAK: RESULTS AND DISCUSSIONS

The location of the break has been selected at the vessel wall opposite the center of the reactor core. Just before the break, the reactor is at steady state operation, the annulus is approximately at 2280 psia, 555°F and the downcomer flow velocity is some 29 fps.

The unit break size is 4.12 ft^2, the cross sectional area of the cold leg. Break sizes in multiples of 1, 2, 3 and 4 times that area have been studied. The rupture is assumed to open up linearly from zero to the specified area over a break time ranging from 0.00025 second to 0.1 second. Subcooled blowdown loadings and two-phase blowdown phenomena are studied. The results are summarized below.

8.1 Subcooled Blowdown Loadings

Description of system leg setup has been illustrated in Chapter 4, Table 4.2.T1 and Fig. 4.2.F3. Table 8.1.T1 describes the real system dimensions and various important parameters necessary for reference in the following discussion.

Leg 1 has been used to simulate the break. Before the rupture, it has the same pressure, temperature, subcooled condition as the location in the annulus opposite the reactor core center. Upon break initiation, liquid starts to blow out the end of leg 1, thereby creating decompression waves which travel to Leg 2 and Leg 4 at the same time because of the junction of these legs with Leg 1. The pressure just outside the break is taken as 1087 psi, the saturation pressure of water at 555°F which

Table 8.1.T1

WHAM NETWORK FOR SIDE BREAK

Leg No.	Initial p (psi)	Initial u (ft/sec)	Area (ft^2)	Length (ft)	Number of Subnodes
1	2279.5	0	4.12X	1.6	2
2	2279.5	29	16.54	6.58	7
3	2276.0	29	16.54	6.67	8
4	2283.0	-29	16.54	6.58	8
5	2283.0	29	10.18	6.58	8
6	2279.5	29	10.18	6.58	7
7	2276.0	29	10.18	6.67	8
8	2286.5	-29	36.4	4.67	5
9	2286.5	0	36.4	4.67	5
10	2272.5	6.0	129.4	5.33	6
11	2269.2	6.5	119.5	3.25	4
12	2265.8	6.5	119.5	1.34	2
13	2262.5	15.5	47.9	3.292	4
14	2254.6	15.5	47.9	3.292	4
15	2246.6	15.5	47.9	3.292	4
16	2276	15.5	47.9	3.292	4
17	2235.5	6.9	134.24	4.67	6
18	2236.5	0	134.24	6.32	8
19	2236.5	0	1.0	4.37	6
20	2262.5	1.4	23.44	3.292	4

Leg No.	Initial p (psi)	Initial u (ft/sec)	Area (Ft^2)	Length (ft)	Number of Subnodes
21	2254.6	1.4	23.44	3.292	4
22	2246.6	1.4	23.44	3.292	4
23	2238.6	1.4	23.44	3.292	4
24	2288	-47.54	16.48	21.16	24
25	2203	-37.8	20.81	11.5	13
26	2203	-7.52	105.8	6.22	6
27	2210.5	-15	54.56	26.16	26
28	2225.5	-17.51	54.56	26.16	27
29	2233	-9.0	105.8	6.22	6
30	2235	-50.47	18.35	17.22	23

(1) Sign of steady state velocity is relative to the positive direction of increasing subnodes in each leg.

(2) Number of subnodes is the integer closest to $L/C\Delta T$ where c is the sound velocity and Δt=0.25 msec.

is present in the annulus. Three different break times are studied, 0.00025 sec., 0.01 sec. and 0.1 sec. As 0.00025 sec. is the time for waves to travel only 1 subnode (Leg 1 has 2 subnodes), it can be considered as the "instantaneous" rupture case.

8.1.1 Transient Pressure Differentials

Figs. 8.1.F1, 8.1.F2 and 8.1.F3 show the pressure differential transients across the core, the core barrel and the thermal shield, respectively. These are the transients for the instantaneous break cases. Cases with longer break times show a similar fluctuating pattern, but with much lesser peaks. A comparison of the magnitudes of these peaks can be obtained from Figs. 8.1.F4 and 8.1.F5.

8.1.1.1 Thermal Shield

As can be expected, the largest pressure differential in the case of side rupture occurs across the thermal shield. The maximum differential is at the first pulse at around 2 to 3 msec. (8 to 12 time steps) when the break has been fully opened, exposing the point immediately at the break to a very low, close to saturation pressure whereas the point on the other side of the shield is still at its initial pressure. For the largest break (16.48 ft^2), the differential is 1130 psi. This value is very close to the maximum value of some 1200 psi which is the difference between the initial pressure and the saturated pressure.

Fig. 8.1.F1
SIDE BREAK: HISTORY OF PRESSURE DIFFERENTIALS ACROSS THERMAL SHIELD

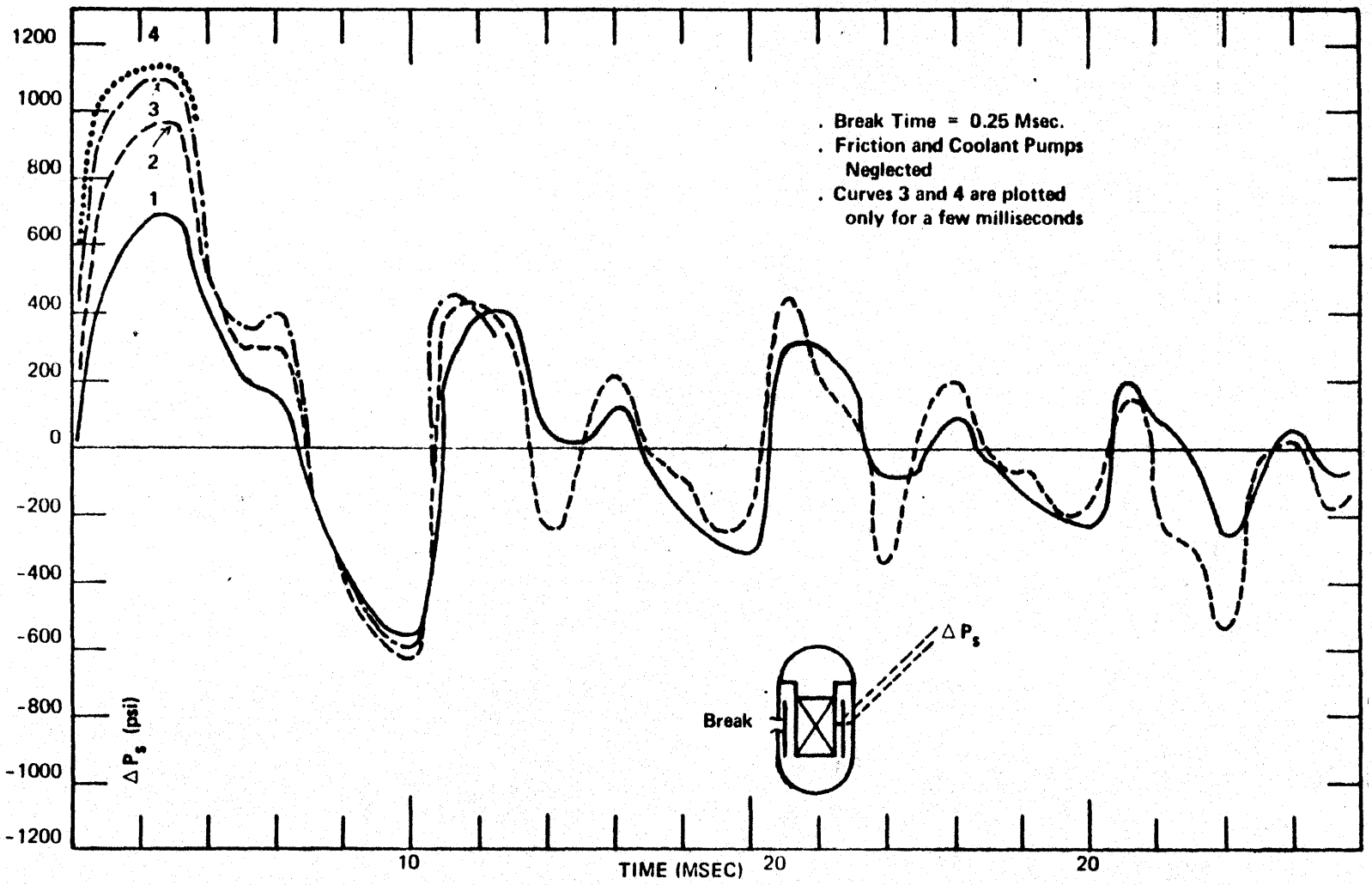

Fig. 8.1.F2
SIDE BREAK: HISTORY OF PRESSURE DIFFERENTIALS ACROSS CORE BARREL

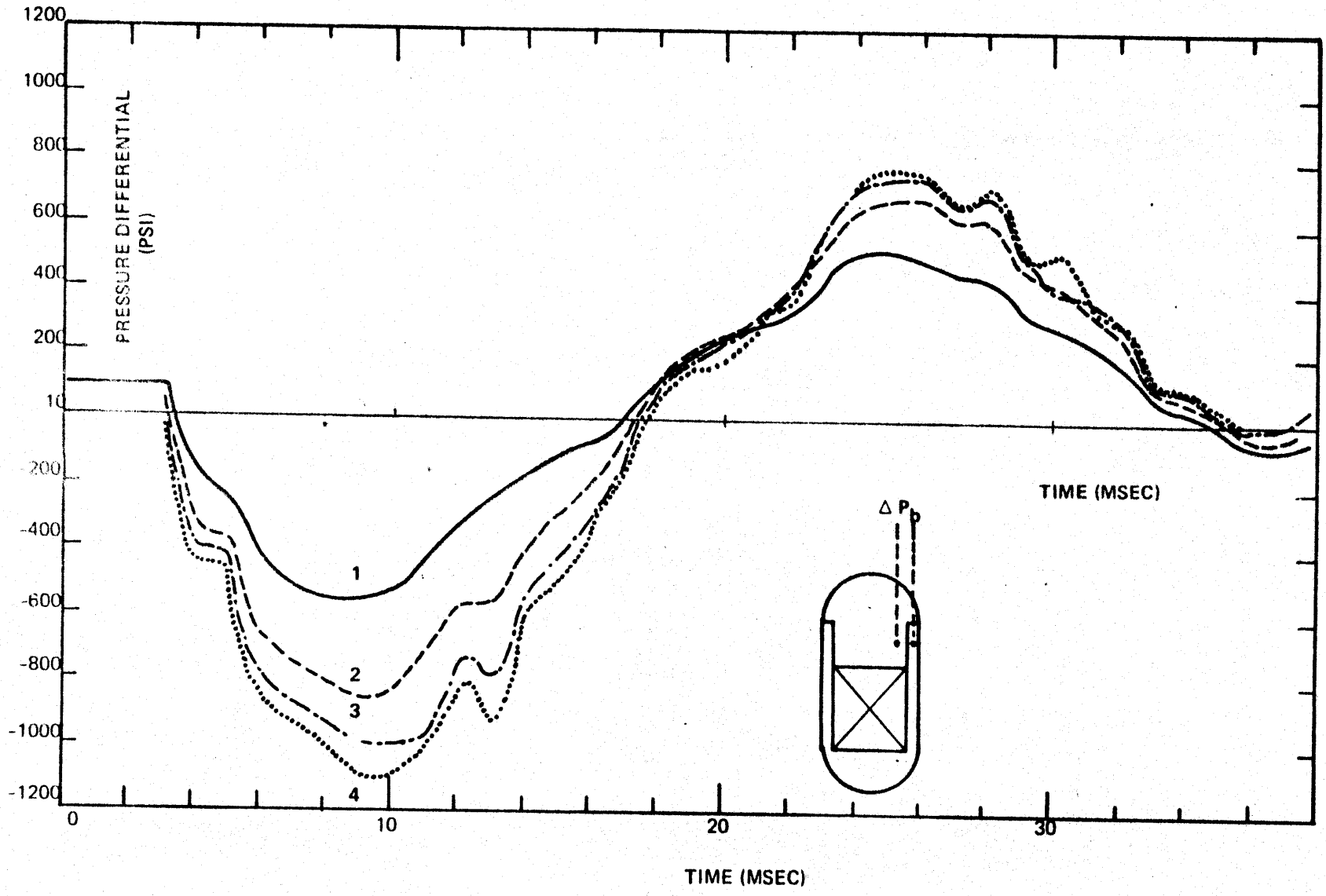

Fig. 8.1.F3

SIDE BREAK: HISTORY OF PRESSURE DIFFERENTIALS ACROSS CORE

(Only 2- and 4-pipe-sizes break cases are shown)

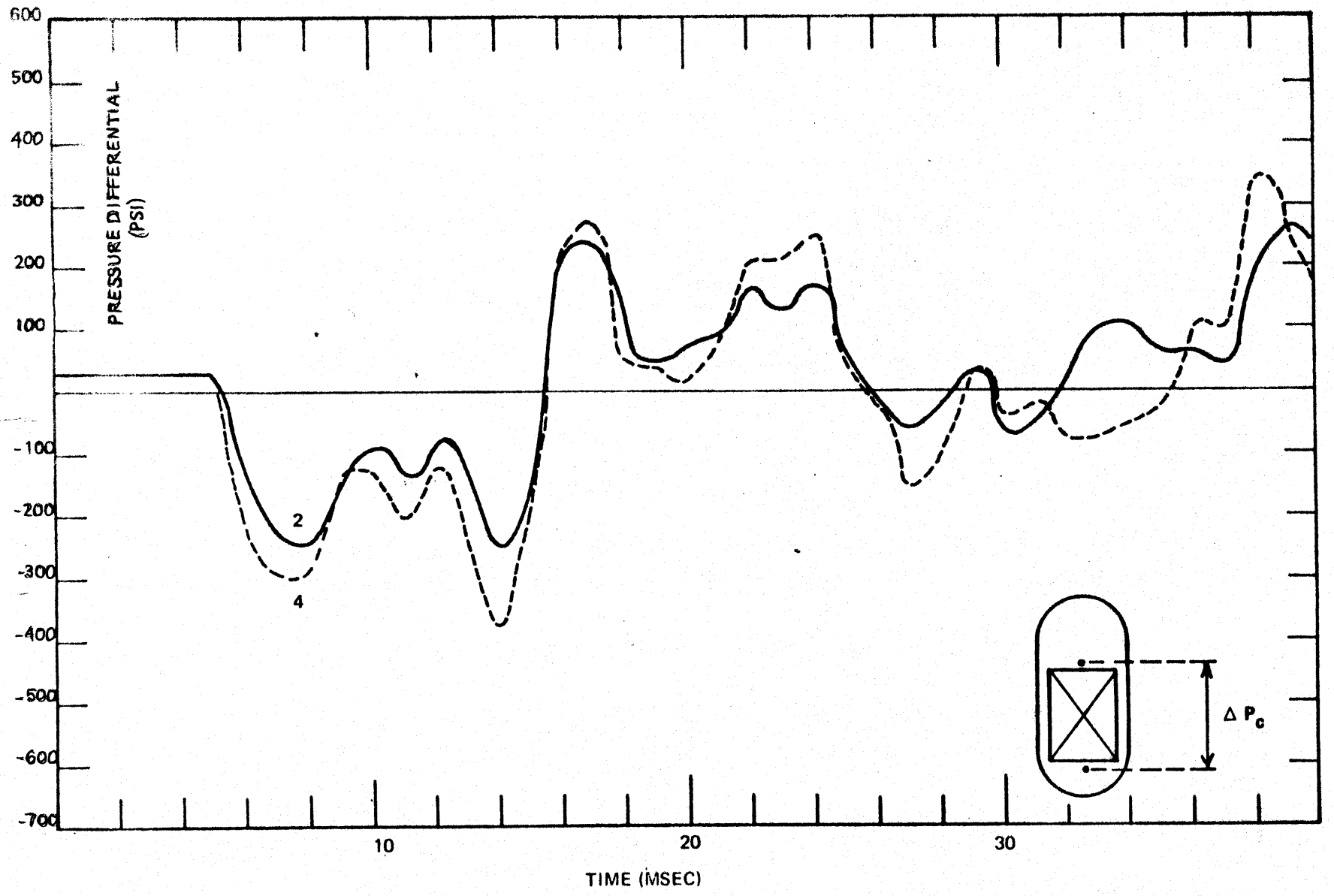

Beyond the first peak, the pressure differential curve assumes a complex oscillatory pattern which is due principally to three reasons: a) The rarefaction waves have traveled to the opposite side of the thermal shield, thus lowering the pressure there. b) Parts of the rarefaction waves have reflected back from leg ends to the break, thus increasing the pressure at the break (a reflected rarefaction wave is a compression wave). c) Compression waves from higher pressurized parts of the leg have traveled towards the break. b) and c) travel towards the break under the same form because tthe WHAM formulation allows only two kinds of wave coming in opposite direction towards any point.

A complete loading cycle takes about 10 msec. or 40 time steps. This is the duration of time needed for a wave to travel a round trip from one side of the shield to the other. The corresponding frequency is of the order of 100 cps.

8.1.1.2 Core Barrel

Fig. 8.1.F2 shows the pressure differential across the upper portion of the barrel as a function of time. The differential is taken as the pressure just at the cold leg nozzle minus the pressure on the other side of the barrel, in the upper plenum. Thus, following a vessel side break, the rarefaction waves reach the cold leg nozzles first, reducing the pressure there. The pressure in the upper plenum remains at its initial value (2236 psi) for quite a while, as one can inspect from Table 8.1.T1 and Fig. 4.1.3.F3, it takes some 50 time steps (12.5 msec.) for the waves to travel to the hot leg nozzles in the upper plenum. Due to this longer path for the waves to travel, the oscillatory pressure differential curve has

Table 8.1.T2

FREQUENCIES OF VIBRATION WITH RESPECT TO CORE AND CORE BARREL FOR SOME VESSEL INTERNALS (1)

Internal Component	Frequency (cps) Blowdown Loading	Seismic Loading
Upper Support System	300	25
Lower Support System		
When in Contact with Core	105	n.a.
When Core is Lifted	120	n.a.
Upper Flange	69	25

(1) Information is extracted from the spring-mass analysis summarized in Ref. C1, p. 14.3.3-8.

a longer period, some 32 msec. The corresponding frequency of loading is 32 cps.

In a similar manner as for the thermal shield, the first pulse has the largest amplitude. The peak pressure differential is 560 psi, 860 psi, 1000 psi, and 1100 psi respectively for 1, 2, 3 and 4 pipe-sizes breaks. Fig. 8.1.F4 shows that the peak value of the diffential levels out as the break size increases, approaching of course to the maximum possible value of 1149 psi which is the difference between the initial 2236 psi in the upper plenum and the 1087 psi that exists at the break as the back pressure.

8.1.1.3 Reactor Core

Fig. 8.1.F3 shows the pressure differential across the core. These curves are somewhat more complex than the corresponding ones for the core barrel and the thermal shield. The differential is taken as the pressure just below the core minus the pressure just above the core. At steady state normal operation. this is about 31.5 psi. Some 6 msec. after the rupture, the first rarefaction wave reaches the core bottom, thus making the pressure differential negative as indicated in the figure. The magnitudes of the pulses are not as pronounced as in the case of the upper core barrel because the magnitude of the rarefaction wave have been reduced through a series of transmission, and bending. Furthermore, the pattern of the curve indicates a series of reflection in the regime between the flow plates and core bottom.

8.1.1.4 Sensitivity of Break Size and Break Time

The above results are for break opening time of 0.25 msec., a duration so short that it has been called instantaneous. Calculations have also been performed for break opening times of 10 msec. and 100 msec. Typically, the longer the break opening time, the smaller the pressure differential across a certain component. This is due to the fact that the train of rarefaction waves emanating from the break consists of waves with magnitudes steadily increasing from 0 to a maximum value, whereas in the instantaneous break case, the train has rarefaction waves of the same maximum magnitude throughout. Due also to the same reason, the largest pressure differential does not necessarily take place at the first peak of the oscillatory curve. A series of transmission, reflection of compression and rarefaction waves of varying magnitudes would indeed result in a oscillatory pressure differential curve with a maximum peak somewhere later in the subcooled blowdown. In this work, the subcooled blowdown has been limited to less than 100 msec. (less than 40 msec. in the case of 4 pipe-sizes break) when the pressure at any point in the network is observed to fall below its normal saturation pressure.

Fig. 8.1.F4 shows the sensitivity of break areas and break opening times on the maximum pressure differentials across the core and the core barrel. Fig. 8.1.F5 shows the same sensitivity for the maximum pressure differential across the thermal shield.

Fig. 8.1.F4
SIDE BREAK

MAXIMUM PRESSURE DIFFERENTIALS ACROSS
THERMAL SHIELD CORE AND CORE BARREL

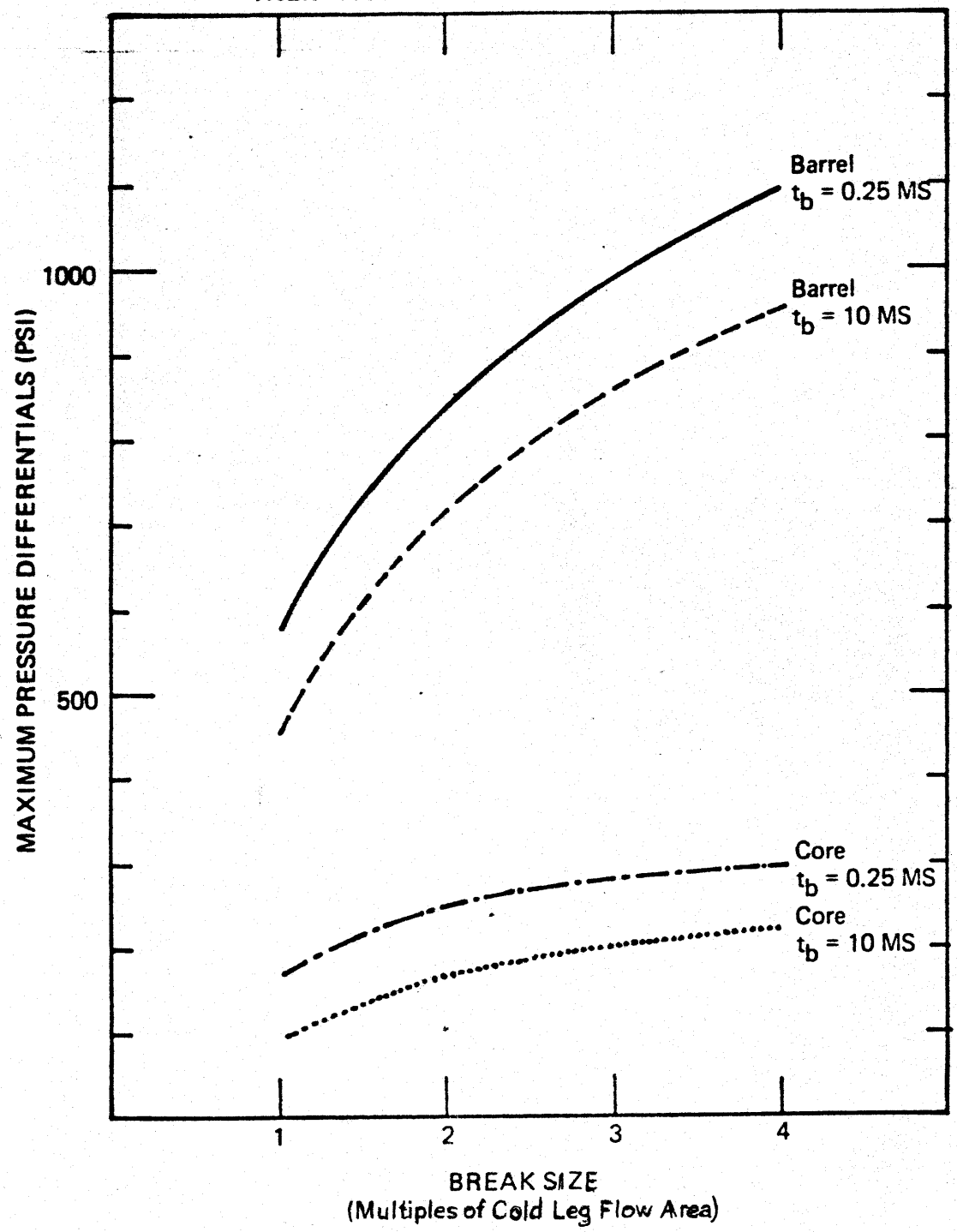

Fig. 8.1.F5
SIDE BREAK
MAXIMUM PRESS. DIFF. ACROSS THERMAL SHIELD

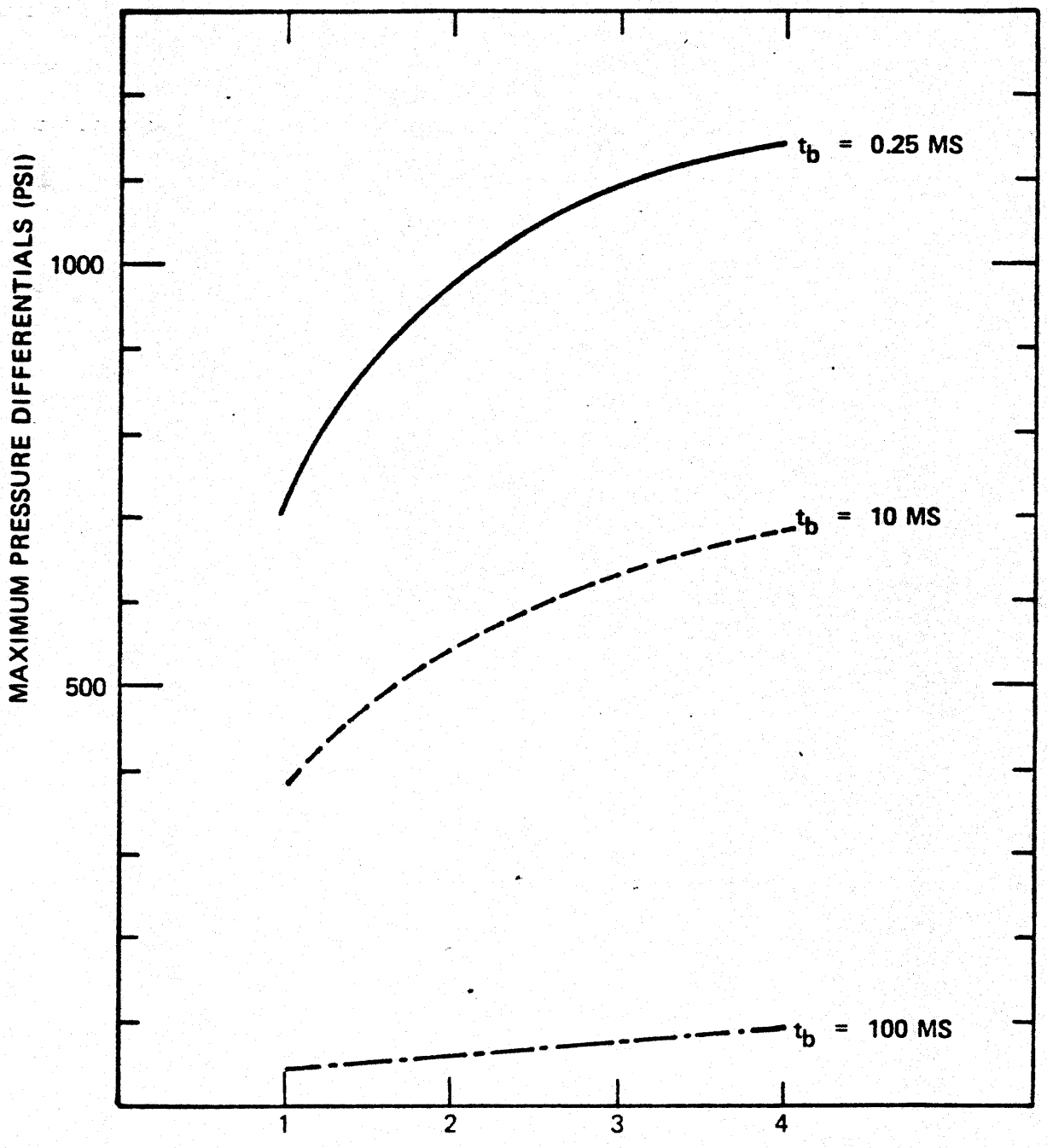

The manufacturer (C1) states that the critical buckling pressure for the core barrel is 2990 psi assuming the upper core barrel is simply supported and the stiffening effect of the fluid environment is neglected. It is obvious that this value is much larger than any pressure differential obtained from this study. The same reference has also cited that a quantitative analysis has been done for the dynamic response of the barrel under compressive pressure waves of 360 psi in magnitude, 25 msec. in pulse time. The maximum resultant stress was found to be 11,844 psi, and the maximum radial deflection was found to be plus or minus 25.6 mils. It is not a part of this study to establish stress and deflection resulting from loadings due to LOCA by vessel rupture.

8.1.2 Subcooled Force Loadings

The manner by which the force loadings are computed have been described in Sections 4.1.2 and 4.1.3. In general, the forces acting on the internal can be classified as the hydrostatic force which is always perpendicular to the surfaces, the shear force due to friction and momentum change which always acts parallel to the surface. The gravity force is very small and has been neglected.

Due to the one to-one relationship between the pressure, velocity and force at any point in the system, the force loading should have the same time behavior as the pressure differentials. Table 8.1.T3 shows the maximum force loadings across the core for the first two pressure differential peaks which take place at about 8 msec. and 14 msec. Only the hydrostatic force and the inertial force have been included. The forces due to gravity, friction, and momentum fluxes are quite negligible compared to the above

Table 8.1.T3

VESSEL SIDE BREAK

MAXIMUM FORCE LOADINGS ACROSS THE CORE*

Cases	Inertial Force (1000 kips)	Hydrostatic Force (1000 kips)	Total (1000 kips)
At 8 msec peak			
Break Size A=1	1.794	-2.321	-0.527
A=2	1.881	-3.428	-1.547
A=3	2.196	-3.889	-1.693
A=4	2.243	-4.089	-1.846
At 14 msec peak			
Break Size A=1	0.912	-1.645	-0.734
A=2	1.778	-3.419	-1.641
A=3	2.374	-4.554	-2.180
A=4	2.761	-5.221	-2.461

*Forces due to momentum fluxes, friction and gravity have been neglected Cross section of the core is taken as the area inside the baffle, or 96 ft^2. Positive direction of the forces is upwards.

two forces. It is seen that, the hydrostatic force is acting downwards as the result of the higher pressure in the upper plenum at these instants. The inertial forces act in the opposite direction. This is due to the fact that the normal fluid velocity is acting upwards, and the transient causes it to slow down. The slowing down of the fluid creates a reactive force on the flow channel wall with an upward direction. Hence, the effect of the pressure differential is cancelled somewhat by the acceleration or deceleration of the fluid. The net forces are in the direction of the hydrostatic force.

Force loadings for the core barrel and the thermal shield have not been evaluated. This is due to two complicating factors:

a) The pressure differentials across these components are different at different elevations.

b) The inertial forces act in a direction perpendicular to the hydrostatic force. Furthermore, different inertial forces act on the two sides of these components.

The present study does not include a detailed analyses of these loadings.

8.2 Two-Phase Blowdown

Similar to the cases of top and bottom vessel rupture, the principal phenomena of the two-phase blowdown have been studied within the capability of the RELAP-3 Mod 36 Computer Code.

The main assumptions and initial conditions are the same as in the case of the bottom break and have been described elsewhere in this study. The break elevation is taken as that of the core center. Four sizes for the break have been considered, with the cold leg flow area taken as unit break size. Thus, the break sizes are 1, 2, 3, and 4 times the size of the cold leg flow area, corresponding to 4.12 ft^2, 8.24 ft^2, 12.36 ft^2 and 16.48 ft^2, respectively.

Most of the runs are based on a break time of 0.1 second, although a few cases have been studied with a break time of 0.01 second. The choice of a 0.1 second break time is conservative on two counts. First, it retards the reactor scram by slower void formation, thus allowing fission to take place over a longer time after break initiation. Second, it retards the flow reversal process, resulting in a longer flow stagnation. A large break time would be unconservative as far as subcooled loadings are concerned, but these have been studied separately in Section 8.1 with break times as small as 0.00025 second.

The principal phenomena followed are the normalized core power history, the flow reversal, the pressure history in the upper and lower plena, the mass loss rate, the ECC injection rate, the core flow and heat transfer coefficient, and the clad surface temperature in the central core region. All values are averaged values computed by following the processes in very small time steps.

8.2.1 Normalized Power History

Fig. 8.2.F1 shows the normalized power histories for the four break sizes (1, 2, 3 and 4) and the history for the LOCA by cold pipe break put forth for essentially the same plant by the manufacturer (C1).

Void formation has been solely responsible for reactor scram. Doppler coefficient has been used but its effect is essentially nil because the temperature of the fuel does not change for the short span of time at the begining of blowdown. No power excursion is deemed possible, hence this mechanism has not been considered. No safety rod action has come into play because any motion of the rod has been conservatively delayed for 30 seconds, an assumption with the same significance as no safety rod insertion at all. The magnitude of the void reactivity are -0.0079, -0.0328, -0.0149 dollar per 1% void respectively for the upper one third, central one third, and lower one third of the core. These values are conservatively small compared to the ranges found in the kinetic characteristics of the same plant (Appendix A) and the values set forth by an independent study by Elbaum (E2) on this kind of accident. A sensitivity study has been done for this void reactivity coefficient and is reported in Chapter 9.

All curves except the DE curve in Fig. 8.2.F1 have been based on a break time of 0.1 second as previously mentioned. The effect of a shorter break time, namely 0.01 second, is also reported in Chapter 9. The DE curve is the manufacturer supplied curve for essentially the same plant but for the case of LOCA by a double ended break in one of the four cold legs. It was obtained with the use of the CHIC-KIN point kinetic computer code (C1, R4), taking

Fig. 8.2.F1
SIDE BREAK
NORMALIZED POWER HISTORY

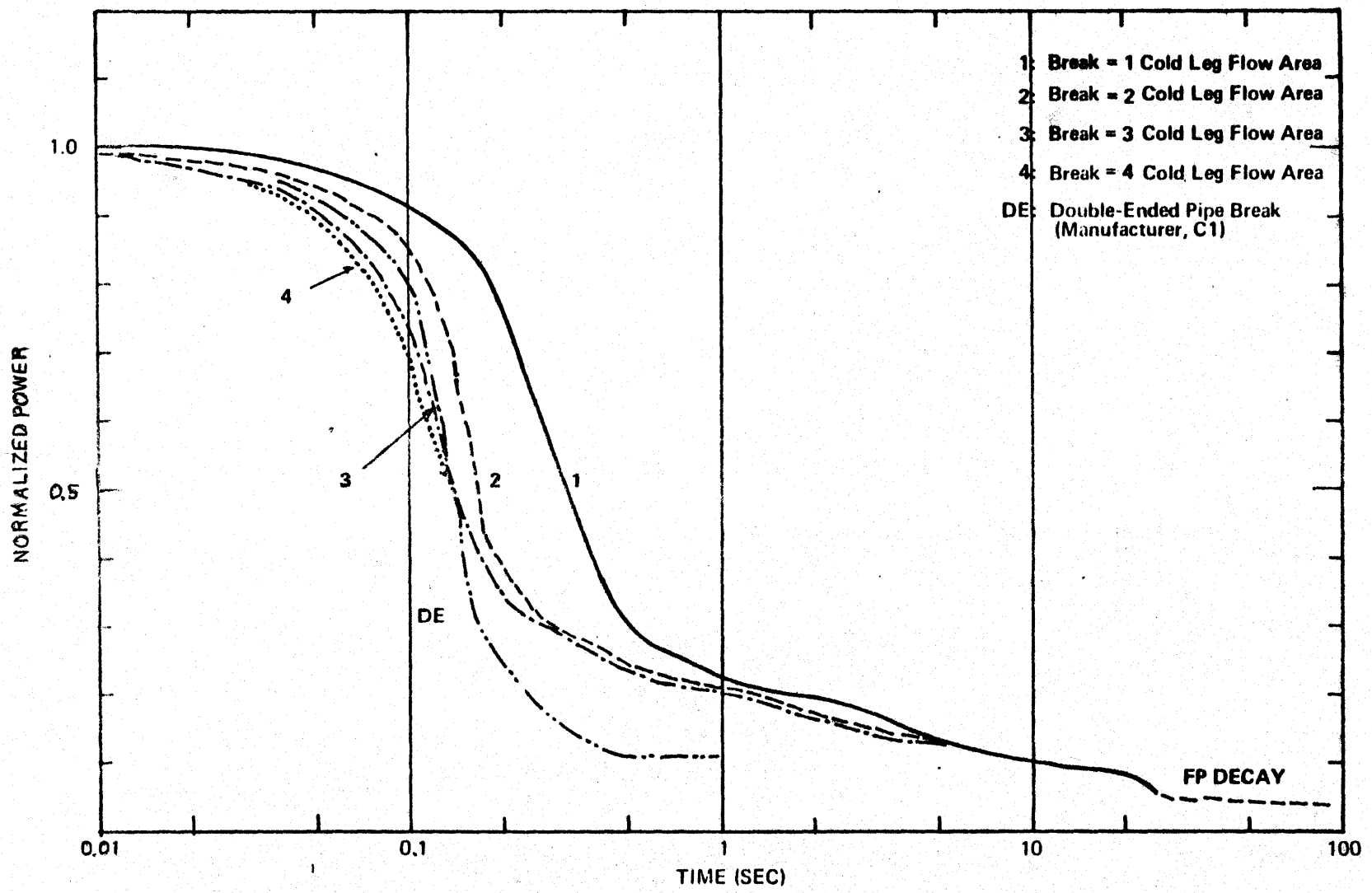

into account of void formation, reactor scram by pressure signals and other reactivity coefficients.

Reactor scram should be slower for the case of pipe break than for the case of vessel break with the same break area. This is because of a faster depressurization, and therefore, a faster void formation in the core region. However, it is apparent from Fig. 8.2.F1 that the DE curve decays faster than curve 2. This is due to the fact that a slower break time has been used in the vessel break postulate, and that all other negative reactivity coefficients have been neglected. Both of these assumptions are conservative, particularly beyond 0.1 second when there is still substantial fission power for the vessel rupture cases under study.

A comparison with Fig. 7.2.F1 (Bottom break) indicates that there is more power generated in the side break cases than in the corresponding cases of the bottom break. This should be of no surprise because a break in the bottom should depressurize the coolant in the core a little faster. Furthermore, the normalized power curves in the side break case are more crowded together, indicating a smaller difference in void formation than in the case of bottom break. This fact is a result of the flow rates and mass loss which are fast in reaching an asymptotic configuration due to flow choking. Further discussion of this phenomenon will be found in the following sections.

8.2.2 Flow Reversal

Fig. 8.2.F2 shows the flow reversal for the four side break cases under consideration. It is noted that the time scale of the figure is in milliseconds. Normal flow rate through the core is of the order of 37,000 lbs/sec. Onset of the break is at 5 msec., a value set for break actuation by the computer.

As the break at the side opens up linearly with time, the flow through the core is slowed down due to a great pressure differential between the upper plenum and the lower plenum. The slowing down of the flow takes place very fast. Stagnation (zero flow) is reached around 56 msec., (51 msec. after the break) for the one pipe size break. For larger breaks, stagnation happens around 20 msec. Since the full break size is not reached until 105 msec. (break time is 0.1 sec.), it is seen that flow reversal takes place quite early in the blowdown.

At the time of stagnation, the pressure differential across the core is of the order of 200 to 400 psi. The fluid in the system is still substantially subcooled.

Fig.8.2.F2

SIDE BREAK: FLOW REVERSAL AT CORE CENTER

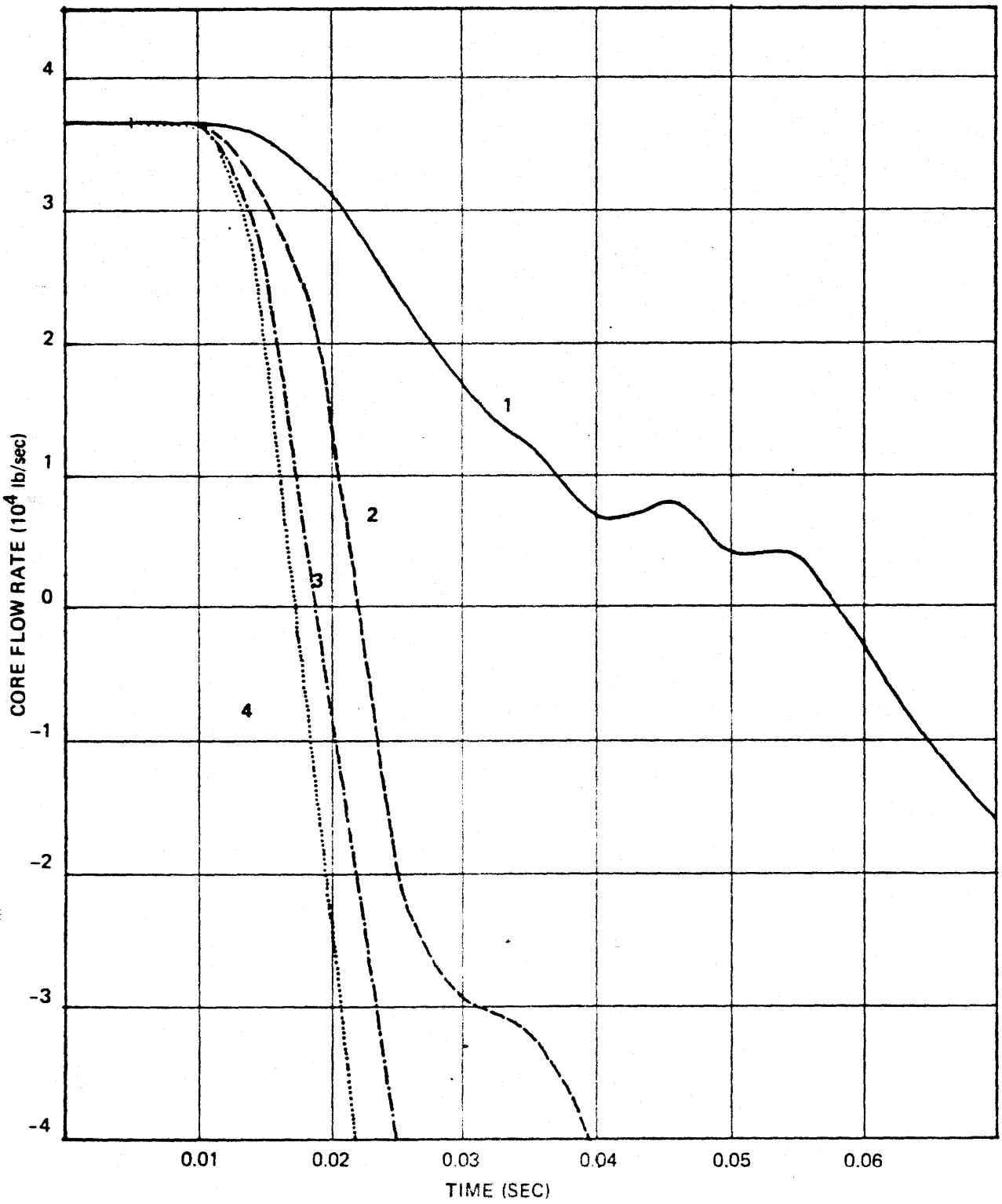

It has been reported (C5) that for the case of LOCA by cold leg break, flow reversal may swing back and forth a few times due to liquid flashing in the upper and lower plena. Thus, soon after the cold leg break, the flow through the core reverses from the normal, positive direction to the negative direction due to the negative pressure differential. Fluid in the upper plenum may flash at this moment and contributes further to the reversed flow. Then, the fluid in the core volume would flash, pushing coolant out at both ends of the core. Shortly after, the fluid in the lower plenum would flash, driving the coolant up the core, thus causing another reversal. Finally, due to the influence of the break, the pressure in the lower plenum drops faster than the pressure in the upper plenum, creating another flow reversal.

For the cases of vessel side break considered, however, no such repeated reversals are observed. This certainly would be due to the fact that flashing in the core and the lower plenum is of no competition to the drop in the lower plenum pressure caused by the rapid blowdown. Later on, when blowdown is completed, there may develop situations whereby the coolant may get to the core, be heated up to a relatively high temperature and pressure, and subsequently is pushed out towards both core ends. Flow starvation, reversal and stagnation in this period are the chief causes for a steep clad temperature transient that will be discussed in Section 8.2.7.

It is also worth noting that during the short duration of flow reversal, the clad temperature rises somewhat. When stagnation point has passed and the reversed flow increases in magnitude, the temperature of the clad drops again and keeps on dropping until close to EOB. There is some exception to this general pattern as will be later discussed in Section 8.2.7.

8.2.3 Rate of Blowdown

Fig. 8.2.F3 shows the blowdown flow rates at the break. Fig. 8.2.F4 shows the mass loss history for the entire primary system. Table 8.2.T1 lists the duration of flow choking in some critical flow paths and Table 8.2.T2 lists some EOB time values for the side break cases considered.

The effect of flow choking displays itself dramatically in the vessel side break of large sizes. Starting from no leak at the onset of the break, the flow through the break is first subcooled, but then quickly becomes two-phase with choking because there is a great pressure differential across the break. The buildup in blowdown flow rates as seen in Fig. 8.2.F3 between 0.01 sec. and 0.1 sec. is mainly due to the fact that the break area still grows linearly in size. For large breaks, a maximum blowdown rate is reached even before the break size has reached a preset maximum. Thereafter, the rate tapers off while still being choked because of the decrease in the driving pressure in the primary system. The larger the break, the sooner the choking disappears due to a faster drop in system pressure.

Fig. 8.2F3
SIDE BREAK $t_b = 0.1$ sec
BLOWDOWN FLOW RATES AT BREAK

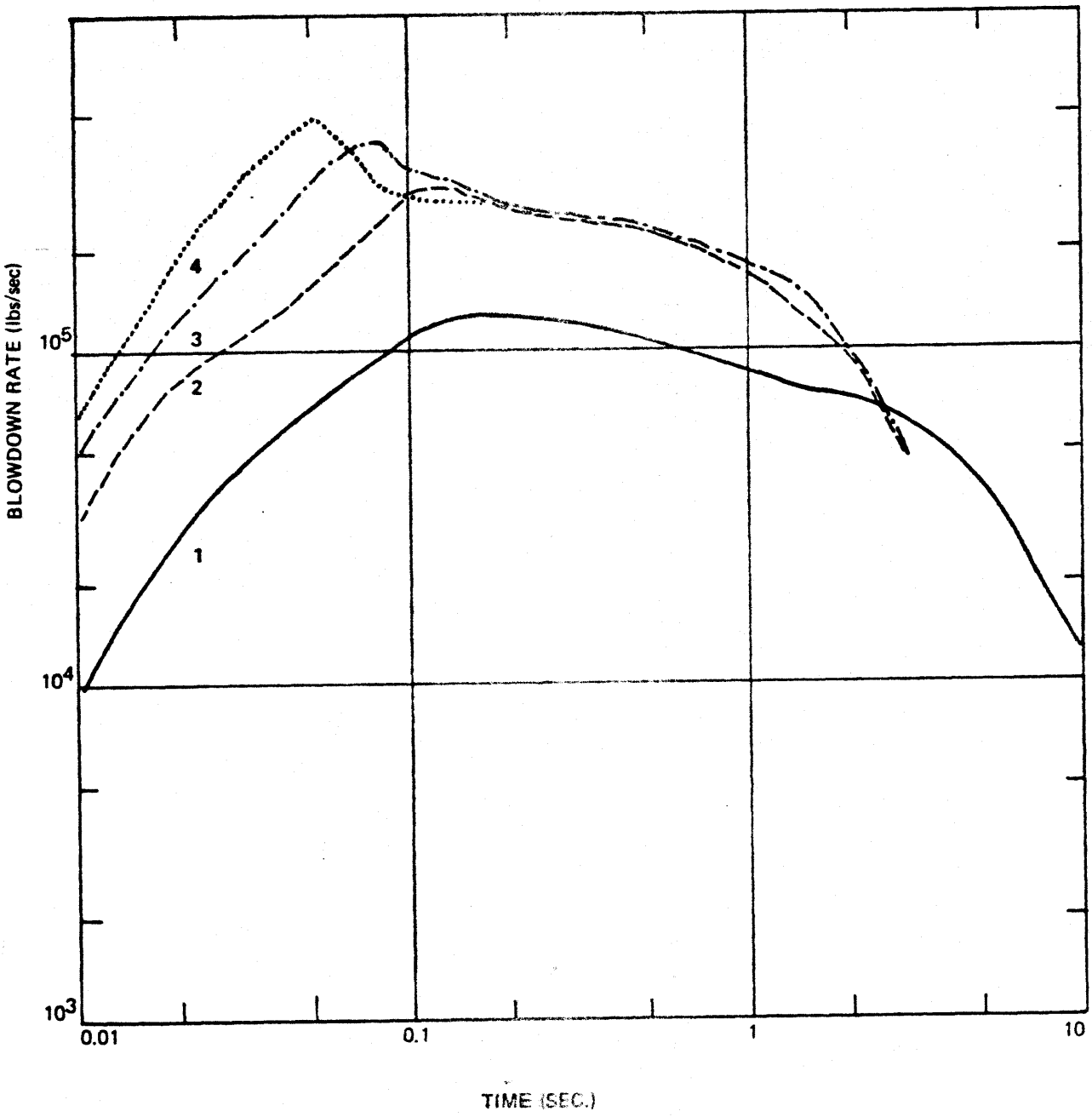

Table 8.2.T1

SIDE BREAK

FLOW CHOKING IN SOME FLOW PATHS

Break Size (Multiples of Cold Leg Flow Area)	Duration of Choking (Sec) J20*	J12	J10
1	0.005 - 10.63	No	No
2	0.005 - 3.5	0.3 - 2.0	NO
3	0.005 - 2.5	0.1 - 3.0	0.2 - 2.5
4	0.005 - 1.8	0.08 - 3.5	0.08 - 2.5

* The flow path indexes correspond to Fig. 5.3.F1, namely J20 is the break, J12 is the flow path between the lower plenum and the annulus between the thermal shield and the vessel wall, and J10 is the flow path between the cold leg nozzle region and the same annulus.

Table 8.2.T2

SIDE BREAK

START OF EMERGENCY CORE COOLING INJECTION

(SECCI) AND END OF BLOWDOWN (EOB)

Break Size (Multiple of Cold Leg Flow Area	SECCI (Sec)	EOB (Sec)
1	5.76	12.35
2	1.78	7.09
3	1.59	2.59 - 7.84
4	1.58	1.85 - 7.85

Fig.8.2.F4

SIDE BREAK

MASS LOSS HISTORIES

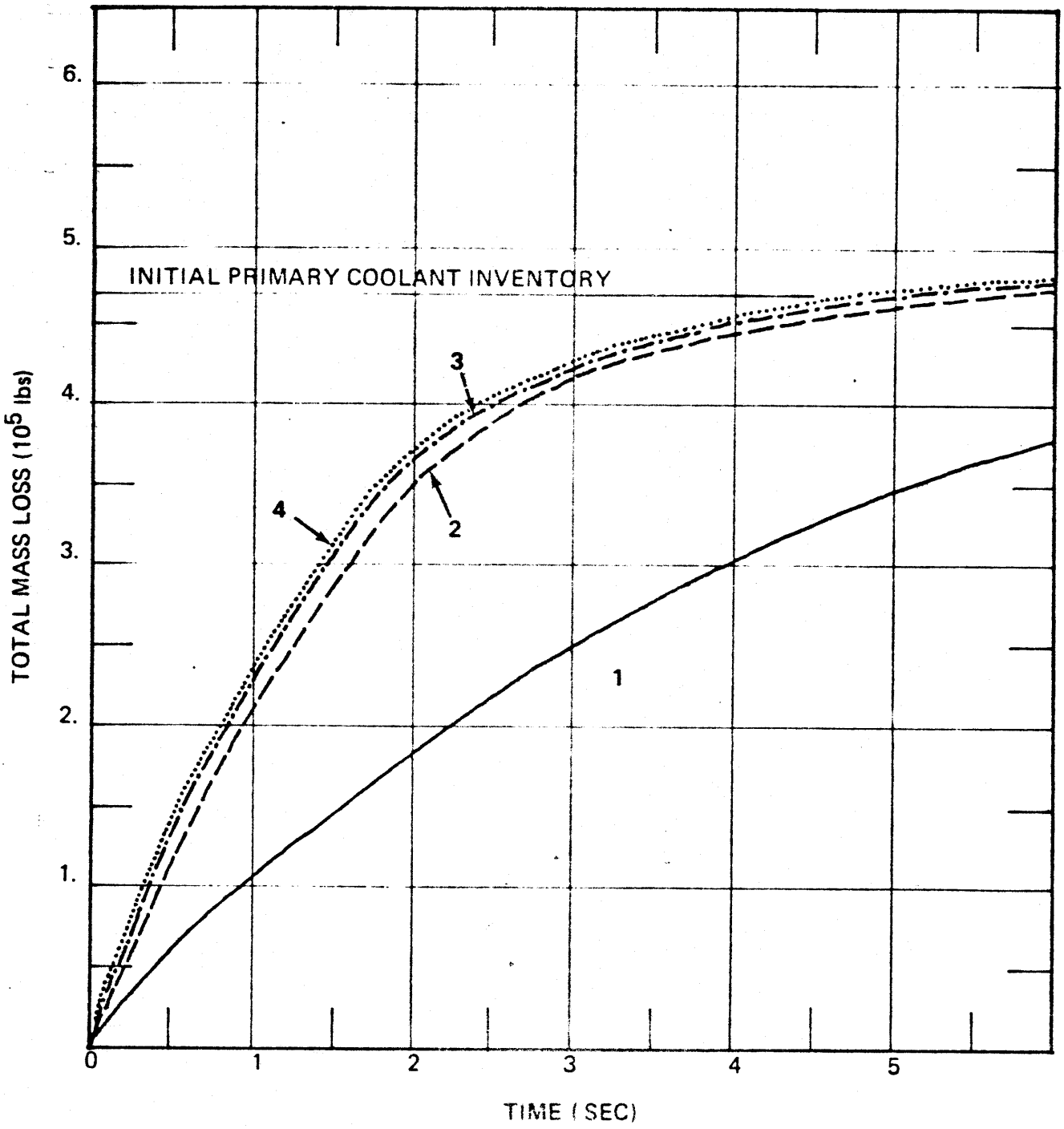

The dramatic asymptotic pattern of the blowdown flow rates for curves 2, 3 and 4 between 0.1 and 3 seconds is due to flow choking at the break and elsewhere in the system. Indeed, the flow area at both ends of the annulus between the thermal shield and the vessel wall is only 16.54 ft^2, the area equivalent to 4 times the cold leg flow area. Table 8.2.T1 indicates that soon after the break, the flow in these flow paths becomes choked. In fact, flow choking in these flow paths can last longer than at the break for large break sizes because they have a higher resistance and are at the immediate outlet of high pressure regions which have flashing coolant, namely the vessel and the cold legs. The limiting flow rates as seen in Fig. 8.2.F3 are the reason for the asymptotic configuration in the system mass loss history, system pressure and other parameters that are seen in Figs. 8.2.F4, 8.2.F5 and 8.2.F6.

Table 8.2.T2 lists some values for the start of emergency core cooling injection from the accumulators and some values for end of blowdown. The ECC water from the accumulator starts to inject into the cold legs when the pressure there drops below 660 psi. Credit has been given to this water as it is, however, it would take some time for this injection rate to build up to a significant value, as can be seen in Fig. 8.2.F7.

End of blowdown (EOB) happens at 12.35 seconds for Case 1, 7.09 seconds for Case 2. EOB has been defined as the first instant when the flow out the break effectively stops. This definition is not rigorous for large break sizes, however, because the flow in such situations fluctuates violently and otherwise is controlled by restrictions in various locations in the system. Thus, the first zero flow rate at the break happens at 2.59 seconds for Case 3 and 1.85 seconds for Case 4. But the primary

system still contains significant amounts of coolant as can be seen in Fig. 8.2.F4. So what happens is a fluctuating flow pattern after the first stagnation at the break. As can be seen in Table 8.2.T2, EOB is not effectively reached until 7.85 seconds for Cases 3 and 4, a value quite similar to EOB for Case 2.

8.2.4 Pressure Histories in the Upper and Lower Plena

The pressure histories in the upper and lower vessel plena are important in the determination of coolant flow rates through the core, hence its heat removal characteristics.

Fig. 8.2.F5 and 8.2.F6 show the pressure histories in the upper plenum and lower plenum for the side break cases considered. As usual, indexes 1, 2, 3 and 4 designate the break size in the multiples of cold leg flow area. The curve marked DE is the pressure history, presumably for the core, presented by the manufacturer for essentially the same 2758 MWth plant undergoing a LOCA by double-ended break in one cold leg. Simple marks on the curves represent start of emergency core cooling in the cold legs, and crosses represent the end of blowdown.

The curves indicate that for all cases the pressure in the upper and lower plena drop faster than is possible when the pipe breaks. This is only to be expected. When the break is at the vessel, fluid in the upper and lower plena can blowdown with very little resistance.

Fig. 8.2.F5
SIDE BREAK
PRESSURE HISTORY IN UPPER PLENUM

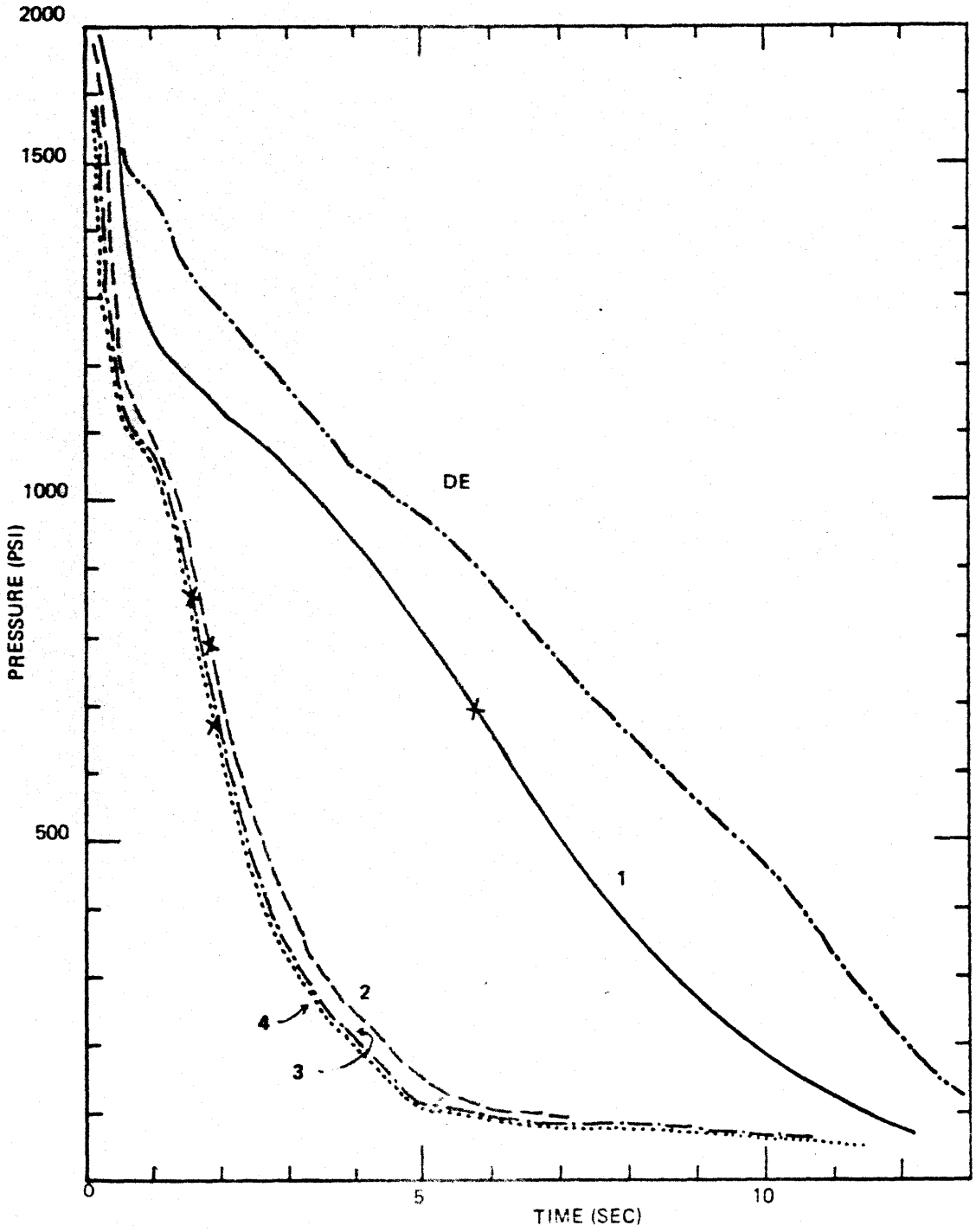

Fig. 8.2.F6
SIDE BREAK

PRESSURE HISTORY IN LOWER PLENUM

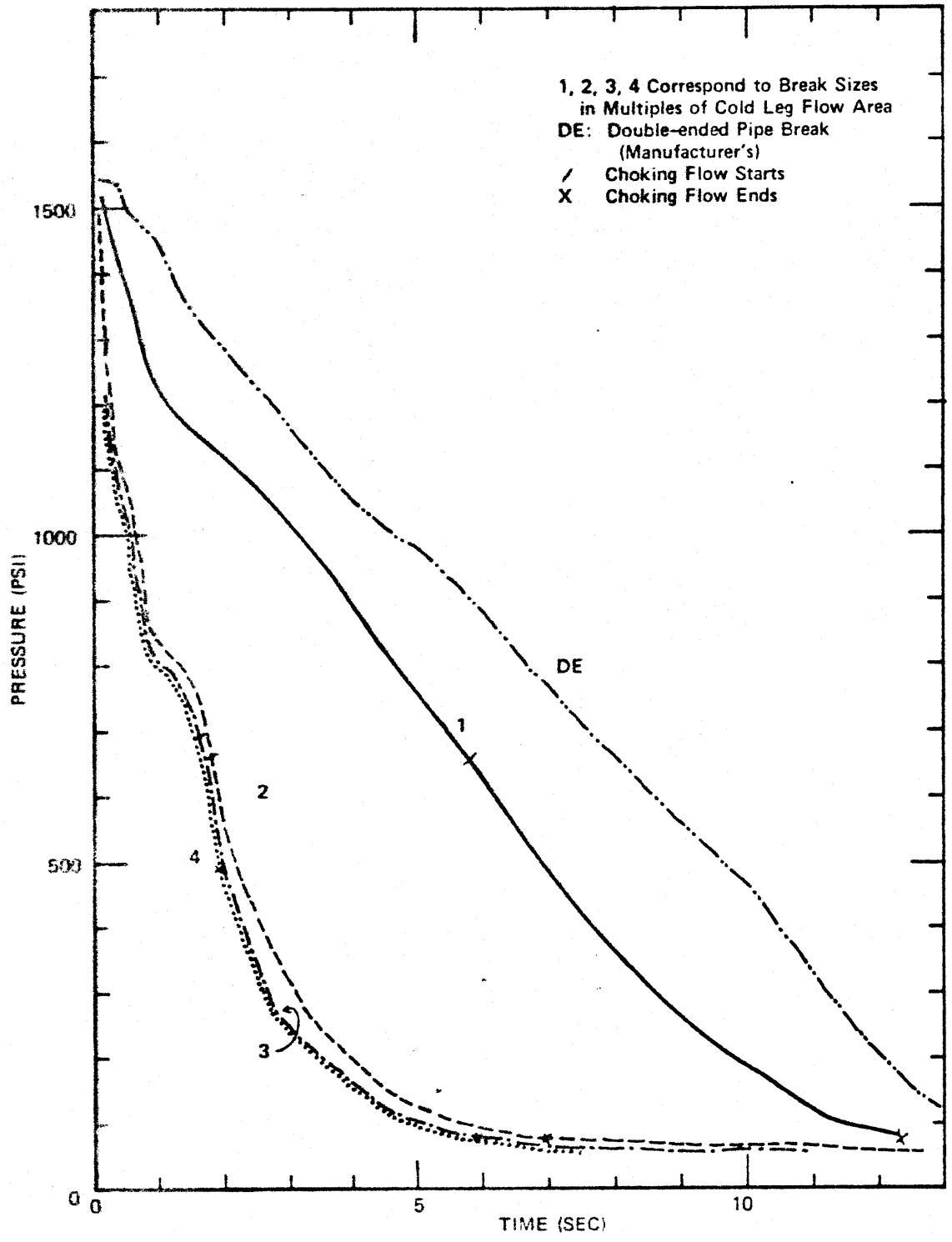

It is noted that the crowding of pressure history curves is apparent for cases of top and bottom breaks but nowhere does it manifest itself so strongly as the present side break cases. The cause of this crowding has been previously explained as the result of flow choking at the outer downcomer annulus, allowing only a limited rate of blowdown.

8.2.5 ECC Water Injection into Cold Legs and Coolant Mass Remaining in Lower Plenum

Fig. 8.2.F7 is a composite graph showing the history of pressure and mass in the cold legs, the ECC water injection rate from the accumulators and the pressure history of the accumulators. The graph is plotted for the case of break size 4 times as large as a cold leg flow area. Other break size cases have similar pressure, mass and injection behavior.

Fig. 8.2.F8 shows the coolant mass remained in the lower plenum of the pressure vessel for all four cases of break size.

The pressure in the cold legs drops in much the same manner as other parts of the system, namely a steep subcooled pressure drop, then a short time at saturation, a less steep drop for the remaining blowdown time, and finally a slower drop as ECC water is slowly building up. At around 660 psi, the ECC water starts to inject, building its velocity from zero to some 2800 lb/sec. in about 2 seconds, then slowly dropping due to the decrease in driving force (pressure differential between the accumulators and the cold legs). The friction in the ECC lines is quite a determinant in the maximum injection rate as will be seen in Chapter 9. The above quoted value of 2800 lb/sec. corresponds to a friction coefficient of 0.004.

Fig. 8.2.F7
SIDE BREAK: ECC INJECTION
M8: MASS IN COLD LEGS; P8: PRESSURE IN COLD LEGS
P17: PRESSURE IN ACCUMULATORS; J19: ECC INJECTION RATE

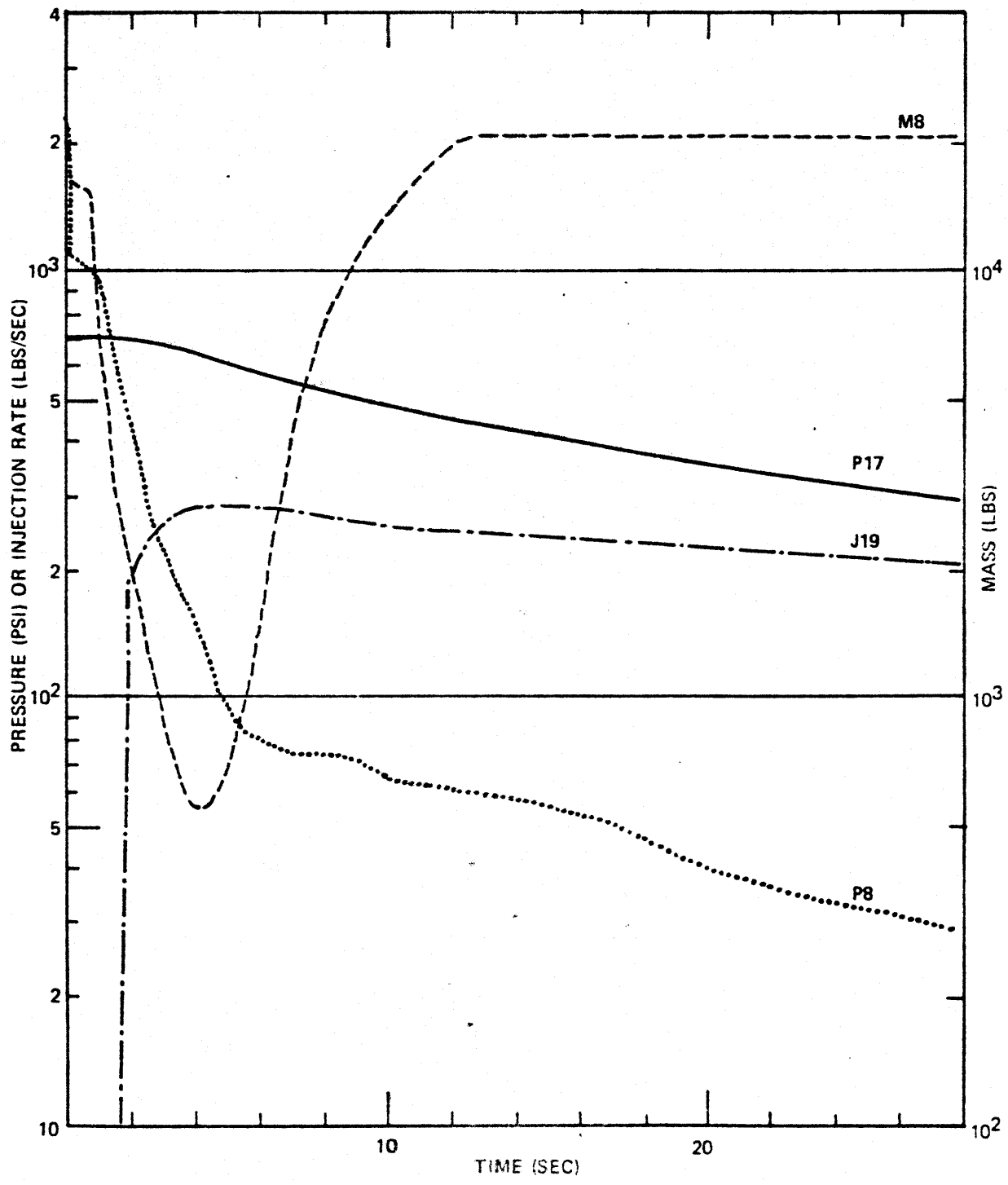

Fig. 8.2.F8
SIDE BREAK
COOLANT MASS IN LOWER PLENUM
(1, 2, 3, 4 Correspond to Breaks In
Multiples of Cold Leg Flow Area)

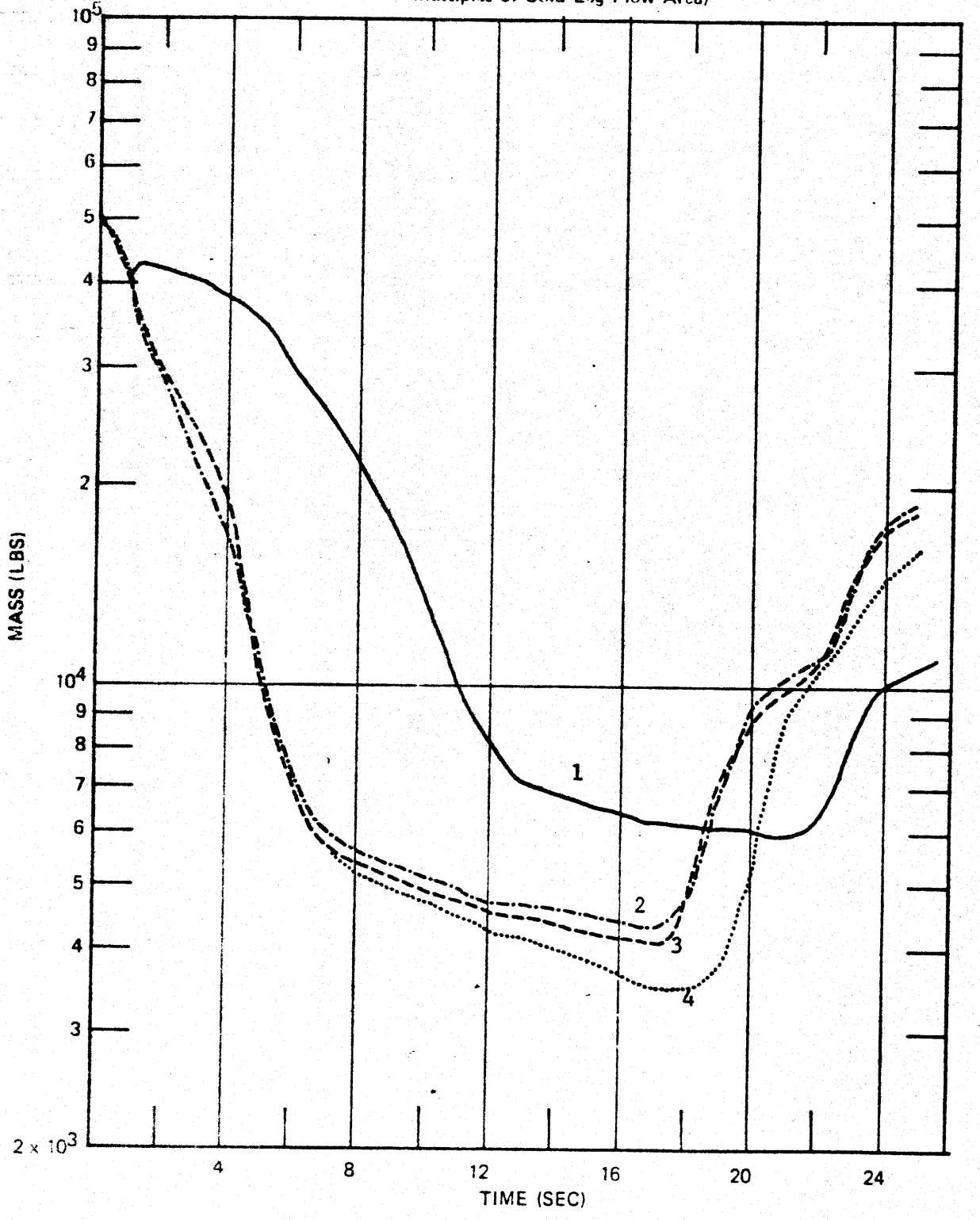

The history of the mass in the cold legs is most indicative of the behavior and effectiveness of the on-line ECC water tanks. It drops from a steady state value of 1.72×10^4 lbs to a low of some 55 lbs in four seconds after the break. The cold legs at that time is practically devoid of coolant except for the steam at approximately 150 psi. The ECC water has actually been injected 2 seconds earlier, having discharged some 5600 lbs of 100°F water. The fact that the total cold leg mass continues to drop between 2 seonds and 4 seconds indicate that some of the injected water did get carried over to the annuli and out the break. Only when the rate of injection has reached a maximum, the pressure of the cold legs has dropped to a value equivalent to or smaller than that of the annuli. then the outflow from the cold legs would effectively stop. The injected ECC water from then on stays in the cold legs to build up the cold leg coolant mass to a value of some 2.06×10^4 lbs at 12 seconds. When the legs have been filled, flow to the annuli again commences with a very high rate equal to or slighly higher than the ECC injection rate at that time.

That the ECC water stays in the cold legs has been explained (A3) more because of the shortcoming of the RELAP3 Code than because of the physical reality. In a physical system, one should expect some carryover due to entrainment, gravity, and the initial ECC velocity. RELAP3 assumes instantaneous thermodynamic equilibrium in any volume of the model. Since the injected ECC water is cold (100°F) this has the effect of dropping the pressure quickly, reversing the flows. and therefore accumulating coolant in that volume. ECC water is, as a consequence. delayed in reaching the next contiguous volume. When the volume to which the ECC water injects is far from the core. the chaining of delays can cause considerable retardation

of the water to reach the core. The core temperature transient must, therefore, be more severe than for the case with allowance for continual entrainment of ECC water.

The coolant mass remaining in the lower plenum as shown in Fig. 8.2.F8 is less for a break larger in size. During blowdown, the rate of mass loss is rapid, but quickly reaches a limiting value as can be judged by the closeness of curves 2, 3 and 4 between 0 and 5 seconds. This, of course, is due to the choking flow in the outer annulus as previously discussed. When EOB occurs, the mass in the lower plenum is still at a respectable value, some 8000 lbs. or 15% that of the initial inventory. This mass continues to drop, but at a slower rate, due to the flashing of steam for flow to other volumes. Some 10 seconds after EOB, ECC water starts flowing in from the annuli, and the mass in the lower plenum starts to build up even through the pressure there continues to drop. At 25 seconds, the lower plenum is still far from being filled for the cases under investigation.

8.2.6 Heat Transfer Coefficient (HTC), and Coolant Flow Rate at Core Mid Plane

Figs. 8.2.F9 and 8.2.F10 show the average flow, heat transfer coefficient and clad surface temperature for the vessel side break with break area in the multiple of 1 and 2 cold leg flow area, respectively.

Fig. 8.2.F9
SIDE BREAK, A = 1

AVERAGE HEAT TRANSFER COEFFICIENT (HTC),
COOLANT FLOW RATE AT CORE MIDPLANE
AND CLAD SURFACE TEMPERATURE IN MIDDLE CORE REGION

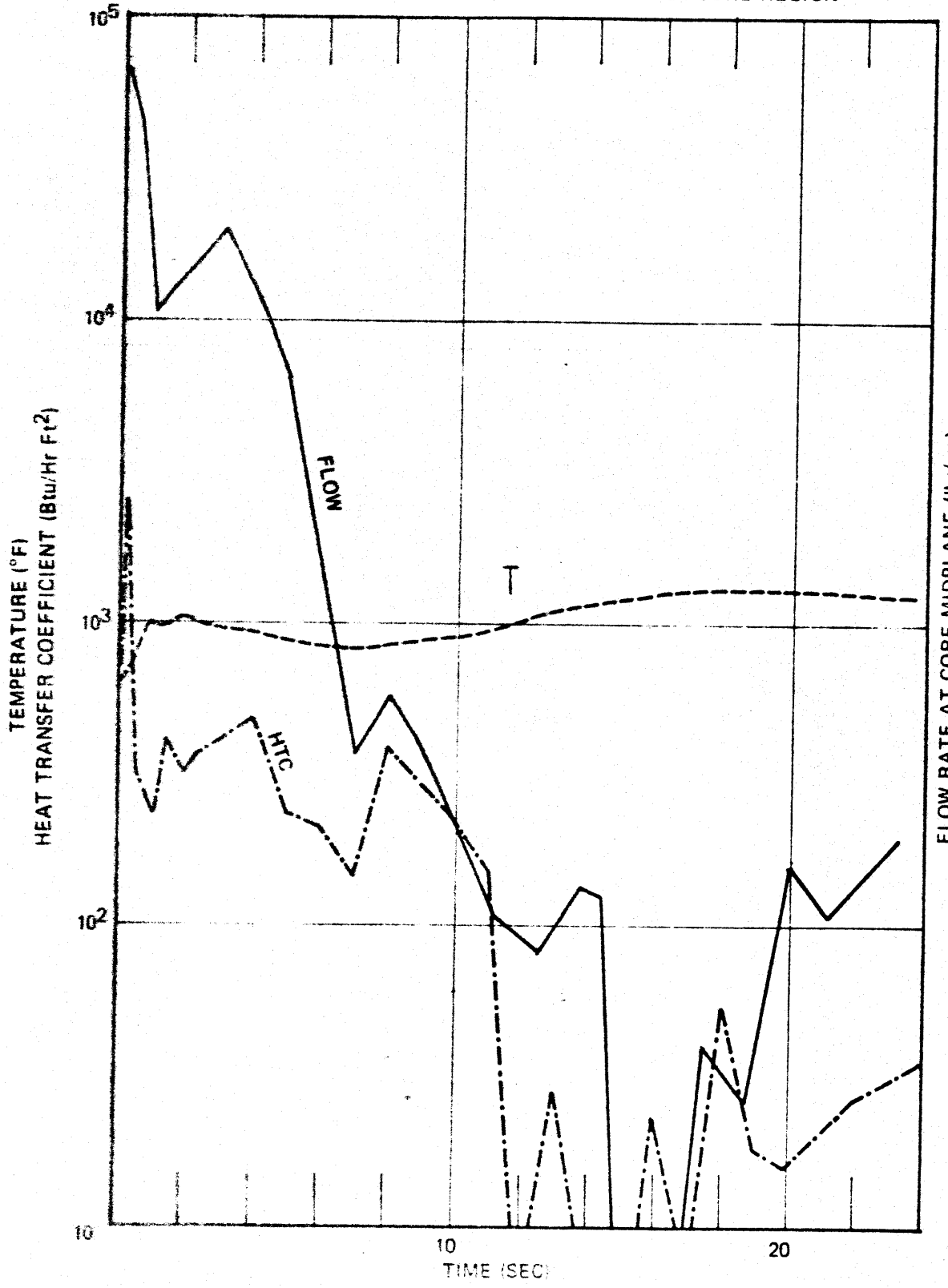

Fig. 8.2.F10
SIDE BREAK, A = 2
AVERAGE HEAT TRANSFER COEFFICIENT, COOLANT FLOW RATE AT CORE MIDPLANE AND CLAD SURFACE TEMPERATURE IN MIDDLE CORE REGION

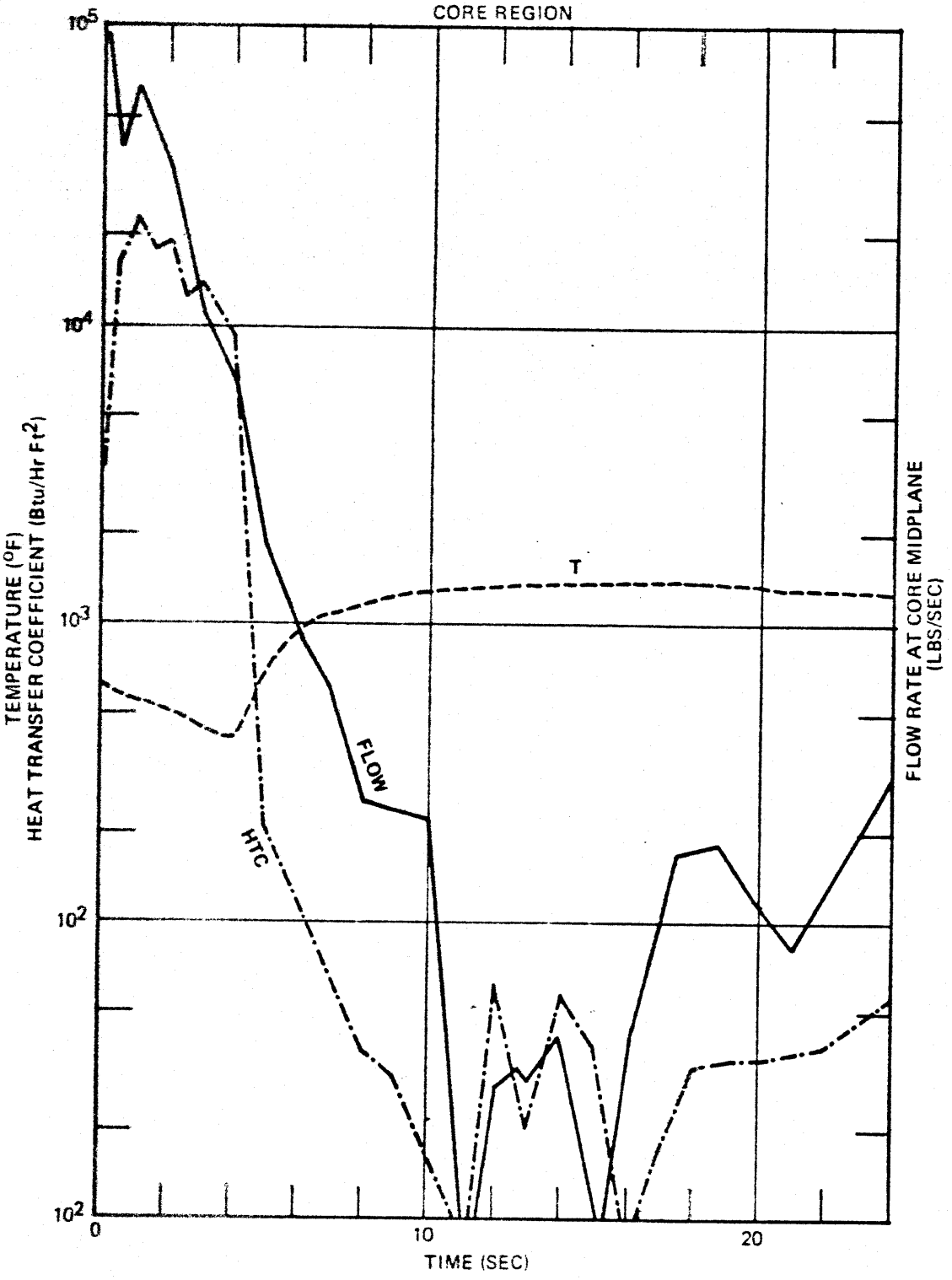

The flow rate has been obtained by taking the average of the flow rates at the two ends of the central core region (the middle one third of the core, or V14 in Fig. 5.3.F1). The temperature curves in these graphs have been somewhat flattened due to the nature of the semi-log plot, but their simultaneous showing with the flow and heat transfer coefficient curves is important in understanding their behavior. A clearer, linear-linear plot of the temperatures is presented in Fig. 8.2.F1[1].

At steady state, the flow through the core is some 3.71×10^4 lbs/sec. in the upwards direction. Upon rupture, loss of mass drops the pressure of the system very fast, reverses the pressure differential, and therefore reverses the flow. Flow reversal has been seen in Fig. 8.2.F2 but cannot be seen here. But very shortly after flow reversal (less than 60 msec.), the coolant flow rate is downwards and is very large. Typical values are about 10^5 lbs/sec or some 3 times the steady state flow rate. This large flow rate decays quickly, however, as the system blows down and drops in pressure. Around 10 seconds, when EOB has been effectively reached, the flow through the core is mainly due to steam flashing from the lower plenum or some leftover coolant from other parts of the primary system. This flow rate is very small, some 10 lbs/sec (for a 47.9 ft^2 flow area of the core). It is also fluctuating in direction. For all practical purposes, the core can be considered as depleted of coolant in this period.

The heat transfer coefficient (HTC) for the central core region and the average clad surface temperature are the direct results of the core flow rates. Thus, at steady state, the average HTC for all cases is around 6200 Btu/hr ft^2 for the central core region (maximum hot spot HTC can be as

high as 125,000 Btu/hr ft^2), just enough to steadily transfer some 45% of total core power through a heat transfer area of 17,200 ft^2. Between onset of the side rupture and flow reversal, the HTC drops due to decrease in mass velocity, but then quickly increases again and stays at a very high value for the major portion of the blowdown. This increased HTC due to increased mass velocity is working in combination with the already effective reactor scram to drop the clad temperature. A very steep drop in HTC subsequently follows, at around 4 seconds, in direct correspondence to the steep drop in mass velocity as EOB is drawing near. This causes the clad surface temperature to turn around and climb steeply. Maximum clad surface temperature is reached when the flow through the core is practically stagnant (between 10 and 20 seconds). Afterwards, the ECC water slowly becomes effective in dropping the temperature of the clad.

The foregoing discussion applies particularly to the cases of two- and three-pipe-sizes breaks. There is an anomaly in the other two cases which will be indicated in the section that follows.

8.2.7 Average Clad Surface Temperature in the Central Core Region

Fig. 8.2.F11 shows the transients of the average clad surface temperature for the vessel side break cases considered. The average clad surface temperature has been computed on the basis of one dimensional heat transfer from cylindrical rods with outside boundary values determined by blowdown conditions.

Fig.8.2.F13

SIDE BREAK
AVERAGE CLAD SURFACE TEMPERATURE IN MIDDLE REGION

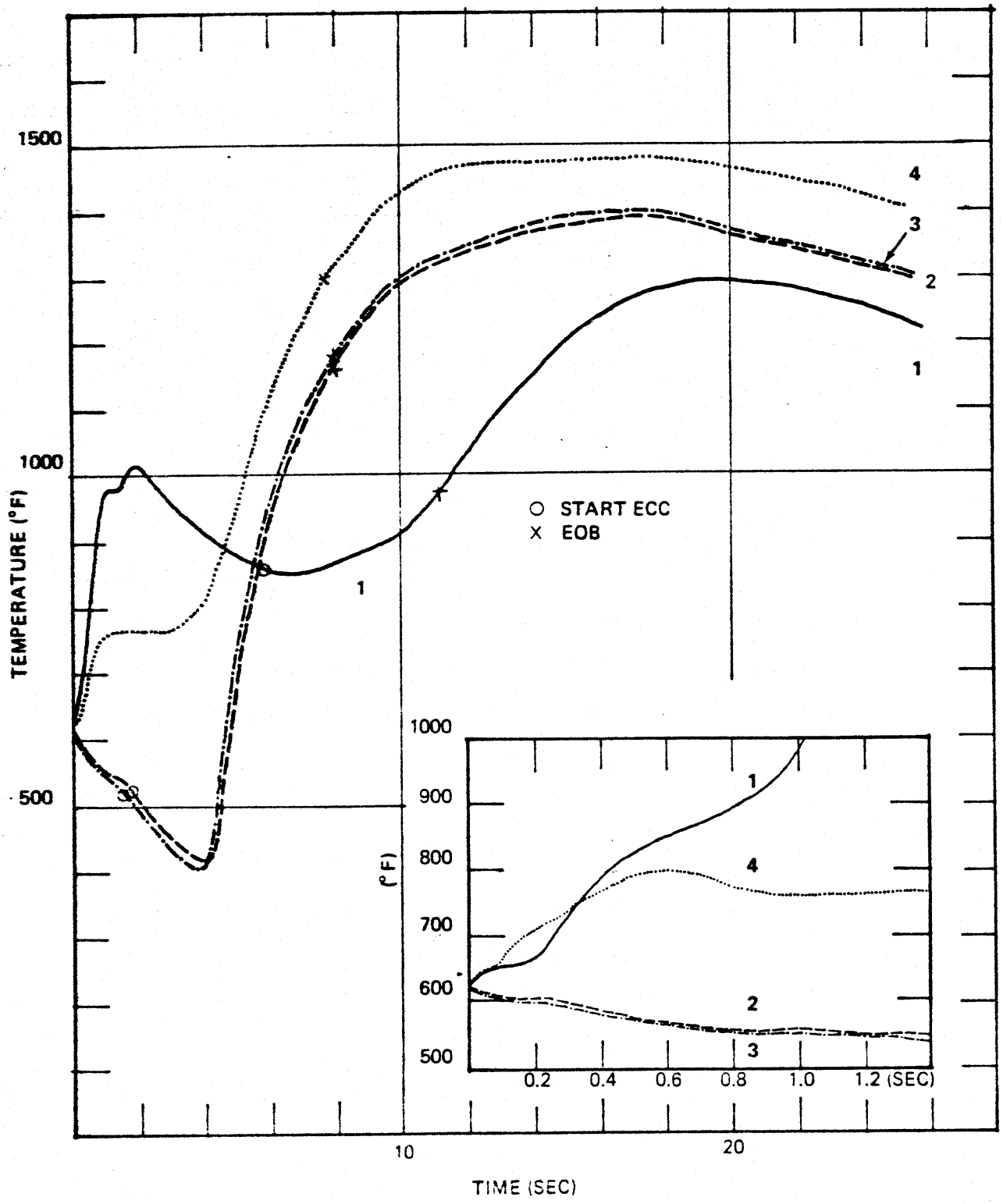

As discussed in the previous section and in Chapter 7, the clad surface temperature should follow a pattern consistent with the core mass velocity and heat transfer coefficient. This pattern consists of a slight (unnoticeable in the linear scale of the graphs shown) increase as the normal flow slows down to reverse, then decreases steadily as the reversed flow occurs and grows in magnitude. Close to EOB, when the mass velocity and consequently the heat transfer coefficient drops drastically, the temperature would rise sharply as the result of film boiling. The maximum would take place when the steam flow through the core is practically stagnant (between 10 and 20 seconds) and before ECC water becomes effective.

Curves 1 and 4 of Fig. 8.2.F11, however, do not strictly comply to this pattern. They feature a rise in clad surface temperature in the first second even though the core flow in this period is larger than the steady state value. The initial rise then reaches a peak, turns around, decreases slightly until close to EOB, then turns upwards again like curves 2 and 3 when the quiescent, stable film boiling period is in effect.

Curve 1 of Fig. 8.2.F11 is similar to curve 1 of Fig. 7.2.F 15 (1-pipe-size break at bottom). Curve 4 is similar to curves 3 and 4 also of Fig. 7.2.F 15. An explanation for this peculiar rise in the clad surface temperature can be tentatively reached in the following manner: The RELAP3 code uses 7 regimes of heat transfer and 5 regimes of critical heat flux. The correct heat transfer regime is determined by the coolant quality and by the comparison of the surface heat flux to the computed DNB flux. The DNB flux, in turn, is determined by system pressure and coolant properties at their pressure. All CHF correlations employed in the RELAP 3 are a function of the mass velocity, and goes to zero when the mass velocity is zero. Thus,

at flow reversal, the ratio of the surface heat flux to the computed CHF can go to a very high value, prompting the use of stable film boiling for that transfer. RELAP 3 seems to allow the heat transfer to get into this regime at flow reversal, but does not allow for a simple exit from it. Thus, the temperature of the clad keeps on rising until the temperature difference between it and the coolant can handle the already lowered heat generation, and the fuel heat redistribution.

In reality, however, it appears that very soon after flow reversal, nucleate boiling or good two-phase heat transfer must be restored thanks to the increased mass velocity. Therefore, as in the case of bottom break, curves 1 and 4 of Fig. 8.2.F11 may not be indicative of the actual average clad surface temperature. They represent a very conservative transient.

8.3 Conclusions

The vessel side break accident is similar to the bottom break case in the subcooled blowdown, two-phase blowdown and their effects. The small differences include a slower reactor scram, a slower blowdown rate, a higher loading on the core barrel and thermal shield and the accentuated asymptotic behavior of many parameters when the break size increases.

The most pronounced behavior of the blowdown observed is the flow choking for a substantial duration of the blowdown not only at the break, but also at both ends of the downcomer. This series of limiting leak flow has the effect of tempering the system mass loss rates, core flow rates, pressure histories in the various nodes, and clad surface temperature transients. The result is an asymptotic configuration for the time behavior of those quantities as the break increases in size.

Towards the end of blowdown, the flow at the break fluctuates significantly. This is due to the small size of the downcomer volume as compared to the upper or lower plena. EOB, therefore, can no longer be taken as the time when break flow first becomes zero, but rather, must be taken as the time when the flow, has gone down to a steady insignificant value, say 100 lbs/sec. When this definition is used, EOB is around 7-8 seconds for all break sizes larger than two times the cold leg flow area.

Similar to the cases of bottom break, the average clad surface temperature would suffer a transient with the following pattern: It would increase slightly around flow reversal (less than 60 msec.), then steadily decrease for a substantial duration of the blowdown, then turns around to climb steeply when the system has practically lost all its coolant, and finally level out and turn downwards when ECC water becomes increasingly effective. This pattern has a fast reaching asymptotic configuration when the break size is equal to or larger than twice the cold leg flow area. The maximum of this asymptotic configuration is around 1400°F at 16 - 18 seconds.

That a certain break size produces a clad surface temperature transient which departs from the above pattern is attributed to the possibility that RELAP3 does not have allowance for heat transfer and CHF correlations for flow reversal, and that its programming logic locks the heat transfer to the stable film boiling regime once the regime is entered. The resulting transient is such that the temperature climb initially to a high value for about 2 seconds, levels out or curving down slightly, then climbs again when EOB is approached. The maximum of the average clad surface temperature is about 1480°F for the case of 4-pipe-sizes break.

The coolant remaining in the lower plenum at EOB represents some 10% of the total initial inventory in that volume but continues to drop slowly due to steam flow out the break. ECC water is injected quite early in the blowdown, but due to the technique of nodalization and the assumption of thermodynamic equilibrium, the ECC effect is not seen until approximately 17-22 seconds when the water mass in the lower plenum starts to build up. The clad surface temperature has then reached a maximum and starts to curve down. ECC maximum injection rate is some 2800 lbs/sec and continues at a slightly smaller rate beyond 40 seconds. The present analyses are sometimes carried to 40 seconds, but mostly only to 25 seconds.

The subcooled blowdown loadings are larger for the thermal shield and the core barrel than in the case of bottom break. The larger the side break the larger the loadings, but the maximum loadings would level out to the peak value which is the difference between the subcooled pressure and the saturation pressure of the coolant.

CHAPTER 9

SENSITIVITY STUDIES

9. SENSITIVITY STUDIES

Beside the physical laws and analytical techniques such as those described in Chapters 4 and 5, a great many parameters must be chosen to properly define the postulated accident before any computation can be made. It is necessary therefore, to study the sensitivity of these parameters to the principal blowdown processes and effects under investigation.

Most of the computations achieved in Chapters 6, 7 and 8 have been made with a set of "base case" parameters. The plant is assumed to be at 100% normal power operation. Coolant pressure, temperature, and flow rates are those of plant design at the indicated power. The core is assumed to have accumulated the maximum quantity possible of fission products. Chemical shim reactivity coefficient is credited in such a manner that the effective reactivity of the reactor is zero at steady state operation. The normal location of the accumulator injection nozzles is at the cold legs, and that of the other diesel-driven ECC lines are at both the hot legs and the cold legs. The maximum ECC injection rate for the base cases is some 2800 lbs/sec.

Other parameters employed in the base case computations are as follows. Void negative reactivity coefficients are -0.0079, -0.0328, -0.0149 $/% void respectively for the upper, middle and lower core regions. The fuel-clad gas gap conductivity is one half the temperature dependent conductivity of helium. The phase separation model for large-volume, low-flow-velocity regions has a bubble population gradient of 0.8 and a bubble rise velocity of 3 ft/sec.

In the sensitivity studies, the effects of break location, break size and break time are pulled together from Chapters 6, 7 and 8. The location of the accumulator ECC water injection is subsequently shifted to the hot legs or the vessel upper plenum to see whether the ECC water is more effective for the cases of bottom and side breaks. The same test is made by increasing the ECC injection rate in the cold legs approximately a factor of 2. The gas gap conductivity effect on the clad surface temperature transient is studied by keeping all base case parameters but varying the gas gap conductivity from 1 to 1/8 the temperature-dependent conductivity of helium. Further sensitivity studies include a change in the void negative reactivity coefficient by a factor of 1 to 4, and a change in the phase separation model to a more homogeneous gradient of 0.5.

Table 9.T1 lists the spectrum of sensitivity studies.

9.1 Break Location

Table 9.1.T1 lists the values of principal parameters for the top, bottom and side break with the break size twice as large as the leg flow area. For the subcooled depressurization, the "instantaneous" break case is considered, that is, the break time is 0.25 msec. For the two-phase blowdown, the break time is 0.1 second.

When the break is at the top or the bottom, there is no pressure loading across the thermal shield because pressure waves move up or down the annuli at the same time and speed. But when a side break occurs, the greatest differential is across the shield. Greater pressure loadings on the core and across the core barrels are also seen for the case of the side break than in the other two locations.

TABLE 9.T1

SPECTRUM OF SENSITIVITY STUDIES

1.	**Break Locations:**	Top, Bottom or Side of Vessel.
2.	**Break Sizes:**	Top Break: 1, 2, 3 and 4 times the size of hot leg flow area. Bottom and Side Breaks: 1, 2, 3 and 4 times the size of cold leg flow area.
3.	**Break Time:**	Subcooled Blowdown: 0.25, 10 and 100 milliseconds. Two-Phase Blowdown: 10 and 100 milliseconds.
4.	**ECC Injection Location:**	Cold legs, Hot legs, and Upper Plenum.
5.	**ECC Injection Rate:**	2800 lbs/sec. and 5200 lbs/sec. at maximum.
6.	**Void Reactivity Coefficient:**	-0.0079, -0.0328, and -0.0149 $/% void respectively for lower, middle, and upper core region. 2 and 4 times the above values were used for sensitivity studies.
7.	**Gas Gap Conductivity:**	1/2, 1/4 and 1/8 the temperature dependent conductivity of helium.
8.	**Phase Separation:**	Gradient 0.8, bubble rise 3 ft/sec. Gradient 0.5, bubble rise 3 ft/sec.

Taking into account of the fact that a break in the upper plenum involves larger unit break size (the hot leg flow area is 4.587 ft^2 while that of the cold leg is 4.12 ft^2) but higher enthalpy coolant, there is no great difference between the top and bottom break of the same unit break size under investigation. The ECC water starts to be injected at about 1.6 seconds when the pressure in the cold legs has fallen below 660 psi. End-of-blowdown is between 7 and 8 seconds. Flow choking is seen at the break and at the pressurizer surge line. Scram to 30% of core power takes place at 0.26 seconds for the bottom break and 0.32 seconds for the top break.

A side break is generally similar to the bottom break, with the blowdown processes being slightly slower due to possible flow choking at the downcomer annuli. Thus, for the case of two-pipe-sizes break, SECCI is 1.775 seconds for a side location, 1.655 seconds for a bottom location, flow reversal is 22 msec. for a side location, 18 msec. for a bottom location, and scram to 30% of core power is at 0.30 sec. for a side location, 0.26 sec. for a bottom location.

The minimum coolant mass in the lower plenum is to a large extent dependent on the phase separation model and the resistance of the flow path through which the coolant from the lower plenum flows towards the break. For the case of the bottom break, it depends further on whether the break is at the lowermost point of the vessel bottom head or at a point higher. Thus, it strikes as a rather abnormal phenomenon that the minimum coolant remaining in the lower plenum should be more for a bottom break than for a side break, 7000 lbs versus 4000 lbs. In this case, the location of the bottom break is at the highest point of the lower plenum. A tentative explanation for this

TABLE 9.1.T1

EFFECTS OF VESSEL BREAK LOCATION

(CASE OF 2-PIPE-SIZES BREAKS)*

Items	Top Break	Bottom Break	Side Break
Subcooled Δp max, psi			
Core	380	370	250
Core Barrel	460	350	860
Thermal Shield	0	0	960
Two-Phase			
SECCI, sec.	1.58	1.655	1.775
EOB, sec.	6.40 -8.60	7.25	7.09 - 8.28
Flow Reversal, msec.	none	18	22
Scram to 30% of power, sec.	0.32	0.26	0.30
Flow choking location**	J20 J2	J20 J2	J20 J12 J2
Minimum Mass Remaining in Lower Plenum			
Lbs.	8000	7000	4000
% of Initial	15.6	13.6	7.8
Peak of Average Clad Surface Temperature in Middle Core Region			
°F	1310	1180	1390

* Top break is twice the hot leg flow area, or 9.174 ft^2. Bottom and side breaks are twice the cold leg flow area, or 8.24 ft^2.

** Refer to Chapter 5 for abbreviation.

TABLE 9.1.T2

EFFECT OF VESSEL BREAK LOCATION

ON THE PEAK OF THE AVERAGE CLAD SURFACE TEMPERATURE

	Temperature (°F)		
Break Size*	Top Break	Bottom Break	Side Break
1	960	1240	1290
2	1310	1180	1390
3	1320	1450	1400
4	1320	1450	1480

*Top break size is in multiples of hot leg flow area (4.587 ft^2). Bottom and side breaks are in multiples of cold leg flow area (4.12 ft^2).

fact is as follows: For the bottom break case, the phase separation model is effective in keeping any water at the bottom and allows only steam to flow out the break at the quiescent stage of the blowdown (which is beyond EOB). On the other hand, should the break be at the side not only all the carried-over coolant (including ECC water) from the cold legs is lost out the break, but also more mass is lost from the lower plenum due to the lingering high pressure there with respect to the downcomer. In other words, both the phase separation model and the ECC water are responsible for the phenomenon described above.

If the bottom break occurs at the lowermost point of the lower plenum, then there is practically no coolant left in this region, as is pointed out in Section 7. Two additional factors are responsible for this case: The flow out the break involves lower quality mixture instead of vapor and the gravity provides an additional driving force for leak flow.

The peak of the average clad surface temperature in the middle core region is higher for the top and side breaks than for the bottom break for the break of two leg flow area. This pattern is not true for other break sizes, such as indicated by Table 9.1.T2. Inspection of this table leads to the conclusion that for large break sizes, the maximum clad surface temperature reaches a somewhat asymptotic value. This value is about the same for the bottom and side break location, and is smaller for the top break location. For smaller break sizes, no similar conclusion can be drawn.

9.2 Break Size

Chapters 6, 7 and 8 have described the effects of break sizes which are dramatic in that most quantities of interest seem to reach an asymptotic value as the break size increases.

Tables 9.2.T1, 9.2.T2 and 9.2.T3 recapitulate these quantities for the top break, bottom break and side break.

Subcooled pressure loadings tend to reach an asymptotic value as the break size increases. This value is the difference between the subcooled pressure and the saturation pressure of the coolant at the location of the break. Thus, when the break is at the bottom or side, the subcooled pressure is 2280 psi, the saturation pressure is 1087 psi, and the asymptotic value is some 1200 psi. When the break is at the top, the subcooled pressure is 2236 psi, the saturation pressure is 1500 psi, and the asymptotic value is some 740 psi. Obviously, the top break involves lesser subcooled loadings on vessel internals than the bottom or side break.

It is obvious that a larger break leads to a faster reactor scram, a faster drop in system pressure, a faster initiation of ECC injection and, in the case of bottom and side break, a faster flow reversal. But it is not obvious that a larger break does not necessarily lead to a shorter EOB, or in other words, a faster loss of the cooling effectiveness of the primary coolant. Flow choking is the key to this latter observation. For the top break, flow choking occurs at the break, at the pressurizer surge line, and as the break size becomes larger, at the hot legs and the core. For the bottom break, flow choking occurs at the break, the pressurizer surge line,

TABLE 9.2.T1

TOP BREAK(1)

EFFECTS OF BREAK SIZE

Items	Multiple of Hot Leg Flow Area* 1	2	3	4
Subcooled, t_b = 0.00025 sec.				
Δp max, psi				
Core	230	380	520	620
Core Barrel	300	460	620	720
Thermal Shield	0	0	0	0
Two-Phase, t_b = 0.01 sec.				
Scram to 30% power, sec.	1.3	0.28	0.13	0.095
SECCI, Sec.	4.68	1.54	1.34	1.30
EOB, Sec. (2)	12.8	6.4-8.6	4.58-8.3	3.96-8.2
Flow Choking Location**	J20	J20	J20	J20
		J1	J1	J1
		J2	J3	J17
			J2	J2
Minimum Mass Remaining In Lower Plenum				
Lbs.	8200	7800	8000	8500
% of Initial Mass	16.0	15.2	15.6	16.5
Peak Average Clad Surface Temperature In Middle Core Region				
°F	960	1310	1320	1320

* Hot leg flow area is 4.587 ft^2.

** Refer to Chapter 5 for abbreviation.

(1) Note that the top break unit size is slightly larger than the bottom and side break unit size, and that the break time is 0.01 sec.

(2) Where there are two numbers for a case, the first number is the time when the flow out the break first becomes zero, and the second number is the time after which break flow rate no longer exists.

TABLE 9.2.T2

BOTTOM BREAK

EFFECTS OF BREAK SIZE

Item	Multiples of Cold Leg Flow Area* 1	2	3	4
Subcooled, t_b = 0.00025 sec. Δp max, psi				
Core	180	370	530	670
Core Barrel	210	350	450	530
Thermal Shield	0	0	0	0
Two-Phase, t_b = 0.1 sec.				
Flow Reversal Time, msec.	56	18.5	14	12.5
Scram to 30% power, sec.	0.5	0.26	0.19	0.16
SECCI, Sec.	5.73	1.655	1.13	1.075
EOB, Sec.	12.2	7.25	7.04	6.53
Flow Choking Location**	J20	J20 J2	J20 J11 J12 J8 J2	J20 J11 J12 J8 J2
Minimum Mass Remaining In Lower Plenum				
Lbs.	8000	7000	9800	11000
% of Initial Mass	15.6	13.6	19.1	21.4
Peak of Average Clad Surface Temperature In Middle Core Region				
°F	1240	1180	1450	1450

* Cold leg flow area is 4.12 ft^2.

** Refer to Chapter 5 for abbreviation.

Table 9.2.T3

SIDE BREAK

EFFECTS OF BREAK SIZE

Items	Multiple of Cold Leg Flow Area* 1	2	3	4
Subcooled, t_b = 0.00025 sec.				
Δp max, psi				
Core	120	250	330	380
Core Barrel	560	860	1000	1100
Thermal Shield	700	960	1080	1120
Two-Phase, t_b = 0.1 sec.				
Flow Reversal Time, msec.	58	22	19	17.5
Scram to 30% power, sec.	0.5	0.3	0.26	0.26
SECCI, sec.	5.76	1.775	1.585	1.572
EOB, sec. (1)	12.35	7.09 - 8.28	2.59 - 7.85	1.85 - 7.85
Flow Choking Location**	J20	J20 J12 J2	J20 J12 J10 J2	J20 J12 J10 J8 J2
Minimum Mass Remaining In Lower Plenum				
Lbs.	6000	4100	4300	3500
% of Initial Mass	11.7	8.0	8.4	6.8
Peak of Average Clad Surface Temperature In Middle Core Region				
°F	1290	1390	1400	1480

* Cold leg flow area is 4.12 ft^2.

** Refer to Chapter 5 for abbreviation.

(1) Where there are two numbers for a case, the first number is the time when the flow out the break first becomes zero, and the second number is the time after which break flow rate no longer exists.

the downcomer annuli, and the cold legs. For the side break, flow choking takes place in the same locations as for the bottom break, and very emphatically at either ends of the downcomer annuli.

Largely due to the flow choking patterns described above that the primary coolant must take some time to flow out the break no matter how large the break is. When the break is very large, there is violent fluctuations of flow rates, particularly at the later stages of the blowdown. The result of these fluctuations is that EOB no longer has meaning according to the definition that it is the time when the flow out the break first becomes zero. For large break size and consequently large flow fluctuations at the later blowdown stages, the flow out the break may temporarily become zero but may reach again a high value at the next instant because there is still significant mass and pressure in the system. Therefore, a liberal interpretation of EOB can be devised as the time when the flow out the break has dropped to an insignificant value (say 100 lbs/sec.) With this interpretation, EOB is somewhere between 7 and 8 seconds after break initiation.

For the top break, the minimum quantity of mass remaining in the lower plenum is practically the same for all break sizes, some 16% of the initial coolant mass in this region. The bottom and side break cases manifest two opposite trends. There seems to be more mass remaining in the lower plenum as the bottom break size increases. The reverse is true for the side break. Explanation of these trends can be tentatively made on the basis of the phase separation model and the pressure transient in the lower plenum. However, it is felt that there exists enough uncertainty to warrant further study in this area.

The general pattern of the clad surface temperature transient is as follows: The temperature is initially at the average clad surface temperature at normal 100% power operation. If there is a flow reversal, it increases momentarily. But the temperature would subsequently drop because the flow rate through the core is increased due to the great pressure differential across it. Close to the EOB only steam is available to flow through the core, and the temperature rises sharply to reach a maximum value just before ECC water becomes effective.

As the break size increases, there is a tendency for the average clad surface temperature to assume an asymptotic pattern. Thus, for the top break case, the asymptotic pattern has been reached for break sizes larger than twice the flow area of the hot leg. The peak of this asymptotic curve is about 1320°F, occurring at approximately 12 seconds after the break.

Although there seems to exist some anomaly in the clad temperature transient involving flow reversal in some bottom and side break cases, it has been argued in Chapter 7 and 8 that the transient should also assume an asymptotic configuration as the bottom and side breaks increase in size. The maximum of this asymptotic configuration should be around 1450°F, occurring at approximately 14-16 seconds after the break.

Further studies on these observations are needed on the ground that if they are indeed true for even more severe vessel break cases, then there exist real possibilities for imaginative passive safeguards that ultimately can cool the core.

9.3 Break Time

The effects of break time is dramatic for the subcooled loadings on vessel internals but only marginal on the two-phase blowdown processes. Break time has been defined before as the duration of time over which the break is assumed to open up linearly to its postulated size.

Three break times have been used in the WHAM computations of the subcooled depressurization, namely 0.25 msec., 10 msec., and 100 msec. The 0.25 msec. break time is termed "instantaneous" because is takes twice that time for the sonic wave to travel through the break. Table 9.3.T1 shows a representative listing of the highest magnitude of the pressure loadings across the core, the core barrel or the thermal shield for the case of two-pipe-size breaks. It is seen from this table that as the break time is longer, the subcooled loadings are smaller. The "instantaneous" break is of the sonic explosion type and is obviously too fast when one considers the fact that the vessel metal behaves in the ductile mode at 100% steady power operation. Reactor manufacturers have used break times of "instantaneous", 1 msec., 10 msec. and 300 msec. in the guillotine pipe break analyses for nuclear plants (C9) and have arrived at the same conclusion. If, therefore, it can be established by theoretical and experimental fracture mechanics that the break takes a finite time which is slower than "instantaneous", then current LWR vessel internals may be sturdy enough to withstand vessel ruptures of large size.

Table 9.3.T1

EFFECTS OF BREAK TIME

ON SUBCOOLED BLOWDOWN PRESSURE LOADINGS

(2-pipe-sizes breaks)

Items	Break Opening Time (sec)		
	0.00025	0.01	0.1
Top Break, Δp max, psi			
Core	380	210	40
Core Barrel	460	445	130
Bottom Break, Δp max, psi			
Core	370	250	40
Core Barrel	350	245	72
Side Break, Δp max, psi			
Core	250	170	36
Core Barrel	840	720	60
Thermal Shield	980	540	60

Table 9.3.T2

EFFECT OF BREAK TIME

ON TWO-PHASE BLOWDOWN PARAMETERS

(2-Pipe-Sizes Break)

Items	Break Time (Sec) 0.01	0.1
Scram (by void) to 30% power, sec.		
Top Break	0.28	0.32
Bottom Break	0.24	0.26
Side Break	0.29	0.30
SECCI, Sec.		
Top Break	1.54	1.58
Bottom Break	1.61	1.655
Side Break	1.735	1.775
EOB, Sec *		
Top Break	6.4 - 6.8	6.4 - 6.8
Bottom Break	7.53 - 8.04	7.25 - 7.92
Side Break	7.11 - 7.93	7.09 - 7.78
Flow Reversal, msec		
Bottom Break	10.2	18.5
Side Break	16.8	22.0
Minimum Mass Remaining In Lower Plenum, % of Initial Mass		
Top Break	15.2	15.2
Bottom Break	10.7	19.1
Side Break	8.2	8.0
Peak of Average Clad Surface Temperature in Middle Core Region, °F		
Top Break	1310	1320
Bottom Break **	1450	1180
Side Break	1380	1390

* Where there are two numbers for a case, the first number is the time when the flow out the break first becomes zero, and the second number is the time after which break flow rate no longer exists.

** Clad surface temperature for this case is explained in Section 7.2

Table 9.3.T2 shows the effect of the blowdown time on principal two-phase processes and effects. Only the case of two-pipe-sizes break are selected for listing. Two break times have been studied with RELAP3, namely 10 msec. and 100 msec. It has been argued elsewhere in Chapters 5, 6, 7 and 8 that contrary to the subcooled decompression case, a slow break time is conservative for the two-phase blowdown. This is because the mass loss over 100 msec. is only a very small fraction of the system mass no matter whether over that period the break has been widely opened (when break time is small) or is still in the process of opening (when the break time is 100 msec.). On the other hand, a slower break allows a slower reactor scram and particularly a slower flow reversal, both of which tend to cause the clad surface temperature to assume a higher value to start in the transient.

Beside the above argument, examination of Table 9.3.T2 leads to the conclusion that the break time is quite insensitive to the two-phase blowdown processes. Start of emergency core cooling injection, end of blowdown and coolant mass remaining in the lower plenum are all quite similar for the 0.01 sec. and 0.1 sec. break times. The peak of the clad surface temperature transient should be slightly larger for the longer break time, and the anomaly seen in Table 9.3.T2 has been tentatively explained in Section 7.2.

9.4 ECC Injection Location

Most of the current PWR plants have the accumulator ECC injection nozzles installed at the cold legs. Some plants feature extra injection nozzles at the upper plenum (Connecticut Yankee) or at the downcomer (B&W). BWR's have a spray system in the upper plenum which has been given credit as having an independent capability to cool the core in the event of a LOCA by pipe break. (S6).

The base case accumulator system in this study include three accumulators which start to inject ECC water when the pressure in the receiving end location drops below 660 psi. Friction factor is provided to control the injection rate. The maximum injection rate for the base case is 2800 lbs/sec. a relatively low value.

Consequences of the location of the ECC injection nozzles have been investigated for the bottom and side breaks with break size twice as large as the cold leg flow area. Cold leg location, hot leg location and upper plenum location are considered. In the case of the upper plenum injection it is noted that the assumption of instantaneous mixing allows the injection to act as sprays but the phase separation model causes the cold water to settle down. No injection velocity is accounted for.

Table 9.4.T1 summarizes the results for the principal blowdown parameters under investigation. For bottom and side breaks, the pressure in the hot legs and the upper plenum obviously drops slightly slower than the pressure of the cold legs (the stagnation point of the system being somewhere in the steam generators), therefore, the ECC injection should start a little

TABLE 9.4.T1

2-PIPE-SIZES BREAK (t_b = 0.1 SEC)

EFFECTS OF ACCUMULATOR ECC INJECTION LOCATION

Items	Accumulator ECC Injection At		
	Cold Legs	Hot Legs	Upper Plenum
Assumed Accumulators	3	3	3
Maximum Injection Rate (lbs/sec)	2820	2820	2820
Bottom Break			
SECCI, sec	1.665	1.915	1.92
EOB, sec	7.25 - 7.92	6.93 - 7.99	6.61 - 7.77
Minimum Mass Remaining In Lower Plenum % Initial	19.1	22.2	22.2
Peak of Average Clad Surface Temperature in Middle Core Region °F	1180	1210	1310
Side Break			
SECCI, sec	1.775	2.10	2.11
EOB, sec	7.09 - 8.28	6.71 - 7.79	6.58 - 7.35
Minimum Mass Remaining In Lower Plenum % Initial	8.0	21.6	25.1
Peak of Average Clad Surface Temperature in Middle Core Region °F	1390	1280	1370

later. EOB, however, still occurs between 7 and 8 seconds according to the new interpretation of its meaning as presented in Section 9.2. The minimum mass remaining in the lower plenum is about the same for the bottom break case but increases significantly for the side break case. The latter increasing trend is certainly due to the fact that the break is between the ECC injection and the lower plenum in the case of cold leg ECC injection, whereas all the injected water has a chance to mix with the coolant in the lower plenum before flowing out the break in the case of hot leg and upper plenum ECC injection.

Figs.9.4.F1 and 9.4.F2 show the transients of the average clad surface temperature in the middle core region. For the bottom break, the ECC location at the cold legs or hot legs makes little difference. For the side break, a hot leg ECC injection seems to be superior in delaying the start of the temperature climb. The peak is also delayed and slower. On the other hand, the location of the ECC injection in the upper plenum seems to hasten the temperature climb and to cause the peak to be slightly higher. This result is contrary to common sense and could only be tentatively explained by the observation that as ECC injection sets in quite early in the blowdown, it serves to depress the pressure in the upper plenum and consequently causes a more stagnant flow through the core at later stages of the blowdown. However, many important features such as the ECC injection velocity and a possible late injection start have not been investigated. It is felt that an ECC injection at the top, may be in the form of sprays, which starts at a pressure lower than 660 psi (maybe 200 psig) should certainly be of great help in cooling the core when the break is at the bottom or side of the vessel.

Fig. 9.4.F1
BOTTOM BREAK, A = 2
EFFECT OF ECC INJECTION LOCATION ON AVERAGE
CLAD SURFACE TEMPERATURE TRANSIENT IN MIDDLE CORE REGION

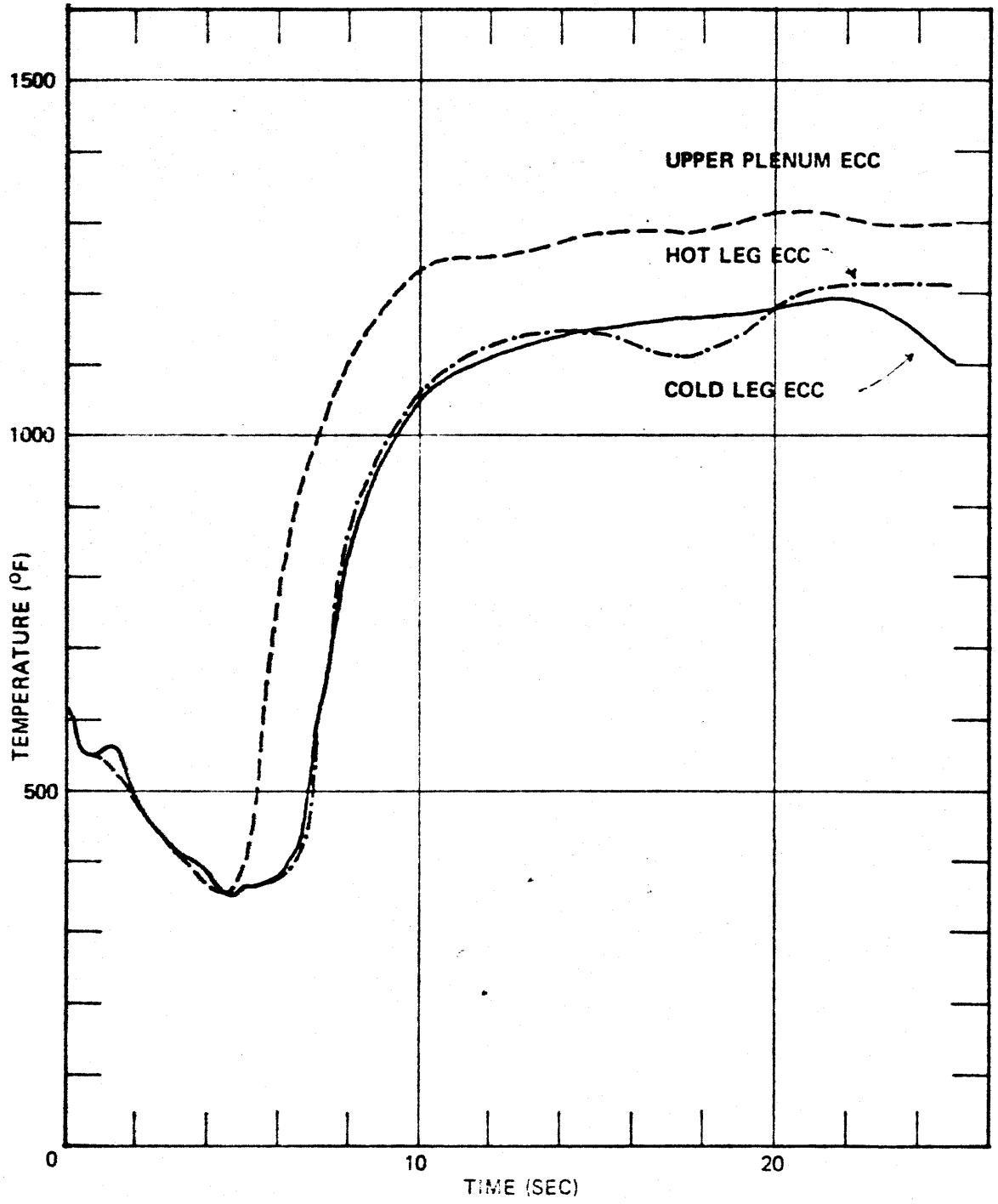

Fig. 9.4.F2

SIDE BREAK, A = 2

EFFECT OF ECC INJECTION LOCATION ON AVERAGE CLAD SURFACE TEMPERATURE TRANSIENT IN MIDDLE CORE REGION

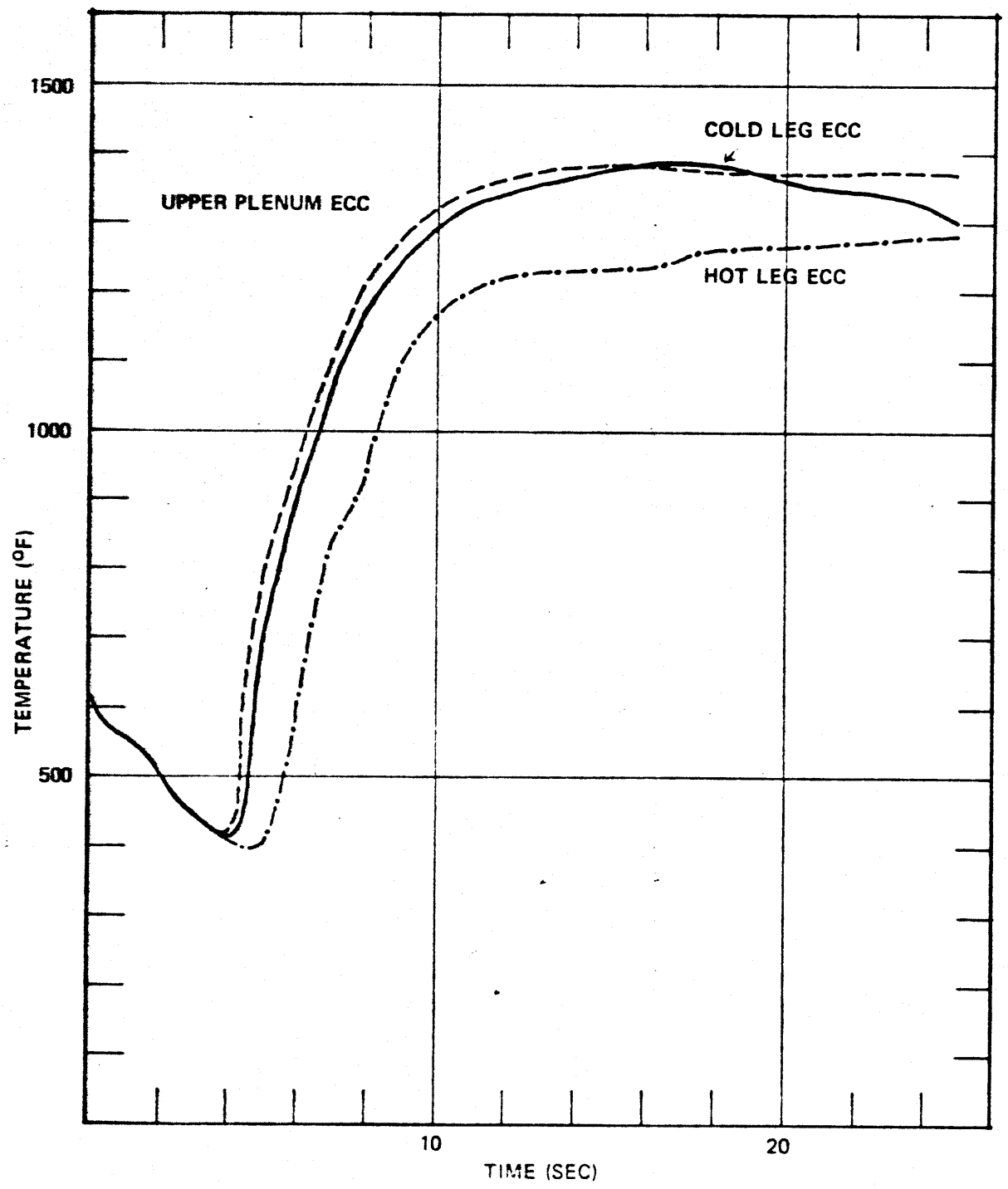

9.5 ECC Injection Rate

The rate of ECC injection can be increased by physically increasing the accumulator pressure, or the size of the ECC injection line, or the number of accumulator tanks, or by decreasing the friction in the injection line. This latter method has been chosen to study the effect of the injection rate on different blowdown parameters.

The base case uses a friction coefficient of 0.004 $lb_f sec^2/lb_m ft^3 in^2$ for the ECC injection line. The resultant injection rate is such that a maximum of 2800 lbs/sec. is attained during the quiescent stage following EOB. The injection rate maintains at the 2000 lbs/sec. level well after 25 seconds. A reduction of the friction factor to 0.001 $lb_f sec^2/lb_m ft^3 in^2$ increases the injection rate by approximately a factor of 2, with a maximum of 5200 lbs/sec. The transients are followed only to 10 seconds after break initiation.

Table 9.5.T1 shows the SECCI and values of the clad surface temperature at 0 sec., 4 sec. and 10 sec. respectively. Cases considered are for side break with size twice the flow area of the cold leg. It is noted that SECCI is the same for the same injection location. Except for the case of upper plenum ECC injection, the minimum clad surface temperature occurs around 4 seconds with the magnitude being approximately 410°F. The climb starts at about 4 seconds and continues beyond 10 seconds as can be seen in Fig. 8.2.F9. Up to 10 seconds, no appreciative difference can be observed in the clad surface temperature transient that can not been explained by other causes. For example, the value of 578°F at 4 seconds for the case of

Table 9.5.T1

EFFECTS OF ECC INJECTION RATE ON

AVERAGE CLAD SURFACE TEMPERATURE TRANSIENT (1)

Rate of Injection at (2) Maximum (lbs/sec.)	SECCI (Sec.)	Temperature of Clad Surface (°F) at 0 sec.	4 sec.	10 sec.
A = 2				
Cold Leg ECC				
2800	1.775	620.8	416	1290
5200	1.775	620.8	414	1303
Hot Leg ECC				
2800	2.10	620.8	421	1163
5200	2.10	620.8	407	1267
Upper Plenum				
2800	2.11	620.8	415	1318
5200	2.11	620.8	578	1332
A = 3				
Cold Leg ECC				
2800	1.585	620.8	407	1297
5200	1.585	620.8	406	1310

(1) Computations are carried out only to 10 seconds after start of accident.

(2) The control of the injection rate is effected by the friction factor in the ECC injection path. The two indicated maximum flow rates correspond to friction factors of 0.004 and 0.001 respectively. (See momentum equation in Section 5.2.2).

upper plenum ECC injection with the larger injection rate has been explained in Section 9.4 as due to the temperature climb which starts slightly before 4 seconds (at 3.5 seconds).

The effects of the injection rate beyond 10 seconds have not been included in this study.

9.6 Void Reactivity Coefficient

The base case uses a constant void reactivity coefficient of -0.0079, -0.0328, -0.0149 $/% void for the top, middle and bottom core region, respectively. These values are taken from the sample problem prepared by the Aerojet Nuclear Company for transmittal along with the RELAP3 Mod 36 Code (A5). The indicated sample problem is a 34-volume RELAP3 setup for a large, 4 loop PWR very similar to the reactor under investigation in this study. The void reactivity coefficients employed are very conservative when compared to the values set forth by Elbaum (E2) in his study of severe power excursion.

Two studies with the void reactivity coefficient twice and four times the base case values have been conducted for the case of one-pipe-size top break. The normalized power histories and the average clad surface temperature transient are shown in Fig. 9.6.F1.

Curves V1, V2 and V3 in Fig. 9.6.F1 indicate the obvious fact that a larger negative void reactivity coefficient brings about a faster reactor scram. The little plateau around 1 second is characteristic of the one-pipe-size top break which seems to be due to flashing of the coolant in the core

Fig. 9.6.F1

TOPBREAK, A = 1

NORMALIZED POWER AND CLAD SURFACE TEMPERATURE
SENSITIVITY TO VOID COEFFICIENT

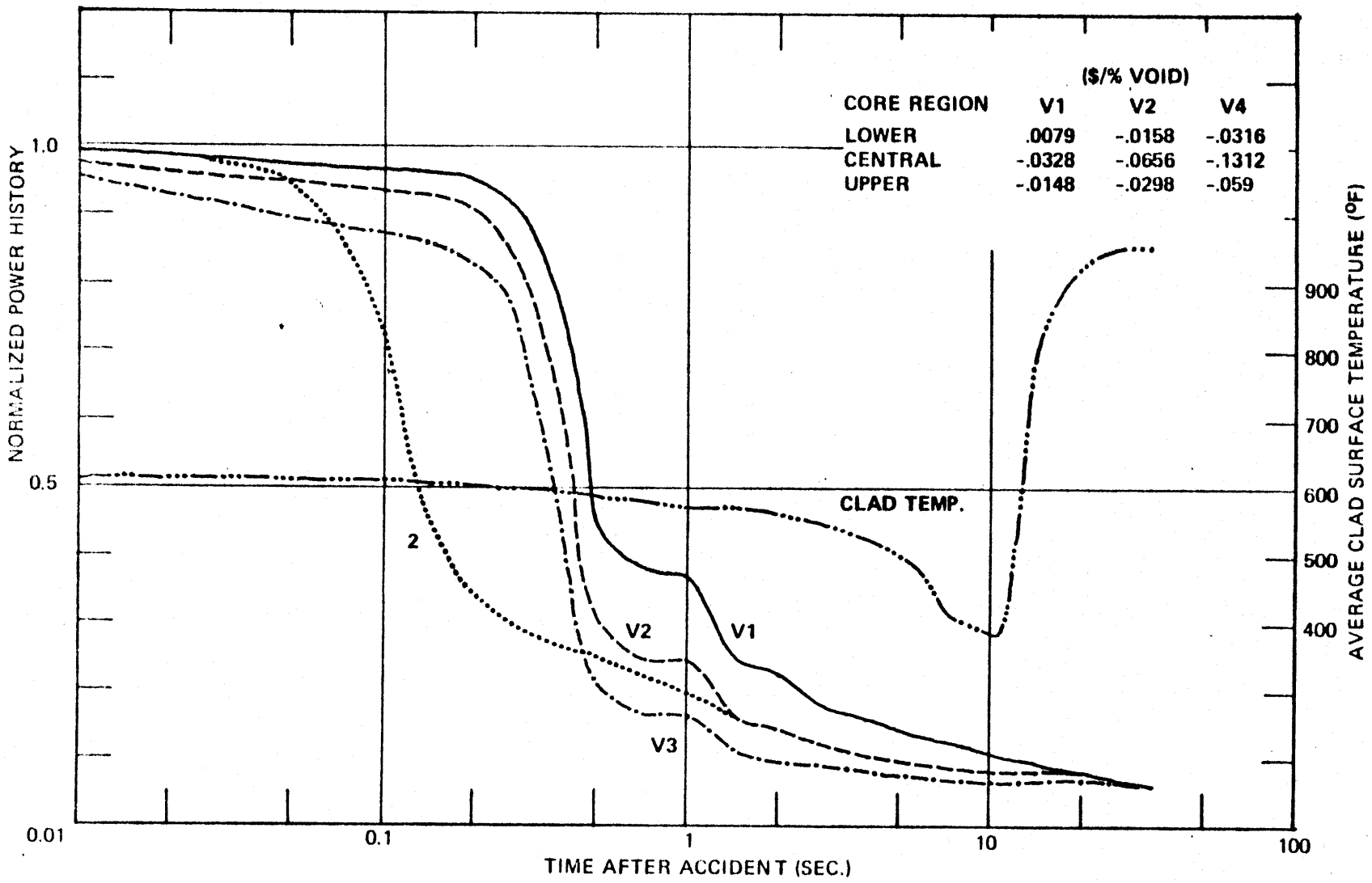

during which the void changes relatively little. For larger break sizes, the steady effect of flashing is of no competition to the fast pressure drop caused by the blowdown, and the plateau is no longer prominent.

For purposes of comparison, the normalized power history for the two-pipe sizes top break has also been drawn into Fig. 9.6.F1. The scram faster than Curves V1, V2 and V3 is indicative of the fact that the amount of void formed is more sensitive than the net void reactivity coefficient. Indeed, the larger the break, the more there is void because void increases very fast for a small increase in coolant quality at the lower end of the quality scale.

The clad surface temperature transient does not show any sensitivity to the change in void reactivity coefficient such as described above. For all three cases, the average clad surface temperature first drops due to increased core flow rate, then at close to EOB, it turns around and climbs sharply to a maximum value of 960°F. This maximum value occurs during the quiescent steam cooling period.

9.7 Gas Gap Conductivity

The conductance of the gas gap between fuel and clad is largely unknown during the blowdown because it depends on the gas pressure, gas composition, the degree of normal operation fuel swelling, clad collapse and blowdown clad swelling.

At normal operation, the manufacturer uses the following empirical formula to determine the gas gap conductance (C1):

$$h = 0.6P + \frac{k}{f(14.4 \times 10^{-6})}$$

where

h is the conductance in Btu/hr ft^2°F.

P is the contact pressure in psi.

k is the thermal conductivity of the gas mixture in the gap.

f is the correction factor for the accommodation coefficient.

A value of approximately 1000 Btu/hr ft^2°F has been obtained when the pellet contacts the clad with zero contact pressure and when the gas composition is 75% fission gas and 25% air.

It is obvious that this calculational technique is unsuitable for computation of gas gap conductivity during the blowdown. RELAP3 has used instead the gap thickness and conductivity in the calculation of heat transfer from the pellet to the clad.

Table 9.7.T1 shows the average fuel and clad surface temperature in the middle core region as a function of gap conductivity. For all cases, the gap is 0.00325 inch thick. Except for the first high value of 0.4687 Btu/hr ft°F, all other conductivity values are referred to the temperature - dependent value of helium (Appendix B). It is seen that for very low conductivities, 1/8 and 1/4 that of helium, the average centerline temperature in the middle core region is quite high when put in proper perspective with the design maximum

Table 9.7.T1

STEADY STATE OPERATION

AVERAGE FUEL AND CLAD SURFACE TEMPERATURES

IN MIDDLE CORE REGION

Gas Gap Conductivity* (Btu/hr.ft.°F)	Temperature (°F) Fuel Centerline	Average for Fuel	Clad Surface
0.4687	1817	1185	620.8
$K_{HE}(T)$	2322	1451	620.8
1/2 $K_{HE}(T)$	2897	1845	620.8
1/4 $K_{HE}(T)$	3720	2514	620.8
1/8 $K_{HE}(T)$	4723	3555	620.8

*The temperature dependent conductivity of helium is listed in Appendix B.

Fig. 9.7.F1
TOP BREAK, A = 1
GAP CONDUCTIVITY EFFECT ON FUEL TEMPERATURE TRANSIENT

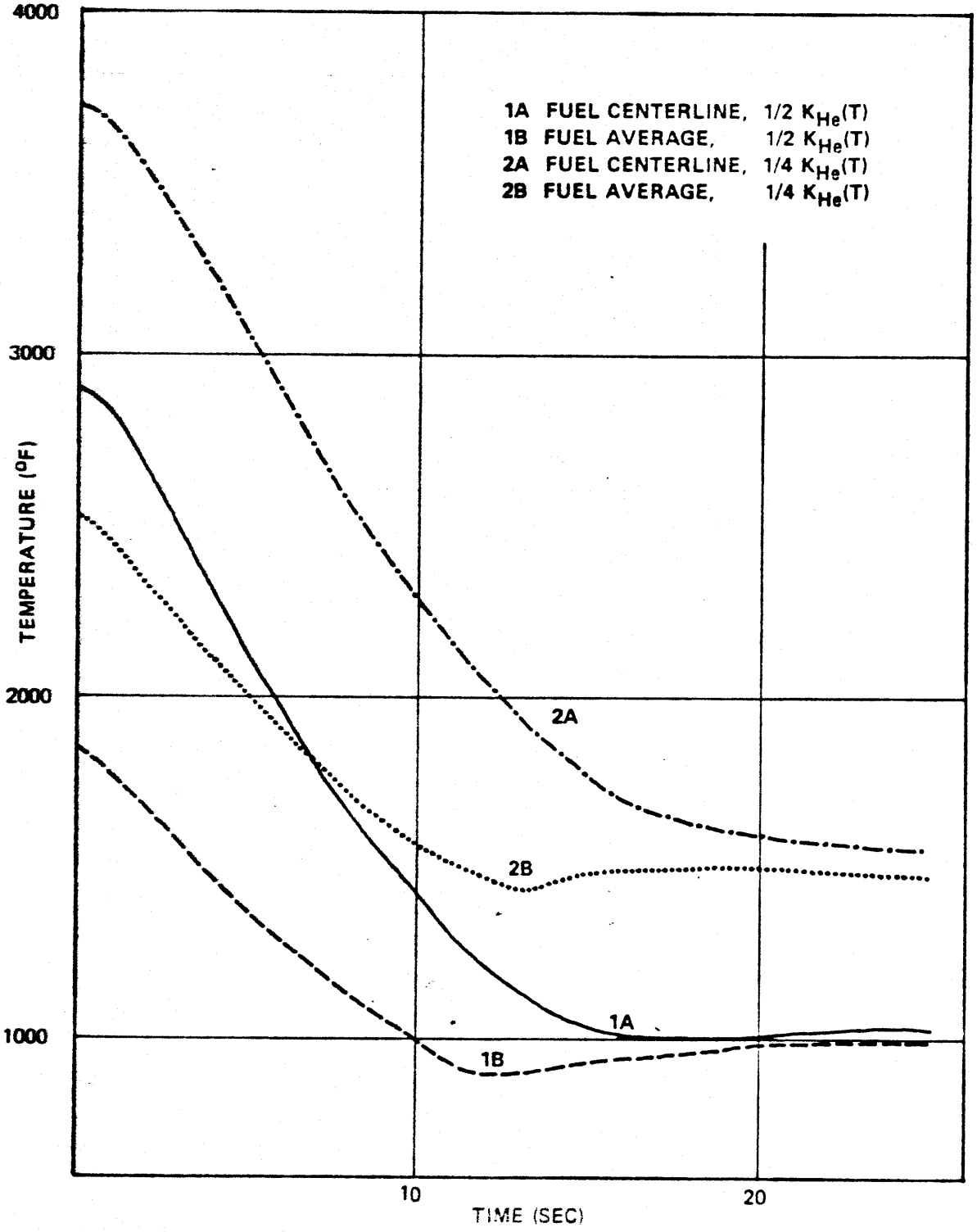

Fig. 9.7.F2
TOP BREAK, A = 1
EFFECT OF GAP CONDUCTIVITY ON
CLAD SURFACE TEMPERATURE IN MIDDLE CORE REGION

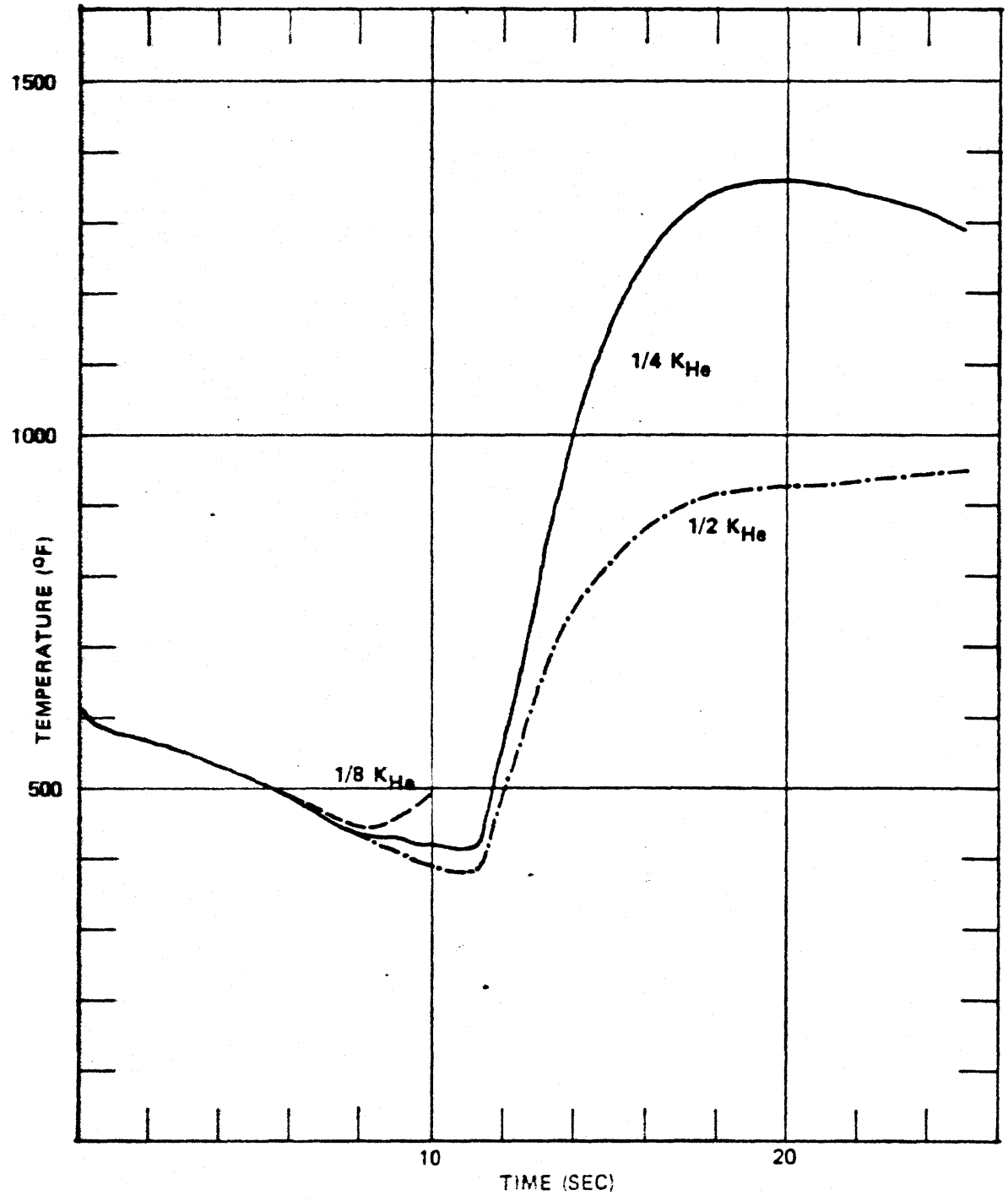

centerline temperature of 4380°F. The base case calculations employ the gap conductivity one half that of helium.

The one-pipe-size top break has been chosen to study the effect of change in gas gap conductivity on the clad surface temperature transient during the blowdown. Fig. 9.7.F1 shows the fuel temperature transients and Fig. 9.7.F2 shows the clad surface temperature transients for 1/2 k_{He} and 1/4 k_{He}. A study with the conductivity 1/8 that of helium was also made, but was carried out only to 10 seconds after the break initiation.

A large difference of approximately 400°F exists between the two peaks in Fig. 9.7.F2. This suggests that the gap conductivity has a strong effect on the behavior of the clad temperature transient. The reason can be found in part in Fig. 9.7.F1. When the gap conductivity is small there must be a great temperature gradient across the gap to transfer the heat produced in the fuel. Thus, at steady state operation, both the centerline temperature and the average fuel temperature are higher, and consequently the energy inventory in the fuel is larger. For one-pipe-size top break, EOB is 12.8 seconds, or about one fuel time constant. Thus at the onset of the stable film boiling regime, there is still approximately half the heat inventory in addition to the fission products heat production. The clad surface temperature climb should, therefore, be steeper and reach higher peak when the gas gap conductivity is smaller.

This effect should be even more pronounced for larger sized break because EOB is shorter for these breaks and consequently there is a larger percentage of the heat inventory still remaining in the fuel at the onset of steam cooling.

9.8 Phase Separation Model

The coolant flow within the primary system following vessel rupture is rapid and extremely turbulent. Flashing of liquid into steam and heat transfer serve to complicate the coolant pressure, enthalpy and flow velocity even further. The two-phase flow in pipes have been investigated by Fauske(F6) and Moody (M9, M10, M11).

For the very short duration of the blowdown, theoretical and experimental evidence indicates that a homogeneous mixture between the two phases can be assumed for small-volume, turbulent flow paths. Where the volume is large enough for the phases to separate, however, a two-phase separation model with bubble rise has been devised to fit experimental blowdown observations. As pointed out in Chapter 5, the currently recommended model uses two parameters, C_o and V_j, one for the bubble population gradient in the vertical direction within the volume, and the other for the bubble velocity as it rises from the mixture volume towards the phase interface. Curet (C8), Moore (M8) and Rettig (R2) all recommend a value of 0.8 for the gradient and 3 ft/sec. for the velocity. These values are based on semi-empirical fit to a number of experimental, high pressure blowdown (C8).

To investigate how sensitive the model is to the blowdown parameters, a value of 0.5 for the gradient has been chosen to study the two-phase blowdown of one-pipe-size top break. Fig. 9.8.F1 shows the coolant mass history in the lower plenum. Fig. 9.8.F2 shows the transient of the average clad surface temperature in the middle core region.

Fig. 9.8.F1

TOP BREAK, A = 1

EFFECT OF PHASE SEPARATION MODELS ON
COOLANT MASS REMAINING IN LOWER PLENUM

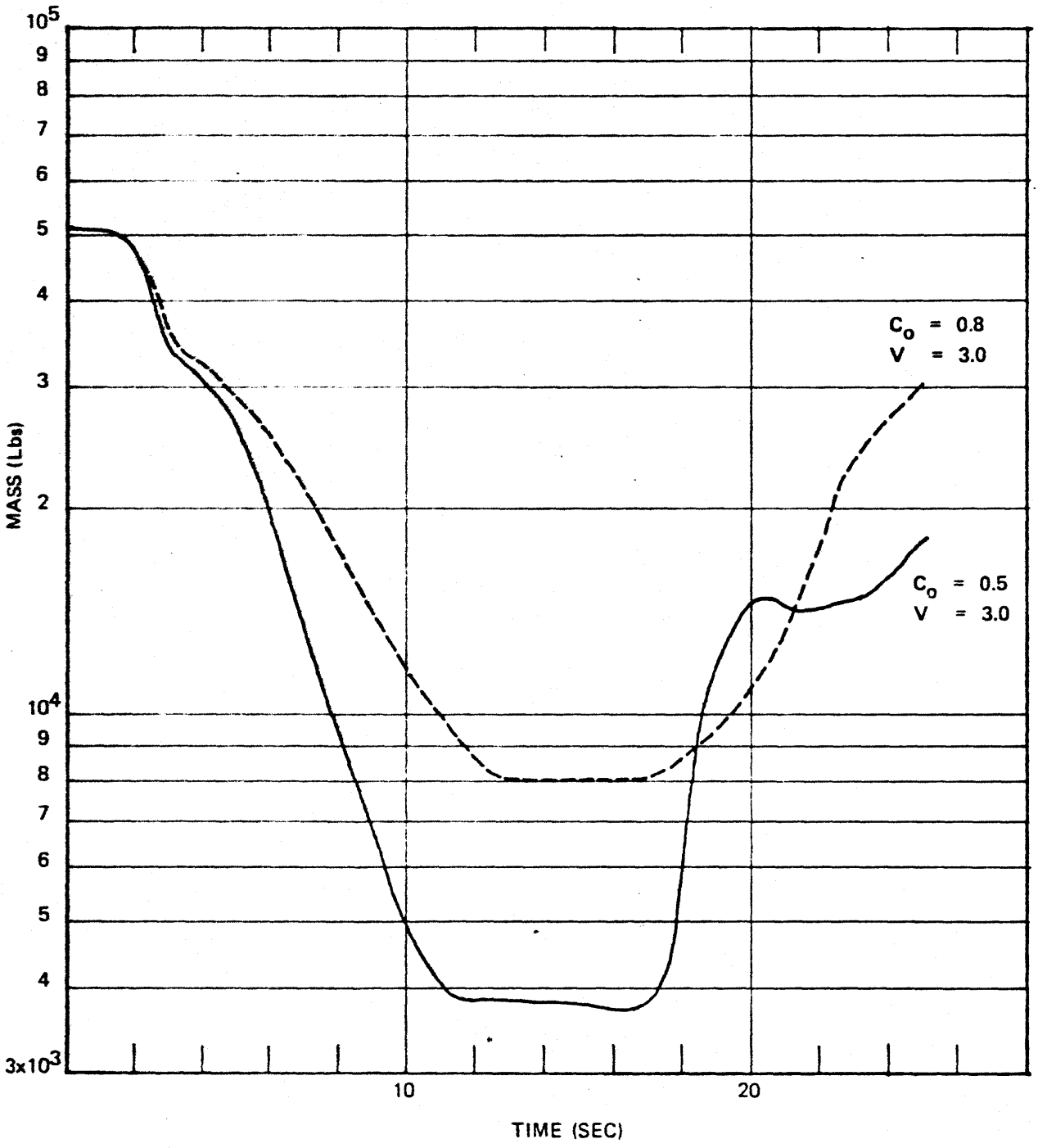

Fig. 9.8.F2
TOP BREAK, A = 1
EFFECT OF PHASE SEPARATION MODELS
ON AVERAGE CLAD SURFACE TEMPERATURE
IN MIDDLE CORE REGION

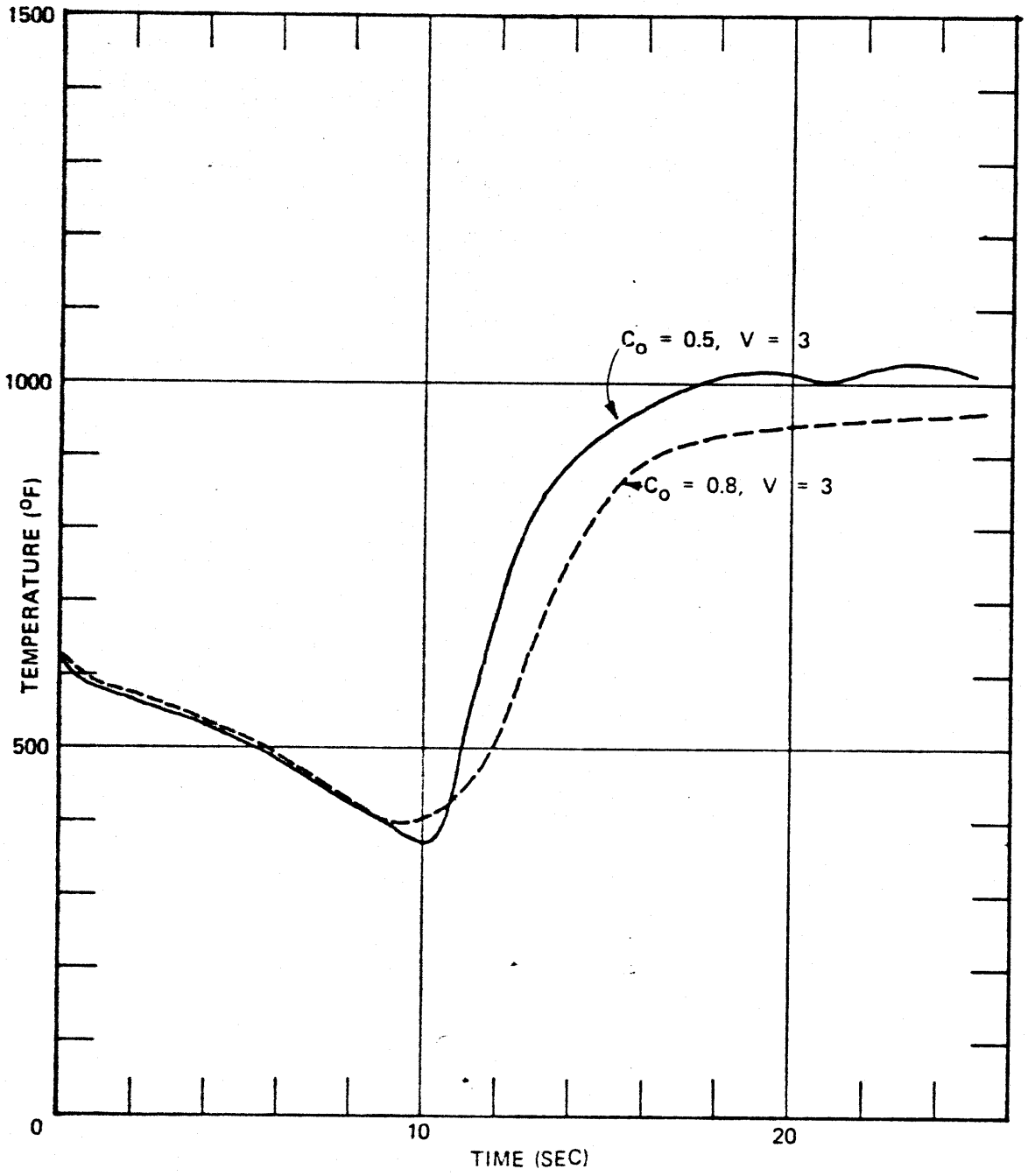

A less steep bubble gradient in the mixture means that the mixture is more homogeneous. When this is the case, then Fig. 9.8.F1 shows that the mass loss from the lower plenum is faster and there is less mass remaining in it during the quiescent, steam cooling stage. This is explained by the fact that a more homegeneous phase model would increase the density of the mass flow, whereas the density is low due to the predominance of the steam phase in the case of a phase model with steeper bubble population gradient. This fact is further illustrated in Fig. 9.8.F2. Between 0 and 10 seconds the average clad surface temperature is slightly lower for the more homogeneous phase model; due certainly to the fact that the mass flow rate through the core is slightly higher. Beyond 10 seconds when steam cooling sets in and before ECC water is effective, the more homogeneous phase model causes the clad temperature to climb more steeply and to attain a higher peak. This is due to the smaller steam flow rate emanating from the low coolant mass left in the lower plenum.

Although analysis has not been made for the bottom and side break, it is felt that the same effects would hold true.

9.9 Conclusions

Some basic parameters of the loss-of-coolant accident analysis have been studied to explore their sensitivity to other blowdown processes, mechanisms and consequences. These basic parameters include the vessel break

location, break size, break time, ECC injection location, ECC injection rate, void reactivity coefficient, gas gap conductivity and phase separation model. The physical laws and computational techniques which form the fundamental structures of the codes WHAM and RELAP3 have been invoked or commented upon where applicable, but otherwise they have been accepted throughout as valid in this work.

For the same break size and break time, a break location in the upper plenum would result in lower subcooled loadings on the vessel internals than a break at the bottom or side. A side break gives rise to the highest loadings on the thermal shield, the core barrel and the core. For all break locations, flow choking would take place at the break and in the high resistance flow paths, establishing limiting conditions for the blowdown rates, mass remaining in the lower plenum, EOB, and clad surface temperature transients.

As the break increases in size, an asymptotic configuration is assumed by most quantities under investigation. At the liberal interpretation of EOB as the time at which the flow out the break has dropped to a low, insignificant value, then EOB is around 7 to 8 seconds for all break sizes, due to the inherent limiting flow in many flow paths of the system. Due to the same reason, the minimum mass remaining in the lower plenum, and the transient of the average clad surface temperature tend to assume an asymptotic configuration. The maximum of the asymptotic temperature curve is comparable to that of the LOCA by guillotine pipe break and is below 1500°F.

The break time is very sensitive to the magnitude of the subcooled loadings but is very insensitive to the rest of the two-phase parameters. Thus, when the break is "instantaneous", the subcooled pressure loadings on vessel internals would be in the vicinity of 1000 psi. If the break time is 10 milliseconds, the loadings decrease manyfold. If the break time is 100 milliseconds, the loadings dropped to quite insignificant magnitudes. The establishment of accurate bounds for the vessel break time is, therefore, important in the economic and safe mechanical design for the vessel internals. On the other hand, a change in break time from 100 milliseconds to 10 milliseconds brings about very little change in EOB, flow reversal, minimum mass remaining in the lower plenum and clad surface temperature transients.

The location of the ECC injection nozzles in the upper plenum seems to cause an earlier and steeper temperature tise of the clad which eventually climb to a higher maximum value as compared to a cold leg ECC location. No such clear observation is seen when the ECC nozzles are placed at the hot legs. This fact suggests that an early ECC injection in the upper plenum works to suppress the pressure there, and consequently causes a lower mass flow through the core (the break being located in the bottom or at the side). It has been argued that a ECC injection at the top in the later stages of the blowdown should help cool the clad, but such studies have not been made to substantiate this argument for pressurized water reactors.

An increase in the injection rate to approximately twice the base case value does not cause any significant change. No larger injection rate has been investigated, but it seems plausible that when the injection time and rate are designed in such a way that massive ECC water is available at the onset of the steam cooling period (around 4 seconds), the clad surface temperature would certainly be suppressed. To do this, a lower ECC injection

pressure to delay the start of injection, a larger injection line or redundancy of injection nozzle, and finally the location of the injection close to the core should be an option for the ECC specialist.

An increase in the negative void reactivity coefficient to twice and four times the base case values causes the reactor to scram slightly faster, but otherwise does not affect significantly other parameters. It is argued that the void fraction, which is a function of the break time and size, is more sensitive to the reactor scram than the precise value of the void reactivity coefficient (within its bounds).

The gas gap conductivity has a large effect on the behavior of the clad surface temperature transient because it determines the inventory of the energy in the fuel at the onset of the accident. Since the fuel time constant is of the order of 10 - 12 seconds, which is larger than EOB for most vessel break accidents under consideration, a large initial energy inventory in the fuel would result in a large energy leftover after EOB. In addition to the fission products heat production, this energy must be removed by the steam during the steam cooling period, and consequently the clad surface temperature is high. It is felt that the accurate determination of the gas gap conductance during blowdown with due account for clad swelling, gas pressure and gas composition, is of prime importance in the accurate calculation of the clad temperature.

The change of the phase separation model to a more homogeneous one results in a lower coolant mass remaining in the lower plenum and a steeper clad surface temperature transient which reaches a higher peak.

APPENDIX A

SELECTED DESIGN DATA OF A TYPICAL LARGE PWR POWER PLANT FOR USE IN THE COMPUTATIONS

APPENDIX A

SELECTED DESIGN DATA OF A TYPICAL LARGE PWR POWER PLANT FOR USE IN THE COMPUTATIONS

This appendix contains the design characteristics of the typical large PWR of the 1967-1970 design that have been used in this study. Except where indicated, all data are the final design data of a Westinghouse 4-loop, 2758 MWt similar to the Indian Point 2 plant[C1].

A.1

GENERAL PLANT DATA

Power Level	
Heat output, MWt	2758
Heat output, Btu/hr	9413×10^6
Net electrical, MWe	873
System Conditions	
Total flow rate, lb/hr.	136.3×10^6
Nominal inlet, °F - psia	543 - 2280
Nominal outlet of hot channel °F - psia	633.5 - 2236.5
Avg. coolant temp. in core, °F	571
Avg. coolant temp. in vessel, °F	569.5
Heat Transfer Data	
Percent of flow through core	91
Avg. coolant velocity along rods, ft./sec.	15.5
Avg. channel cross section, ft^2	1.225×10^{-3}
Heat transfer surface area, ft^2	52,200
Avg. heat flux, Btu/hr-ft^2	175,600
Max. heat flux, Btu/hr-ft^2	567,300
Max. clad surface temp. at nominal pressure, °F	657
Fuel Centerline Temperature for Nominal Rod dimensions, °F	4090
Hot Channel Factors	
Nuclear	3.12
Engineering	1.03
Total	3.23
Enthalpy rise	1.75
Avg. thermal output, kW/ft.	5.7
Max. thermal output, kW/ft.	18.4
Max. thermal output at 112% power, kW/ft.	20.6
General Plant Data	
Number of loops	4
Design pressure, psia	2,485
Design temperature, °F	650
Total primary coolant volume, ft^3	12,600
Total reactor flow, gpm	358,800

A.2

VESSEL DESIGN DATA

Physical Dimensions	
Overall height of vessel and closure head	43'-9-11/16"
ID at shell (in.)	173
ID of flange (in.)	167-1/16
OD of flange (in.)	205
Inlet nozzle ID (in.)	27.5
Outlet nozzle ID (in.)	29
Closure head thickness (in.)	7
Lower head thickness, min. (in.)	8-5/16
Beltline thickness (in.)	8-5/8
Clad thickness, min. (in.)	5/32
Thickness of reflective SS insulation (in.)	3
Number of closure head studs (in.)	54
Diameter of closure head stud (in.)	7
Water Volumes (ft^3)	
Total water volume with core and internals in place (design)	4647
Upper head (above upper plate)	494
Upper plenum (estimated)	1451
Core (estimated)	637.5
Bypass (estimated)	286.5
Lower plenum (design)	1106
Downcomer annuli	678
Design Conditions	
Design/operating pressure, psig	2485/2235
Hydrostatic test pressure, psig	3110
Design temperature, °F	650
Reactor coolant inlet temperature, °F	555
Reactor coolant outlet temperature, °F	612.6
Coolant flow, lbs/hr	1.34×10^8
Code requirements	ASME III, Class A
Pressure Drops	
Across Vessel, including nozzles	46.7
Across core	31.5
Transient Design Cycles	
Heatup at 100°F per hour	5/yr.
Cooldown at 100°F per hour	5/yr.
Loading at 5% of full power per minute	1/day
Step load increase of 10% of full power (but not to exceed full power)	1/week
Step load decrease of 10% of full power	1/week
Step load decrease of 50% of full power	5/yr.

A.3

PRESSURE VESSEL INTERNALS

UO_2 weight (lbs.)	216,000
UO_2 average specific gravity	10.117
Number of fuel rods	39,372
Total Zircaloy weight (lbs.)	44,600
Zircaloy specific gravity	7.17
Core barrel	Austenitic steel 304
ID (in.)	148
OD (in.)	152.5
Thickness (in.)	4.5
Area inside (ft^2)	119.5
Area outside (ft^2)	126.84
Thermal Shield	Austenitic steel 304
ID (in.)	158.5
OD (in.)	164.0
Thickness (in.)	5.5
Area inside (ft^2)	137.02
Area outside (ft^2)	146.695
Cross Section of Annulus between Core barrel and thermal shield (ft^2)	10.177
Fuel Baffle	Austenitic steel 304
Area inside	96.06
Cross Section of area between baffle and barrel (ft^2)	23.44
Top core plate thickness	2 inches
Top Support plate thickness	3 inches
Bottom core plate thickness	2 inches
Bottom flow distribution plate	1.5 inches
Bottom flow inlet casting	8.8 inches
Reactor trip	10/yr.
Hydrostatic test at 3110 psig pressure, 400°F temperature (preoperational)	5
Hydrostatic test at 2485 psig pressure, 400°F temperature (post operational)	40
Life, years	40
weeks	2080
days	14600

A.4

REACTOR CORE DATA

Fuel Assemblies	
Number	193
Design	Canless, 15 X 15
Rod pitch, in.	0.563
Overall dimensions, in.	8.426 X 8. 426
Total UO_2 (lbs)	216,000
Total weight (lbs)	276,000
Total clad (lbs)	44,600
Fuel Rods	
Number	39,372
OD, in.	0.422
Diametrical gap, in.	0.0065
Clad thickness, in.	0.0243
Clad material	Zircaloy - 4
Fuel Pallets	
Material	UO_2 sintered
Density (% T.D.)	94-92-91
Diameter, in.	0.3669
Length, in.	0.600
Physical Dimensions	
Core diameter, in.	132.75
Core height, in.	144
Reflector	
Top - water plus steel, in.	10
Bottom - water plus steel, in.	10
Side - water plus steel, in.	4.18
Cross section inside baffle, ft^2	96.06
Solid cross section, ft^2	48.16
Coolant channel cross section, ft^2	47.9
Some Thermal Hydraulic Data	
Avg. temp. in core, °F	571
Avg. temp. rise in core, °F	55.5
Percent of total flow that passes through core	91
Avg. coolant speed (ft/sec.)	15.5
Avg. coolant density (lb/ft^3)	45.552
Avg. coolant enthalpy (Btu/lb)	572
Equivalent hydraulic diameter (ft)	0.00444
Total pressure drop across core (psi)	31.5
Equivalent dimensionless Moody friction coefficient	0.0224

A.5

REACTOR CORE KINETIC DATA

Reactivity Coefficients	
Moderator temp. at full power ($°F^{-1}$)	-0.3×10^{-4} to -3.0×10^{-4}
Moderator pressure (psi^{-1})	$+0.3 \times 10^{-6}$ to $+3.0 \times 10^{-6}$
Moderator Density ($\Delta k/gm/cm^3$)	+0.03 to +0.30
Doppler ($°F^{-1}$)	-1.1×10^{-5} to $+1.8 \times 10^{-5}$
Neutrons	
Delayed fraction (%)	0.52 to 0.72
Prompt neutron lifetime (sec.)	1.4×10^{-5} to 1.80×10^{-5}
Control Rods	
Effective k at BOL, full power, rods in., no boron, Xe Sm in equilibrium	1.152
Boron ppm	780
Total worth of inserted rods at hot, full power (% $\Delta k/k$ = \$)	6.35% = 9.478\$
Worst rod bank (% $\Delta k/k$)	0.5%
Void Coefficients for 3 Axial Core Regions (\$/% Void)	
Upper one-third	-0.0079
Central one-third	-0.0328
Lower one-third	-0.0149

A.6

COLD LEG DATA

ID, in.	27.5
Length (est.), ft.	21.16
Cross section, ft^2	4.12
Volume, ft^3	87.2
Mass. flow, lb/hr.	33.5×10^6
gpm	$.8978 \times 10^5$
ft/sec.	48.55
Average pressure, psia	2288
Average temperature, °F	555
Average density, ft/sec.	46.52
Average enthalpy, Btu/lb.	552.8
Psat, psia	1087

*These data are for one leg. The nominal pressure and temperature are taken from Indian Point 2 Final Safety Analysis Report, Fig. 1.1.F1. It is realized later that these data slightly differ from other data elsewhere in the FSAR, but the small difference does not matter in the results of the present study.

A.7

HOT LEG DATA*

ID, in.	29
Length, (est.), ft.	17.22
Cross section, ft^2	4.587
Volume, ft^3	79
Mass flow, lbs/hr.	33.5×10^6
gpm	$.9958 \times 10^5$
ft/sec.	48.4
Average pressure, psia	2235
Average temperature, °F	596
Average density, lb/ft^3	43.5
Average enthalpy, Btu/lb.	610
Psat, psia	1500

*These data are for one leg. The nominal pressure and temperature are taken from Indian Point 2 Final Safety Analysis Report, Fig. 1.1.F1. It is realized later that these data slightly differ from other data elsewhere in the FSAR, but the small difference does not matter in the results of the present study.

A.8

DATA FOR VESSEL UPPER PLENUM, LOWER PLENUM AND DOWNCOMER ANNULI

Upper plenum	
Cross section (est.), ft^2	163.24
Length (est.), ft.	10.5
Volume (est.), ft^3	1714
Coolant volume (est.), ft^3	1451
Mass. flow, lbs/hr.	134×10^6
Average coolant speed (est), ft/sec.	6.9
Average pressure, psia	2236.5
Upper Head Region	
Volume of region above upper grid plate, ft^3	494
Lower Plenum	
Cross section (est.), ft^2	163.24
Length (est.)	6.74
Volume (est.)	1106
Average coolant speed (est.), ft/sec.	4.56
Average pressure	2266.5
Annuli	
Cross section above shield (ft^2)	36.4
Cross section between shield and barrel, ft^2	10.177
Cross section between shield and vessel wall, ft^2	16.543
Nominal downcomer	
ft^2/sec.	776.3
ft/sec.	29
Volume above reactor region, ft^3	278
Volume at reactor region, ft^3	400
Height above reactor region, ft.	10.5
Height at reactor region, ft.	15

A.9

PRESSURIZER DATA

Height (est.), ft.	46.8
Nominal water volume, ft^3	1080
Nominal steam volume, ft^3	720
Design operating pressure, psig	2485–2235
Design operating temp. 1°F	680–653
Surge line	
ID, in.	14
Length, ft.	41
Volume, $ft.^3$	38

A.10

STEAM GENERATOR DATA

Number	
Design, pressure, reactor coolant/ steam, psig	2485/1085
Design temp., reactor coolant/steam, °F	650/600
Reactor coolant flow, lbs/hr.	33.5×10^6
Heat transfer surface, ft²	44,430
Heat transferred, Btu/hr.	$2,631 \times 10^6$
Overall height, ft-in.	63-1.625
Shell OD upper/lower, in.	166/127.5
Shell thickness, upper/lower, in.	3.5/2.63
U-tubes	
Number	3260
ID, in.	0.875
Cross section, ft²	4.176×10^{-3}
Avg. wall thickness, in.	0.050
Length (est.) ft.	63.6
Total flow area (est.) ft²	13.614
Shell side conditions	
Feed water temp., °F	427.2
Steam temp., °F	513.8
Steam pressure, psig	755
Steam flow, lb./hr.	3.315×10^6
Volumes, ft.³	
Reactor coolant water volume	924
Inlet plenum volume	
Outlet plenum volume	
Secondary side water volume	1613
Secondary side steam volume	2966
Line leading to coolant pump	
ID., in.	31
Cross section, ft.²	5.21
Volume, ft.³	113.5

A.11

EMERGENCY WATER INJECTION SYSTEMS

Accumulators	
Number assumed working	3 out of 4
Injected into	Cold legs
Injection line size (est.), in.	14
Equivalent $\frac{L}{A}$ for all lines, ft^{-1}	20
Equivalent friction factor	0.004 lb_f sec^2/lb_m ft^3 in^2
Total volume, $ft.^3$	3300
Water volume, $ft.^3$	2100
Nitrogen volume, $ft.^3$	1200
Initial pressure, psi	700
Elevation head, ft.	neglected
Actuation pressure differential, psi	660
Safety injection lines	
Working condition and capability	Fill Curve 2, Fig. 14.3.2-29 of IP2 FSAR (2 pumps on three loops)
Injection into	Hot legs and cold legs
Delay time after actuation	25 sec.
Charging Lines	
Injection into	Hot legs
Delay time after actuation	25 sec.
Reservoir pressure and temperature	14.7 psia 100°F

Pressure (psig)	gpm
100	578
600	514
1080	455
1400	414
1700	369
2000	309
2300	228
2600	86

Recirculation Lines

Injection into	Cold legs
Delay time	25 sec.
Reservoir-pressure/temp.	14.7 psia 100°F

Pressure (psig)	gpm
10	4734
30	4482
50	4140
70	3780
100	3150
130	2430
150	1800
170	540

*The Safety Injection Lines, charging lines and recirculation lines were provided for the system but were not used due to a decision to stop at 25 sec. to save computer time.

A.12

COOLANT PUMPS

General design data

Number per coolant loop	1
Type	Centrifugal
Overall height, ft.	28.38
Water volume, $ft.^3$	192
Capacity, gpm	89,700
Developed head, ft.	272
NPSH, ft.	170
Suction temperature/pressure	555°F/2235 psi
Design temperature/pressure	650°F/2485 psi
Suction line nozzle, ID, in.	31

Motor data

Type	AC Induction Single Speed, Air Cooled
Voltage	6600
Insulation class	B. Thermalastic Epoxy
Phase	3
Frequency, cps	60
Starting current, amp	2950
Input to hot coolant, kw	4250
Input to cold coolant, kw	5600
Nameplate rpm	1189
Nameplate horsepower	6000

A.13

PUMP HEAD CHARACTERISTICS (S5.C6)

Actual Flow / Nominal Flow	Actual Head / Nominal Flow
-1.0	2.8
-0.5	2.02
-0.25	1.75
0	1.6
0.25	1.52
0.5	1.4
0.75	1.26
0.9	1.14
1.0	1.0
1.1	0.915
1.25	0.7
1.5	0.32
1.69	0
2.0	-0.65
2.25	-1.18
2.5	-1.75

A.14

PUMP COASTDOWN CHARACTERISTICS*

Time (Sec.)	Core Flow (% of nominal flow)
0	1
2	0.855
4	0.735
6	0.65
8	0.59
10	0.54
12	0.50
14	0.46
14	0.46
16	0.43
18	0.40
20	0.38
40	0.32
70	0.25

*Taken from D. C. Cook Preliminary Safety Analysis Report (11).

APPENDIX B

PHYSICAL PROPERTIES USED IN THE COMPUTATIONS

APPENDIX B

PHYSICAL PROPERTIES USED IN THE COMPUTATIONS

This appendix contains other physical properties employed in the computations. Efforts have been made to use the most current or recommended data. Where these data are absent and must be estimated, they are so indicated.

B.1

UO_2 THERMAL CONDUCTIVITY

Uranium thermal conductivity obtained by Lyons et al (L3) is used.

The formula approximating the data measured for UO_2 pellet under irradiation with central melting is:

$$k = \frac{1}{3600}\left\{\frac{3978.1}{T+629.61} + (6.0237 \times 10^{-12})\ (T + 460)^3\right\}$$

$$77°F < T < 5072°F$$

where T is in °F and k is Btu/hr. ft. °F.

A few computed values for k_{uo_2} are listed below:

Temperature °F	k_{uo_2} (Btu/hr. °F ft.)
100	5.45343
300	4.28199
500	3.52703
700	3.00140
1000	2.46002
1200	2.20210
1500	1.91368
1800	1.70740
2000	1.60314
2500	1.42849
3000	1.34736
3500	1.34013
4000	1.39761
4500	1.51596
5000	1.69431
5100	1.70000

B.2

UO_2 HEAT CAPACITY

The heat capacity data for UO_2 is recommended by Brassfield at el (B2)

$$C_p = 0.0726 + (3.33 \times 10\text{-}6)\ T - \frac{4.74 \times 10^3}{(T + 460)^2}$$

$$77°F \leq T \leq 2240°F$$

$$C_p = -0.18426 + (3.8303 \times 10^{-4})\ T - (2.0447 \times 10^{-7})\ T^2 + (4.6457 \times 10^{-11})\ T^3 - (3.6289 \times 10^{-15})\ T^4$$

$$2240°F < T \leq 5072°F$$

where C_p is in Btu/lb. °F

A few values of C_p are:

Temperature °F	C_p (UO_2) (Btu/lb °F)
100	.05782
300	.06539
500	.06912
800	.07228
1000	.07371
1500	.07636
2000	.07848
2500	.07951
2800	.08195
3000	.08500
3200	.08945
3400	.09537
3600	.10270
3800	.11122
4000	.12059
4300	.13513
4700	.15176
5000	.15820
5100	.16000

B.3

ZIRCALOY-4 THERMAL CONDUCTIVITY

The thermal conductivity of Zircaloy-4 is proposed by Touloukian et al (T3).

$$k = \frac{1}{3600}\left\{4.14 + (1.044 \times 10^{-2})\,T - (5.276 \times 10^{-6})\,T^2 + (1.536 \times 10^{-9})\,T^3\right\}$$

$572°F < T \leq 2732°F$

where k is in Btu/hr. ft. °F.

A few values of k are:

Temperature °F	k_{zirc} (Btu/hr. ft. °F)
600	8.83642
700	9.38961
800	9.90179
900	10.38218
1000	10.84000
1100	11.28446
1200	11.72477
1300	12.17015
1400	12.62982
1500	13.11300
1600	13.62890
1800	14.79571
2000	16.20400
2200	17.92749
2400	20.03990
2700	24.09905

B.4

ZIRCALOY-4 HEAT CAPACITY

Data for Zircaloy-4 heat capacity is recommended by Brassfield et al (B2).

$C_p = 0.068 + (1.33 \times 10^{-5})\ T; \quad 32°F < T < 1376°F$

$C_p = 0.086; \quad T \geq 1376°F$

The unit of C_p is in Btu/lb. °F.

At 1584°F, a latent heat effect is of 19.2 $\frac{Btu}{lb.}$ is present.

A few values of C_p for Zircaloy-4 are:

Temperature °F	C_p (Btu/lb. °F)
100	.06933
200	.07066
300	.07199
400	.07332
500	.07465
600	.07598
700	.07731
800	.07864
900	.07997
1000	.08130
1100	.08263
1200	.08396
1300	.08529
1376	.086
2700	.086

B.5

FISSION-PRODUCTS DECAY HEAT

During blowdown, the reactor power is calculated by means of coded point kinetic subroutine in RELAPS, with seven neutron groups, eleven gamma groups, void and Doppler coefficients but no control rod action.

When the reactor has been well shutdown, the power is calculated by the ANS-5 Proposed Standard "Energy Release Following Shutdown of Uranium - Fueled Thermal Reactors" (R1).

Approximated representation of fission products decay power over nominal reactor power is:

Time (Sec.)	P/P_o
0.1 - 10	$0.06025t - .0639$
10 - 150	$0.07655t - .1807$
150 - 4×10^6	$0.1301t - .2834$
4×10^6 - 2×10^8	$0.2659t - .335$

Some values for P/P_o are listed below:

Time (Sec.)	P/P_o
.1	.069
1	.059
10	.052
25	.0428
100	.035
10^3	.024
10^4	.013
10^5	.006
10^6	.0026

B.6

HELIUM PROPERTIES

The basic properties of helium as listed by Rohsenow and Choi (R3) are presented here. Fresh PWR fuel rods have a helium filled gap. As soon as the rod is irradiated, fission product gases and other elements diffuse out to the gap and mix with helium. Also, thermal processes are such that the gap would change in size and would no longer maintain the assumed original symmetry. The gap conductance is therefore largely dependent on locations, and is unknown. Except where mentioned otherwise, most computations have been based on the assumption that the gap thickness does not change and the gap conductivity is half that of helium.

Temperature °F	C_p (Btu/lb. °F)	k (Btu/hr.ft. °F)
0	1.24	0.078
200	1.24	0.098
1000	1.24	0.16
5000	1.24	0.4688*

*This value is not listed in Rohsenow and Choi, but is adopted from ANC sample pipe break LOCA calculations (A10).

APPENDIX C

HEAT TRANSFER AND CRITICAL HEAT FLUX CORRELATIONS

USED IN RELAP3, MOD. 36

C.1

HEAT TRANSFER CORRELATIONS

The regimes of heat transfer can be summarized by Fig. C.1.F1 Following is a description of the correlations and their validity.

1) $x < 0$, $T_s < T_{NB}$ Subcooled Forced Convections

Seider-Tate Correlation

$$h = \frac{q''}{T_s - T_w} = 0.023 \frac{k_f(T_w)}{D} \left[Re(T_w)\right]^{0.8} \left[Pr(T_w)\right]^{1/3} \left[\frac{\mu_f(T_w)}{\mu_f(T_s)}\right]^{.14}$$

where

x = quality of the water steam mixture

T_s = fuel rod surface temperature, °F

T_{NB} = minimum surface temperature for nucleate boiling

$$T_{NB} = T_{sat} + 0.072\, e^{-p/1260}\, q''^{0.5}$$

T_{sat}	Saturation temperature, °F
p	Coolant pressure, psi
q''	Surface flux, Btu/hr. ft.^{2}
T_w	Coolant temperature, °F
D	Hydraulic diameter of flow channel, ft.
Re	Reynolds number, Re = $\rho VD/\mu$
Pr	Prandtl number, Pr = ν/α

and $k_f, \mu_f, \nu_f, \alpha_f$ are the thermal conductivity (Btu/hr. ft.°F), viscosity (lbs/hr. ft.), kinematic viscosity (ft.^{3}/hr) and thermal diffusivity (Ft^2/hr.) of the coolant mixture, respectively. These quantities are evaluated at the indicated temperature.

2) $x < 0$, $T_s = T_{NB}$ Subcooled Nucleate Boiling

Thom Correlation

$$h = \frac{q''}{T_s - T_w}$$

where the quantities have been defined.

3) $0 \leq x < 0.1$ Nucleate Boiling

The heat transfer coefficient is calculated by interpolating with respect to quality between Thom Correlation and Schrock-Grossman Correlation.

4) $0.1 \leq x < 0.6$ Forced Convection Boiling

Schrock-Grossman Correlation with Wright Constant

$$h = 6700A\left[\frac{q''}{GH_{fg}} + 0.00035\ B^{0.66}\right]$$

$$A = 0.023\ \frac{k_f}{D}\ (1-x)^{0.8}\ Re^{0.8}\ Pr^{0.4}$$

$$B = \left(\frac{x}{1-x}\right)^{0.9} \left(\frac{v_g}{v_f}\right)^{0.5} \left(\frac{\mu_g}{\mu f}\right)^{0.1}$$

where

v_g Specific volume of vapor, ft.^{3}/lb.
v_f Specific volume of liquid, Ft.^{3}/lb.
H_{fg} Heat of vaporization, Btu/lb.
0.66 Wright Constant

5) $0.6 \leq x < 1.0$ Forced Convection Boiling

The heat transfer coefficient is calculated by interpolating with respect to quality between Schrock-Grossman Correlation and Dittus-Boelter Correlation.

6) $x \geq 1.0$ Single Phase Steam Heat Transfer

Dittus-Boelter Correlation

$$h = 0.023\ \frac{k_g}{D}\ Re^{0.8}\ Pr^{0.4}$$

Physical properties are evaluated at $\frac{T_w + T_s}{2}$

7) Stable Film Boiling*

Effective when the surface heat flux is greater than CHF. Dougall Rohsenow Correlation (D1).

$$h = 0.023 \frac{k_g}{D} \left[x + \frac{v_f}{v_g} (1 - x) \right]^{0.8} Re_g^{0.8} Pr_g^{0.4}$$

The physical properties are evaluated at saturation conditions.

If x 0.0, the term $\frac{S_g}{S_f} (1 - x) + x)$ is set equal to 1.0

which reduces this correlation to the Dittus Boelter Correlation.

---

* The Groeneveld Correlation, which is recommended by the Interim Policy Statement (U2) provides values of the heat transfer coefficient somewhat similar but more conservative than Dougall Rohsenow Correlation. For heated cylindrical rods, the Groeneveld Correlation is: (G1):

$$h - 0.052 \frac{k_g}{D} \left[x + \frac{v_f}{v_g} (1 - x) \right]^{0.688} Re_g^{0.688} Pr_s^{1.26} Y^{-1.06}$$

where Pr_s is the Prandtl number evaluated at the surface temperature,

and Y is the Miropolskyi two-phase flow factor (M4).

$$Y = 1 - 0.1 (v_g/v_f - 1)^{0.4} (1 - x)^{0.4}$$

Fig. C.1.F1

RELAP 3 Mod 36 Heat Transfer Regimes

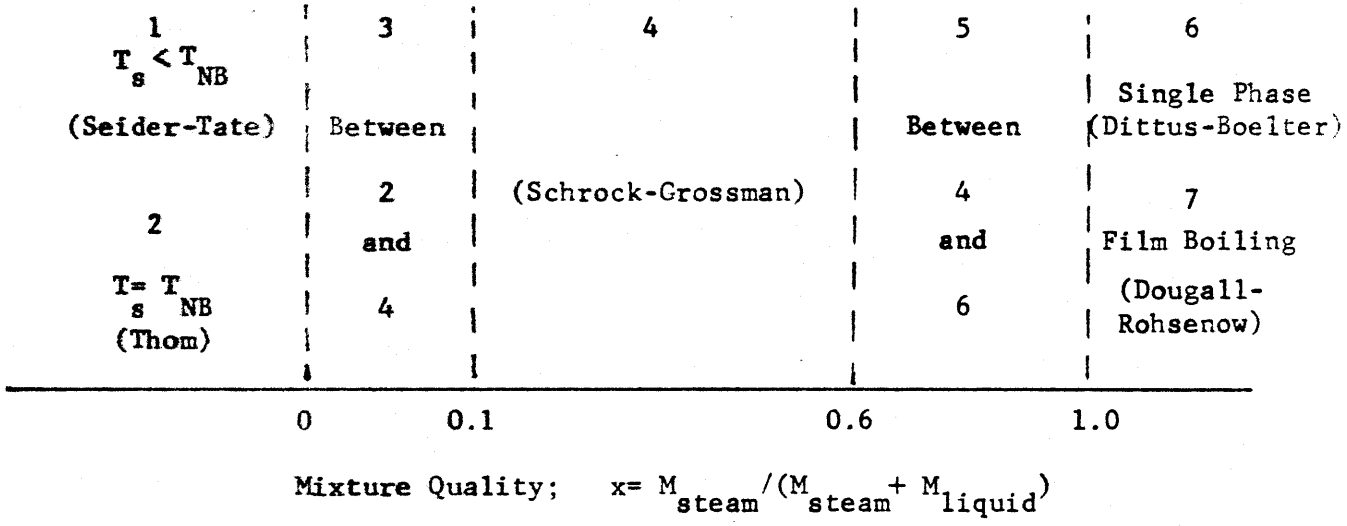

C.2

CHF CORRELATIONS

In RELAP3, Mod. 36, stable film boiling (Dougal$_1$ Roshenow) is assumed to occur when the calculated surface heat flux is larger than the calculated CHF. The CHF is predicted on the basis of pressure and mass flow. Fig.C.1.F2 is a schematic diagram of different CHF regimes.

1) $p \leq 725$ psi: Modified Barnett Correlation With Idaho Nuclear Corporation Constants

$$\frac{CHF}{10^6} = \frac{B+E\ (H_f - H_{in})}{F + L}$$

$$B = 73.71\ D^{0.0523}\ G^{0.663}\ \frac{888.6}{H_{fg}}\ (1.0 - 0.315e^{-11.34CG})$$

$$E = 0.104\ D^{1.445}\ G^{0.691}$$

$$F = 45.55\ D^{0.0817}\ G^{0.587}$$

where

CHF = Critical heat flux, Btu/hr. ft.^{2}

H_f = Saturated liquid enthalpy, Btu/lb.

H_{in} = Inlet enthalpy, Btu/lb.

L = Channel length, in.

D = Heated equivalent diameter, in.

C = $\left[d(d + D)\right]^{0.5} - d$, in.

d = Fuel rod diameter

G = Mass flux, 10^6 lbs/hr. ft.^{2}

H_{fg} = Heat of vaporization, Btu/lb.

2) 725 psi < p ≤1000 psi

The CHF is calculated by linear interpolation with respect to pressure between Modified Barnett Correlation and Barnett Correlation. (B3)

3) 1000 psi ≤ p < 1500 psi: Barnett Correlation (B3)

$$\frac{CHF}{10^6} = \frac{J + M\,(H_f - H_{in})}{R + L}$$

$$J = 67.45\, D^{0.68}\, G^{0.192}\, (1.0 - 0.744e^{-6.512GC})$$

$$M = 0.2587\, D^{1.261}\, G^{0.817}$$

$$R = 185\, D^{1.415}\, G^{0.212}$$

All parameters have been previously defined

4) 1500 psi ≤ p < 1800 psi

The CHF is calculated by linear interpolation with respect to pressure between Barnett Correlation and B & W-2 Correlation. (G1)

5) p ≥ 1800 psi, G > 0.5 X 10^6 lbs/hr. $ft.^2$
B&W-2 Correlation (G1)

$$\frac{CHF}{10^6} = \frac{S}{12.71Y^N}\,(37.02\, W^Z - 0.15208\, GH_{fg}x)$$

$$S = 1.15509 - 0.40703\, D$$

$$W = 0.59137\, G$$

$$Z = 0.8304 + 6.8479 \times 10^{-4}\,(p-2000)$$

$$N = 0.71186 + 2.0723 \times 10^{-4}\,(p-2000)$$

$$Y = 3.0545\, G$$

where

G = Mass flux, 10^6 lb/hr. $ft.^2$

x = Mixture quality

6) $p \geq 1800$ psi, $G \leq 0.5 \times 10^6$ lbs/hr. ft.^{2}

The CHF is evaluated by using the average value between B&W-2 value and Barnett value.

In the above CHF correlations, the inlet enthalpy is dependent on the flow direction and is determined as follows:

Normal Inlet Flow	Normal Outlet Flow	H_{in}
> 0	≥ 0	H at normal inlet
≤ 0	< 0	H at normal outlet
All other cases		H of core volume

Fig. C.2.F1

RELAP 3 Mod 36 CHF Regimes

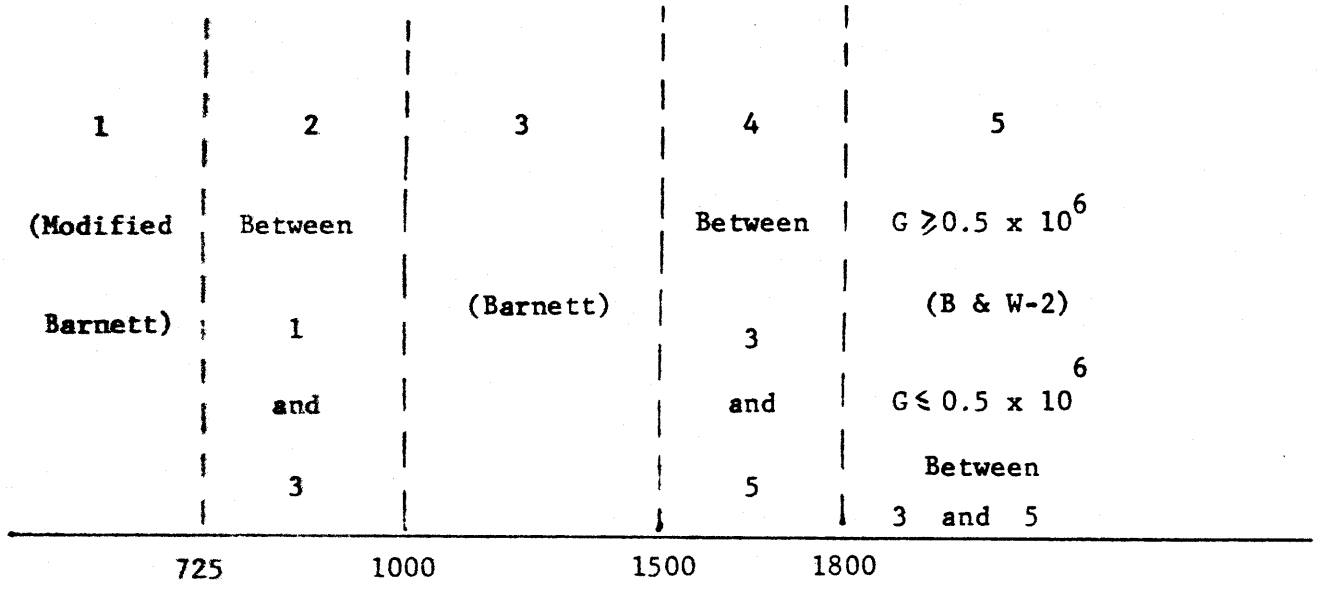

APPENDIX D

SURVEY OF CURRENT REACTOR VESSEL CODE AND THE ANALYSIS OF VESSEL FAILURE

D.1 ASME Section III, Nuclear Vessel

The design, manufacture, testing and maintenance of pressure vessels have traditionally been done with professional codes. Older naval and medium sized reactor vessels were fabricated in accordance with Section I and VIII of the ASME Boiler and Pressure Vessel Code. Today all reactor pressure vessels are designed, manufactured, tested and maintained in accordance with the ASME Boiler and Pressure Vessel Code, Section III, Nuclear Vessels, which was published in 1964. This section is primarily concerned with temperatures below 800°F the creep limit for the material of interest. Provisions for limiting primary, secondary and other stresses as well as stress concentrations are incorporated. Rules for the control of external influences and environmental factors, such as corrosion and radiation effects, are not specified, but the designer or owner is made responsible for taking these factors into consideration.

The four major areas of requirements spelled out by Section III are:

a) Hydrostatic Test Requirements

The vessel must undergo a complete hydrostatic test to verify that it has enough strength and no leak. The test pressure is determined by:

$$P_{test} = 1.25\, P_{dsgn} \frac{\text{Allowable design stress intensity at test temperature}}{\text{Allowable design stress intensity at design temperature}}$$

The P_{test} represents about 40% of minimum tensile strength and 80% of minimum yield strength of the material.

b) Stress Report Requirements

A complete stress analysis report must be prepared. All pertinent analytical and experimental data must be included. This report must be certified by a qualified Professional Engineer.

c) Quality Assurance Requirements

The quality assurance must cover the rank and file of the manufacturer's organization and every phase in the history of the vessel. These include material specifications, preparations and testings of material samples, heat treatments, welding, non-destructive and mechanical testings, chemical analyses, mechanical property determinations, and flaw detection.

d) Post Operation Testing

After the vessel has been put into operation, there must be supplied periodic monitoring of vessel conditions. Checks of brittle fracture transition must also be made.

D.2 Reactor Vessel Design, Analysis and Experimentation On Failure Modes

To comply with the design rules of Section III, the designer must perform a complete stress analysis for the vessel. However, due to its complex geometry, particularly around reinforcements and penetrations, rigorous solution is not possible. Current practice is to identify those areas of uncertainty, to use the best approximate solution, and to apply a margin for conservation. In a broad context, the pressure vessel is subject to the following failure modes:

a) Excessive plastic deformation, including plastic instability and buckling.

b) Cracking leakage or brittle fracture due to initial flaws or flaw growth by fatigue or corrosion.

c) Elastic distortion.

d) Excessive creep deformation or creep rupture.

Section III provides only partial analytical treatments for the first two modes, the remainder being the responsibility of the designer. The recommended techniques are based on the following assumptions:

a) Ductility of construction material remains significant throughout the operating history.

b) Tresca maximum shear-stress theory describes the limiting stress loading.

c) Secondary and local stresses exceeding the yield can be accommodated by material ductility.

d) The adequacy of protection against fatigue failure can be achieved by the use of Goodman's diagram and Miner's hypothesis, and by comparison with strain-controlled fatigue data.

e) Thin-shell theory, discontinuity analysis, and linear superposition of stresses are valid.

f) Unverified approximations must be supplimented with experimental data.

g) Provision must be made for deterioration of materials due to radiation, material instability, and loading effects such that the preceding assumptions are always valid.

All vessel manufacturers employ large and sophisticated computer codes to handle various phases of vessel design. But the most rigorous analytical stress analyses are obviously not adequate enough in view of limitations of the theory and possible inadequate assessment of loading conditions. There has been no unique, theoretically acceptable way of determining elastic distortion and creep rupture. Transient conditions that give rise to thermal and pressure loading present another category of difficult problems,

as consequences of pressure-pulse loadings have not been included in the code at present. Table 3.1.T1 list the types of transients and the number of cycles designed for the pressure vessel of a 2758 Mwt PWR power plant (C1).

Defects such as cracks, flaws may propagate with catastrophic speed when the tensile stress is equal to the dynamic yield stress. Depending on the size and shape of a structural element and on its stress environment history during service, a critical condition for crack propogation may develop gradually in the following modes:

a) Crack growth by fatigue.

b) Crack growth by stress corrosion (or hydrogen embrittlement)

c) Reduction of crack toughness (such as by radiation damage)

The fracture behavior for which a suitable analysis is needed is termed progressive crack extension. The combination of local plastic strains advance separations, elastic constraint, and tension near the loading edge of a crack may be sufficient to cause sudden rapid spreading of the crack. If that combination is less than sufficient, there may be plastic strain reversals near the loading edge that cause the crack to grow. Onset of rapid crack extension provides a relatively abrupt expansion of the flaw. The environment, with or without fatigue assistance, may cause stable spreading of the crack.

Full-scale tests have been conducted to verify and improve the theoretical design calculations for large steel pressure vessels. The most well known tests are the series undertaken by the Pressure Vessel Research Committee (PVRC), the British, the PM-2A, and the SKODA (USSR) projects. The results indicate that neither the transition-temperature approach nor the fracture-mechanics approach is entirely adequate for design against failure. Some of the large scale tests have shown that cyclic crack growth is a significant problem which has not been fully understood. Catastrophic failure usually has multiple causes, such as in the case of the December 22, 1965 failure of a large, thick-walled pressure vessel intended for high pressure use in a British ammonia plant. Although the design test pressure was 6950 psi, 50°F, the vessel failed at 5100 psi, 50°F and threw a 2-ton steel segment 153 feet away. Post-mortem analysis indicated a series of possible causes, such as marginal steel strength, low design safety factor, faulty heat treatment and possible undetected flaws in the heat affected zone. (W3)

The most recent efforts in heavy section pressure vessel technology have been undertaken by the Heavy-Section Steel Technology Programs (HSST) with major emphasis on LWR vessel materials, namely ASTM A533, Grade B, Class 1 plate steel and ASTM A-508, Class 2 forging steel. For all tests, the steel has been purchased to specifications used by industry in the fabrication of reactor vessels. Dynamic tear tests on specimens up to 12-inch thick and drop weight NDT tests on specimens up to 4-inch thick has revealed that as the thickness increases, so does the temperature at which significant increase in toughness occurs. This leads to the conclusion that plastic constraints bring about an increase in fracture transition temperature.

A major series of the tests involves the use of flawed sbusized pressure vessels which will be overloaded to failure. These vessels are designed to include as far as practicable the actual vessel configuration and construction features. The fracture toughness property, K_{Ic}, which relates nominal stress, flaw size and geometry has been shown to be a quantitative measure of the potential for brittle fracture. Fracture toughness values for the plate specimens as thick as 12 inches have been measured at about 50°F, and results indicate that relatively large flaws (at least 1/4 the plate thickness deep and 3/4 the plate thickness long) could be tolerated without failure. At high operating temperatures around 550°F, even larger flaws can be tolerated without failure. Crack arrest tests have revealed a similar increase in toughness for increasing temperatures. In general, welds and forgings have exhibited higher toughness levels than the plate at the lower temperatures. Crack propagation rates at relatively high frequency, 60 to 600 cycles/min., measured under reactor service temperatures and pressure are similar to those measured in an inert gas environment.

The fracture toughness factor, K_{Ic}, for specimens under the influence of radiation has also been investigated for a fast neutron fluence of 2×10^{19} nvt, K_{Ic} of a 2-inch specimen increased from 50,000 at 120°F to more than 150,000 at 300°F. (T6)

Concurrent to the HSST program, there is also a on-going program for nuclear piping components and pressure vessel nozzles. The loads under investigation are internal pressure, external force and moments, and the thermal stress induced by non-uniform temperature distributions in the components. Significant information, including codes, standaridization and computer codes have been contributed by this program to the nuclear component industry.

REFERENCES

The references are organized in alphabetical blocks to facilitate their use in the text and their location when necessary. However, no attempt has been made to classify the items within each block any further.

A

A1. 10 CRF 50, Appendix A, "General Design Criteria For Nuclear Power Plants", Definitions.

A2. Criteria For Emergency Core Cooling Systems for Light Water Power Reactors - Interim Policy Statement, Federal Register, Vol. 36, No. 125, June 29, 1971 and Vol. 36, No. 244, December 18, 1971.

A3. Testimony of the AEC Regulatory Staff at a Public Rulemaking Hearing on Interim Acceptance Criteria for Emergency Core Cooling Systems for Light Water Power Reactors, January 27, 1972.

A4. Aerojet Nuclear Company, Statement Relating to the "Interim Acceptance Criteria for Emergency Core Cooling Systems for Light Water Power Reactors", December 28, 1971.

A5. Aerojet Nuclear Company, Transmittal letter, RELAP 3 Package and 34-volume Sample Problem, From E. Larene Smith to D. D. D. Lanning (MIT) on December 3, 1971.

A6. Advisory Committee on Reactors Safeguards, Letter the Chairman of ACRS, W. Manly, to the Chairman of the Atomic Enery Commission, November 24, 1965.

B

B1. Babcock & Wilcox Co., J. S. Goellerstedt et al, "Correlation of CHF in a Bundle Cooled by Pressurized Water", Two-Phase Flow and Heat Transfer in Rod Bundles, Winter Meeting, ASME, Los Angeles, pp 63-71 (November, 1969).

B2. H. C. Brassfield, J. F. White, L. Sjokahl, J. T. Bittel, Recommended Property and Reaction Kinetics Data for Use in Evaluating a Light-Water Cooled Loss-of-Coolant Incident Involving Zircaloy-4 or 304 SS Clad UO_2, GEMP-482 (April, 1968).

B3 P. G. Barnett, A Correlation of Burnout Data for Uniformly Heated Annuli and Its Use for Predicting Burnout in Uniformly Heated Rod Bundles, AEEW-R-463 (1966).

B4. F. W. Buckman, Severe Reactivity Transient in Boiling Water Reactors, Ph.D. Thesis, Dept. of Nuclear Engineering, M.I.T. (1970).

B5. N. T. Berta, Approximation of Subcooled Depressurization and Core Hydraulic Loading in PWR Vessels - An Empirical Method and Computer Application, ANCR- 1009, Aerojet Nuclear Corp., October, 1971.

B6. Babcock & Wilcox Co., Multinode Analysis of B & W's 2568 - MWT Nuclear Plants During A Loss-of-Coolant Accident, BAW-10015 (February, 1971), BAW-10015 Suppl. 1 (June, 1971), BAW-10034 (October, 1971).

B7. Babcock & wilcox Co., CRAFT, Description of Model for Equilibrium LOCA Analysis Program, BAW-10030 (October, 1971), Proprietary.

B8. F. M. Bordelon, "A Comprehensive Space-Time Analysis of Loss-of-Coolant (SATAN Digital Code), WCAP-7236 (Westinghouse Proprietary), March, 1968.

C

C1. Consolidated Edison Company of New York, Inc., Indian Point Nuclear Generating Unit No. 2. Final Facility Description and Safety Analysis Report, Vols. 1, 2, 3, 4, and supplements. USAFC Docket 50-247.

C2. H. D. Curet, "Experimental Blowdown Phenomena Applicable to Pressurized Water Reactor Systems", ANS Transaction, 9, No. 2 (1966), pp 560-561.

C3. R. Curtis and E. Hogan, Perils of the Peaceful Atom, The Myth of Safe Nuclear Power, Doubleday & Co., Inc., Garden City, New York, 1969.

C4. Consolidated National Intervenors, Direct Testimony Before the Specially Set Atomic Safety and Licensing Board in the Matter of Certain Hearings with Respect to Amendment, Rescission or Adoption of Interim Acceptance Criteria For Emergency Core Cooling Systems - Light Water Cooled Nuclear Power Reactors, USAEC Docket No. RM-50-1, March 23, 1972.

C5. Combustion Engineering, Inc., State of Affirmative Testimony And Evidence of Combustion Engineering, Inc. In the Matter of Rule Making Hearing on the Acceptance Criteria for Emergency Core Cooling Systems For Light Water Cooled Nuclear Power Reactors, Docket No. Rm-50-1, March, 1972.

C6. G. N. Cox and F. J. Germano, Fluid Mechanics, Von Nostrand Company, Inc.

C7. Carolina Power and Light Co., Burnswick Steam Electric Plant Units 1 & 2, USAEC Dockets 50-324, 50-325.

C8. H. D. Curet, "Experimental Blowdown Phenomena Applicable to Pressurized Water Reactor Systems", ANS Transactions, Vol. 9, No. 2 (1966), pp 560-561.

C9. Combustion Engineering, Inc., Chapter 14 of the Fort Calhoun Nuclear Power Plant Preliminary Safety Analysis Report.

D

D1. R. S. Dougall and W. M. Rohsenow, Film Boiling on the Inside of Vertical Tubes with Upward Flow of the Fluid at Low Qualities, MIT-TR-9079-26 (1963).

D2. F. W. Dittus and L. M. K. Boelter, "Heat Transfer in Automobile Radiators of the Tubular Type", Univ. of California, Pub. in Eng., 2 No. 13 (1930) pp 443-461.

E

E1. Ergen et al, Emergency Core Cooling: A Report of the Advisory Talk Force on Power Reactor Emergency Core Cooling, USAEC (1967).

E2. G. J. Elbaum, Rapid Excursions In Water Reactors Involving Fuel Element Rupture, Ph.D. Thesis, Department of Nuclear Engineering, M.I.T., 1967.

F

F1. F. R. Farmer, ed., Quantitative Safety Analysis, Chap. 8, Steel Pressure Vessels, Nucl. Eng. Design 13 (1970), pp183-244.

F2. M. H. Fontana, "Core Meltthrough As a Consequence of Failure of Emergency Core Cooling", Nuclear Safety, Vol. 9, No. 1, Jan.-Feb., 1968.

F3. S. Fabic, "Computer Code WHAM for Calculation of Pressure, Velocity, and Force Transients in liquid Filled Piping Networks", Kaiser Engineers Report 67-49-R, Nov. 1967.

F4. S. Fabic, "BLOWDN-2" Westinghouse APD Computer Program for Calculation of Fluid Pressure, Flow, and Density Transients During a Loos-of-Coolant Accident", ANS Transaction, 12, p. 358 (1969).

F5. S. Fabic, "Two- and Three-Dimensional Fluid Transients", ANS Transactions, June, 1971, Boston, Mass., pp 360-361.

F6. H. K. Fauske, Contribution to the Theory of Two-Phase, One-Component Critical Flow, USAEC Report ANL-6633 (October, 1962).

F7. H. K. Fauske, "The Discharge of Saturated Water Through Tubes", AIChE, Reprint 30, Seventh National Heat Transfer Conference, AIChE and ASME, Cleveland, Ohio (August 9 to 12, 1964).

G

G1. D. C. Groeneveld; An Investigation of Heat Transfer in the Liquid Deficient Regime, AECL-3281 (December, 1969).

G2. G. E. Gruen; WHAM Prediction of Semiscale Test Results, IN-1431 (October, 1970).

H

H1. J. C. Haire and G. F. Brockett; LOFT Core Length Study, USAEC Report IN-1391, Idaho Nuclear Corporation, (August, 1970).

H2. C. J. Hocevar and I. W. Wineiger; Theta 1-B: A Computer Code For Nuclear Reactor Core Thermal Analysis, IN-1445 (Feb., 1971)

H3. E. D. Hughes; A Correlation of Rod Bundle CHF For Water in the Pressure Range 150 to 725 psia, USAEC Report IN-1412, Idaho Nuclear Corporation, July, 1970.

H4. G. H. Hanson, "Subcooled Blowdown: LOFT-Quarter Scale Experimental Procedures and Calculated Transients During a Loss-of-Coolant Accident", ANS Transaction, 12, p 359 (1969).

I

Il. Indiana & Michigan Electric Company: D. C. Cook Plant, Preliminary Safety Analysis Report, USAEC Docket.

L

L1. C. G. Lawson, Emergency Core Cooling Systems For Light Water Cooled Power Reactors, ORNL-NSIC-24 (October, 1968).

L2 C. G. Lawson, Heat Transfer From Electrically Heated Rods During A Simulated Loss-of-Coolant Accident, Chemical Engineering Progress Symposium Series, No. 119, Vol. 67 (1971).

L3. M. F. Lyons, et al, UO_2 Pellet Thermal Conductivity From Irradiations With Central Melting, GEAP-4624 (July, 1964).

L4. Lacrosse Nuclear Plant, Dairyland Power Cooperative, Letter and Analyses transmitted to the AEC Division of Reactor Licensing, january 24, 1972, on vessel stud failures, Docket 155-156.

M

M1. Z. R. Martinson, Behavior of 5-Inch Long 1/4-Inch OD Zircaloy-2 Clad Oxide Fuel Rods Subjected to High Energy Power Bursts, USAEC Report IN-TR-107, Idaho Nuclear Corporation, August, 1969.

M2. J. E. Meyer, "Hydrodynamic Models for the Treatment of Reactor Thermal Transients", Nuclear Science and Engineering, 10 (July, 1961), pp 269-277.

M3. E. C. Miller, The Integrity of Reactor Pressure Vessels, ORNL-NSIC-15 (May, 1966).

M4. Z. L. Miropolsky, "Heat Transfer in Film Boiling of a Steam-Water Mixture in Steam Generating Tubes", Teploenergetika, Vol. 10, No. 5, pp 49-53 (1963).

M5. F. H. Moody, "Maximum Flow Rate of A Single component, Two-Phase Mixture", ASME Paper 64-HT-35 (1964).

M6. F. H. Moody, Maximum Two-Phase Vessel Blowdown From Pipes, APED-4827 (April 20, 1965).

M7. D. L. Morrison et al, An Evaluation of the Applicability of Existing Data to the Analytical Description of a Nuclear Reactor Accident. BMI-1910 (July - September, 1971).

M8. K. V. Moore and R. P. Rose, "Application of a Lumped Parameter Bubble Rise Model to Coolant Blowdown Analysis", ANS Transaction, Vol. 9, No. 2 (1966), pp 559-560.

M9. F. H. Moody, Maximum Two-Phase Vessel Blowdown From Pipes, APED-4827 (April 20, 1965).

M10. F. H. Moody, "Maximum Flow Rate of a Single Component, Two-Phase Mixture", Transaction ASME, Ser. C, Journal Heat Transfer, 87(1): 134-142 (1965).

M11. F. H. Moody, "Liquid/Vapor Action in Vessel During Blowdown", ASME Paper 68-WA/NE-2 (December 1-5, 1968).

N

N1. S. Novick, The Careless Atom, Houghton Mifflin Co., Boston, Mass. (1969).

P

P1. J. F. Proctor; "Explosion Containment for Nuclear Reactor Vessels", Nuclear Safety, Vol. 7, No. 4, pp. 459-468 (Summer, 1966).

P2. J. F. Proctor; "Adequacy of Explosion Response Data in Estimating Reactor Vessel Damage", Nuclear Safety, Vol. 8, No. 6, (November - December, 1967).

R

R1. M. E. Remley, ANS Proposed Standard: "Energy Release Following Shutdown of Uranium - Fueled Thermal Reactors", Approved by Subcommittee ANS-5 on June 11, 1968.

R2. W. H. Rettig et al, RELAP 3 - A Computer Program for Reactor Blowdown Analysis, IN-1321 (June, 1970).

R3. W. M. Rohsenow and Harry Choi, Heat, Mass and Momentum Transfer, Prentice Hall, 1961.

R4. V. A. Redfield, "CHIC-KIN, A Fortran Program for Intermediate and Fast Transients in a Water Moderated Reactor", WAPD-TM-479 (January, 1965).

R5. J. A. Redfield et al, FLASH, FLASH2, FLASH3, A Fortran IV Program for the Digital Simulation of a Multinode Reactor Plant During Loss-of-Coolant (1966, 1967, 1968), WAPD-TM-534, 666 and 800.

R6. J. A. Redfield, T. S. Porsching et al, FLASH-4: A Fully Implicit Fortran-IV Program for the Digital Simulation of Transients in a Reactor Plant, WAPD-TM-840 (March, 1969).

S

S1. E. N. Seider and G. E. Tate, "Heat Transfer and Pressure Drop of Liquids in Tubes", Indus. Eng. Chem., 28, No. 12 (December 1936), pp 1429-1435.

S2. H. C. Sorensen and S. H. Fistedis, "A Hydrodynamical Analysis for Reactor Primary Containment by Energy Absorption", Nuclear Engineering and Design, 7 (1968), pp 547-577.

S3. V. E. Schrock and L. M. Grossman, Forced Convection Boiling Studies, Final Report on Forced Convection Vaporization Project, TID-14632 (1959).

S4. V. L. Streeter and E. B. Wylie, Hydraulic Transients, McGraw Hill, New York (1967).

S5. A. J. Stepanoff, Centrifugal and Axial Flow Pumps, John Wiley and Sons, Inc, (1948).

S6. Bruce C. Slifer, Loss-of-Coolant Accident & Emergency Core Cooling Models for GE Boiling Water Reactors, NEDO-10329, April 1971, Class 1 and NEDO-10329, April 1961, Class 1, Supplement 1.

T

T1. H. Thielsch, Defects and Failures in Pressure Vessels and Piping Rheinhold Pub., New York (1965).

T2. J. R. S. Thom et al, "Boiling in Sub-Cooled Water During Flow Up Heated Tubes or Annuli", Proc. Instru Mech. Engrs., Vol. 180, (1965-1966), pp226-246.

T3. Y. S. Touloukian (ed.), Thermodynamical Properties of High-Temperature Solid Materials, Vol. 2, Part II, New York, McMillan (1967).

T4. S. E. Turner et al, "Industrial Sabotage in Nuclear Power Plants", Nuclear Safety, Vol.11, No. 2, March-April, 1970.

T5. G. A. Tingate, " Some Thoughts on Sound Practices With Particular Reference to Contingency Allowances and Reactor Pressure Vessels" Australian Atomic Energy Commission (1962). Also Private Communication with P. L. Doan (April, 1971).

T6. D. B. Trauger, Testimony During the AEC Rule Making Hearing on Emergency Core Cooling Systems in Large Civilian Nuclear Power Plants, January 27, 1972.

U

U1. USAEC, Testimony of the AEC Regulatory Staff at the Public Rule Making Hearing on Interim Acceptance Criteria for Emergency Core Cooling Systems for Light Water Power Reactors, Washington, D. C., January 27, 1972.

U2. USAEC, Criteria for Emergency Core Cooling Systems for Light Water Power Reactors - Interim Policy Statement, Federal Register, Vol. 36, No. 125, June 29, 1971, and Vol. 36, No. 244, December 18, 1971.

U3. USAEC Report WASH-1146 on Light Water Reactor Safety Program Plan (1970). Reviewed by H. F. Bradburn et al in Nuclear Safety, Vol. 11, No. 5, September - October, 1970.

W

W1. Westinghouse Electric Corporation; Analysis of Anticipated Reactor Transients Without Trip, WCAP-7655.

W2. Westinghouse Electric Corporation, An Evaluation of Anticipated Operational Transients in Westinghouse PWR, WCAP-7486-L (December, 1970).

W3. G. D. Whitman, Technology of Steel Pressure Vessels for Water-Cooled Nuclear Reactors, Nuclear Safety, Vol. 8, No. 5, Sept. - Oct., 1967, also ORNL-NSIC-21.

W4. Westinghouse Electric Corporation, Testimony at the Rule Making Hearings in the Matter of Acceptance Criteria for Emergency Core Cooling Systems for Light-Water-Cooled Nuclear Power Reactors, March 23, 1972, Docket Rm 50-1.